How Dynamic Bond results in the unique viscoelastic behavior of the associating polymers

A Dissertation Presented for the

Doctor of Philosophy

Degree

The University of Tennessee, Knoxville

Sirui Ge

August 2022

Acknowledgements

First of all, I would like to express my gratitude to my advisor, Dr. Alexei P. Sokolov for his guidance, patience, encouragement and support throughout my doctoral research. I feel extremely lucky to be able to work closely with him and learn about various aspects of polymer physics and many professional skills. He is my life mentor not only in the field of scientific research, but also in how to become a kind, considerate, decent and wise person with critical thinking and professional spirit. Besides the Ph.D. research, he cares deeply for students' future development and is super supportive for us to explore various opportunities. His kindness to students, diligent and professional working spirit, aspiration to knowledge and passion for science have influenced me profoundly in the past five years and will keep inspiring me in my future life. I also would like to thank him for writing several letters of recommendations for some postdoctoral research associate positions that I applied for my next step as a researcher.

I would like to thank my doctoral committee members: Dr. Kevin M. Kit, Dr. Takeshi Egami and Dr. S. Michael Kilbey for serving on my doctoral committee and for their valuable suggestions and efforts to help me with my graduation.

I feel greatly blessed to work in our group with so many talented and kind colleagues. I would like to thank Dr. Martin Tress who worked closely with me on my first project by teaching and discussing with me how to understand the experimental results correctly on the molecular level. I would like to thank Dr. Subarna Samanta who worked with me on my following projects on the study of associating polymer with microphase separation. Not only he gave me quite a few suggestions on my research project, but also he gave me quite a few guidance on my future

career. I would like to thank Dr. Shiwang Cheng who taught me rheology and dielectric measurements. I would like to thank Dr. Kunyue Xing, Bingrui Li, Dr. Peng-Fei Cao and Dr. Sheng Zhao who greatly helped me on the synthesis of associating polymers. I would like to Thank Dr. Anne-Caroline Genix and her student Philippe Dieudonné-George on part of the X-ray scattering measurement in France. I would like to thank G. Peyton Carden under my mentorship who helps me finish some experimental measurement, including X-Ray Scattering and dielectric measurement. I would like to thank Katrina D. Pangilinan for training me on several necessary research facilities in Polymer Characterization Lab which was used in my research work.

I would also like to acknowledge the collaborative efforts and many valuable discussions with members and former members in the group: Dr. Tomonori Saito, Dr. Vera Bocharova, Dr. Md Anisur Rahman, Dr. Catalin Gainaru, Dr. Alexander Kisliuk, Dr. Vladimir Novikov, Dr. Ivan Popov, Dr. Amanda Young-Gonzales, Dr. Zhengping (Jim) Zhou, Dr. Xiao Zhao, Dr. Dmitry N. Voylov, Dr. Zaneta Wojnarowska, Dr. Seung Pyo Jeong, Dr. Lingyao Meng, Dr. Lu Han, Dr. Sungjin Kim, Dr. Arif Arifuzzaman, Dr. Kostas Misichronis, Dr. Michelle L. Lehmann, Dr. Dustin B. Gilmer, Dr. Zheng Zhang, Dr. Jiadeng Zhu, Dr. Jiancheng Luo, Dr. Zoriana Demchuk, Dr. Ke Cao, Dr. Tao Hong, Dr. Bobby Carroll, Dr. Mengyuan Wang, Dr. Andrew J. Erwin, Dr. Tianyi Liu, Dr. Gaukhar Toleutay, Dr. Yu Kashiwagi, Jacky Zheng, Natasha Ghezawi, Tony Su, Md Dipu Ahmed, Justin C. Powell, Leo Parsons, Ben Stacy, Maria Furukawa, Alexander Huynh and other group members.

I would also like to thank other researchers in UT and ORNL on some discussion and collaboration such as Dr. Mark Dadmum, Dr. Akan A. George, Dr. Halie Martin, Dr. Neiko

Levenhagen, Kaizhong Guan, Dr. Guang Yang, Dr. Runming Tao, Dr. Yiman Zhang, Dr. Alexandar Buhse Brady, Dr. Aimee Lu Church, Dr. Jinbo Dou, Dr. Tianyu Li, Dr. Fang Liu, Dr. Yu Yan, Dr. Lengwan Li, Dr. Ashleigh Locke Barnes, Dr. Liu Cao, Dr. Nan Huang, Dr. Youxiong Ye, Dr. Chengze liu and some others who I met in Tennessee Areas.

Last but not least, I would like to thank my Master's thesis advisor Dr. Shi-Qing Wang, as well as other group member including Dr. Jianning Liu, Dr. Xiaoxiao Li, Dr. Yexin Zheng, Dr. Zhichen Zhao, Dr. Panpan Lin, Dr. Gengxin Liu, Yue Zhao, Mengchen Wang and Dr. Xianggang Li in the University of Akron. Working in that group not only helped me to learn how to use rheometer and something about polymer dynamics, but also opens the door for me to scientific research in my life.

I dedicate this dissertation to my beloved parents, Ning Fan and Wenjian Ge, for their unconditional love, support and encouragement.

Abstract

Associating polymer is a special kind of polymer possessing transient reversible bonds in addition to the conventional covalent bonds. The reversible bonds provide unique dynamics and fascinating viscoelastic properties, resulting in attractive applications for these polymers, such as self-healing and shape memory materials. Despite many years of studies, the understanding of dynamics of polymers with reversible bonds, especially on molecular level, is still in the rudimentary stage, preventing the rational design of the potential novel functional materials based on associating polymers.

In this dissertation, we provide a detailed and quantitative understanding of the dynamics and viscoelastic properties of associating polymers. The functional groups form both binary association and microphase separation.

For the associating polymer with binary association, the bond lifetime renormalization model was experimentally tested on telechelic associating polymers with PDMS and PPG backbone, different chain length and different H-bonding functional groups, unravelling the mechanism of how bond dissociation results in the network rearrangement in such system.

For associating polymers forming microphase separation, the microphase separated structure was characterized through X-ray scattering. In addition, a layer of polymer segments with restricted mobility was found at the interface of the microphase separated clusters and the polymer matrix through the dielectric measurements. The layer plays a critical role in mechanical reinforcement of the associating polymers with microphase separation. In addition, we unraveled the mechanism of how network rearrangement happens in associating polymers. Finally, a general

molecular picture of stress relaxation mechanism in such associating polymer system was proposed.

The microscopic understanding of the dynamics and viscoelastic behavior of associating polymers is instructive for rational design of novel functional polymeric materials, i.e, how to control viscoelasticity by tuning the structure and position of the functional groups in such materials. In addition, the research can be essential for the understanding of the dynamics of general soft matter, and even biological materials in which dynamic bonds play an important role.

Table of Contents

List of Tables

List of Figures

Introduction

Associating polymer is a special kind of polymer with both covalent bonds and transient reversible bonds. This kind of polymer have been studied due to their potential applications in the fields of self-healing materials and shape memory materials. However, the microscopic understanding of the mechanisms controlling viscoelastic properties in associating polymers is still in rudimental stage.

Binary association is the simplest form of association in which two complementary functional groups form reversible bonds. Sticky Rouse and Sticky Reptation models have been utilized to study the associating polymers. However, some contradictions have been reported, such as different bond lifetimes between different measurement techniques. The new bond lifetime renormalization model was proposed later, which theoretically explained the contradiction. However, it has not been thoroughly tested experimentally. In addition to the binary association, it is also possible for functional groups on associating polymers to aggregate, forming clusters. With microphase separation, the associating polymer can demonstrate enhanced mechanical modulus. However, the reason for the elevated mechanical modulus is still not well-understood. Besides mechanical reinforcement, microphase separation makes the dynamics and viscoelastic properties of associating polymers more complicated. Also, the terminal relaxation behavior has not been well understood. Thus, the main goal of this research is to provide a detailed and quantitative understanding of the dynamics and viscoelastic properties of associating polymers forming both binary association and microphase separation. Throughout the research, the associating polymers with hydrogen bonding are telechelic so that the spatial hindrance will have

the least impact on dynamics of the physical bonds. Also, the chemical structure of the telechelic polymer is more well-defined.

Firstly, we used both rheology and dielectric spectroscopy to characterize bond lifetime for telechelic associating polymers with only binary association. The terminal relaxation time from rheology is much longer than the bond dissociation time from dielectric spectroscopy, indicating that rheological measurement has additional contribution on the estimation of bond lifetime. Detailed analysis of experimental data revealed that the bond lifetime renormalization model describes the results well. Through the analysis of the model, the sticker diffusion indicates a Rouse to Reptation dynamics transition with longer backbone, suggesting that the dynamics of super-chains must be considered. When bond strength is high, bond lifetime renormalization model predicts no difference between the timescale of bond lifetime from rheological measurement and dielectric measurement, which is verified by experiments.

Then, we are focusing on the associating polymer with microphase separation. We verified microphase separation and characterized its structure using X-ray scattering. Taking the interfacial layer model analysis of dielectric spectra from the polymer nanocomposite field, we illustrated the existence of a layer of polymer segment with restricted mobility surrounding the microphase separated cluster (In the later part of the dissertation we called it interfacial layer). The thickness of the interfacial layer was found to be ~0.7−0.9 nm surrounding these microphase separated clusters. The critical role of the interfacial layer on the mechanical reinforcement was also confirmed through the analysis of both mechanical interfacial layer model as well as mechanical percolation model.

As the next step, we proposed a mechanism of network rearrangement in associating polymer

with microphase separation by borrowing the idea of chain exchange kinetics in block copolymer micelles. The mechanism also successfully explains the separation between timescales of the end group dynamics within microphase separated cluster and the terminal relaxation time from rheological measurement. Finally, we formulated a general molecular picture describing the viscoelastic properties of associating polymers with microphase separation.

This dissertation is organized in the following way.

Chapter 1 gives a concise overview of the background of associating polymers and classic theories and model describing the dynamics and viscoelastic properties of associating polymers.

Chapter 2 describes experimental techniques involved in the research. An introduction to the principles and instrumentation of Differential Scanning Calorimetry (DSC), rheology, Broadband Dielectric Spectroscopy (BDS), and X-ray Scattering is presented.

Chapter 3 presents the detailed experimental test of the bond lifetime renormalization model on a variety of telechelic associating polymers. Our analysis verifies the mechanism of network rearrangement in associating polymers with binary association. This analysis also suggests the formation of superchain in the studied telechelic polymer system.

Chapter 4 extends the work of Chapter 3 by introducing a hydrogen bonding functional group (single urea) with higher bonding energy. This functional group also forms binary association. Our analysis demonstrates that the rheological terminal relaxation time equals to the bond dissociation time from dielectric measurement, which also agrees with the prediction from bond lifetime renormalization model.

Chapter 5 presents the detailed structural characterization of the associating polymers with

microphase separation using X-ray scattering, the unusually high mechanical modulus from rheological measurements, the study of segmental dynamics using BDS with the analysis of the spectra based on the dielectric interfacial layer model. Our analysis reveals the presence of interfacial layer with thickness of 0.7 to 0.9 nm, and demonstrates the crucial role of the interfacial layer on the mechanical reinforcement.

Chapter 6 presents analysis of the percolation phenomenon through the overlapping of interfacial layer in associating polymer with microphase separation. We show that the mechanical percolation model explains well the observed reinforcement. In addition, through the careful comparison of shear modulus spectra and dielectric modulus spectra, the mechanism of how network rearrangement happens was unraveled for associating polymer with microphase separation. Finally, the general molecular picture of how stress relaxation happens in such system is presented.

At the end, conclusions are summarized and some future directions are proposed as well.

CHAPTER 1 BACKGROUND AND LITERATURE REVIEW

1.1 Associating polymers and their applications

Associating polymers are a unique class of polymers possessing functional groups which form a transient network via reversible bonds[1, 2]. These reversible bonds can associate and dissociate based on their own binding energies, which has different dynamics from the polymeric chains to which they are linked[3, 4]. Thus, by incorporating the reversible bond into the associating polymer, it adds new timescales that gives additional manipulation of dynamics of the whole polymer chains. As a result, the properties of the polymers, especially the viscoelastic properties, can be significantly tuned thanks to the incorporation of these reversible bonds. Due to the unique dynamics of associating polymers, they have quite a few applications. One of the applications is self-healing materials[5-7]. For example, they can be used as the binder of the silicon electrode for lithium batteries[8]. The silicon electrodes are prone to cracking during the recharging process, resulting in a shortened lifetime. By incorporation of the self-healing binder made from associating polymer, the electrode can self-heal during the charging process (Fig. 1.1a), so that the lifetime of the lithium battery is prolonged[9-11]. Another application is the shape memory materials[12]. In shape memory materials, crosslinks determine the permanent shape. Reversible interaction is used to fix the temporary shape[13]. At low temperature, the resulting transient bond has a long lifetime. Thus, the shape of the material after being stretched will be fixed upon cooling. At high temperature, the transient bond has a very short lifetime and will rearrange towards equilibrium, allowing the shape of material to recover. Fig. 1.1b shows a typical

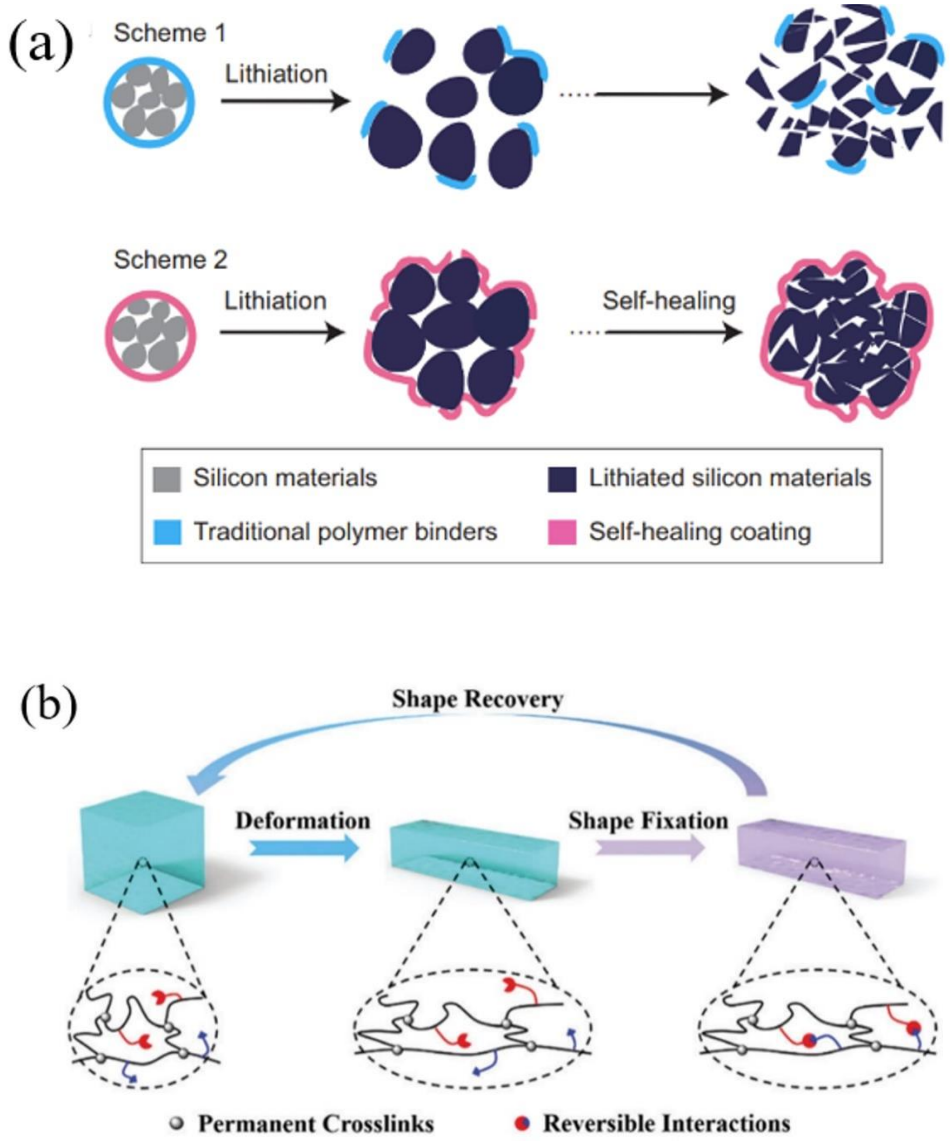

Figure 1.1 (a) illustration of self-healing materials made of associating polymers[14]. (b) illustration of shape memory materials made of associating polymers[13].

procedure of shape memory.

1.2 Different type of associating bonds

Several kinds of physical bonds can work as the transient reversible bonds for associating polymers. These physical bonds include hydrogen bonding[15, 16], ionic bonding[17-19], metal-ligand bonding[20, 21], π–π stacking[22], etc. Different type of associating bonds has different bond energies (Fig. 1.2). In this research, we are focusing on the associating polymer with hydrogen bonding.

1.3 Associating polymers with hydrogen bonding

Hydrogen bonding is the most common associating bond in associating polymers because of its directionality, cooperative property[23]. In addition, the strength of the transient bond can be tuned by increasing the number of H-bonding centers on the functional groups[24], in other words, the hydrogen bond strength can be tuned in a wide range based on rational molecular design of the functional groups. One classical example of this kind of associating polymer utilized urea as function groups, which form strong association bonds[8] (Fig. 1.3). With the hydrogen-bonded functional group, not only they can link together, forming binary association, but also functional group can aggregate together to form microphase separation. Recent study shows that hydrogen bonding has an impact on the dynamics of hydroxyl, amine and carboxylic acid terminated PDMS[25, 26] and PPG[27] associating polymers.

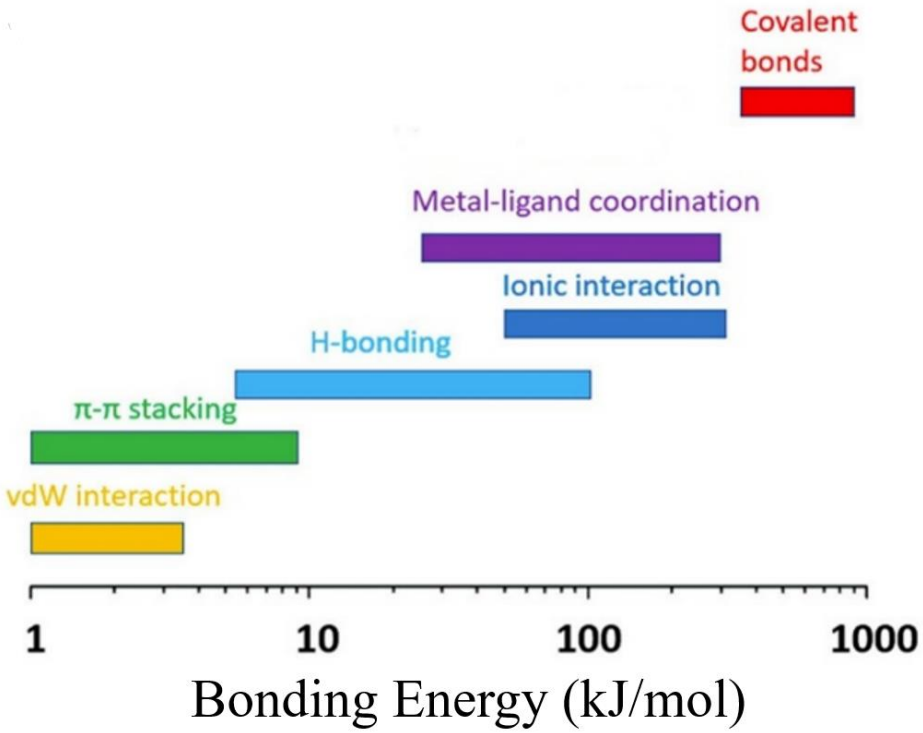

Figure 1.2 The bond energy for different association types.

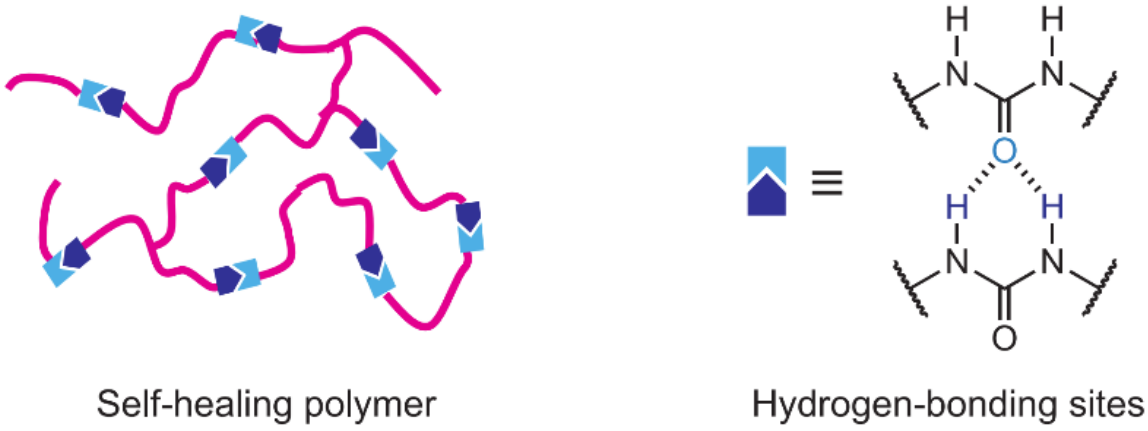

Figure 1.3 Associating polymer with hydrogen bonding[8]

1.4 Hydrogen bond forming binary association

Binary association is the most fundamental hydrogen bonding interaction when two sticky groups on associating polymers form a transient bond. In such a case, the complimentary a associating groups can associate and dissociate, with dynamics controlled by the lifetime of the associating bonds. In the past few decades, associating polymers with hydrogen bonded functional groups randomly distributed along the polymer backbone, have been investigated in melt[28, 29] and solution state[30-32]. The overall dynamics of such associating polymers is determined by bond strength, i.e., the activation energy for bond dissociation.

1.5 Activation energy for bond dissociation and its estimation

If hydrogen bonds form binary association, it is the activation energy for bond dissociation that controls the lifetime of the transient bonds. The illustration of activation energy is shown in Fig. 1.4. In associating polymers, the free energy level at associated state (E_{assoc}) is lower than that at dissociated state (E_{diss}). Their difference is called binding energy (E_{bind}). However, in order for the transient bond to dissociate, it needs to overcome an energy barrier larger than E_{bind}. This energy barrier is the activation energy (E_a) for a transient bond to dissociate[33]. Since activation energy is of paramount importance to determine the lifetime of the transient bond, several studies have been conducted to estimate this activation energy. Matsumiya et al. acquired bond lifetime of end-carboxylated polyisoprene associating polymers at different temperatures and used Arrhenius fit to acquire the activation energy to be ~100-130 kJ/mol[34]. Xing et al. conducted analogous analysis on a PDMS associating polymer with carboxylic acid functional groups and acquired the similar activation energy[26]. The reason for the unusually high activation energy is

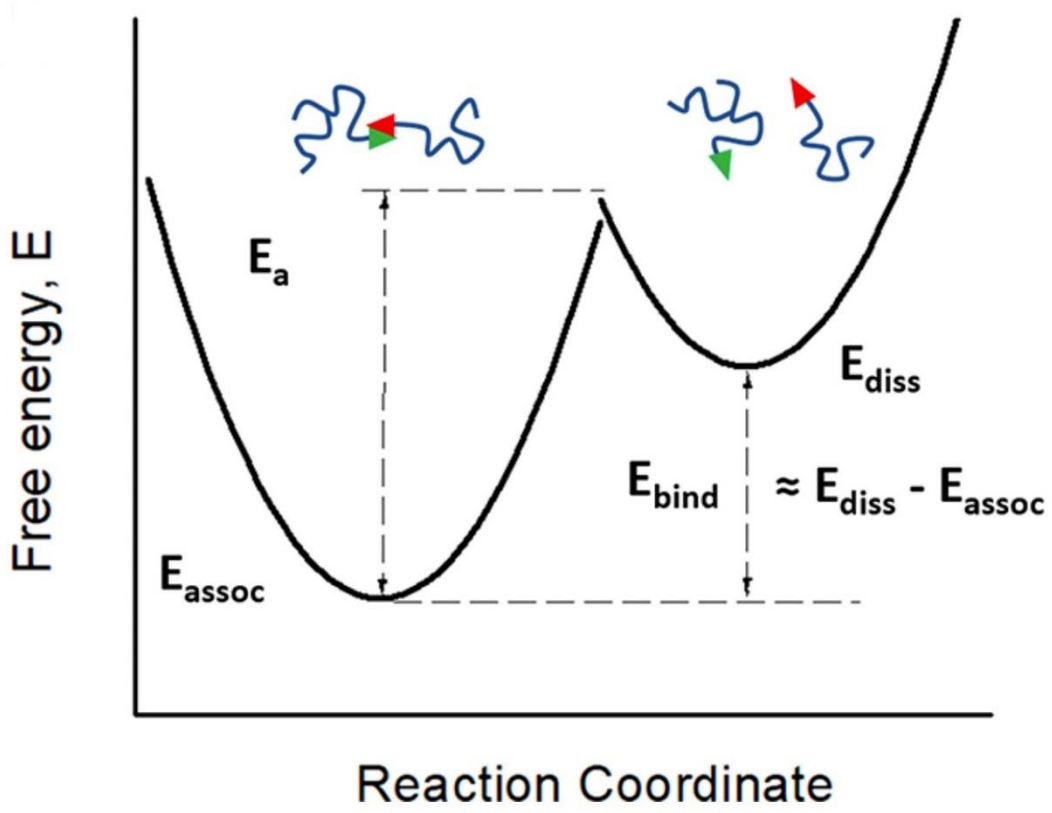

Figure 1.4 Different range of activation energy for associating polymers with different kind of transient bonds[35]

that they did not take into account changes in segmental dynamics of associating polymers. In associating polymers, τ_{dis} (the characteristic relaxation time of bond dissociation acquired from experimental measurement) is controlled not only by the activation energy, but it is also affected by the temperature dependence of segmental relaxation of the polymer, $\tau_\alpha(T)$. The segmental dynamics defines the attempt frequency for the dissociation in this case[36]. Thus, $\tau_{dis}(T)$ is not only correlated to the activation energy (E_a), but it is also correlated to the segmental relaxation, i.e., $\tau_\alpha(T)$, so that $\tau_{dis}(T)$ is expressed as:

$$\tau_{dis}(T) = \tau_\alpha(T)\exp\left(\frac{E_a}{RT}\right) \quad (1.1)$$

in which the activation energy (E_a) can be estimated from the measured $\tau_{dis}(T)$ scaled by $\tau_\alpha(T)$:

$$E_a = RTln\left[\frac{\tau_{dis}(T)}{\tau_\alpha(T)}\right] \quad (1.2)$$

1.6 Characterization of bond lifetime

To estimate the activation energy, the bond lifetime characterization from experiment is quite important. Both dielectric spectroscopy and rheology can are used for characterizing bond lifetime.

1.6.1 Characterizing bond lifetime through dielectric spectroscopy

Dielectric spectroscopy is a powerful tool to characterize the bond lifetime. After the dissociation process of the transient bond, the absolute value of the dipole moment changes with a value of $\Delta\mu$. With the assumption that cross-correlations between different polymer chains can be neglected, the microscopic correlation function $\gamma(t)$ can be expressed by dielectric function[37]:

$$\frac{\varepsilon^*(\omega)-\varepsilon_\infty}{\varepsilon_S-\varepsilon_\infty} = \hat{L}(-\frac{d}{dt}\gamma(t)) \qquad (1.3)$$

where $\hat{L}$ is the operator for Laplace transform whose general formalism for a time dependent function is given by $\hat{L}[f(t)] = \int_0^\infty e^{-i\omega t} f(t)dt$. Since the variation of a dipole moment originates from the time-dependent variation in the absolute value of the dipole moment $|\vec{\mu}(t)|$ rather than orientation, the microscopic correlation function $\gamma(t)$ can be expressed by

$$\gamma(t) = \frac{\langle|\overrightarrow{\mu_i}(0)||\overrightarrow{\mu_i}(t)|\rangle}{\langle|\overrightarrow{\mu_i}(0)||\overrightarrow{\mu_i}(0)|\rangle} \qquad (1.4)$$

Through this mechanism, the breaking of transient bonds results in a dielectric relaxation process. The characteristic bond dissociation time can be acquired through the peak position of the dielectric relaxation process.

In recent study, bond dissociation process in associating polymers with binary association has been detected by dielectric spectra. In telechelic associating polymer with PDMS backbone (different chain length) and amine functional groups (PDMS-NH_2)(Fig. 1.5 (a)(b)(c))[26], the dielectric spectra demonstrates the bond dissociation process as a low frequency process, which is on the left side of the segmental relaxation process. The bond dissociation process is also verified by its dielectric strength increasing with the weight fraction of NH_2 groups (Fig. 1.5d).

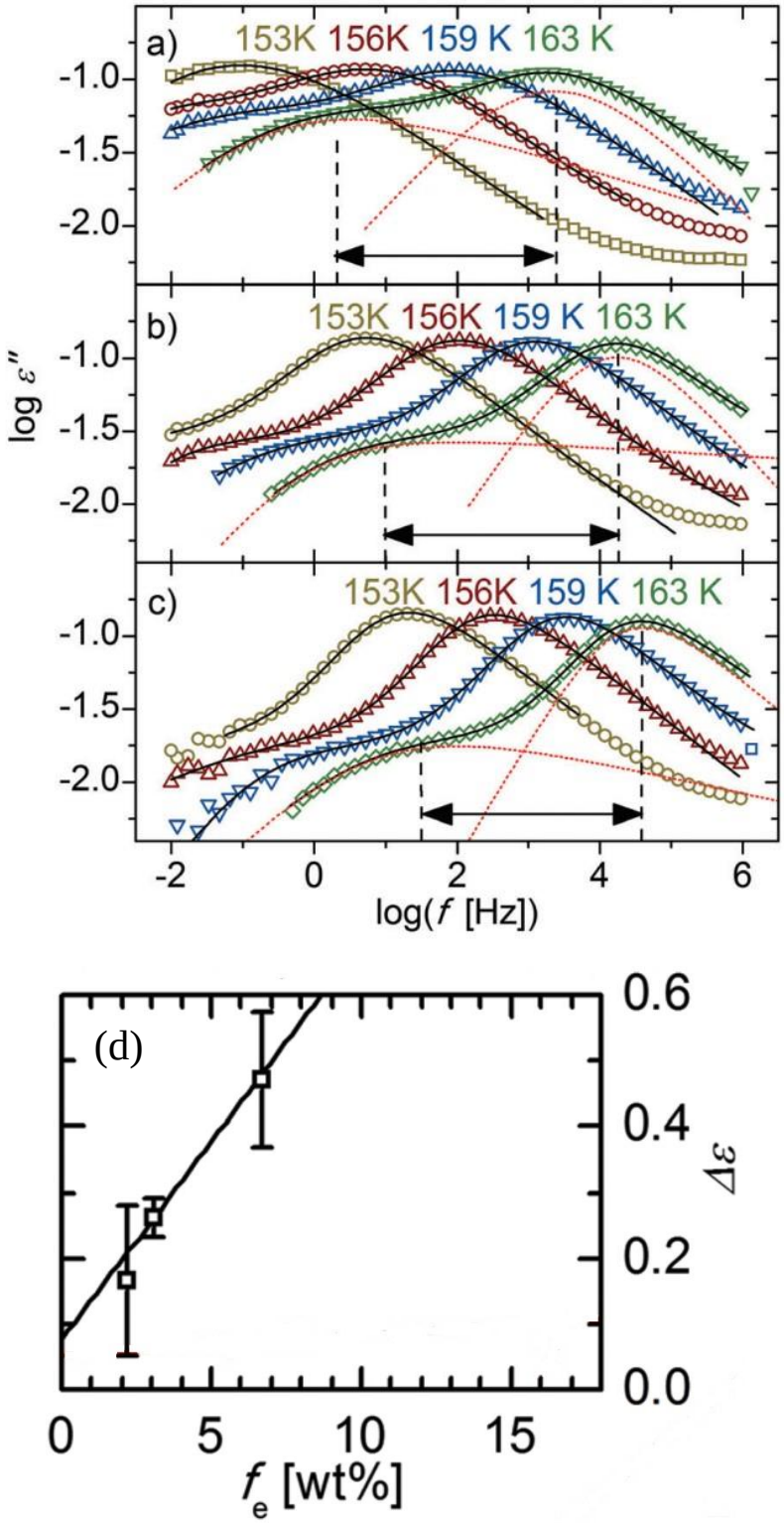

Figure 1.5 Dielectric spectra for PDMS-NH_2 with (a) DP of 22, (b) DP of 50 and (c) DP of 74[26]. (d) Dependence of the dielectric relaxation on the weight fraction of stickers for PDMS-NH_2.

1.6.2 Characterizing bond lifetime through rheology

Besides dielectric spectroscopy, rheology is another technique to characterize the bond lifetime for associating polymer with binary association. The time it takes for bond rearrangement (τ_{rearr}) can be acquired using rheological measurement. With the addition of the functional groups, the terminal relaxation time, i.e., the time it takes for the macroscopic flow to happen, of the polymer system can be prolonged until the network rearrangement happens, which originates from bond dissociation. In addition, it can also result in a rubbery plateau which is defined by the rubber elasticity theory. Quite a few models have been proposed in order to explain the experimental results, including Sticky-Rouse model[36] and Sticky Reptation model[38]. Both models have been applied to study the associating polymer with functional groups randomly distributed along the polymer backbone. Before introducing these two models, rubber elasticity theory needs to be introduced first.

1.6.2.1 Rubber elasticity theory

The rubber elasticity theory was proposed decades ago. It was utilized to predict the mechanical modulus of polymers which have rubber-like behavior. To simplify the case, all the polymer chains are considered Gaussian chains whose probability distribution of the end-to-end distance is Gaussian distribution. For each Gaussian chain i, the conformational entropy can be expressed as:

$$S_i = k_B \, ln \, \Omega_i \qquad (1.5)$$

in which k_B is the Boltzmann constant and Ω_i is the number of different conformational states.

Because of Gaussian distribution, we can have:

$$\Omega_i \sim P(R_i) = e^{-\frac{3R_i^2}{2<R^2>}} \qquad (1.6)$$

in which R_i is the end-to-end distance of each Gaussian chain and the $<R^2>$ is the mean-square end-to-end distance. Assuming that the total number of Gaussian chains is n, the total entropy can be denoted as:

$$S = \sum_{i=1}^{n} S_i = k_B \, ln \, \Omega \text{ in which } \Omega = \prod_{i=1}^{n} \Omega_i \qquad (1.7)$$

All the chains are assumed to be uncorrelated with each other so that the entropy can be simply added. Thus, the Helmholtz free energy can be expressed as:

$$A = U - TS = U + \frac{3}{2} k_B T \sum_{i=1}^{n} \frac{R_i^2}{<R^2>} \qquad (1.8)$$

Then consider a simple shear, the chain end-to-end vector changes from $\vec{R}$ to $\overrightarrow{R'}$ (Fig. 1.6a). The y and z components do not change during the simple shear, whereas x-component of the end-to-end distance is displaced so that:

$$R_{ix} \rightarrow R_{ix} + \gamma R_{iy} \qquad (1.9)$$

As a result, after the simple-shear deformation, Helmhotz free energy should be:

$$A(\gamma) = A(0) + \frac{3k_B T}{2<R^2>} \sum_{i=1}^{n} \gamma^2 R_{iy}^2 = A(0) + (\frac{nk_B T}{2})\gamma^2 \qquad (1.10)$$

in which A(0) is the free energy without the deformation. The total elastic force F is given by the variation of the free energy A with the displacement X= γH (Fig. 1.6), that is,

$$F = \left(\frac{\partial \triangle A}{\partial x}\right)_{T,V} = \frac{\partial \triangle A}{\partial \gamma} \frac{\partial \gamma}{\partial x} = \frac{nk_B T \gamma}{H} \qquad (1.11)$$

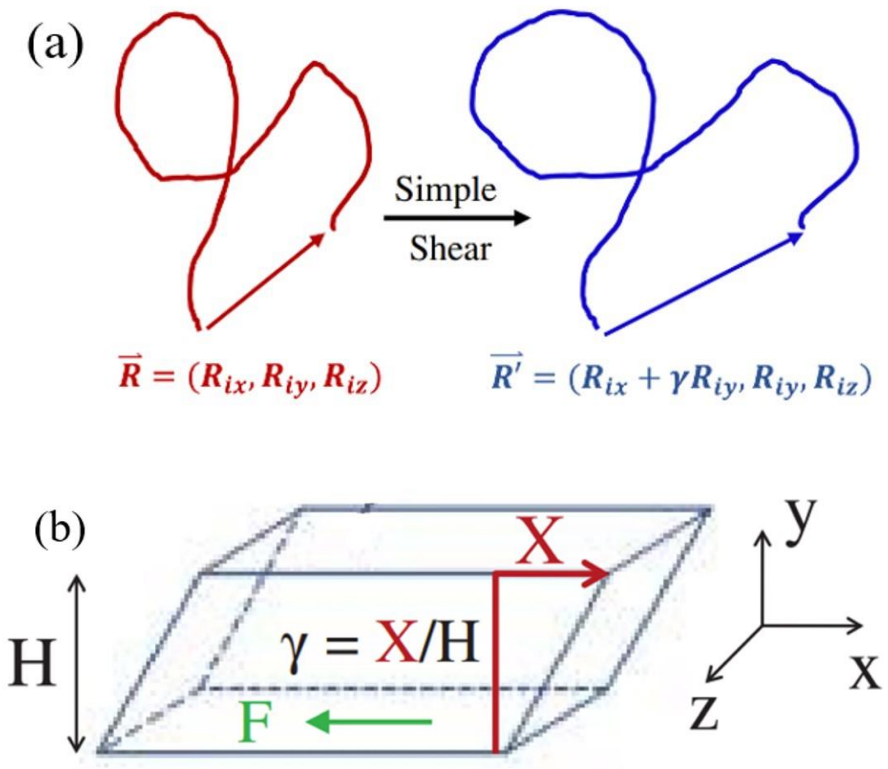

Figure 1.6 (a) Illustration of transformation in the end-to-end vector from **R** to **R'** during a simple shear. (b) An illustration of simple shear

Thus, the shear stress has the form:

$$\sigma = G\gamma \tag{1.12}$$

in which G is the shear modulus which is given by:

$$G = \frac{nk_BT}{V} = \frac{\rho RT}{M} \tag{1.13}$$

in which V is the total volume and M is molecular weight between crosslinks.

1.6.2.2 Sticky-Rouse model

The Rouse model is utilized to describe unentangled polymers in melt states. For timescale longer than the segmental relaxation time, the polymer chain can be considered as a chain with a many flexible segments, called Rouse segments. The motion of the polymer starts from the single Rouse segment, and then expands to the whole chain[39]. The shear modulus relaxation function in Rouse model can be expressed as

$$G_R(t) = G_0 \sum_{p=1}^{N} \exp\left(\frac{-tp^2}{\tau_0 N^2}\right) \tag{1.14}$$

in which N indicates the number of Rouse segments per chain. τ_0 is the elementary Rouse time. G_0 is the Rouse modulus defined as $G_0 = \frac{\rho RT}{M}$ which follows the rubber elasticity theory.

Here ρ is the density of the polymer, R is the gas constant, T is the temperature, M is the molecular weight of the polymer.

For associating polymers, the Rouse modes can persist until the chain feels constraints of transient crosslinks from the associating bonds. The chain motion on scales larger than the

distance between functional groups is controlled by bond lifetime. Then, the low order Rouse modes from p=1 to p=N_s should be delayed, here N_s is the number of segments between functional groups. Meanwhile, the high order chain modes are still Rouse-like. This enables us to express the relaxation of the whole chain as a combination of high order Rouse modes with $N_s + 1 \leq p \leq N$ with τ_0 and low order sticky Rouse modes with $1 \leq p \leq N_s$ that are delayed by τ_{rearr}:

$$G_R(t) = G_0 \left\{ \sum_{p=N_s+1}^{N} \exp\left(\frac{-tp^2}{\tau_0 N^2}\right) + \sum_{p=1}^{N_s} \exp\left(\frac{-tp^2}{\tau_{rearr} N_s^2}\right) \right\} \qquad (1.15)$$

In the bracket, the first term indicates the conventional Rouse mode, and the second term indicates the sticky Rouse mode. In addition, eq. 1.15 is equivalent to eq. 1.14 if $\tau_{rearr} \leq \tau_0 (\frac{N}{N_s})^2$, and the Rouse time of the chain between stickers will be replaced by $\tau_0 (\frac{N}{N_s})^2$. In such a case, the contribution from bond rearrangement can be neglected. On the other hand, if $\tau_{rearr} > \tau_0 (\frac{N}{N_s})^2$, the chain motion will be delayed due to the bond rearrangement. The Sticky-Rouse model has been utilized to acquire τ_{rearr} of the P(MEA-co-UPy-MA) associating polymers (Fig. 1.7a)[40]. In Fig. 1.7a, τ_{rearr} was labeled as τ_s, through which we know that the τ_{rearr} is the shortest Rouse time in the Sticky Rouse mode.

1.6.2.3 Sticky Reptation model

In the situation with entanglement of the polymeric chains in the system, the Sticky Reptation model needs to be employed. When the molecular weight polymer reaches a threshold, i.e., M_e, the entanglement happens in polymers, which leads to a modulation of Rouse dynamics. In other

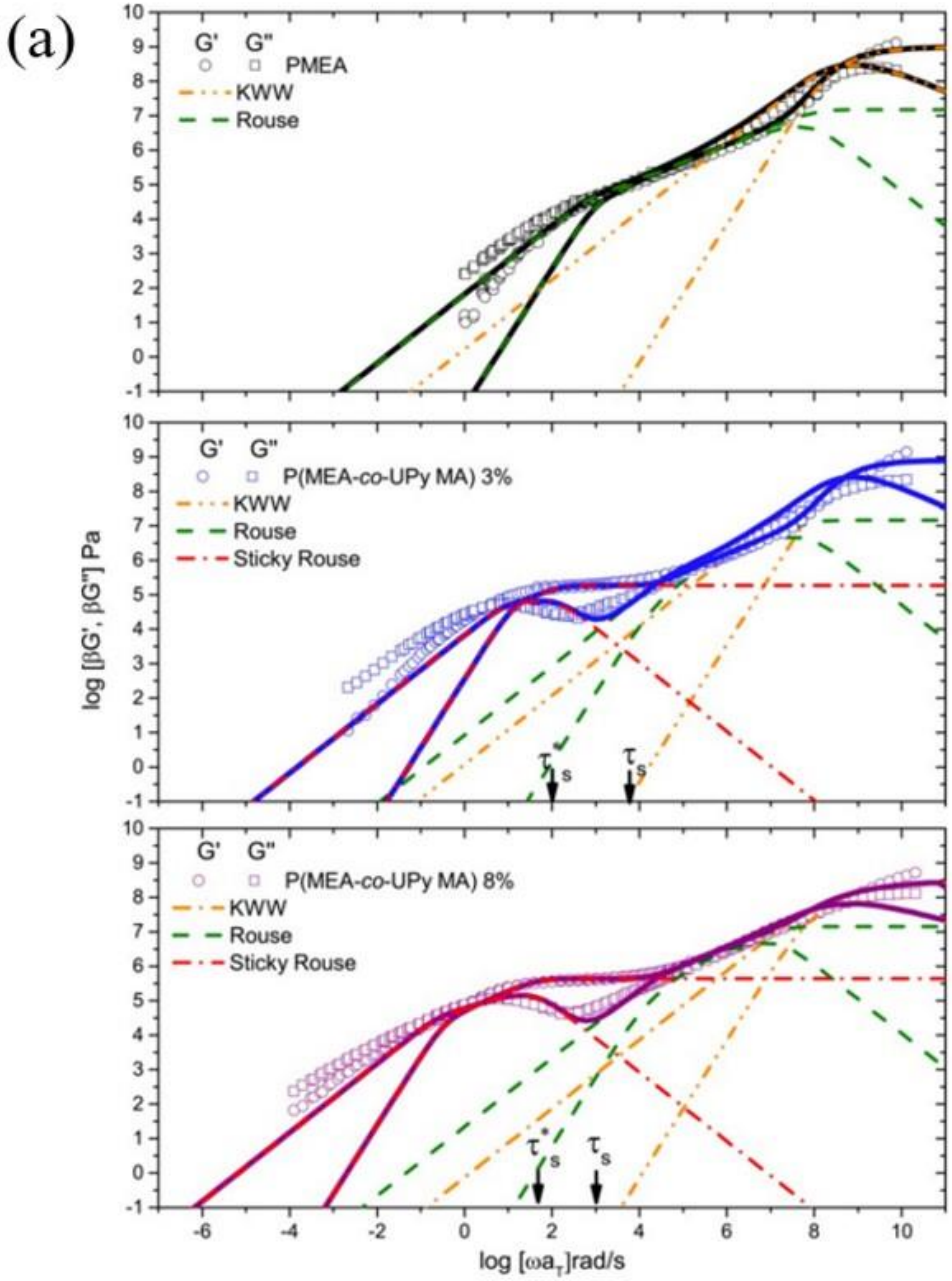

Figure 1.7 (a) Sticky Rouse model and its usage on acquiring bond lifetime of the P(MEA-co-UPy-MA) associating polymers[40]. (b) Sticky Reptation model and its scaling behavior[38]

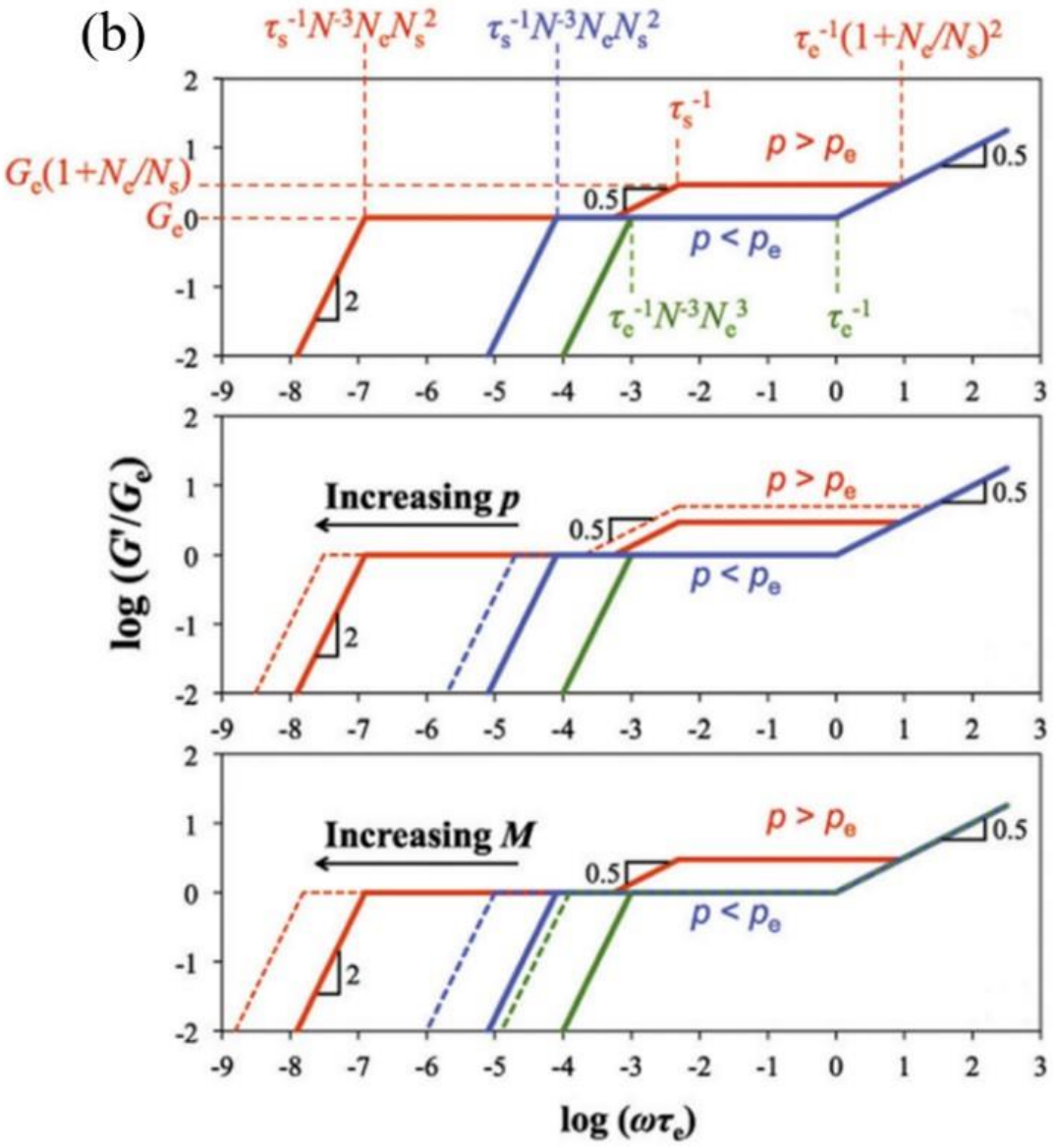

Figure 1.7 continued

words, a polymeric chain performs Rouse relaxation at short times. However, further relaxation process is confined when it encounters entanglement. Within the scenario of entanglement, the polymers are confined in a "tube" formed by the surrounding polymeric chains. Then, it takes the reptation time τ_d for the chain to be pulled out, resulting in terminal relaxation[41, 42]. In entangled polymer, τ_d is calculated as

$$\tau_d = 3\tau_e(\frac{N}{N_e})^3 \quad (1.16)$$

in which N_e indicates the number of Rouse segments between entanglement points and τ_e is tube constraint time defined as

$$\tau_e = \tau_0 N_e^2 \quad (1.17)$$

According to the Tube model from Doi and Edwards[43], the relaxation modulus for representing the relaxation process due to reptation is expressed as

$$G(t) = G_N^0 \sum_{q;odd} \frac{8}{q^2\pi^2} \mathrm{e}^{\frac{-q^2 t}{\tau_d}} \quad (1.18)$$

in which G_N^0 is defined as $G_N^0 = \frac{\rho RT}{M_e}$ according to the transient network model.

When functional groups are incorporated into the entangled polymer, the dynamics gets modified as well, depending on whether the number of functional groups is larger than the number of entanglements[38]. If the number of functional groups (p) is larger than the number of entanglements (p_e), there will be 2 rubbery plateaus (Fig. 1.7b). The rubbery plateau at high frequency reflects the contribution from both entanglements and transient bonds, which persist till τ_{rearr}. Because of the sticky bond, the tube constraint time becomes even longer, which is

modified as $\tau_e = \tau_{rearr}(\frac{N_e}{N_s})^2$. Then, the second rubbery plateau shows up, persisting until the sticky reptation time.

$$\tau_{rep} = \tau_e(\frac{N}{N_e})^3 = \frac{\tau_{rearr}N^3}{N_e N_s^2} \quad (1.19)$$

If the number of functional groups (p) is less than the number of entanglements (p_e), the Rouse equilibration of entanglement strands does not necessarily require bond dissociation. The plateau modulus is still the sum of entanglements and reversible bonds. Whereas reptation is still delayed by the reversible crosslinks (Fig. 1.7b). On the timescale of τ_{rearr}, a fraction $\frac{N_s}{N}$ is able to reptate a distance of $bN_s^{0.5}$ in which b is the segmental size. Then, the reptation of the whole chain over a contour length of $L = \frac{Na}{N_e}$ becomes

$$\tau_{rep} = \frac{\tau_{rearr}L^2}{\frac{N_s^2 b^2}{N}} = \frac{\tau_{rearr}N^3}{N_e N_s^2} \quad (1.20)$$

in which $a = N_e^{0.5}b$ is the entanglement length. Thus, no matter whether the number of functional groups is larger than the number of entanglement or not, the expression of sticky reptation time, namely the timescale when terminal relaxation time happens, are identical. Thus, τ_{rearr} can be acquired on condition that we know the exact chemical structure of the associating polymer as well as the terminal relaxation time.

1.6.2.4 Bond lifetime characterization for telechelic associating polymers from rheological measurement

Recently, the viscoelastic behavior of unentangled telechelic associating polymers with binary association was also studied through rheological measurement. For telechelic associating polymers, the chemical structure is more well-defined. Using the idea of the Sticky Rouse model, only the lowest order Rouse mode was delayed. Thus, a Maxwellian relaxation behavior happens at the low frequency end of the shear modulus spectra. In other words, terminal relaxation time (τ_c) is the characteristic τ_{rearr} for unentangled telechelic associating polymers with only binary association. Xing et al. characterized τ_c for PPG-COOH and PPG-NH_2[27]. Fig. 1.8 indicates the shear modulus master curve as well as the shifting factor for PPG-COOH with DP of 6, 33 and 67. From the samples with DP of 33 and 67, there is significant delay of the terminal relaxation time which shows apparent Maxwellian behavior at the low frequency end.

1.6.3 Disagreement of relaxation times from rheology and dielectric spectroscopy

Sticky Rouse Model and Sticky Reptation Model have been tested many times and quantitatively reasonable results have been acquired. However, some problems arise on the quantitative side. In recent study, τ_{rearr} from rheological measurement appears several orders longer than τ_{dis} from dielectric measurement. Shabbir et al. reported this phenomenon in the study of P(MEA-co-UPyMA) associating polymer with hydrogen bonding[40]. In their research, the separation is ~40 for associating polymer containing 3% of functional groups and ~25 for associating polymers containing 8% of functional groups. Xing et al. also found the similar situation in unentangled PPG-COOH[27]. Terminal relaxation time estimated from rheology is several times larger than

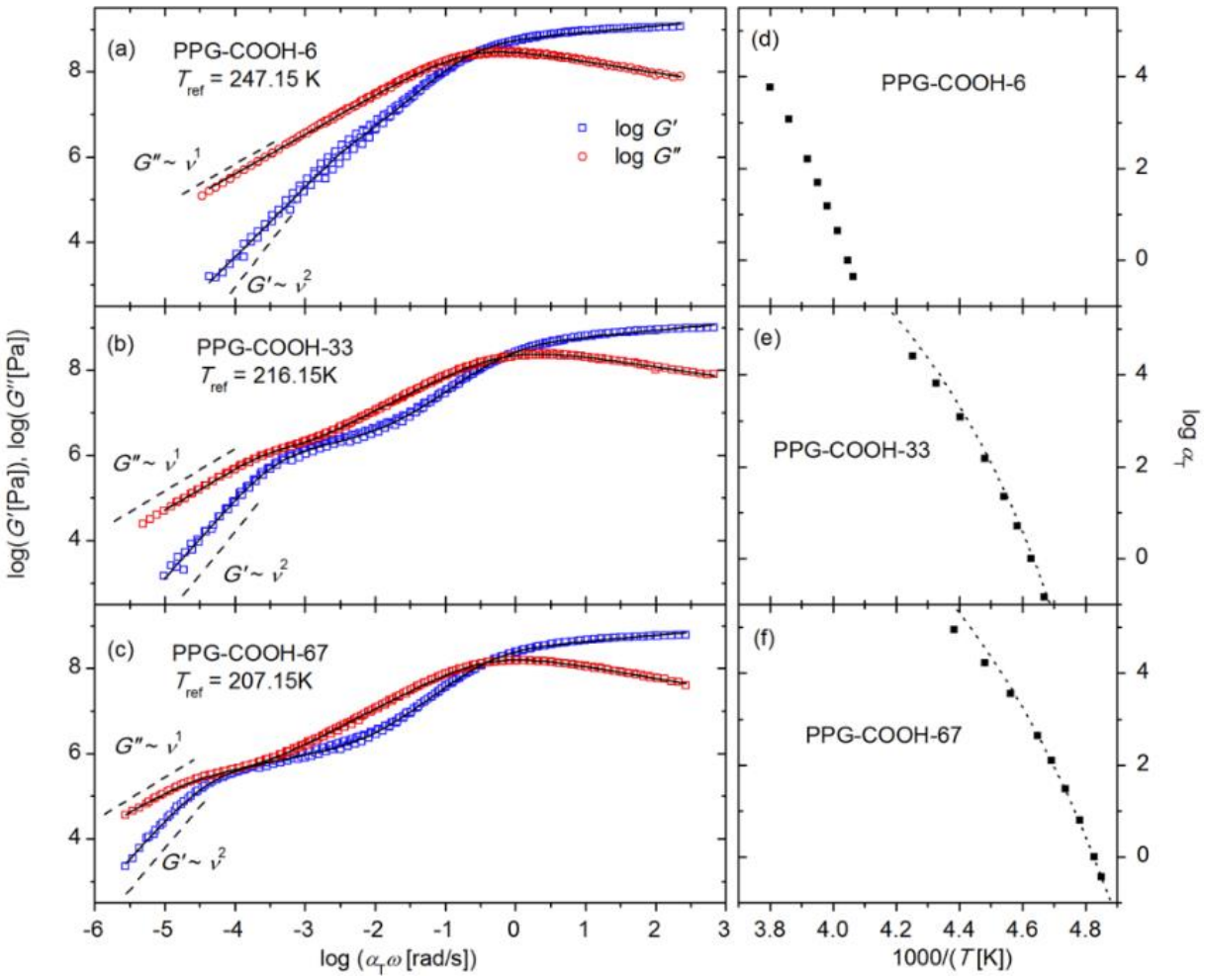

Figure 1.8 Shear modulus master curve for telechelic PPG-COOH with DP of (a) 6, (b) 33 and (c) 67, whose shifting factor is shown in (d), (e) and (f) respectively[27].

bond dissociation time estimated from BDS for PPG-COOH. In addition, with a longer PPG backbone, the separation of these two relaxation times is greater. To explain the disagreement of these two timescales, bond lifetime renormalization model was proposed.

1.6.4 Bond Lifetime renormalization model

The disagreement of τ_{rearr} from rheological measurement and τ_{dis} dielectric measurement can be explained by the bond lifetime renormalization model which was first used to study the autonomic self-healing of unentangled polymer networks[44]. In this model, one of the two end monomers of each polymer chain is fixed in space mimicking dangling chains attached to a polymer network, while the sticky monomer at the other end of each chain can form a pairwise reversible bond with the sticky end of another chain. Below is the review of this model:

For binary association, the state of associating groups (stickers) is expressed as

$$A + A \rightleftharpoons A_2 \qquad (1.21)$$

in which A and A_2 indicate the open stickers and closed sticky pairs, respectively. The total concentration of sticky groups can be $c_t = c_{eq}(A) + 2c_{eq}(A_2)$ in which $c_{eq}(A)$ and $c_{eq}(A_2)$ indicate the concentration of A and A_2 at the equilibrium state. At the equilibrium state, the concentration of the open and closed stickers is expressed as:

$$\frac{c_{eq}(A_2)}{c_{eq}^2(A)} = \frac{c_t - c_{open}^{eq}}{2(c_{open}^{eq})^2} = K_{eq} \qquad (1.22)$$

in which $K_{eq} = b^3 \exp\left(\frac{E_a}{k_B T}\right)$ is the equilibrium constant and b is the molecular size. The total

concentration of sticky groups c_t is one per volume of a dangling chain with N Kuhn segments. Each Kuhn segment has a molecular size of b.

$$c_t \approx \frac{1}{b^3 N} \tag{1.23}$$

$$c_{open}^{eq} = \frac{\sqrt{1+8K_{eq}c_t}-1}{4K_{eq}} \approx \left(\frac{c_t}{2K_{eq}}\right)^{\frac{1}{2}} \approx \frac{1}{\sqrt{2}b^3 N^{0.5}} \exp\left(-\frac{E_a}{2k_B T}\right) \tag{1.24}$$

Thus, if the transient bond is weak, i.e., $E_a < k_B T ln N$, then $K_{eq} < \frac{1}{c_t}$, meaning that most of the stickers are open and the associations between stickers are not important. However, if the transient bond has intermediate bond strength, i.e, $k_B T ln N < E_a < 2k_B T ln N$, there is one open sticker per pervaded volume (the volume that an open sticker can explore) of a dangling chain. The dynamics of bonding in this case is controlled by Rouse subdiffusive motion of stickers. The average time (τ_b) two stickers spend in a bonded state before a successful separation on molecular distance can be expressed as

$$\tau_b \approx \tau_0 \exp\left(\frac{E_a}{k_B T}\right) \tag{1.25}$$

in which τ_0 indicates the time scale for segmental motion.

After the dissociation of two stickers, each open sticker moves by Rouse subdiffusive motion. The mean-square displacement increases as the square root of time t.

$$\langle \Delta r^2(t) \rangle \approx b^2 \left(\frac{t}{\tau_0}\right)^{0.5} \tag{1.26}$$

Thus, the volume explored by the open sticker is expressed by

$$V_{expl}(t) \approx \langle \Delta r^2(t) \rangle^{\frac{3}{2}} \approx b^3 \left(\frac{t}{\tau_0}\right)^{\frac{3}{4}} \tag{1.27}$$

This subdiffusive process belongs to the class of compact space exploration due to multiple returns of the sticker to the same elementary volume. The number of returns to the same elementary volume can be estimated as the ratio of the total number of elementary steps n ($n = \frac{t}{\tau_0}$) to the number of elementary volumes $\frac{V_{expl}(t)}{b^3}$ "explored" during time t. In most cases, the excursion of the open stickers after bond breaking ends by two stickers encountering each other and forming a bond again. There are still a small number of open stickers whose excursion is relatively long. The long excursions dominate the average lifetime of stickers in the open and nonlinked state. This time τ_{open} is estimated as the time that the open sticker diffuses to a new open sticker whose distance is estimated as $r_{open} \approx (c_{open})^{-\frac{1}{3}}$. Thus, τ_{open} is estimated as

$$\tau_{open} \approx \tau_0 (\frac{r_{open}}{b})^4 \qquad (1.28)$$

Then, the renormalized bond lifetime τ_b^{renm} is defined as the average time it takes from the first formation of a bond between a particular pair of partners until the formation of a bond with a new partner. This time is the sum of the total time two stickers stay bonded during multiple returns and the time the sticker takes to diffuse to a new sticker. Thus, the renormalized lifetime can be expressed by:

$$\tau_b^{renm} \approx J(\tau_{open})\tau_b + \tau_{open} \qquad (1.29)$$

As mentioned before, the number of returns can be estimated by

$$J(t) \approx \frac{n}{\langle \Delta r^2(t) \rangle^{\frac{3}{2}}/b^3} \approx n^{\frac{1}{4}} \qquad (1.30)$$

The model can be illustrated in Fig. 1.9. τ_{rearr} from rheology indicates the structural

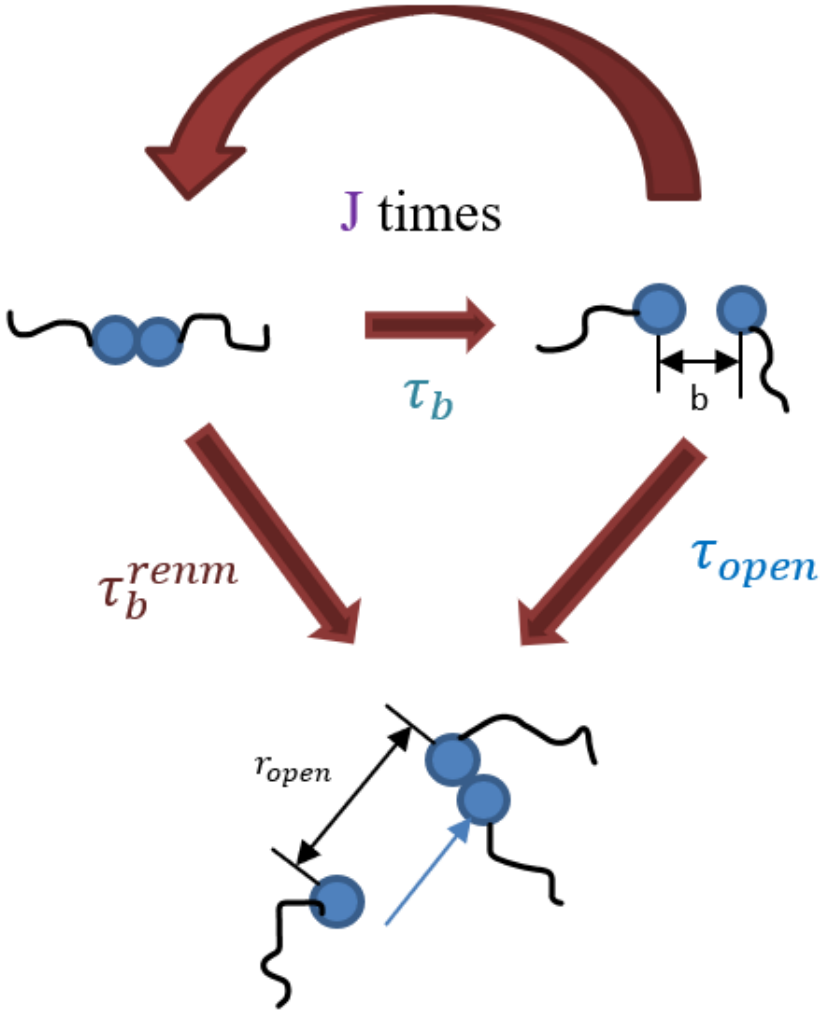

Figure 1.9 Cartoon about the Bond Lifetime Renormalization Model

rearrangement of the network formed by transient bond and τ_{dis} from dielectric measurement originates from the direct transient bond dissociation. This model can explain reasonably the separation between τ_{rearr} from rheology and τ_{dis} from dielectric measurement. The breaking of the binary association bond may not result in the topological rearrangement since the sticker can reassociate with its previous partner. Only when the sticker changes the partner the transient network can rearrange, and τ_{rearr} can be probed by rheological measurement.

In the case that the transient bonding is stronger, i.e., $E_a > 2k_BTlnN$, there will be less than one open sticker in the volume pervaded by a dangling chain. In such case, a more complex process, called hopping (partner exchange), is required for two open stickers to recombine. This mechanism predicts $\tau_{rearr} = \tau_{dis}$.

Several groups have used this model to explain the combined dielectric and rheology data. Gold et al. applied this model to the study of associating polymers with polyisoprene backbone and urazole functional groups[45]. In the study, they also found separation between τ_{rearr} from rheological measurement (denoted as τ_{rheo}) and τ_{dis} from dielectric measurement (denoted as τ_{α}^{*}) (Fig. 1.10). In addition, they did some modification on the original model by considering the open sticker diffusion process to be

$$\langle \Delta r^2(t) \rangle \approx b^2 (\frac{t}{\tau_0})^x \qquad (1.31)$$

in which x is an adjustable exponent, with x = 0.5 for Rouse dynamic and 0.25 for reptation dynamics. Finally, they achieved x value to be ~0.365, indicating an open sticker diffusion behavior between Rouse dynamics and Reptation dynamics. This research shows good qualitative agreement of the model with experimental result. However, there has been no

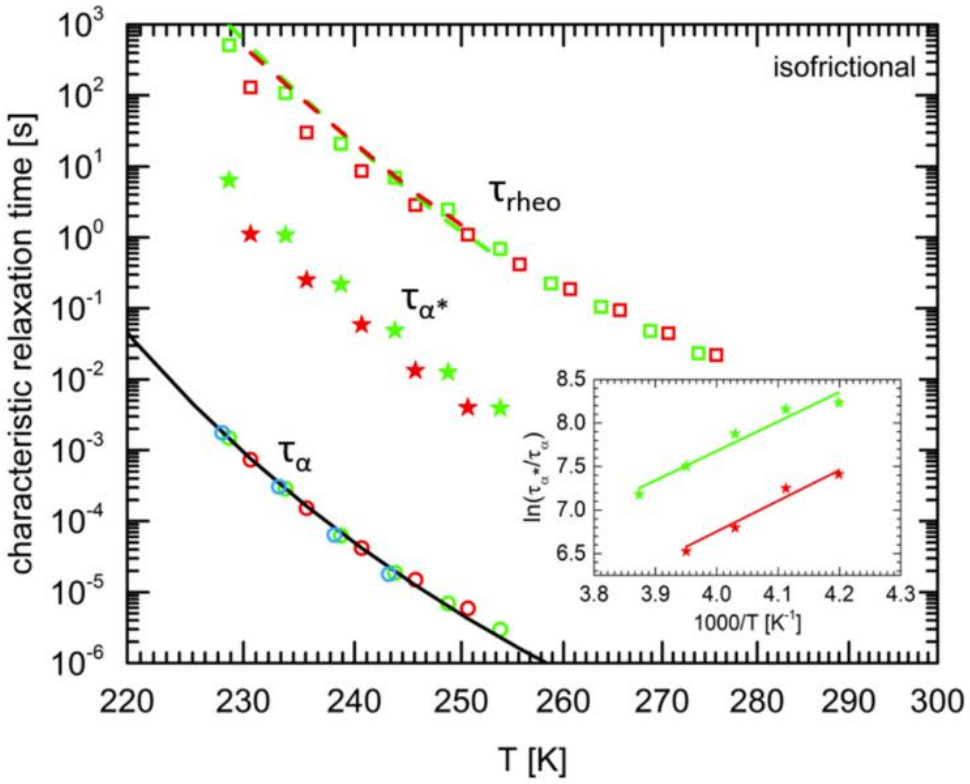

Figure 1.10 Separation between characteristic relaxation time from dielectric measurement and rheological measurement in Gold et al.[45]

thorough experimental test of this model yet.

1.7 Associating polymers with microphase separation

Binary association is the simplest model of association. However, if the polymeric backbone and the functional groups of associating polymers are immiscible, then microphase separation happens[46]. In such case, functional groups with binary association can aggregate together, resulting in the formation of clusters separated from polymeric backbone[47]. The microphase separation can happen in associating polymer with different type of transient bonds, including hydrogen bonding[48], ionic interaction[17, 49], and even in vitrimers[50].

1.8 Microphase separation in associating polymers based on hydrogen bonding

Functional groups with hydrogen bonding are usually polar. When the polymeric backbone is non-polar, the functional groups are prone to form microphase separation due to immiscibility. For example, Goldansaz et al. studied the diblock copolymers based on poly(n-butyl acrylate) and (PnBA) and poly(hydroxyethyl acrylate) segments[28]. In addition, Yan et al. found that the microphase separation happens on mono-and bi-functional associating polymers with poly(isobutylene) (PIB) backbone and functional groups such as thymine, diaminotriazole, and barbituric acid, that form hydrogen bonding with each other (Fig. 1.11a)[51, 52]. Xing et al. proposed a molecular picture of the microphase separated PDMS-NHCO-COOH associating polymers with not only binary association, but also chain ends aggregate together to form clusters (Fig. 1.11b). In addition, it is the PDMS backbone that connects the clusters, forming a

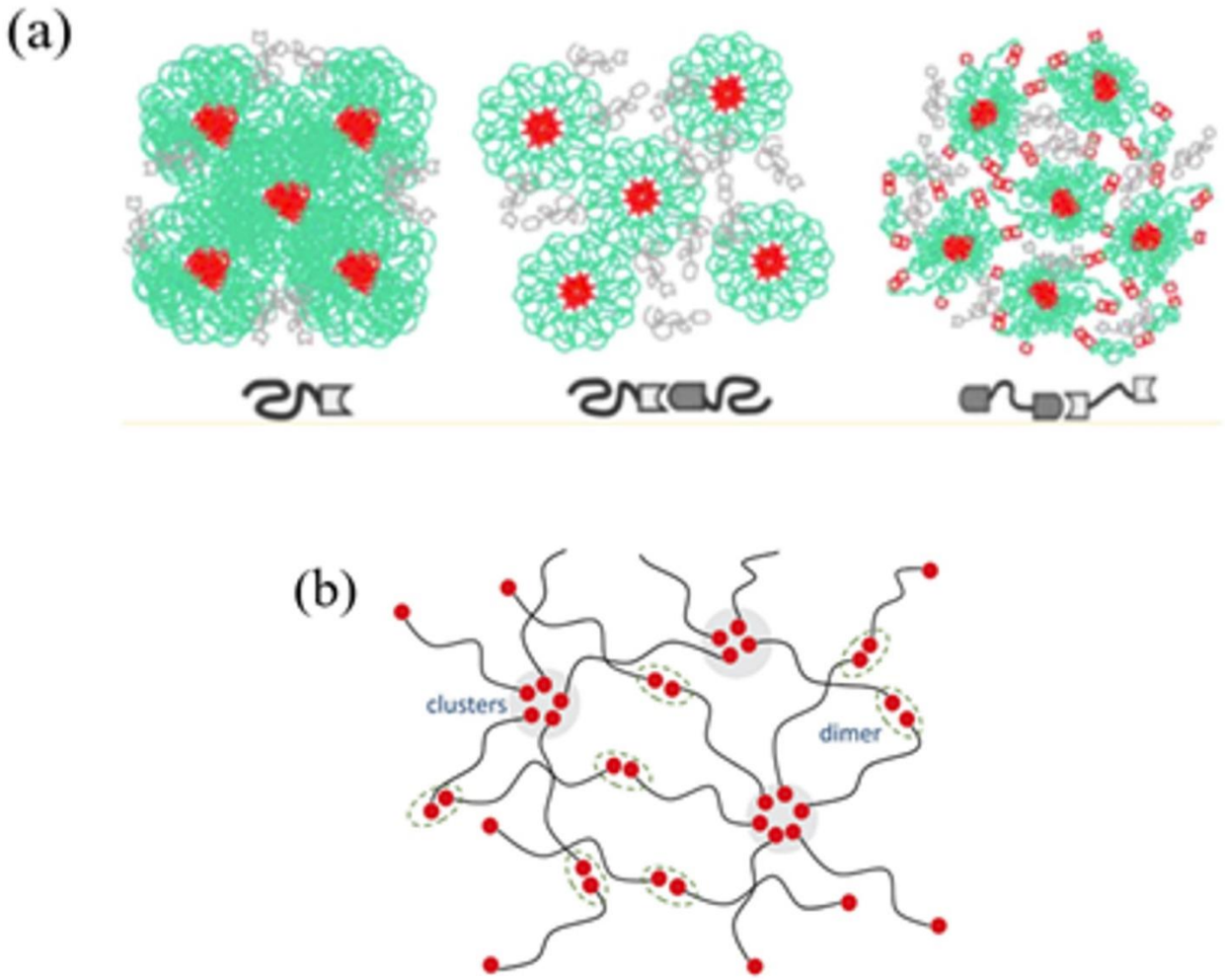

Figure 1.11 (a) Microphase separation in associating polymers with hydrogen bonding from Yan et al.[51] (b) Molecular picture of microphase separated PDMS-NHCO-COOH proposed by Xing et al.[26]

physical crosslinking network.

1.9 Ways of characterizing microphase separation in associating polymers

To determine whether associating polymers form microphase separation, the thermal analysis and X-ray scattering are two powerful tools.

1.9.1 Thermal analysis

One of the most widely used thermal analysis methods to characterize microphase separation in associating polymer is differential scanning calorimetry (DSC) through which the thermal transition of associating polymers can be detected[53, 54]. If microphase separation happens in associating polymers, usually it shows two glass transition temperatures, while those without microphase separation show only one glass transition temperature. Xing et al. found 2 glass transition temperatures in telechelic associating polymers with PDMS backbone and NHCO-COOH chain ends[26]. This indicates the microphase separation in these polymers.

1.9.2 Scattering method

In comparison to thermal analysis methods, scattering methods provides more direct evidence of microphase separation. Scattering results from the interaction of incident radiation and structures within materials[55]. Thus, scattering techniques are very powerful to probe inhomogeneous structures, such as microphase separation in associating polymers[56].

X-ray scattering method is widely used to probe the structure of microphase separation in associating polymers, no matter whether the aggregate is crystalline or amorphous. The aggregation domain usually results in a characteristic peak in the X-ray scattering measurement. Herbst et al. studied the PIB functionalized with 2,6-diaminotriazine and Thymine groups using X-ray scattering, in which they witnessed ordered scattering peaks showing that aggregates form BCC lattice[57]. Also, X-ray scattering was used to study the UPY-based associating polymers which unraveled the nanofiber structures within it[58].

1.10 The mechanical properties influenced by microphase separation

If microphase separation happens in associating polymers, mechanical properties change dramatically. Due to the existence of microphase separated structure, the rate of network rearrangement is much slower than that from binary association. Usually, microphase separation results in the gel-like behavior in associating polymers. Xing et al.[26] found that in microphase separated associating polymers, the shear modulus spectra show a prominent rubbery plateau regime before the final terminal relaxation (Fig. 1.12a). This prominent rubbery plateau does not show up in PDMS-NH_2 with only binary association. Hawke et al. describes the linear rheological properties of associating PnBA copolymer with microphase separation[59] (Fig. 1.12b). They attributed the featured prolonged rubbery plateau to the trapped strands between clusters. Later, Ahmadi et al. found a way to deconvolute the binary association and cluster dissociation on the rheological properties of associating polymer[60]. Not only the rubbery plateau becomes more prominent, the modulus level in associating polymers with microphase separation also increases a lot. Wu et al. found significantly elevated rubbery plateau modulus in the ionomers

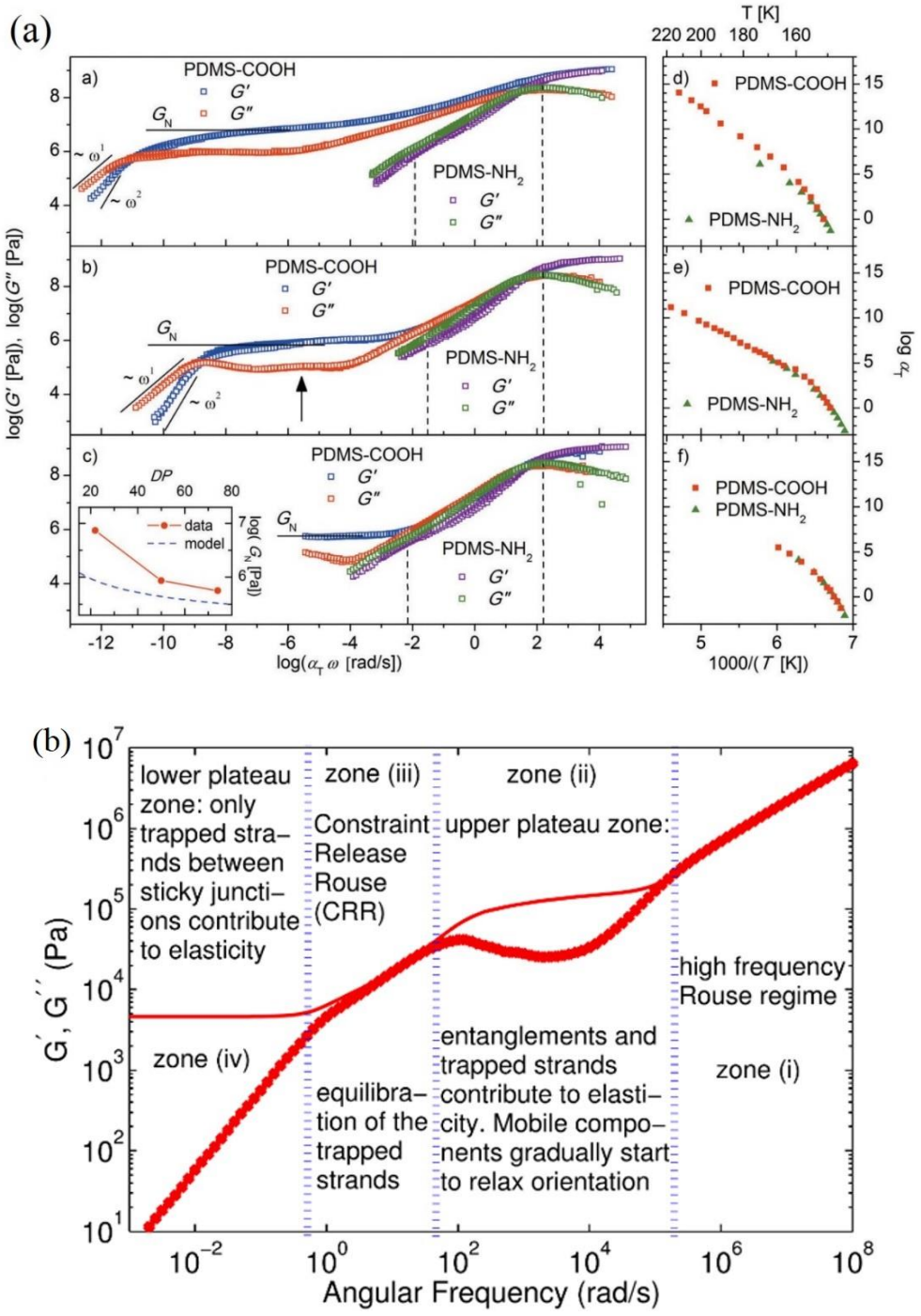

Figure 1.12 (a) Rheological spectra of telechelic PDMS-NHCO-COOH and PDMS-NH_2, with (upper) DP of 22 and shifting factor, (middle) DP of 50 and shifting factor, (lower) DP of 74 and shifting factor. The inset indicates how plateau modulus level changes with DP with both experimental data (red) and prediction from rubber elasticity theory (blue)[26]. (b) A typical viscoelastic behavior of associating polymer with microphase separation[59]

with higher volume fraction of clusters[61]. Xing et al. also found that rubbery plateau modulus demonstrates abnormal behavior[26]. When DP is 50 or 74, the plateau modulus for PDMS-NHCO-COOH is ~ 1 MPa. This is a typical value for a crosslinked polymer network following the rubber elasticity theory. However, when DP is 22, the plateau modulus appears at G'~10 MPa. This is around 1 order of magnitude higher than predicted by the rubber elasticity theory, indicating strong mechanical reinforcements. The microphase separation also affects the shift factor of associating polymers, leading to a failure of time-temperature superposition. For conventional polymer, the shift factor shows Williams-Landel-Ferry (WLF) behavior[62]. This also applies for the associating polymer with only binary association. However, for associating polymers with microphase separation, the temperature dependence of the shift factor becomes complicated. Xing et al. found that at low temperature close to T_g, the shift factor has WLF-like behavior. At high temperature, the shift factor becomes Arrhenius-like[26]. The reason is that at low temperature, shift factor follows segmental dynamics whereas at high temperature, the cluster dynamics dominates the shift factor. Similar behavior was also found in Stadler et al.[63] and Wu et al.[61].

1.11 Dielectric behavior influenced by microphase separation

Not only mechanical property is significantly altered by the microphase separation, but also dielectric property gets significantly modified. When microphase separation happens in associating polymers, dielectric measurement results also show some interesting behaviors. Goldansaz et al. studied the dielectric behavior of partially hydrolyzed poly(n-butyl acrylate). They discovered three characteristic relaxation processes correlated with transient bond

dissociation, which is originated internal structural relaxation of the microphase separated clusters besides binary association (Fig. 1.13a)[28]. Xing et al. studied dielectric behavior of microphase separated PDMS-NHCO-COOH and found a third process which originates from microphase separation. This third process is attributed to the sticker motion inside the clusters (α_2 process) (Fig. 1.13b)[26]. The weight fraction of the functional groups participating in microphase separation was also estimated based on the dielectric strength of this process, through which they found that the majority of chain ends are aggregated into microphase separated clusters. In addition, the broadening of the segmental relaxation process is also observed. With microphase separation, the dielectric spectra of the segmental relaxation process broaden, especially on the low frequency side (Fig. 1.13c)[26]. In addition, with shorter PDMS backbone, the broadening becomes more severe. The broadening of the spectra indicates strong dynamic heterogeneity of the segmental motion.

1.12 Dynamic heterogeneity in associating polymer with microphase separation

When microphase separation happens in associating polymers, motion of the polymer backbone segments is restricted, especially for the polymeric segments in the vicinity of the clusters formed by the microphase separated functional groups. The restricted segments form a layer around the clusters. Since this layer is between the clusters and polymer phase, it is called interfacial layer throughout this research. The idea of this interfacial layer in associating polymer was first proposed by Eisenberg et al. in their Multiplet-Cluster Model for ionomers. They assume that there is an interfacial layer around the multiplets formed by ionic groups, as is shown in Fig. 1.14a[17]. The layer has a thickness of the order of a persistence length of the

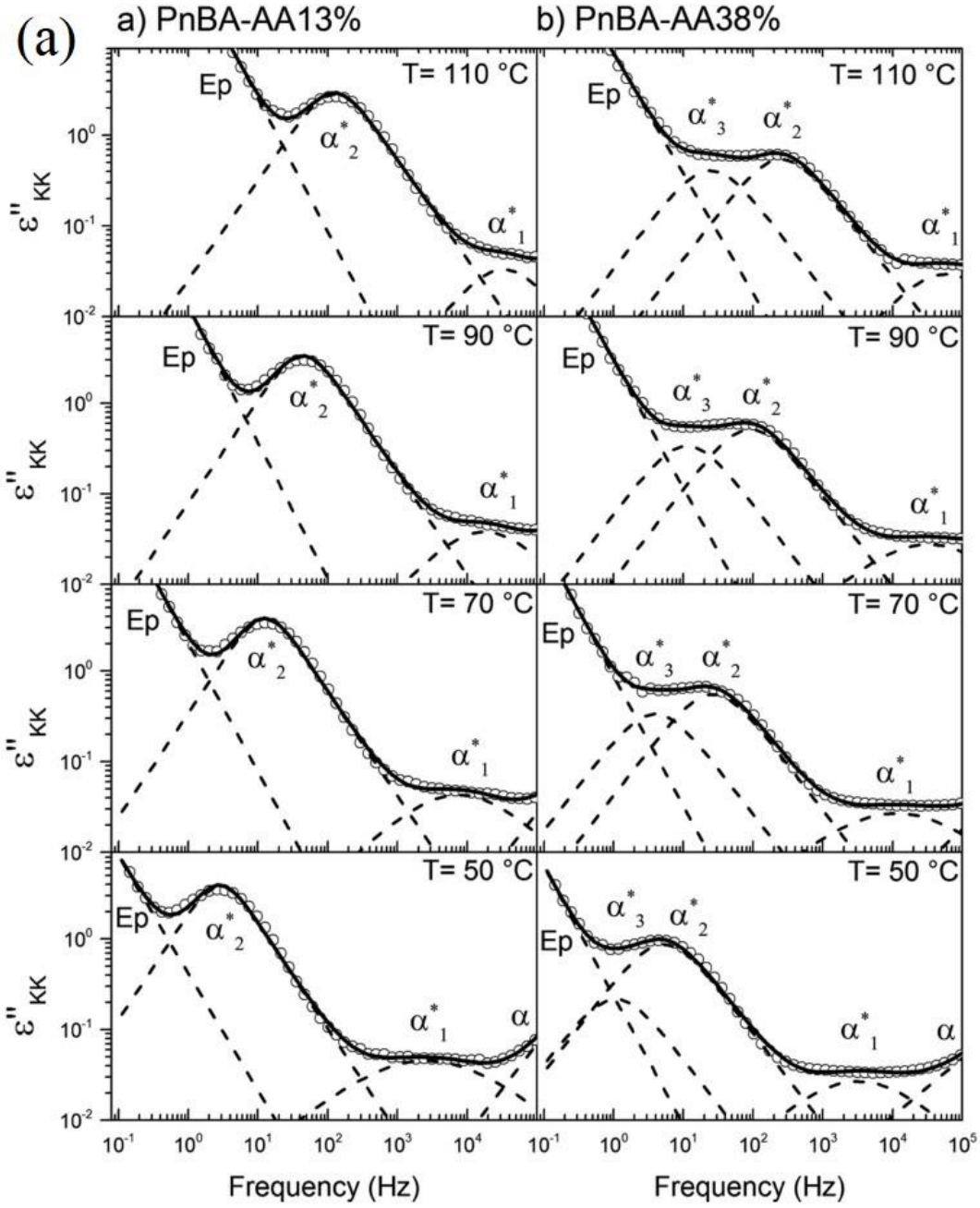

Figure 1.13 Dielectric behavior in (a) partially hydrolyzed poly(n-butyl acrylate)[28] (b) PDMS-COOH associating polymer[26] (c) ε" spectra of α relaxation normalized to its maximum for regular PDMS-H (DP=22) and telechelic PDMS-NHCO-COOH with DP of 22 and 50[26]

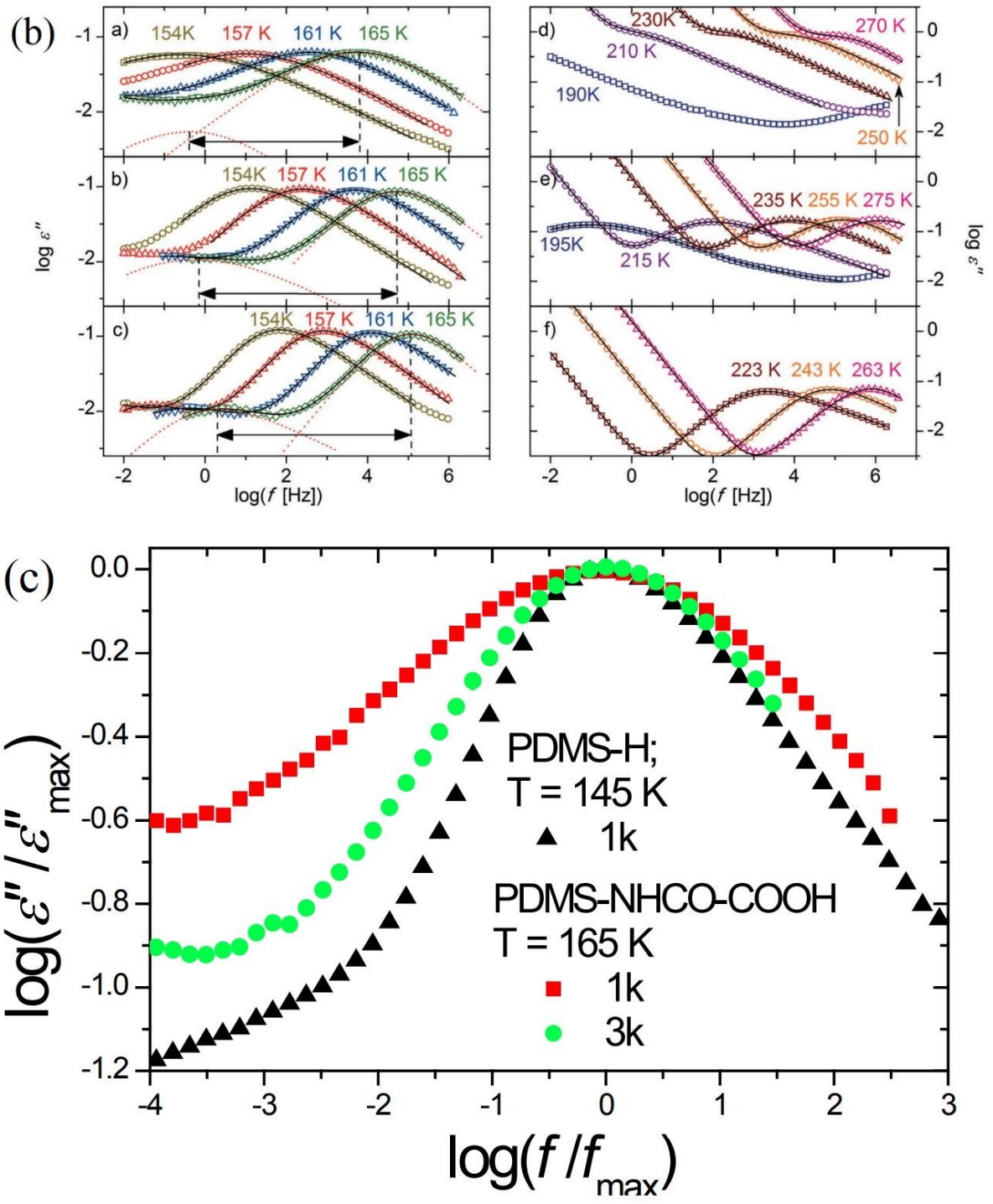

Figure 1.13 Continued

polymeric backbone. Nyrkova et al. did some further theoretical study on the ionomer with microphase separation and found that polymeric chains are grafted on the clusters which is a Super-strong segregation microdomain[64]. Thus, the polymeric segments in the vicinity of the clusters get stretched, implying the restriction on their mobility. This is analogous to the situation in polymer grafted nanoparticle, a kind of polymer nanocomposite sample in which the similar interfacial layer has been found. Moreover, Vanhoorne et al. found direct experimental evidence from NMR measurement that there is a local restriction in segmental chain mobility in the vicinity of clusters formed in ionomers[65]. Besides ionomers, the interfacial layer was also found in associating polymers with hydrogen bonding. Goldansaz et al. studied the dynamics of partially hydrolyzed poly(n-butyl acrylate) through rheology and dielectric measurement and proposed a general microstructure (Fig. 1.14b) that there is an interfacial layer around the clusters formed by poly(acrylic acid) functional groups based on experimental observation and wealth of literature[28]. Thus, the idea of interfacial layer in microphase separated associating polymers has been well established. However, it has never been quantitatively studied. For example, the interfacial layer thickness has never been characterized yet. In addition, its effect on the mechanical properties of associating polymers have never been analyzed. On the other hand, the polymer nanocomposite, which is analogous to the microphase separated associating polymer, has been well studied and quite a few models have been utilized to quantitatively characterize the interfacial layer formed by the restricted polymer segments and quantitatively describe the effect in the overall properties, i.e, mechanical reinforcements.

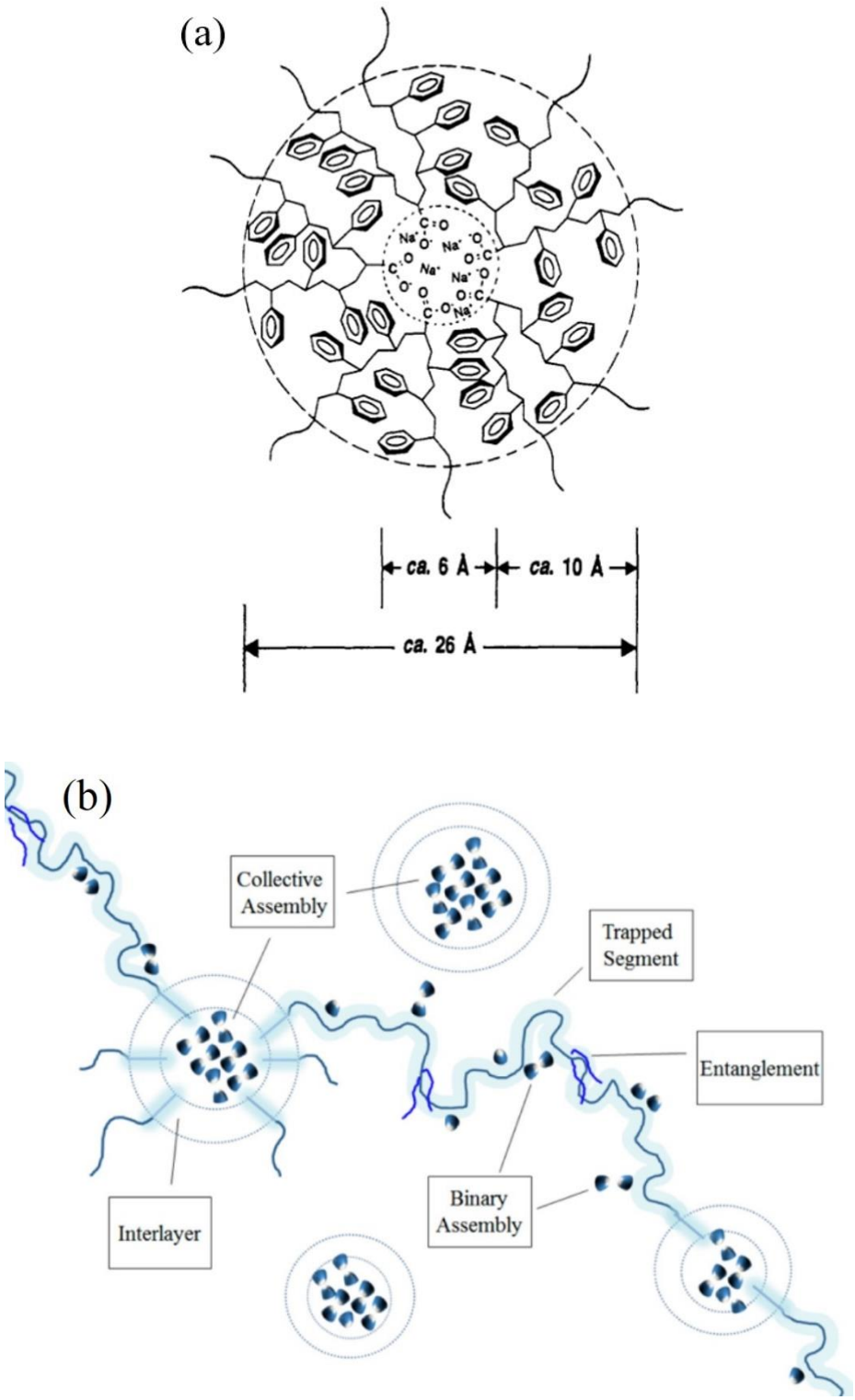

Figure 1.14 (a) Interfacial layer formed in ionomer[17]. (b) Interfacial layer formed in partially

1.13 Models for studying the polymer nanocomposite sample

1.13.1 Dielectric studies of the interfacial layer in polymer nanocomposites

Dielectric spectroscopy is an effective tool to provide an approach to estimate the thickness of the interfacial layer in polymer nanocomposite samples. Several approaches to fit the dielectric spectra had been applied to decipher the contribution from an interfacial layer in such heterogeneous systems[66-71]. Previously, a simple two-HN functions fit (an additional HN function to represent the interfacial layer process) and a more convoluted dielectric interfacial layer model have been used to study the interfacial layer properties in polymer nanocomposite samples[66]. The interfacial layer model is the most accurate method to study the interfacial layer using dielectric spectroscopy since it considers the non-additive feature of the dielectric response in heterogeneous systems[70]. Although the two-HN functions approach is less accurate[66], it is much simpler and has been utilized in quite a few studies[67, 68, 71] providing reasonable results. Through the results, the effects of an interfacial layer on polymer nanocomposites have been unraveled as well. The segmental relaxation time in the interfacial layer was found to be about one order of magnitude slower than that in the bulk polymer also in polymer nanocomposites[66, 72] and polymer grafted nanoparticle samples[73]. In addition, in the case of nanocomposites, the slowdown of segmental dynamics in the interfacial layer depends on the particular polymer-nanoparticles interactions[74, 75]. Not only the timescale, but also the dielectric strength is also affected by the interfacial layer. It is now well documented that the dielectric strength of the segmental relaxation in the interfacial layer of thin polymer films and polymer nanocomposite samples is strongly suppressed[66, 73, 76]. It was ascribed to a strong restriction on segmental reorientation in the crowded interfacial layer[73]. Thus, the dielectric strength of the interfacial

region does not reflect the true volume fraction of the polymer interfacial layer[73], and the remaining dielectric strength from the bulk polymer should be used to estimate the volume fraction of the bulk-like polymer, $\Delta\varepsilon_{bulk}$ [66, 73]. Then the interfacial volume fraction can be estimated using $\varphi_{int} = 1 - \varphi_{NP} - \varphi_{bulk}$, where φ_{NP} is the volume fraction of nanoparticles in the polymer nanocomposite samples.

1.13.2 Mechanical Two-Phase Model (TPM)

By taking the analogy of our microphase separated associating polymer to polymer grafted nanoparticles, we expect that the mechanical reinforcement in microphase separated associating polymer can be explained through the mechanical model for the polymer nanocomposite materials. Mechanical reinforcement happening in polymer nanocomposite materials have been discussed for many years[77-79]. One of the models is the mechanical Two-Phase Model (TPM) which considers that the mechanical reinforcement is only originated from the hard phase (i.e., nanoparticles) (Fig. 1.15a). In TPM, assuming no-slip boundary conditions between the matrix and nanoparticles, the bulk modulus of the composite, K_c, can be calculated as[77, 78, 80]:

$$K_c = \frac{K_f\varphi_f + K_m\varphi_m S}{\varphi_f + \varphi_m S} \quad (1.32)$$

With

$$S = \frac{3K_f + 4G_m}{3K_m + 4G_m} \quad (1.33)$$

and

$$\varphi_m + \varphi_f = 1 \quad (1.34)$$

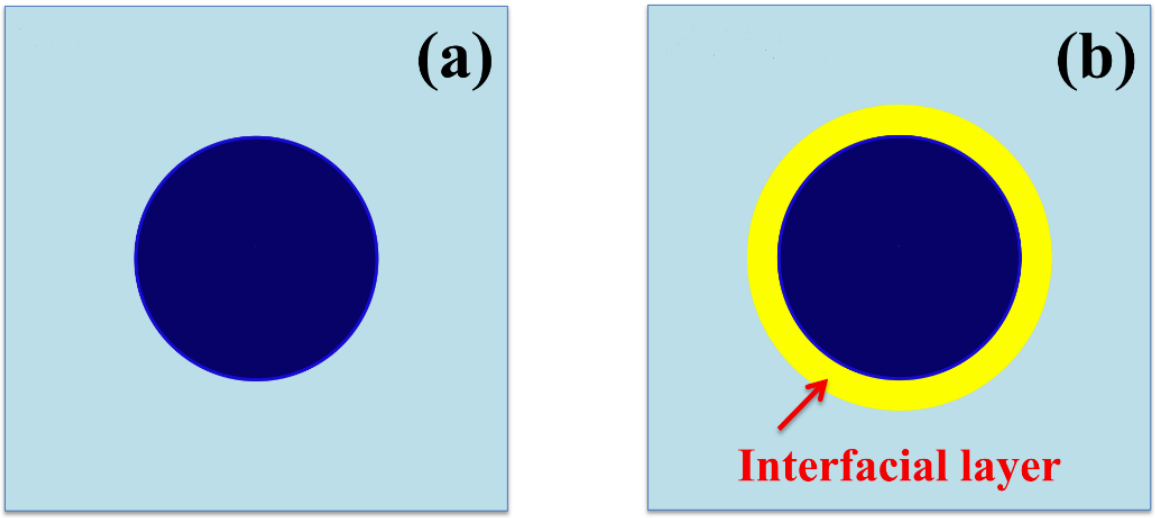

Figure 1.15 A sketch of the (a) mechanical Two-Phase Model (TPM) and (b) mechanical Interfacial Layer Model (ILM). The dark blue core represents nanoparticles, and the cyan background represents the polymer matrix. The yellow shell surrounding nanoparticles represents the interfacial polymer layer.

where K_f and K_m are the bulk modulus of the nanoparticles and the neat matrix; G_m is the shear modulus of the neat matrix; φ_f and φ_m are the volume fraction of the nanoparticle and the matrix. The overall shear modulus, G_c, can be calculated by solving an 8×8 determinantal equation, which can be simplified as $AX^2 + BX + C = 0$ with $X = \frac{G_c}{G_m} - 1$ to be the positive root of the equation[77, 79]. The index A, B and C are functions of $\frac{G_m}{G_f}$, φ_f , σ_f and σ_m, and can be found in Ref.[79] . Here, G_f is the shear modulus of the nanoparticle, σ_f and σ_m are the Poisson's ratio of nanoparticle and neat matrix respectively.

1.13.3 Mechanical Interfacial Layer Model (ILM)

Another mechanical model considering the mechanical reinforcement in polymer nanocomposites is the mechanical interfacial layer model (ILM). The mechanical ILM considers not only the contribution from the nanoparticles, but also the contribution from the interfacial layer around the nanoparticles, and provides a relationship between the interfacial layer thickness, modulus and the overall macroscopic mechanical strength of the composite material (Fig. 1.15b). It assumes a no-slip boundary condition between both interfaces of the nanoparticle-interfacial layer and the interfacial layer-bulk layer[81]. K_c can be analytically calculated as[81]

$$K_c = \frac{K_f\varphi_f + K_l\varphi_l R + K_m\varphi_m S}{\varphi_f + \varphi_l R + \varphi_m S} \qquad (1.35)$$

With

$$R = \frac{3K_f+4G_l}{3K_m+4G_l} \quad (1.36)$$

$$S = \frac{(3K_f+4G_l)(3K_f+4G_m)-12d(K_l-K_f)(G_l-G_m)}{(3K_m+4G_m)(3K_l+4G_l)} \quad (1.37)$$

$$d = \frac{\varphi_f}{\varphi_f+\varphi_l} \quad (1.38)$$

$$\varphi_m + \varphi_l + \varphi_f = 1 \quad (1.39)$$

where K_l , G_l and φ_l are the bulk modulus, shear modulus and the volume fraction of the interfacial layer. The overall shear modulus of the sample G_C is calculated as:

$$40(G_c/G_m)^2|X| + \left(\frac{G_c}{G_m}\right)\{2|Y| + 8|Z|\} - 5|T| = 0 \quad (1.40)$$

where |X|, |Y|, |Z| and |T| are the determinant of a 10×10 matrices which depend on the shear moduli, Poisson's ratio, and volume fractions of filler (i.e., end group clusters), interfacial layer and bulk-like matrix, respectively. The full expression of each matrix can be found in Maurer et al.[81]

1.13.4 Mechanical percolation model

The mechanical ILM assumes the independent nanoparticle with interfacial layer[81]. In the case that interfacial layer gets overlapped, the mechanical ILM becomes questionable, whereas the mechanical percolation model is able to explain the mechanical reinforcement. The idea of percolation is used to describe the disconnected clusters merging into significantly larger and spanning phase[82, 83]. The percolated network has been discovered and extensively studied in polymer nanocomposite samples[84-86]. When the volume fraction of the nanoparticles reaches a

threshold, at which the interfacial layer gets overlapped, the percolation happens[87-89]. In such a case, the interconnection of clusters is reached so that the rigid phase becomes infinitely large in the system and a percolated network form[90, 91]. The percolated network changes the physical properties of polymer nanocomposite samples dramatically, increasing the mechanical modulus[92-94]. To illustrate how the percolated network affects the mechanical modulus, the mechanical percolation model is applied to illustrate the idea[95]. It is a phenomenological series/parallel model that was derived by Takayanagi et al.[96] and extended by Ouali et al.[97] with the idea of percolation, as is shown. The overall shear modulus can be expressed as

$$G_c = \frac{(1-2\psi+\psi X_r)G_s G_r+(1-X_r)\psi G_r^2}{(1-X_r)G_r+(X_r-\psi)G_s} \quad (1.41)$$

in which G_r is the shear modulus of the rigid phase. G_s is the shear modulus of the soft phase. X_r is the volume fraction of the rigid phase. ψ is the volume fraction of the "infinite" rigid phase formed by connected clusters which actively propagates the forces from one cluster to another. ψ can be estimated by the following equation:

$$\psi = \begin{cases} 0, & X_r < X_c \\ X_r\left(\frac{X_r-X_c}{1-X_c}\right)^b, & X_r \geq X_c \end{cases} \quad (1.42)$$

in which X_c is the volume fraction of the rigid phase at the percolation threshold. b is the percolation exponential number evaluating the rapidity that the rigid phase forms. The mechanical percolation model has successfully explained the mechanical reinforcement of the polymer nanocomposite sample in the case that the interfacial layer gets overlapped[84, 91].

1.14 Network rearrangement in associating polymers with microphase separation

Besides the mechanical reinforcement, how network rearrangement happens in microphase separated associating polymers is another puzzle. In microphase separated associating polymers, the mechanism of network reorganization becomes more complicated. Although the terminal relaxation, namely the macroscopic flow, has been found in microphase separated associating polymers, the understanding of its mechanism is still in rudimental stage.

The understanding of the network rearrangement started from the micelle model describing the dynamics in solutions of associating polymers[98, 99] in which the network rearrangement (terminal flow) is considered to be only possible upon debridging of all chains emanating from the cluster, followed by hopping of the cluster to a new position. In contrast, the transient network model[100, 101] claims that it is the single sticker breaking and hopping from cluster to cluster that results in the terminal flow (Fig. 1.16a). Through the combination of rheological study and NMR study, Mordvinkin et al. validated that the transient network model can be used to explain the network rearrangement[102]. However, the mechanism of how a single sticker hops from cluster to cluster is not well formulated. Through computer simulation, a more detailed mechanism was proposed by Amin et al.[103] In that model, network arrangement happens through partner exchange. Specifically, when two clusters are in proximity, they can merge into a large cluster (Fig. 1.16b). Since the large cluster is entropically unfavorable and short-lived, it will break apart into 2 new clusters which contain different member stickers. However, this mechanism has not been tested experimentally yet. And this mechanism was challenged by Mordvinkin et al. who claimed that the distance between clusters in their studied system is well-defined, so that the possibility of the cluster merging is small[104]. Moreover, Xing et al. found that τ_C from rheological measurement

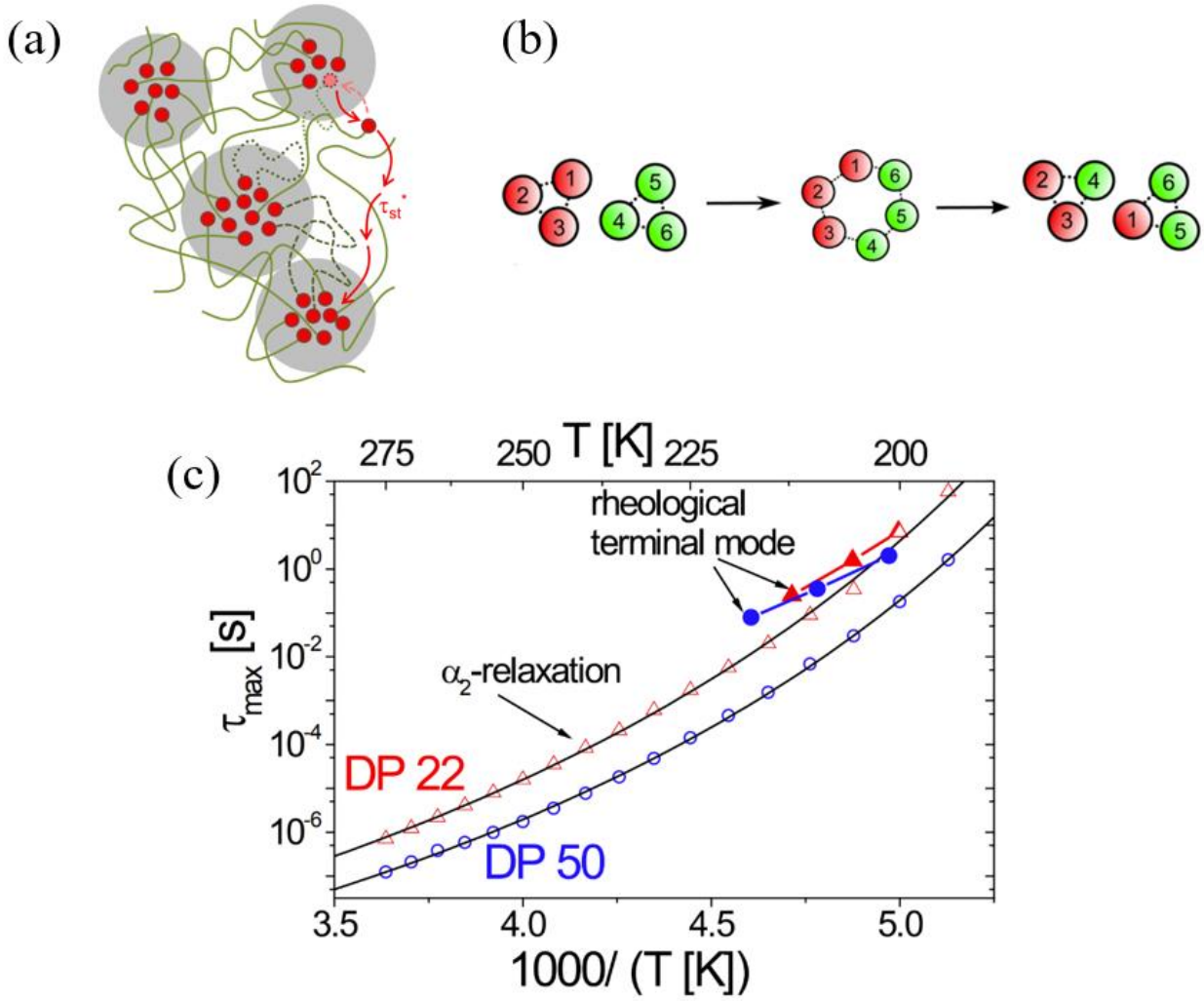

Figure 1.16 (a) The sketch of the network structure includes a single-chain relaxation process predicated by transient network model[102]. (b) Sketch of a partner exchange mechanism through cluster merging−dissociation process[103]. (c) Activation plot of α_2 relaxation process and terminal relaxation time for telechelic PDMS-NHCO-COOH with DP of 22 and 50[26].

(indicating network rearrangement) is significantly longer than τ_{α_2} which indicates the characteristic structural relaxation time in chain end aggregates for PDMS-NHCO-COOH with DP of 50 through dielectric measurement (Fig. 1.16c)[26]. Mordvinkin et al. found similar results[104]. This separation prevents an accurate quantitative description of dynamics and viscoelastic properties of associating polymers. The reason of this separation is still unknown. Thus, more research is necessary to determine the detailed mechanism of chain rearrangement between clusters in microphase separated associating polymers.

1.15 Research objectives

The main goal of this research is to provide a detailed and quantitative understanding of the dynamics and viscoelastic properties of associating polymers. In addition, we formulated a detailed plan for each objective:

Objective 1: (Experimental test of the bond lifetime renormalization model in associating polymers with only binary association)

I. To acquire characteristic timescales (i.e., τ_α, τ_α^* and τ_C) at different temperatures through dielectric and rheological measurement for all associating polymers.
II. To estimate the transient bond activation energy by considering the contribution from polymer segmental relaxation.
III. To test experimentally the bond lifetime renormalization model using associating polymer with different polymer backbone, different chain length and different functional

groups. The transient bond here should have intermediate bond strength (i.e., $k_B T ln N < E_a < 2k_B T ln N$).

IV. To test experimentally associating polymers with stronger transient bond interactions (i.e., $E_a \gg 2k_B T ln N$).

Objective 2: (To characterize microphase separation of functional groups in associating polymers and to understand why microphase separation results in mechanical reinforcement)

I. To verify microphase separation of telechelic associating polymer using X-ray scattering. Provide estimates of cluster-to-cluster distance, the radius of clusters, the number of functional groups in each cluster, etc.

II. To estimate the interfacial layer volume fraction and thickness in microphase separated associating polymer using dielectric spectroscopy.

III. To unravel the critical role of the interfacial layer in mechanical reinforcement in microphase separated associating polymers.

Objective 3: (To develop better understanding of how microphase separation controls dynamics and viscoelastic properties of associating polymers)

I. Unravel the mechanism of chain rearrangements and terminal relaxation in the microphase separated associating polymers.

II. Provide qualitative model description of the shear modulus spectra in microphase separated associating polymers.

CHAPTER 2 EXPERIMENTAL TECHNIQUES

Throughout the dissertation research, differential scanning calorimetry (DSC), rheology, dielectric spectroscopy and X-ray scattering were used to characterize the associating polymers. Differential scanning calorimetry (DSC) was used to study the glass transition temperatures of associating polymers. Rheology was used to study the viscoelastic properties of associating polymers. Dielectric spectroscopy was used to study the microscopic dynamics of associating polymers. X-ray scattering was used to study the structure of the microphase separated associating polymers.

2.1 Differential scanning calorimetry (DSC)

2.1.1 The principle of DSC

DSC is a thermoanalytical technique in which the difference in the amount of heat required to increase the temperature of a sample and a reference is measured as a function of temperature. During the DSC measurement, the sample and the reference are kept at the same temperature all the time and then the thermal energy required to maintain the zero-temperature difference is measured. During a thermal event in the sample, it transfers heat flow to or from the sample pan to maintain the sample with the same temperature as it is in the reference pan, which can be monitored by a computer (Fig. 2.1).

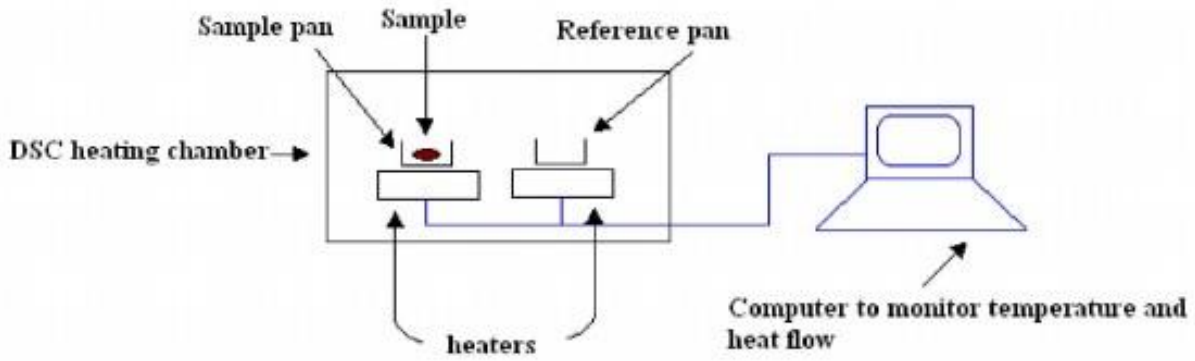

Figure 2.1 Scheme describing DSC

2.1.2 The DSC instruments

The DSC instrument we used is DSC Q2000 and DSC 2500 from TA Instruments. Both are heat flux DSC. The heat flux DSC consists of a single furnace in which the sample and reference are heated or cooled together under a controlled temperature program. The sample encapsulated in an aluminum pan and a vacant reference pan are placed on thermoelectric disks surrounded by the furnace. As the furnace temperature is changed, heat is transferred to the sample and reference. The differential heat flow to the sample and reference is measured by area thermocouples using the thermal equivalent of Ohm's law. The heat flow of the sample is defined by the equation below:

$$q = C_p \frac{dT}{dt} + f(T, t) \qquad (2.1)$$

in which C_p is the sample specific heat capacity, $\frac{dT}{dt}$ is the heating/cooling rate. $f(T, t)$ is a kinetic response at a specific temperature or time. Any thermal transitions, i.e., crystallization, melting, glass transition, can show up as sharp change in C_p. Figure 2.2a indicated how these thermal transition results in the final DSC curves. During the glass transition process, there is a change of the specific heat capacity on the polymeric material, showing as a step. Then T_g can be characterized by midpoint temperature (Fig. 2.2b).

2.2 Rheology

We used the small amplitude oscillatory shear (SAOS) in rheological measurement to study the viscoelasticity of the associating polymers. SAOS is often utilized to investigate the viscoelastic property of the polymeric material in the linear region.

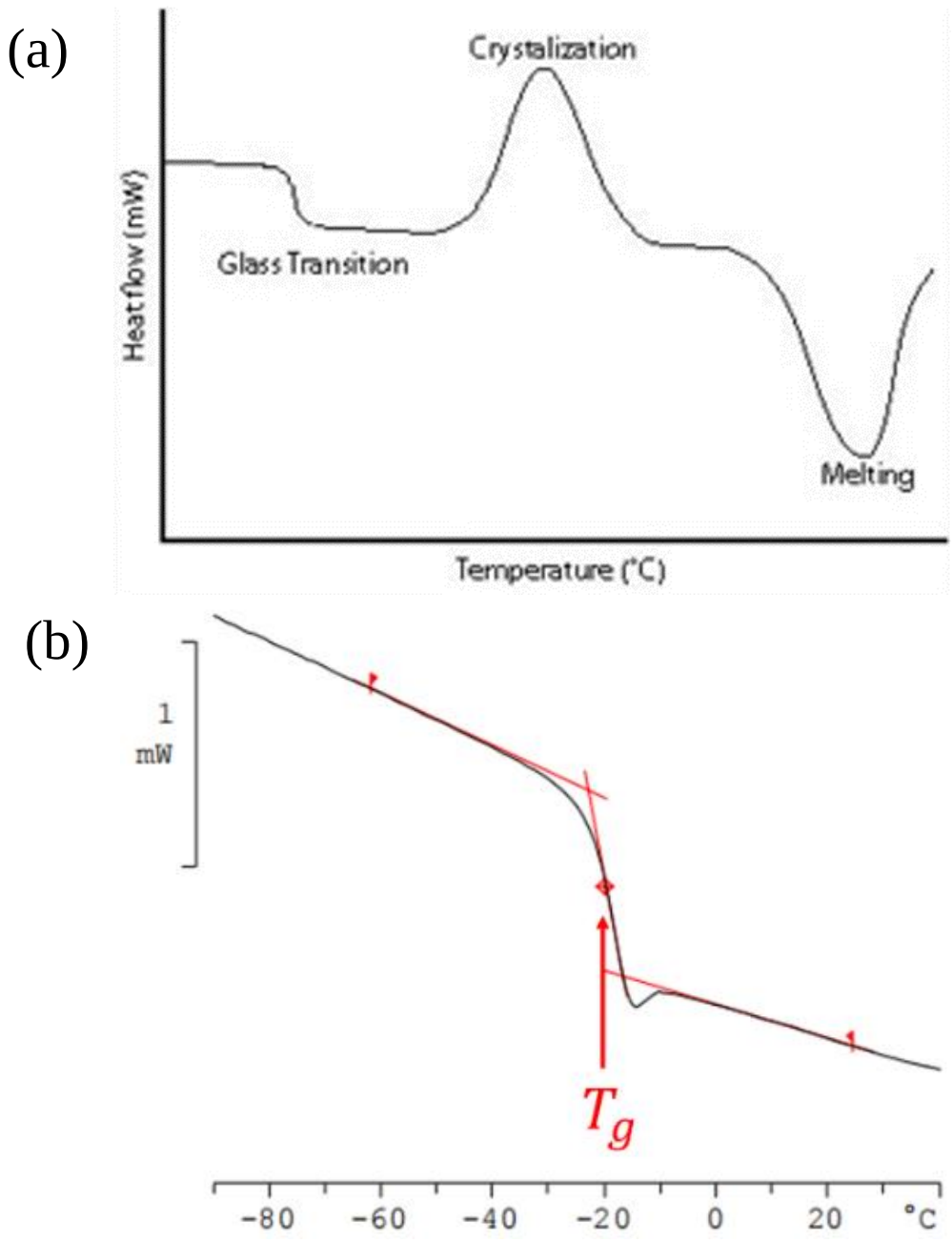

Figure 2.2 (a) Featured DSC curve with glass transition, crystallization and melting. (b) Featured DSC curve with glass transition and how T_g is defined.

2.2.1 Startup shear

Before the discussion of SAOS, the startup shear needs to be introduced. In shear measurement in rheology, the sample is sandwiched between two parallel plates. We also assume that there is no slip at the interfaces between the sample and the plate. To produce startup shear, the lower plate is held stationary, while the upper plate is made to suddenly displace in the X direction with a velocity of V (Fig. 2.3). In such case, sample's upper boundary will move by X=Vt at time t. The shear strain γ is defined by the displacement over the thickness H of the sample, expressed as

$$\gamma = \frac{X}{H} \tag{2.2}$$

Then the shear rate is defined as

$$\dot{\gamma} = \frac{d\gamma}{dt} = \frac{V}{H} \tag{2.3}$$

During the deformation, the sample resists the shear so that a finite horizontal force F arises along the X axis. The shear stress σ can be defined as the total resistance force on the bottom surface divided by the surface area Σ.

$$\sigma = \frac{F}{\Sigma} \tag{2.4}$$

2.2.2 Linear Responses and small amplitude oscillatory shear (SAOS)

Perfectly elastic solids can result in an instantaneous deformation with a shear strain γ when a shear stress σ is suddenly applied. At small enough shear strain, a linear relationship often exists

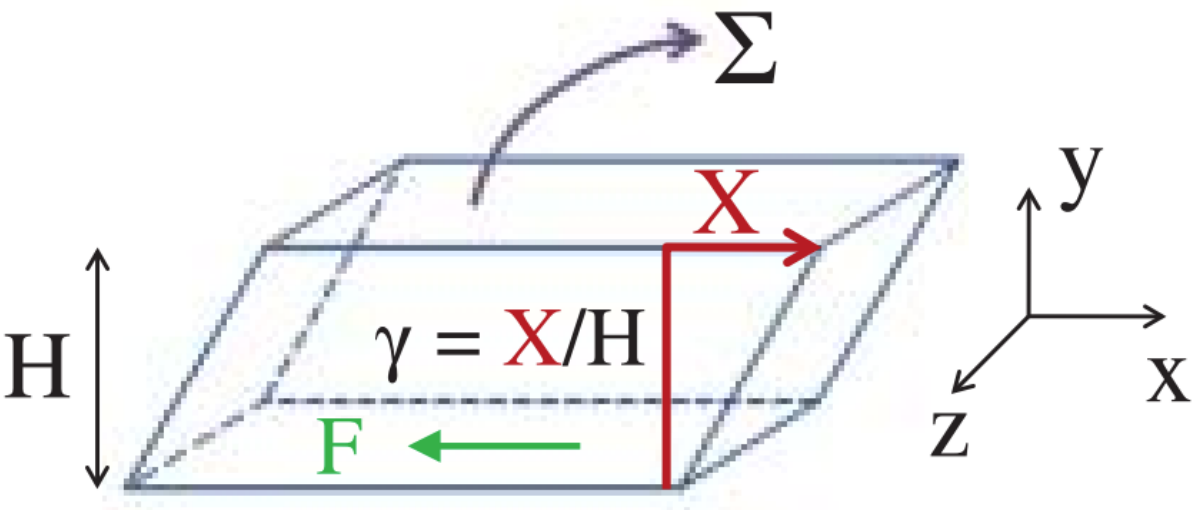

Figure 2.3 An illustration of startup shear in three dimensions

between the time dependent shear strain $\gamma(t)$ and the time dependent stress $\sigma(t)$:

$$\sigma(t) = G\gamma(t) \qquad (2.5)$$

in which G is the elastic shear modulus. For viscoelastic materials like polymers, the shear modulus is typically a decreasing function of time t, i.e., $G(t)$, in the stress relaxation process (Fig. 2.4). Thus, the relationship between $\gamma(t)$ and $\sigma(t)$ becomes more complicated. Based on linear response theory, their relationship can be described by[105]

$$\sigma(t) = \int_{-\infty}^{t} G(t-t')\frac{d\gamma(t')}{dt'}dt' \qquad (2.6)$$

During the SAOS measurement, instead of displacing the upper plate with a constant shear rate, a small oscillatory deformation was applied to the sample:

$$\gamma(t) = \gamma_0 \sin\omega t \qquad (2.7)$$

in which γ_0 is the amplitude of the oscillatory shear strain. The stress response in the linear response regime is also oscillatory according to the linear response theory, which is expressed by:

$$\sigma(t) = \sigma_0(\omega)\sin[\omega t + \delta(\omega)] = \gamma_0(G'(\omega)sin\omega t + G"(\omega)cos\omega t) \qquad (2.8)$$

in which $G'(\omega) = \frac{\sigma_0(\omega)}{\gamma_0}\cos[\delta(\omega)]$ is the storage modulus and $G''(\omega) = \frac{\sigma_0(\omega)}{\gamma_0}\sin[\delta(\omega)]$ is the loss modulus. The relationship between $G'(\omega)$, $G''(\omega)$ and $G(t)$ is

$$G'(\omega) = \omega\int_0^{\infty} G(t)\sin(\omega t)\,dt \qquad (2.9)$$

$$G''(\omega) = \omega\int_0^{\infty} G(t)\cos(\omega t)\,dt \qquad (2.10)$$

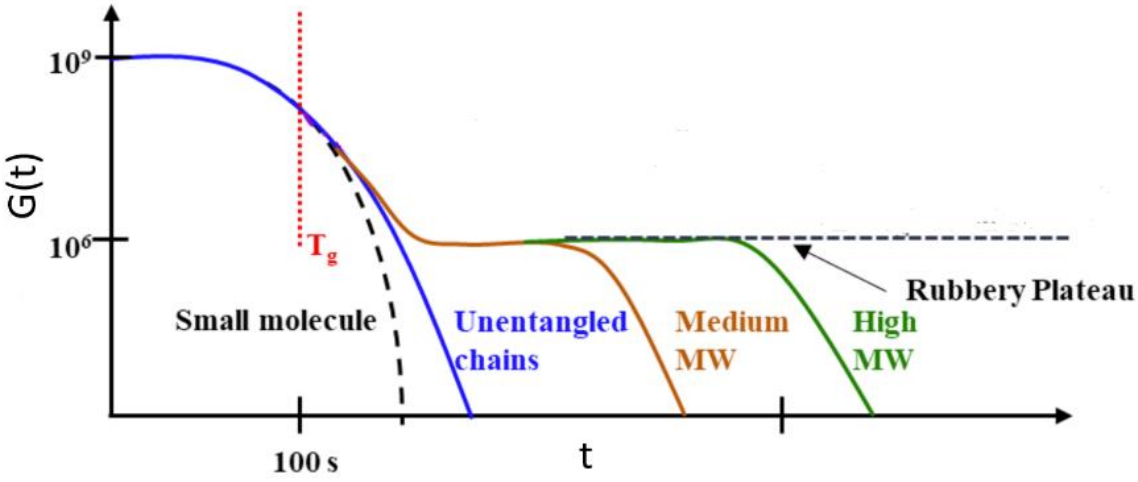

Figure 2.4 A scheme indicating how mechanical modulus changes with time in polymer

In other words, the $G'(\omega)$ and $G''(\omega)$ are the result of Fourier Transformation of $G(t)$.

In practical rheological measurement, $\sigma_0(\omega)$ and $\delta(\omega)$ can be acquired in the frequency range between 10^{-1} rad/s to 10^{2} rad/s, through which $G'(\omega)$ and $G''(\omega)$ can be calculated.

2.2.3 Time-temperature superposition

One of the limitations of SAOS is that the frequency range is quite limited, to overcome the limited frequency range, master curves are constructed which combine results of measurements performed at various temperatures to a single reference temperature but representing the material properties in a much broader frequency range. To construct the rheological master curve, a reference temperature at which one of the spectra was measured is first chosen. Then other measured spectra are horizontally shifted so that they can overlap with each other (Fig. 2.5). The shifting factor $\alpha_T(T)$ is used to represent how much horizontal shift of the measured results has been done.

2.2.4 Maxwell relaxation

Maxwell was the first to propose a phenomenological treatment of viscoelastic phenomena, famously known in the field as Maxwell model[105]. It is a combination of a spring and a dashpot in series, as shown in Fig. 2.6a. The spring represents the elastic component of the material, and the dashpot represents the viscous component of the material. Because the spring and dashpot are connected in series, they will suffer the same amount of stress during the deformation. Thus, the following equation can be written:

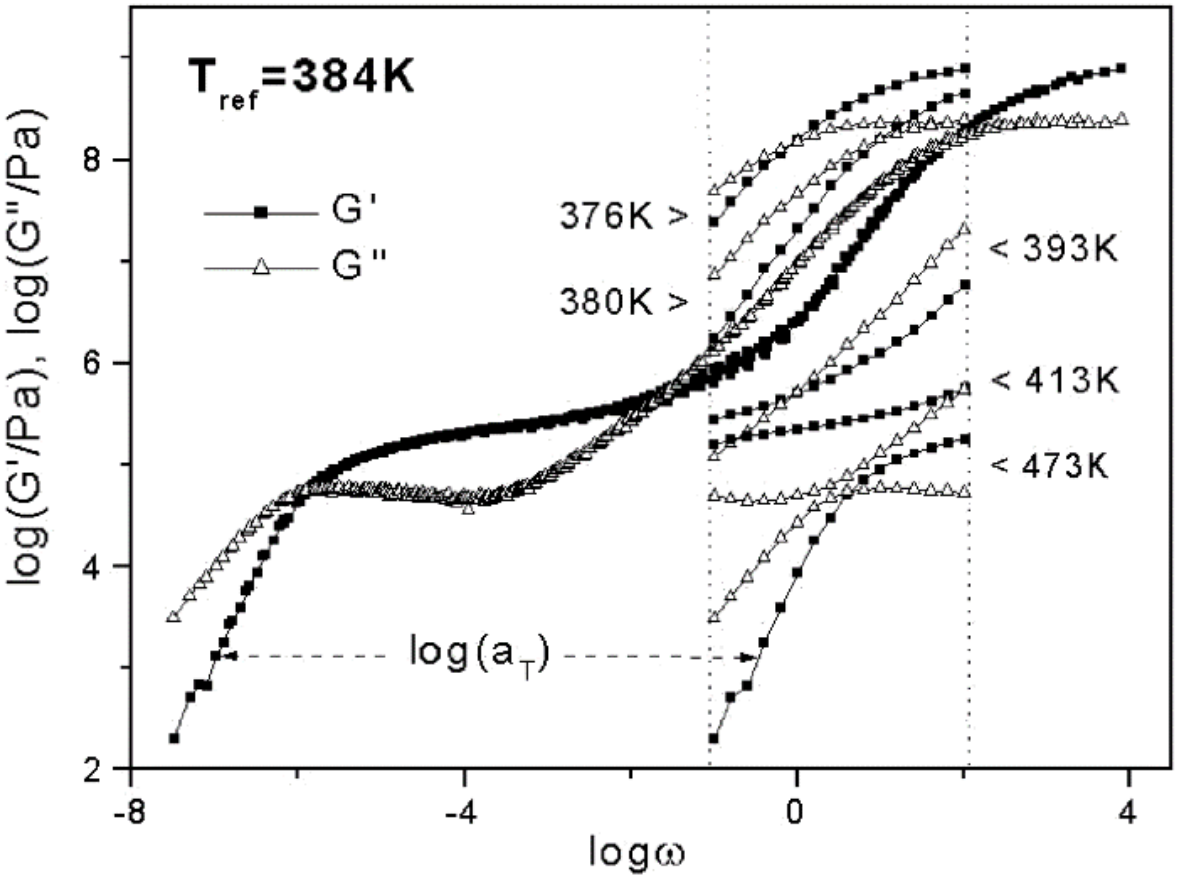

Figure 2.5 An example of Time-temperature Superposition in rheological measurement[106]

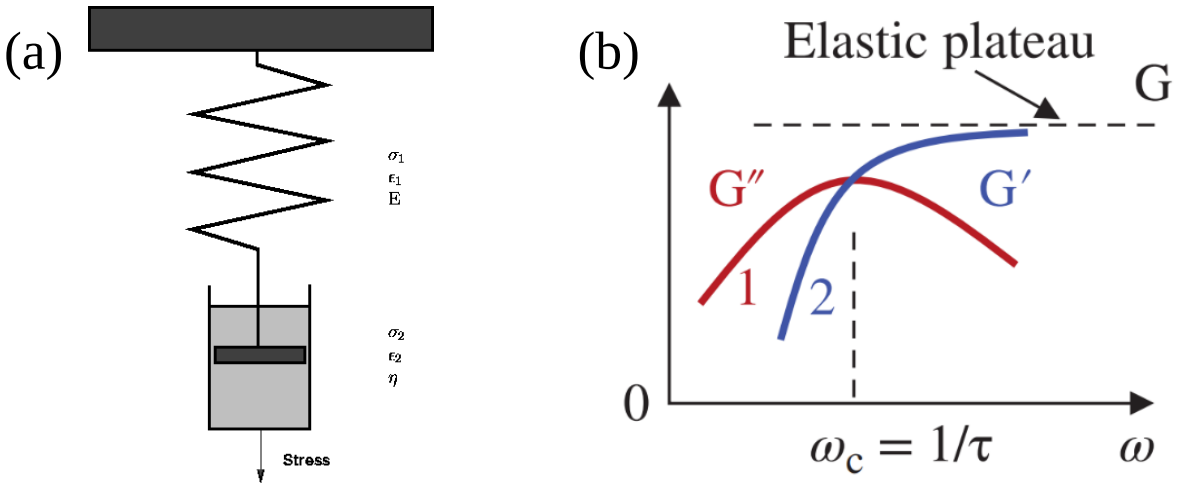

Figure 2.6 (a) An illustration of the spring-dashpot model. (b) The prediction of rheological spectra from Maxwell Model

$$\dot{\gamma} = \frac{\dot{\sigma}}{G} + \frac{\sigma}{\eta} \quad (2.11)$$

For a stress relaxation measurement, during the shear cessation ($\dot{\gamma} = 0$) after a small step shear, the stress decay can be observed. If the condition $\dot{\gamma} = 0$ is given, eq. 2.11 can be written as:

$$\frac{\dot{\sigma}}{G} + \frac{\sigma}{\eta} = 0 \quad (2.12)$$

By solving the differential equation, we can get:

$$\sigma(t) = \sigma_0 e^{-\frac{Gt}{\eta}} \quad (2.13)$$

where σ_0 is the stress when t=0. Here a characteristic relaxation time can be defined, which is $\tau=\eta/G$. So, eq. 2.13 can be written as:

$$\sigma(t) = \sigma_0 e^{-\frac{t}{\tau}} \quad (2.14)$$

Thus, the modulus relaxation function for the Maxwell relaxation can be expressed as

$$G(t) = Ge^{-\frac{t}{\tau}} \quad (2.15)$$

According to eq. 2.9 and eq. 2.10, the $G'(\omega)$ and $G''(\omega)$ for the Maxwell behavior can be expressed as

$$G'(\omega) = G\frac{\omega^2\tau^2}{1+\omega^2\tau^2} \quad (2.16)$$

$$G''(\omega) = G\frac{\omega\tau}{1+\omega^2\tau^2} \quad (2.17)$$

The typical rheological spectra for Maxwell relaxation are shown in Fig. 2.6b. In the graph, a peak can be seen in $G''(\omega)$. Whereas $G'(\omega)$ shows a plateau on the high frequency side of the

peak. For the low frequency side, $G'(\omega)$ and $G''(\omega)$ show a slope of 1 and 2 in log-log scale. From crossover of $G''(\omega)$ and $G''(\omega)$, the characteristic relaxation time is considered as $\tau = \frac{1}{\omega_C}$ in which ω_C is the angular frequency at the crossover. Sometimes, the frequency of the maximum in $G''(\omega)$ is taken for the relaxation time. These two definitions are identical for the Maxwell model but might differ for real systems.

2.2.5 A phenomenological generic peak description in shear modulus spectra

Maxwell model provides the simplest viscoelastic behavior. Usually, the relaxation behavior is more complicated. For instance, the Rouse relaxation behavior, as reviewed in Chapter 1, is a superposition of many Maxwell relaxation processes. Maxwell relaxation process is usually utilized to describe terminal relaxation behavior. In some more complicated scenario, i.e., the segmental relaxation, the relaxation process happens with a distribution of the timescale. This results in the broadening of the rheological spectra for both $G'(\omega)$ and $G''(\omega)$. Thus, a phenomenological generic peak description was proposed[106]:

$$G'(\omega) = \frac{A}{(\omega\tau_1)^{b_1} + (\omega\tau_1)^{b_2}} \quad (2.18)$$

$$G''(\omega) = \frac{A}{(\omega\tau_1)^{c_1} + (\omega\tau_1)^{c_2}} \quad (2.19)$$

Here A represents the modulus level. b1, b2, c1, c2 describe low- and high-frequency slopes of the G′ and G″ curves, respectively. Although these equations do not satisfy Kramers− Kronig relationship which is known to be valid for linear viscoelastic regime, their generic shape not only describe the broadening of segmental relaxation process, but also includes the contribution

of additional dynamics like Rouse modes which are very difficult to fit separately. This method is sufficient to estimate the characteristic relaxation time.

2.2.6 Analysis of the data from shear modulus spectra

Usually, rheological spectra demonstrate a segmental relaxation process as well as a terminal relaxation process. The shear modulus master curve involved in the proposed research can be analyzed through the function set with a Maxwell term describing the contribution from terminal relaxation (right term) as well as a phenomenological generic peak term describing the contribution from segmental relaxation, which is presented below (left term):

$$G'(\omega) = \frac{A}{(\omega\tau_1)^{b_1}+(\omega\tau_1)^{-b_2}} + G_e \frac{\omega^2\tau_2^2}{1+\omega^2\tau_2^2} \quad (2.20)$$

$$G''(\omega) = \frac{A}{(\omega\tau_1)^{c_1}+(\omega\tau_1)^{-c_2}} + G_e \frac{\omega\tau_2}{1+\omega^2\tau_2^2} \quad (2.21)$$

Here A and G_e represent the plateau moduli in the glassy and terminal regime, respectively. τ_1 and τ_2 indicates the characteristic relaxation time of the segmental and terminal relaxation, respectively. This fitting function set has been successfully estimating segmental relaxation time and terminal relaxation time for PPG-COOH[27]. Then relaxation time as a function of temperature can be acquired through time temperature superposition.

2.2.7 Rheological measurement setup

Rheological experiments were performed at an AR2000ex rheometer from TA instrument. Three different types of measurements were carried out. They are small amplitude oscillatory shear

(SAOS), startup shear and creep. For all the experiments, parallel plate geometry with a separation between upper and lower plate of ~700 μm was used (Fig. 2.7). Small amplitude oscillatory shear (SAOS) was used to probe the linear viscoelasticity of the associating polymers, and 4mm plate was used. For viscosity measurement, 8mm plate was used. The startup shear was used to measure viscosity lower than 10000 Pa.s. and creep was used to measure viscosity higher than 10000 Pa.s.

2.3 Broadband Dielectric Spectroscopy (BDS)

2.3.1 Electrostatics

In order to understand the principle of BDS, we need to understand the electrostatics first. If an external dielectric field E is imposed on a material with permanent dipole moments, the external field forces the dipoles to align parallel to the field. This is the polarization behavior. The polarization P describes the dielectric displacement which originates from the response of a material to an external field, which is expressed as

$$P = (\varepsilon_s - 1)\varepsilon_0 E \qquad (2.22)$$

Here ε_0 is dielectric permittivity of vacuum. ε_s is the dielectric permittivity of the material. The overall polarization P consists of two components: the instantaneous polarization P_∞ because of the atomic and electronic polarizations and the orientational polarization P_0because of the reorientation of the permanent dipoles. Thus,

$$P = P_\infty + P_0 = \varepsilon_0(\varepsilon_\infty - 1)E_0 + \varepsilon_0\Delta\varepsilon E_0 \qquad (2.23)$$

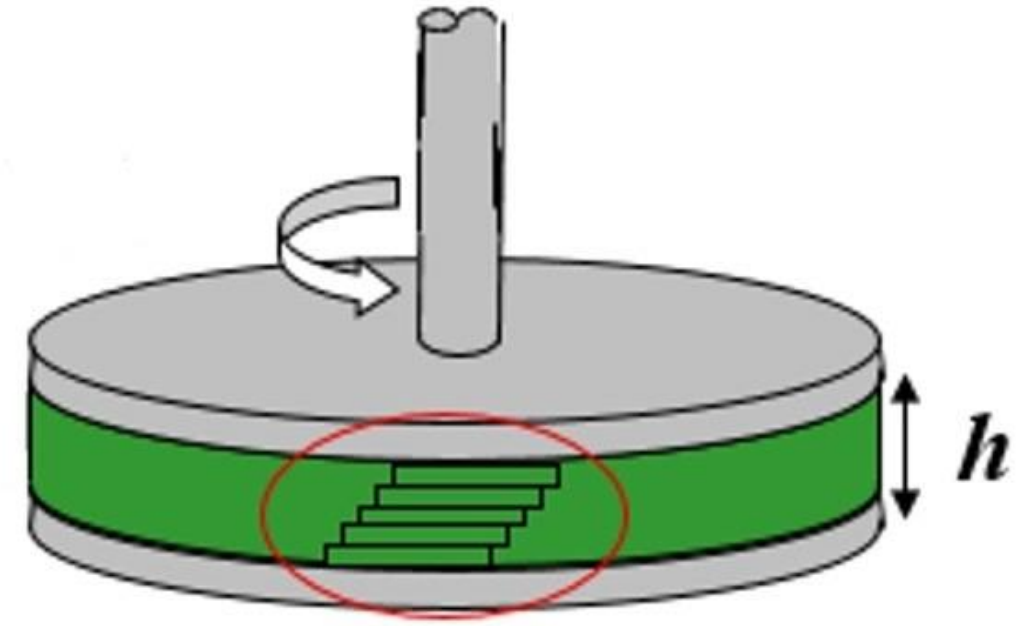

Figure 2.7 Parallel plate measuring system

In such case, $\varepsilon_s = \varepsilon_\infty + \Delta\varepsilon$ in which $\Delta\varepsilon$ is the relaxation strength. ε_∞ is the permittivity of short-time response.

$$P_0 = \frac{N}{V}\langle\mu\rangle_z \tag{2.24}$$

Here N is the number of permanent dipoles in the volume V. After the electric field is applied, the new equilibrium state is only partially oriented parallel with the applied field due to the thermal fluctuations. Thus,

$$\langle\mu\rangle_z = \frac{\int_0^\pi \mu cos\theta \exp\left(\frac{\mu cos\theta E_0}{KT}\right) 2\pi sin\theta d\theta}{\int_0^\pi \exp\left(\frac{\mu cos\theta E_0}{KT}\right) 2\pi sin\theta d\theta} = \frac{\mu^2 E_0}{3KT} \qquad (\mu E_0 \ll kT) \tag{2.25}$$

Thus, according to the Curie law,

$$\Delta\varepsilon = \frac{N\mu^2}{3\varepsilon_0 VKT} \tag{2.26}$$

2.3.2 Dielectric linear response and dielectric relaxation (dielectric retardation)

If an external electric field is applied to a dielectric material, the macroscopic polarization will not reach its equilibrium value instantaneously but after a certain time (Fig. 2.8). In other words, dielectric permittivity changes with time, which can be expressed by $\varepsilon(t)$. Then the relationship between $P(t)$ and $E(t)$ can be expressed by

$$P(t) = P_\infty + \varepsilon_0 \int_{-\infty}^{t} \varepsilon(t - t') \frac{dE(t')}{dt'} dt' \tag{2.27}$$

according to linear response theory. In BDS measurement, an oscillatory electric field is imposed on the material, which is expressed as

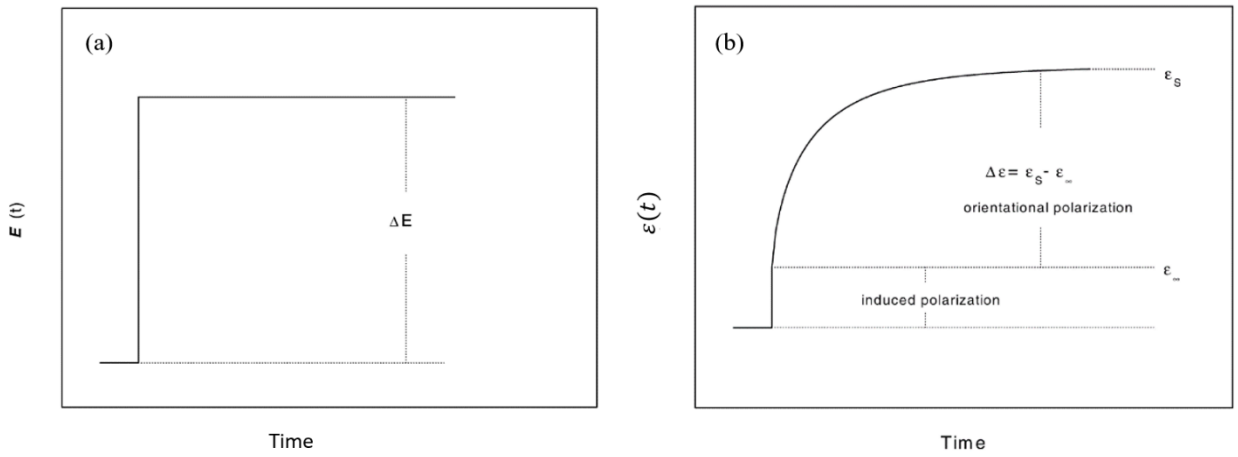

Figure 2.8 Schematic relationships between (a) time dependence of the electric field and (b) time dependent dielectric relaxation function

$$E(t,\omega) = E_0 \exp(-i\omega t) \quad (2.28)$$

The polarization response is also oscillatory according to the linear response theory, which is expressed by:

$$P(t,\omega) = \varepsilon_0[\varepsilon^*(\omega) - 1]E_0 \exp(-i\omega t) \quad (2.29)$$

where

$$\varepsilon^*(\omega) = \varepsilon'(\omega) - i\varepsilon''(\omega) = \varepsilon_\infty - \int_0^\infty \frac{d\varepsilon(t)}{dt} \exp(-i\omega t)dt \quad (2.30)$$

In other words, $\varepsilon^*(\omega)$, the complex permittivity, is the result of one-sided Fourier or full imaginary Laplace transformation of $\varepsilon(t)$. $\varepsilon'(\omega)$ and $\varepsilon''(\omega)$ are the real and imaginary part of the complex permittivity.

The dielectric relaxation strength can be expressed as

$$\Delta\varepsilon = \frac{2}{\pi}\int_0^\infty \varepsilon''(\omega) d ln\omega \quad (2.31)$$

Both dielectric functions $\varepsilon(t)$ and $\varepsilon^*(\omega)$ are generalized compliances, which reflects dielectric retardation behavior. The related modulus is called electric modulus M(t) in the time domain and $M^*(\omega) = M'(\omega) + iM"(\omega)$ in the frequency domain, which reflects true relaxation behavior. The relationship between dielectric permittivity and electric modulus is

$$M^*(\omega)\varepsilon^*(\omega) = 1 \quad (2.32)$$

2.3.3 BDS measurement techniques

Broadband dielectric measurements were performed using Novocontrol Concept 80 system, including Alpha-A impedance analyzer, ZGS active sample cell interface, and Quatro Cryosystem temperature control unit. If the sample is liquid-like, it is placed into a parallel-plate dielectric cell made of sapphire and invar steel, with a defined electrode diameter and electrode separation (Fig. 2.9a). If the sample is solid-like throughout the temperature range of measurement, it is placed in dielectric cell with upper and lower gold plate (Fig. 2.9b). The measurements were in the frequency range of 10^{-2} – 10^{6} Hz. Fig. 2.9c illustrates the application of a sinusoidal electric field. There is a phase lag between the applied electric field and the resulting current. Thus, the impedance is a complex number. Impedance Z^* is measured as $Z^* = \frac{U^*}{I^*}$. So that complex capacitance and permittivity can be derived as $C^* = \frac{1}{i\omega Z^*}$ and $\varepsilon^* = \frac{C^*}{C_0}$.

2.3.4 Description of dielectric relaxation behavior

The simplest description of the dielectric relaxation behavior is Debye relaxation. Assumption that the change of the polarization is proportional to its actual value, which is expressed by the differential equation:

$$\frac{dP(t)}{dt} = -\frac{1}{\tau_D}P(t) \qquad (2.33)$$

in which τ_D is a characteristic relaxation time. This relationship leads to the complex dielectric function:

$$\varepsilon^*(\upsilon) = \varepsilon_\infty + \frac{\Delta\varepsilon}{1+2\pi i\upsilon\tau_D} \qquad (2.34)$$

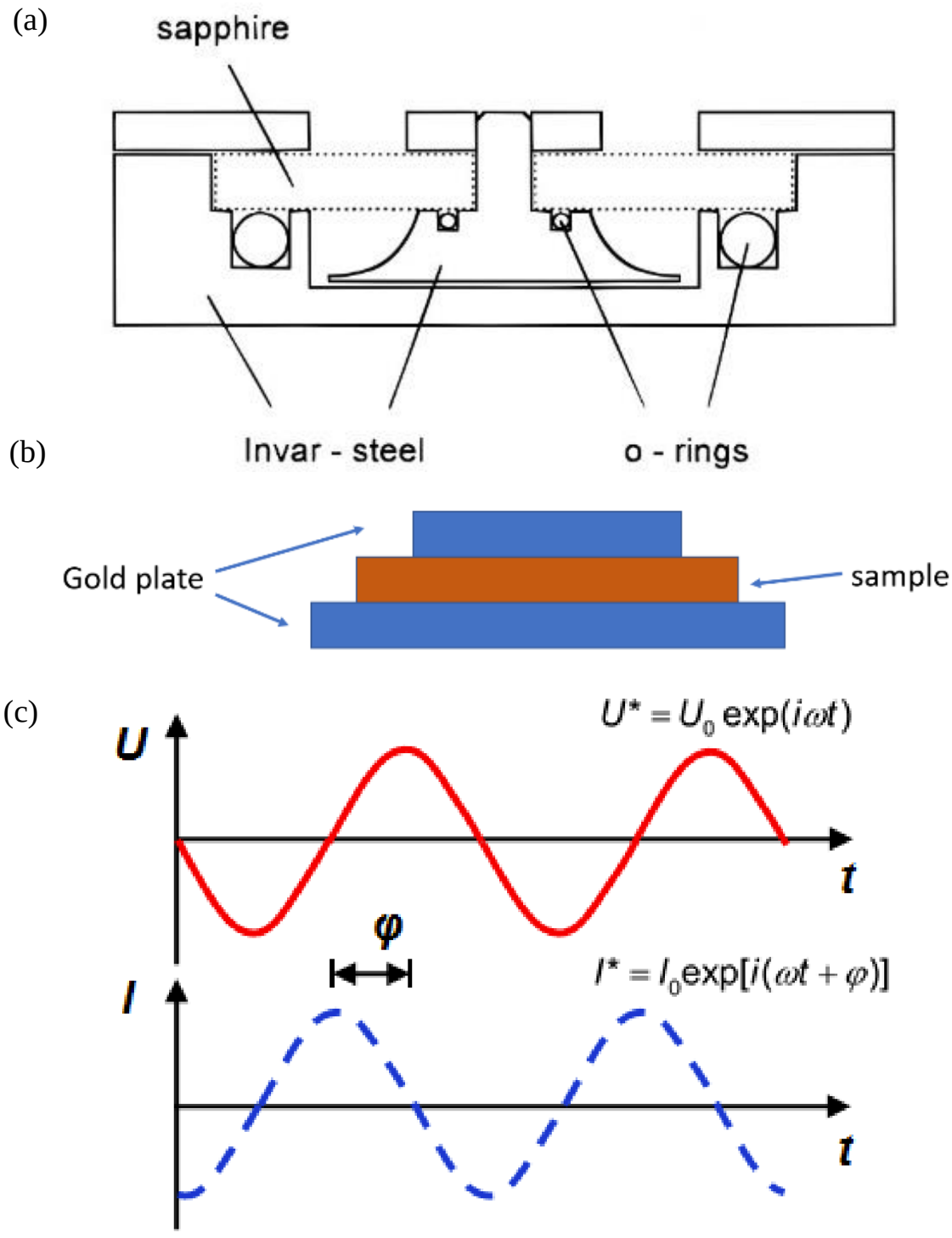

Figure 2.9 (a) Depiction of the sample cell for liquid-like sample. (b) Depiction of the sample cell for solid-like sample. (c) Depiction of the input sinusoidal electric field and the resulting current.

This is most fundamental dielectric relaxation behavior which considers the no distribution of timescale. Usually, the measured dielectric spectra are broader and more asymmetric. The Havriliak and Negami (HN) equation is often used to analyze ε^* spectra in which both broadening and asymmetry are considered[107, 108].

$$\varepsilon^*_{HN}(\upsilon) = \varepsilon_\infty + \frac{\Delta\varepsilon}{[1+(2\pi i\upsilon\tau_{HN})^\alpha]^\gamma} \qquad (2.35)$$

Here, α and γ are the shape parameters denoting broadening and asymmetry. τ_{HN} is the characteristic relaxation time from HN function fitting. It is used to estimate the relaxation time at the loss maximum τ_{max}.

$$\tau_{max} = \tau_{HN}\left[\sin\left(\frac{\alpha\pi}{2+2\gamma}\right)\right]^{-\frac{1}{\alpha}}\left[\sin\left(\frac{\alpha\gamma\pi}{2+2\gamma}\right)\right]^{\frac{1}{\alpha}} \qquad (2.36)$$

If there are several dielectric processes in the ε^* spectra, then the fitting function is a sum of several HN functions, depending on the number of processes. Conductivity can contribute to the dielectric spectra. It appears as a power law with a slope of -1 in ε'' spectra. The conductivity contribution added another term $\frac{\sigma}{2\pi i\upsilon\varepsilon_0}$ to eq. 2.35.

The conductivity mentioned above might cover some dielectric processes from ε^*. However, conductivity does not contribute directly to ε', only conductivity relaxation process can. Thus, derivative analysis for the ε' spectra has been utilized to extract the relaxation processes. According to Kramers-Kronig relationship, it should be similar to ε". Based on the logarithmic derivative[109], ε'_{der} is express as follow:

$$\varepsilon'_{der} = -\frac{\pi}{2}\frac{\partial\varepsilon'(\upsilon)}{\partial ln\upsilon} = \frac{\pi}{2}\frac{\alpha\gamma\Delta\varepsilon(2\pi\upsilon\tau)^\alpha\cos\left[\frac{\alpha\pi}{2}-(1+\gamma)\theta_{HN}\right]}{[1+2(2\pi\upsilon\tau)^\alpha\cos\left(\frac{\pi\alpha}{2}\right)+(2\pi\upsilon\tau)^{2\alpha}]^{\frac{1+\gamma}{2}}} \qquad (2.37)$$

in which

$$\theta_{HN} = \arctan \frac{\sin\left(\frac{\pi\alpha}{2}\right)}{(2\pi\upsilon\tau)^{-\alpha}+\cos\left(\frac{\pi\alpha}{2}\right)} \quad (2.38)$$

Also, if two dielectric processes are too closely adjacent in $\varepsilon^*(\upsilon)$ spectra, they can be distinguished through derivative analysis because the peaks appear narrower in this analysis. In terms of M^* spectra, the process can be fit using HN functions as well and τ_{max} can be acquired through eq. 2.36 as well. In dielectric modulus analysis, the fitting function can also be a sum of HN function based on the number of processes.

2.4 X-ray scattering

2.4.1 Definition of scattering vector q

For inhomogeneous materials, the scattering of X-ray originates from electronic density fluctuations on length scales assessed by the scattering wave vector $\vec{q} = \overrightarrow{k_s} - \overrightarrow{k_\iota}$ in which $\overrightarrow{k_\iota}$ and $\overrightarrow{k_s}$ are wave vector of the incident and scattered X-ray beam, respectively (Fig. 2.10). For elastic scattering, $\left|\overrightarrow{k_\iota}\right| = \left|\overrightarrow{k_s}\right| = \frac{2\pi}{\lambda}$ and thus $|\vec{q}| = \frac{4\pi}{\lambda}\sin\left(\frac{\theta}{2}\right)$ in which λ is the radiation wavelength and θ is the scattering angle.

2.4.2 1st order Bragg's law

When X-ray beam encounters any inhomogeneity or individual atoms in a system (i.e., nanoparticle in amorphous polymer), it will scatter at different directions with different θ. At a specific direction, the scattered beam interferes with another scattered X-ray beam from an

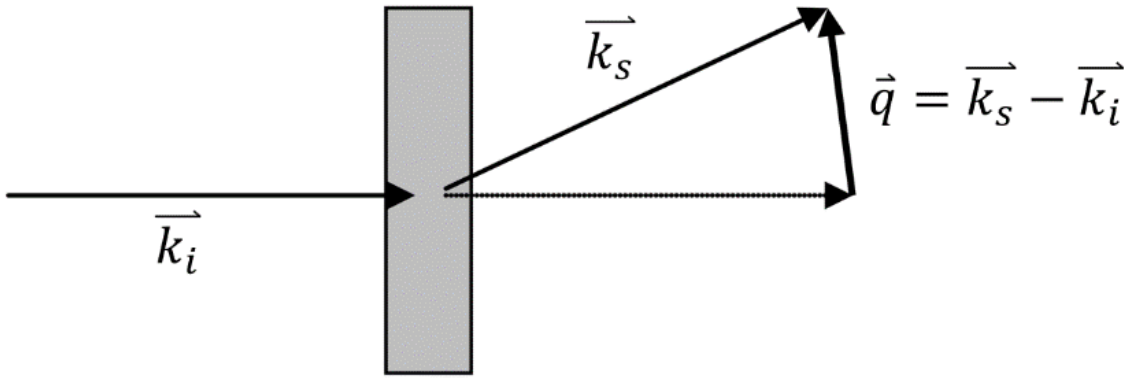

Figure 2.10 Illustration of the wave vector of incident X-ray beam, scattered X-ray beam and scattering wave

adjacent piece of inhomogeneity (Fig. 2.11). The constructive interference, when the two scattered waves are coming in phase, results in stronger X-ray intensity. Through this mechanism, the spacing between this two adjacent inhomogeneity is calculate, which is the 1st order Bragg's law.

$$\lambda = 2dsin\frac{\theta}{2} \quad (2.39)$$

in which d is the distance between 2 adjacent inhomogeneity. Thus, the d can be expressed as a function of scattering wave vector:

$$d \approx \frac{2\pi}{|\vec{q}|} \quad (2.40)$$

2.4.3 X-ray scattering setup

X-ray scattering measurement was conducted on XEUSS 3.0 (Xenocs, France) equipped with a Cu Kα microfocus source and a Pilatus 300k detector (Dectris, Switzerland) (Fig. 2.12). The scattering vector (q) is calibrated by a silver behenate standard material. The distance between sample and detector is 0.9m and 0.55m for SAXS and WAXS, respectively). The sample was squeezed into a capillary tube made of quartz glass with diameter 1.5mm and the wall thickness 0.01mm. Then the capillary was placed perpendicularly to the X-ray beam. The measurement mentioned above was also done on the empty capillary to subtract the background. X-ray measurements were performed at room temperature.

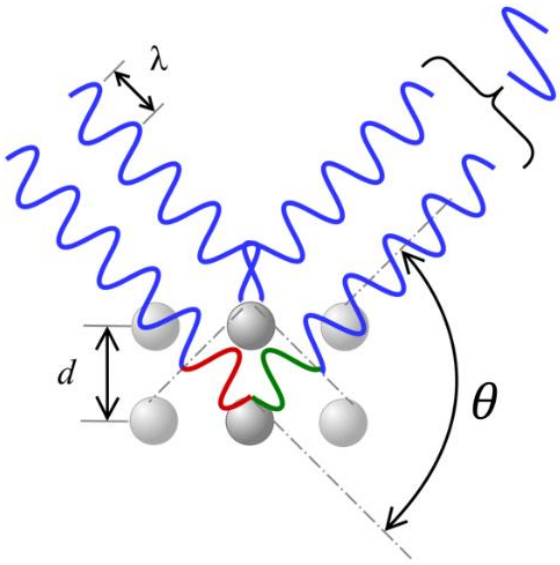

Figure 2.11 Depiction of how constructive interference is generated by the adjacent inhomogeneity during the X-ray scattering measurement

Figure 2.12 X-ray scattering equipment. The left part is the X-ray beam generator. The right part is the sample and detector.

2.4.4 Analysis of the X-ray scattering spectra

The Gaussian equation was used to fit the peaks in X-ray scattering spectra:

$$I(q) = y_0 + (\frac{A}{w\sqrt{\pi/2}})\exp\left[-(\frac{q-q_c}{w})^2\right] \quad (2.41)$$

where y_0 is the background. A is the intensity of the peak defined by the amount of clusters present and their contrast, w is the width of the peak.

CHAPTER 3 EXPERIMENTAL TEST OF BOND LIFETIME RENORMALIZATION MODEL IN ASSOCIATING POLYMER WITH BINARY ASSOCIATION

A version of this chapter was published in *Soft Matter*, by Sirui Ge, Martin Tress, Kunyue Xing, Peng-Fei Cao, Tomonori Saito, and Alexei P. Sokolov "Viscoelasticity in associating polymers: experimental test of bond lifetime renormalization model" (Soft Matter, 2020,16, 390-401)

Alexei P. Sokolov formulated the concept and managed the entire project. Sirui Ge did most of the rheology and dielectric measurement, did all the model analysis and wrote most of the manuscript under the guidance of Alexei P. Sokolov and Dr. Martin Tress. Kunyue Xing provided the chemical synthesis and some of the preliminary measurements, Peng-Fei Cao and Tomonori Saito provides the general guidance and supervision of the synthesis.

3.1 Introduction

Associating polymers with stickers randomly distributed along the polymeric chains have been studied in both melt[28, 38] and solution[32, 110, 111]. Recently, also much better defined systems like telechelic polymers are in focus[112-115 116, 117]. Due to the mechanical robustness established by the supramolecular network, many studies employ rheological measurements. Several models were proposed to explain the experimental results on a molecular level, such as the Sticky Rouse model[36]

and the Reversible Gelation model[118]. A central parameter in these descriptions is the activation energy E_a required to dissociate the bond between stickers[119]. E.g., Tanaka et al.[33, 101] and Indel et al.[120, 121] proposed models to calculate this energy for cluster associations and pairwise associations, respectively, from the characteristic relaxation times revealed in rheology. It is basically agreed that the structural relaxation time τ_α is the pre-factor in an Arrhenius type equation[36, 119] describing the temperature dependence of the characteristic dissociation time τ_b of the supramolecular network.

$$\tau_b(T) = \tau_\alpha(T)\exp\left(\frac{E_a}{RT}\right) \qquad (3.1)$$

where R is the gas constant. The earlier rheological studies considered the terminal relaxation time τ_C in shear modulus spectra to reflect the characteristic time of the sticker dissociation τ_b. However, the recent investigations combining rheology and dielectric spectroscopy challenged this interpretation[45, 122].

Dielectric spectroscopy[106] can provide insight not only into the orientational dynamics but also into association behavior of such polymers, because the dissociation of stickers is accompanied by a change in the dipole moment (since the stickers are often polar groups)[123]. This means that the dissociation can be observed in dielectric spectra and is commonly referred to as α*-relaxation[124] with the characteristic relaxation time τ_α^*. In addition, dielectric spectroscopy is also a common method to probe the segmental relaxation of polymers[106]. Thus, besides rheological measurement, dielectric spectroscopy can also be utilized to detect the relevant processes in associating polymers[125]. In recent studies of entangled polyisoprene randomly functionalized with urazole groups, it has been found that the rheological terminal relaxation time τ_C and the sticker

dissociation time probed by dielectric spectroscopy τ_α^* differ with the former being several orders of magnitude longer than the latter[45, 122]. The authors explained this observation with the concept of lifetime renormalization proposed by Stukalin et al.[44]. The model demonstrated two relevant contributions to the bond rearrangement timescale: (1) after dissociation the sticker returns to its former partner *J* times and remains associated with it for τ_b each time, before (2) it diffuses to another free chain-end (sticker), which requires the additional diffusion time τ_{open}:

$$\tau_b^{renm} = J(\tau_{open})\tau_b + \tau_{open} \qquad (3.2)$$

Considering the assignments $\tau_b = \tau_\alpha^*$ and $\tau_b^{renm} = \tau_C$, this model explains at least on a qualitative level why the terminal relaxation time from rheological measurements is often larger than the α*-relaxation time deduced from the dielectric data. However, the previous research lacks detailed quantitative analysis of the bond lifetime renormalization model.

To provide thorough and quantitative test of the lifetime renormalization model, we utilized both rheology and dielectric spectroscopy to probe the characteristic relaxation times of several telechelic polymers with different chain length and associating groups[126, 127]. We find that the separation between terminal relaxation time and sticker dissociation time ranges from less than one decade to about 4 decades and depends strongly on molecular weight (MW) and activation energy of the end group dissociation. The model of lifetime renormalization as generalized by Gold et al.[45, 122] allows the calculation of the diffusion exponent *x*, which exhibits a systematic transition from $x \sim 0.5$ (Rouse dynamics) to $x \sim 0.25$ (reptation dynamics) with increasing MW. This transition appears well below the entanglement MW M_e, which suggests the formation of super-chains with an effective MW above M_e. According to this analysis, the generalized model

of lifetime renormalization seems to describe the behavior of associating telechelics quantitatively; though, a definite verification requires means to check independently the extracted values of the diffusion exponent *x* and the number of returns *J*.

3.2 Materials

In this research, the telechelic associating polymer used are associating polymers with polydimethylsiloxane (PDMS) backbone and polypropylene glycol (PPG) backbone. The associating polymers with PDMS backbone are terminated with amine ($-NH_2$) and thioether-linked carboxylic acid (-S-COOH) as end groups, labeled as PDMS-NH_2 and PDMS-S-COOH, respectively. The associating polymers with polypropylene glycol (PPG) backbone are terminated with amine ($-NH_2$) and urethane-linked carboxylic acid (-NHCO-COOH) as end groups, labeled as PPG-NH_2 and PPG-COOH.

3.2.1 Commercially available polymers

Some of these associating polymers involved in this research are commercially available, including amine-terminated PDMS (PDMS-NH_2), vinyl terminated PDMS (PDMS-V) and amine-terminated PPG (PPG-NH_2). PDMS-NH_2 with MW of 850-900, 900-1000, 3000 and 5000 g/mol, vinyl terminated PDMS (PDMS-V) with MW of 800 and 6000 g/mol, were purchased from Gelest Inc. PPG bis(2-aminopropyl ether) (PPG-NH_2) with DP 6, 33, 67 (Mn of 480, 2046 and 4018 g/mol was purchased from Sigma-Aldrich and used directly without further purification. The chemical

structures are verified by NMR measurement (Fig. 3.1). The peaks in the NMR spectra indicate the different organic groups on the chemical structure.

The degree of polymerization (DP) of PDMS-NH_2, PDMS-V and PPG-NH_2 were calculated by the end group analysis through the Nuclear Magnetic Resonance (^{1}H NMR) spectra, i.e., for PDMS-NH_2, comparative integration of the peaks assigned to the methyl groups in the repeating units and methylene groups adjacent to amines. Then, DP is calculated by the ratio of integration of methyl groups in the repeating units to the integration of methylene groups adjacent to amines.

In this research, the number of Kuhn segments needs to be used. The number of Kuhn segments in the chain N (Table 3.1) is obtained from the DP and the characteristic ratio C_∞ (6.3 for PDMS[128] and 5.76 for PPG[129]) according to $N = \frac{n}{C_\infty}$ where n denotes the number of atomic bonds in the main chain[130] (n equals to 2×DP in PDMS and 3×DP in PPG). The labeled Mw, degree of polymerization, number of Kuhn segments and the actual molecular weight (M_n) of each commercially available polymer is shown in the Table 3.1.

3.2.2 Synthesis of non-commercially available associating polymers

PDMS-S-COOH, PPG-COOH involved in the research are not commercially available. They were synthesized by other colleagues in the research group. The synthesis routes and the structural characterizations are shown below:

PDMS-S-COOH was synthesized from PDMS-V and react with 3-Mercaptopropionic acid. The synthesis route is shown in Fig. 3.2a. The chemical structure is verified by ^{1}H NMR

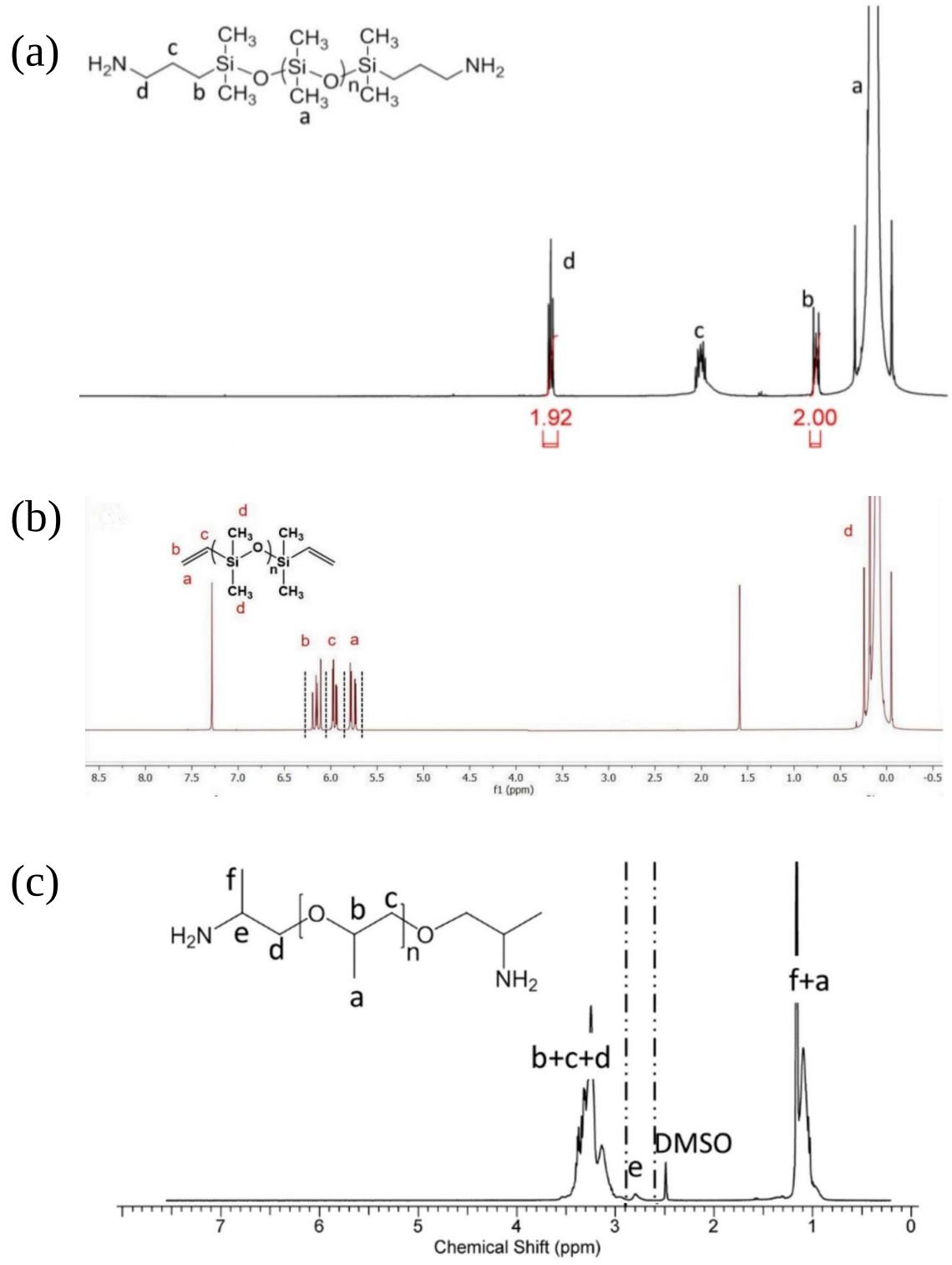

Figure 3.1 Chemical structure and ^{1}H NMR results of (a) PDMS-NH_2, (b) PDMS-V (c) PPG-NH_2.

Table 3.1 The labeled Mw, degree of polymerization, number of Kuhn segments and the actual molecular weight (M_n) of each commercially available polymer

Material	Labeled M_W [g/mol]	DP	N	M_n [g/mol]
PDMS-NH2-13	850-900	13	4	1194
PDMS-NH2-19	850-900	19	6	1522
PDMS-NH_2-22	900-1000	22	7	1744
PDMS-NH_2-50	3000	50	16	3816
PDMS-NH_2-74	5000	74	23	5592
PDMS-V-13	800	13	4	1016
PDMS-V-83	6000	83	26	6196
PPG-NH_2-6	900-1000	6	3	1744
PPG-NH_2-33	3000	33	17	3816
PPG-NH_2-67	5000	67	35	5592

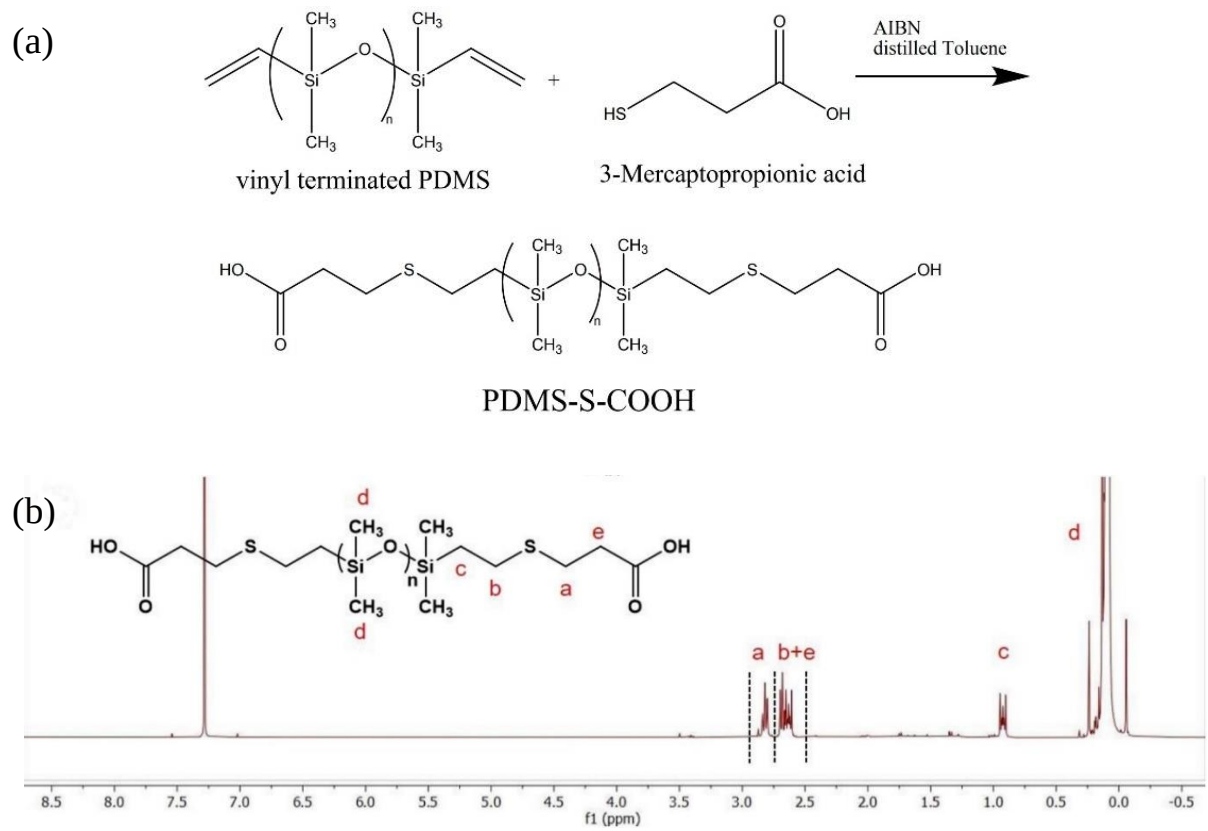

Figure 3.2(a) Synthesis of amide-acid terminated polydimethylsiloxane (PDMS-S-COOH) from the vinyl-terminated polydimethylsiloxane (PDMS-V). (b) ^{1}H NMR spectra of PDMS-S-COOH.

measurement (Fig. 3.2b). The peaks in the NMR spectra (labeled from a to e) indicate the different organic groups (labeled from a to e) on the chemical structure. PPG-COOH was synthesized from PPG-NH_2 and react with succinic anhydride. The synthesis route is shown in Fig. 3.3a. The quantitative end-group modification was confirmed by ^{1}H NMR (Fig. 3.3b). The peaks in the NMR spectra (labeled from a to h) indicate the different organic groups (labeled from a to h) on the chemical structure.

3.3 Methods

3.3.1 Differential scanning calorimetry (DSC)

Differential scanning calorimetry (DSC) was performed using a Q-1000 differential scanning calorimeter (TA Instruments). All the samples were dried in a vacuum oven for several days in order to remove remaining solvent and moisture, and subsequently sealed in hermetic aluminum pans. Scans were performed with a rate of 10 K/min. For associating polymers with PPG backbone, the temperature range is from 150 K to 350 K. For associating polymers with PPG backbone, the temperature range is from 113 K to 376 K. Before the first run, each sample was equilibrated at the highest temperature for 5 minutes. Two subsequent cooling and heating cycles were conducted to verify reproducibility and to eliminate the thermal history. The glass transition temperature (T_g) was determined from the middle point of the respective step in the heat flow.

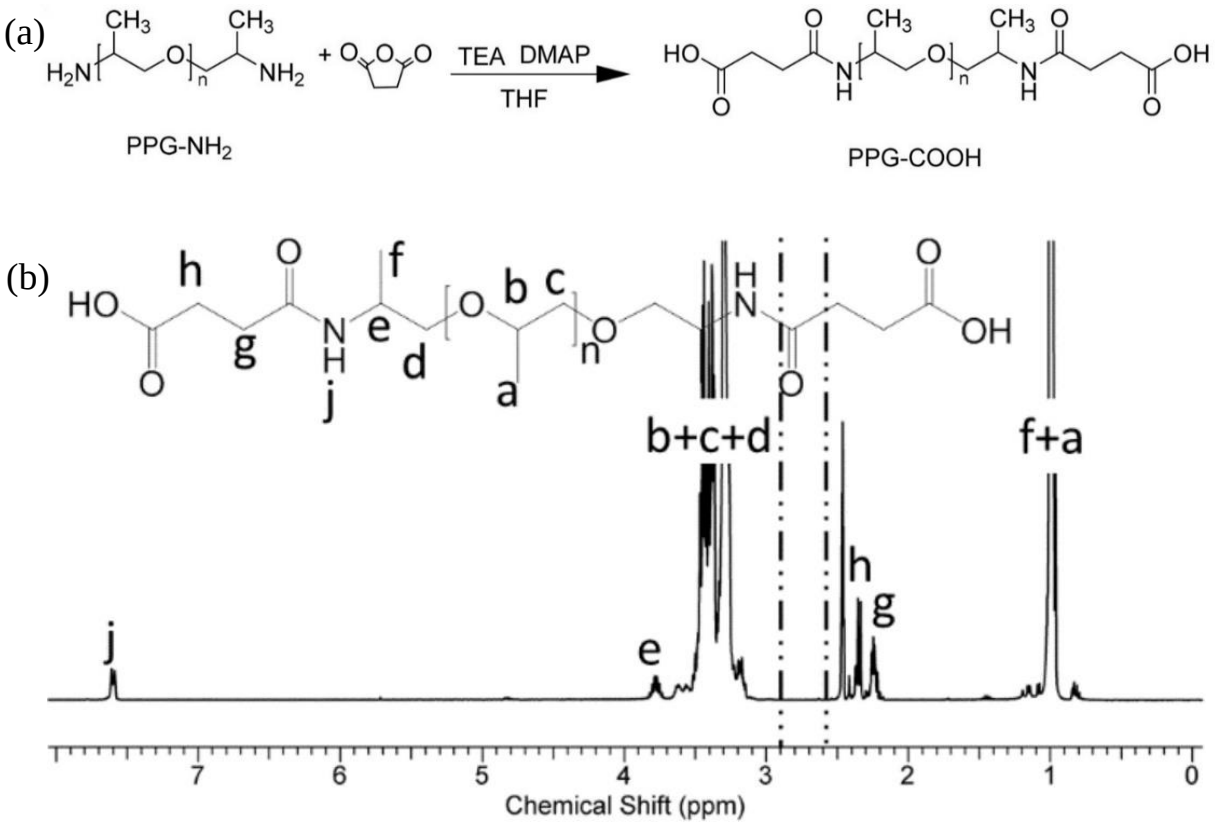

Figure 3.3(a) Synthesis of carboxylic acid-terminated polypropylene glycol (PPG-COOH) from amine-terminated polypropylene glycol (PPG-NH_2). (b) ^{1}H NMR spectra of PPG-COOH.

3.3.2 Broadband dielectric spectroscopy (BDS)

Broadband dielectric spectroscopy (BDS) measurements were conducted with an Alpha-A impedance analyzer connected to a Quatro Cryosystem temperature controller (both from Novocontrol) in a frequency range from 10^{-2} – 10^{7} Hz. Thermalized in a dry nitrogen flow, the maximum permitted deviation in temperature was 0.2 K with an equilibration time of at least 10 minutes before recording each spectrum. Prior to the measurement, each sample was dried according to the sample protocol described for DSC measurements. All PPG associating polymers were prepared in a parallel-plate dielectric cell made of sapphire and invar steel particularly designed for the investigation of liquids[131]. The electrodes of the cell have a diameter of 12 mm and a separation of 49 µm; the capacity of the empty cell is 20 pF. The PDMS associating polymer were measured in a capacitor composed of two gold-plated electrodes of 20 mm diameter separated by a Teflon spacer of 34.4 µm thickness.

3.3.3 Rheology

Small amplitude oscillatory shear (SAOS) measurements were conducted with the strain-controlled mode of an AR2000ex rheometer (TA Instruments) in the angular frequency range of 10^{2}-10^{-1} rad/s utilizing a parallel plate geometry. Plate diameters of 4 and 8 mm were employed depending on the magnitude of the shear modulus. The gap distance between the top and bottom plate was approximately 500 µm and kept constant throughout the temperature range. Prior to the measurement each sample was dried as described for the DSC measurements. A strain sweep was conducted before each spectral sweep to determine the appropriate strain keeping the SAOS in the

linear regime. Before each scan, the samples were thermally equilibrated for 10 minutes, the maximum permitted temperature deviation was 0.2 K.

Zero shear viscosity measurements were performed with the same AR2000ex rheometer. The measurements were conducted with parallel plates of 8 mm diameter and a distance of ~800 µm. For temperatures at which the viscosity was low, i.e. $\eta_0 < 10^5$ Pa.s, the viscosity was determined by continuous ramp measurements with a shear rate ranging from $0.002s^{-1}$ to $0.1s^{-1}$. For temperatures at which the viscosity was high, i.e. $\eta_0 > 10^5$ Pa.s, the viscosity was determined from creep test with the shear stress ranging from 5 Pa to 40 Pa.

3.4 Results

3.4.1 Differential scanning calorimetry

DSC measurements were conducted on all associating polymers to acquire the glass transition temperatures (T_g) that are listed in Table 3.2. From the table, we observed that: For PDMS associating polymers, T_g is dependent strongly on the chain length of backbone with no significant dependence on the functional groups. While for PPG associating polymers, T_g indeed depends on the type of functional group. With NH_2 functional group, T_g depends little on the chain length of the backbone. With COOH functional group, T_g depends strongly on the chain length of the backbone.

Table 3.2 Degree of polymerization DP, total number-averaged MW M_n including end-groups, as well as main chain M_n (excluding end-groups), number of Kuhn segments N, and glass transition temperature T_g of the studied polymers.

Polymer	***DP***	***M*n [g/mol] (total)**	***M*n [g/mol] (main chain)**	***N***	***T*g (DSC)**
PPG-NH_2-6	6	480	348	3	194
PPG-NH_2-33	33	2046	1914	17	199
PPG-NH_2-67	67	4018	3886	35	199
PPG-COOH-6	6	680	348	3	246
PPG-COOH-33	33	2246	1914	17	218
PPG-COOH-67	67	4218	3886	35	207
PDMS-NH_2-22	22	1738	1622	7	153
PDMS-NH_2-50	50	3816	3700	16	150
PDMS-NH_2-74	74	5592	5476	23	149
PDMS-S-COOH-13	13	1228	962	4	168
PDMS-S-COOH-83	83	6408	6142	26	149

3.4.2 Dielectric spectroscopy

3.4.2.1 Dielectric derivative analysis results for telechelic associating polymers with PPG backbone

We did not initially see clearly the α^* process from ε" spectra for PPG-NH_2. This was likely related to a rather weak change of the dipole moment for NH_2 dissociation in the PPG matrix. We then attempted derivative analysis on this kind of associating polymer. Through the derivative analysis, it does not shift the peaks positions, but make them narrower. Thus, it helps to resolve the strongly overlapping peaks. In Fig. 3.4, the ε" spectra and ε_{der} spectra were compared at different temperatures. Both α process and the normal mode process (marked by the dashed and dotted lines) have the same peak position in ε" spectra and ε_{der} spectra. The ε'_{der} spectra of PPG-NH_2 with DP of 6 and 67 exhibit the α*- relaxation as a shoulder of the α-relaxation and normal mode peak, respectively (Fig. 3.4 a and c). A sum of three Havriliak-Negami (HN) functions modified for the ε'_{der} spectra was used to fit these datasets in order to extract the characteristic relaxation times. However, in PPG-NH_2 with a DP of 33 (Fig. 3.4b), the α*-relaxation could probably not be resolved since it is expected to be located close to the normal mode peak.

In terms of PPG-COOH with DP of 6, dielectric derivative analysis also exhibits the α-relaxation peak which is not directly visible in ε" spectra. Thus, through the dielectric derivative analysis, τ_α and τ_α^* at different temperatures for all telechelic associating polymers with PPG backbone have been successfully acquired.

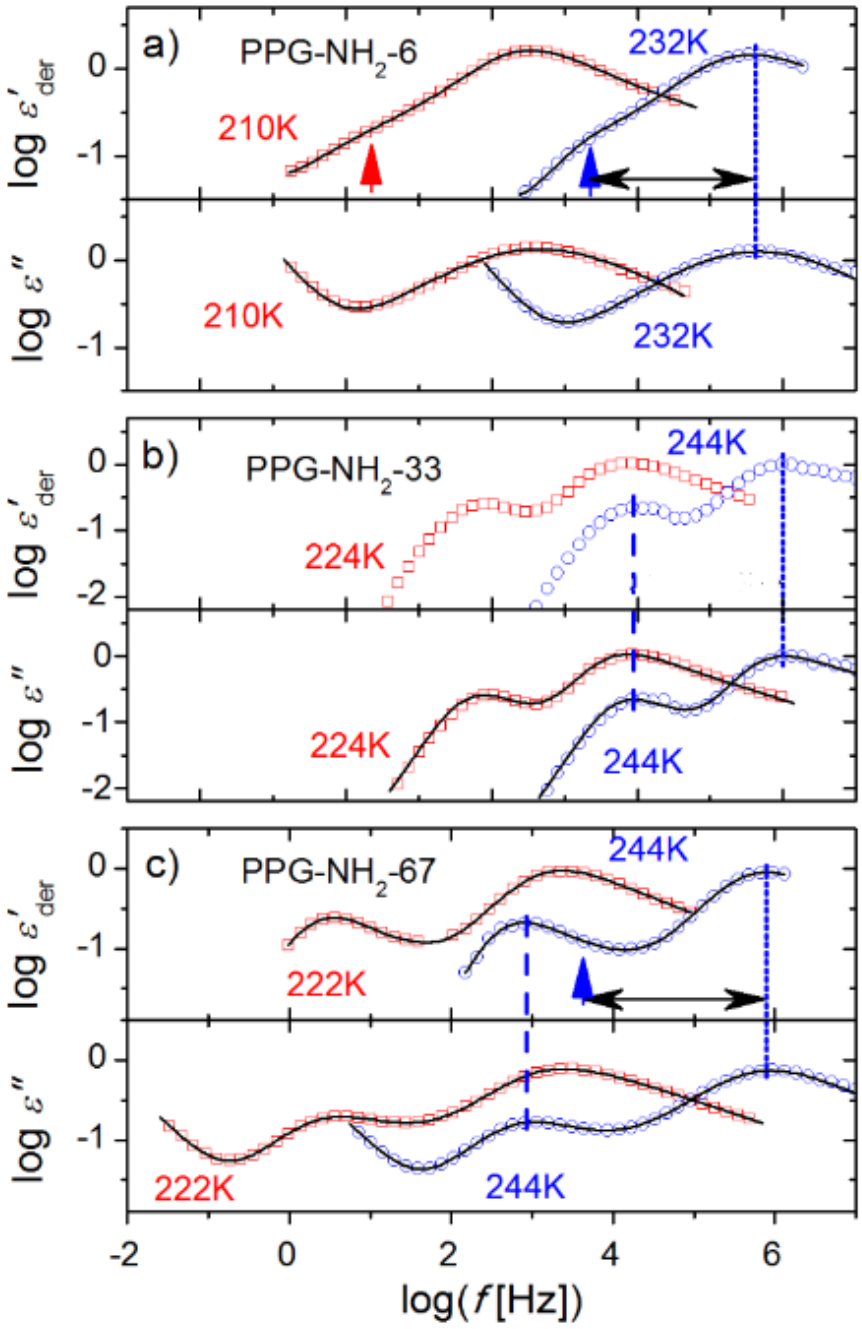

Figure 3.4 ε'_{der} and ε" spectra of PPG-NH_2 with DP of (a) 6, (b) 33, (c) 67 at different temperatures as indicated. The solid lines are fits to HN functions; the dotted and dashed vertical lines indicate the position of the α-relaxation and normal mode, respectively, for the spectrum at higher temperature; the vertical arrows highlight the position of the α*-relaxation where it can be detected. The horizontal double-arrow approximates the separation between α- and α*-relaxation.

3.4.2.2 BDS measurement result for PDMS-S-COOH

PDMS-S-COOH with DP of 13 and 83 were studied. The acquired ε'' spectra are analogous to those for PDMS-NH_2 associating polymers (Fig. 3.5). A second dielectric relaxation process is clearly visible for both samples. The second process is separated by 2-3 orders in frequency from the α process. In addition, the second process exhibits a dielectric strength which scales inversely with DP of PDMS backbone. This clearly indicates that the dielectric process is associated with the functional group. Here we assumed that the process originates from bond dissociation, and we ascribe it to α*-relaxation. Conductivity contribution can be seen at low frequencies in PDMS-S-COOH with DP of 13 at high T, whereas there is no such contribution in PDMS-S-COOH with DP of 83. Instead, a third dielectric process can be seen in PDMS-S-COOH with DP of 83. The assignment of the third relaxation process is unclear and yet to be determined. It might reflect some supramolecular network, which is similar to the Debye-like process in mono-hydroxyl alcohol[132]. Using these BDS measurements of PDMS-S-COOH, τ_α and τ_α^* at different temperatures have been estimated.

3.4.3 Rheology

The shear modulus master curves and their shifting factor for PPG-NH_2 with DP of 6, 67 and PDMS-S-COOH with DP of 13, 83 are shown in Fig. 3.6. Two relaxation processes are visible in the shear modulus spectra of these telechelic associating polymers. The first process occurs at high frequencies exhibits storage modulus values between 0.1 and 1 GPa; it is assigned to the segmental relaxation. The peak position of G″ is used to determine the corresponding segmental relaxation

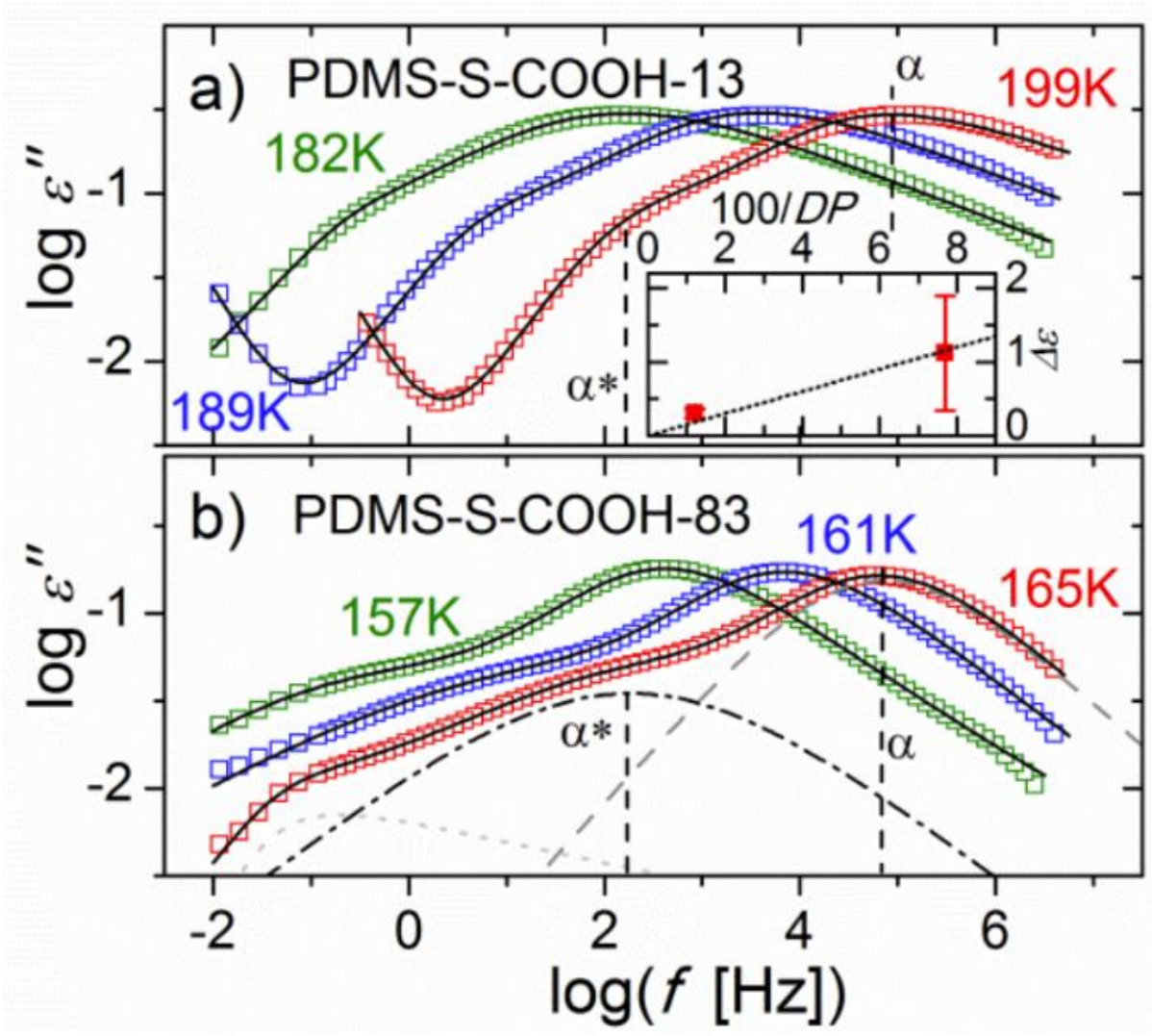

Figure 3.5 ε" spectra of PDMS-S-COOH with DP of (a) 13 and (b) 83 at different temperatures. The dielectric contributions form α process, α* process and the third process are illustrated in Fig. 3.5b. The inset shows the dielectric strength of α* process as a function of 100/DP.

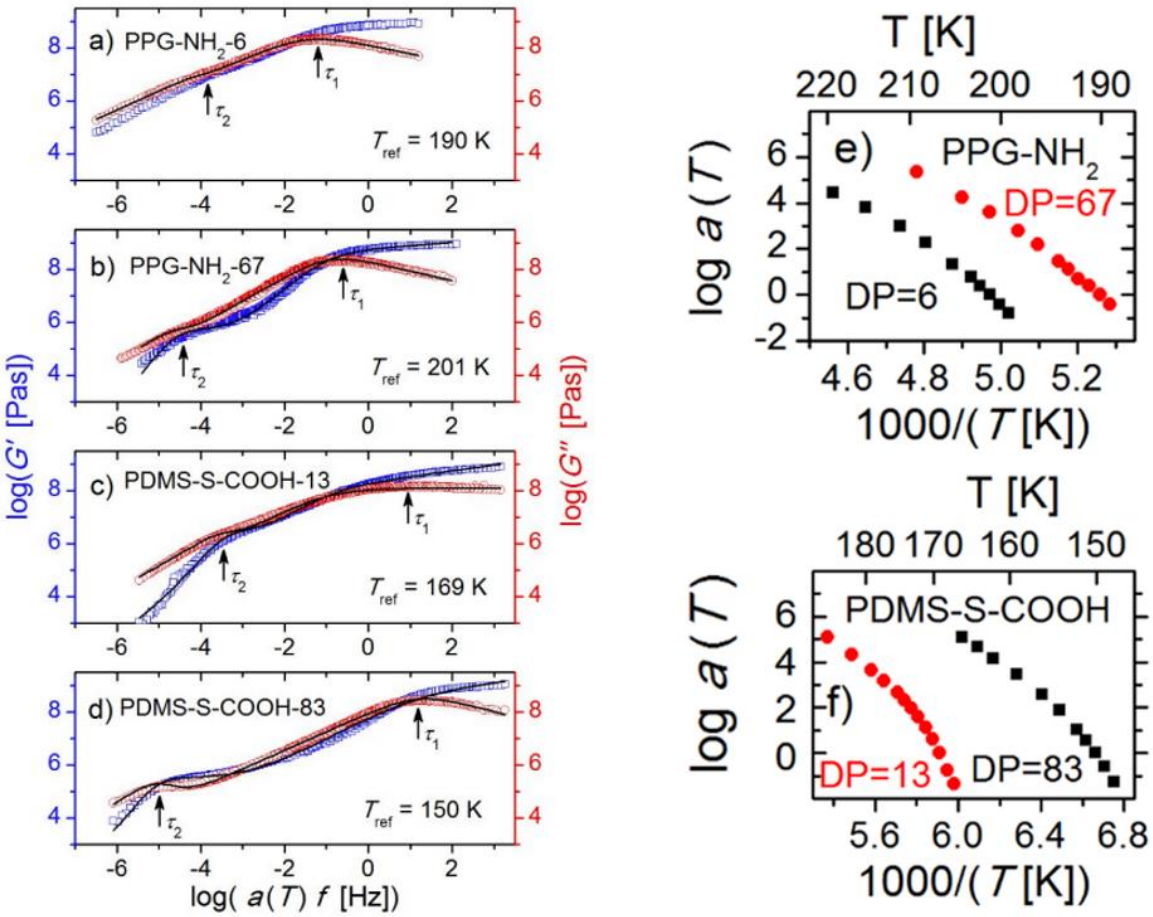

Figure 3.6 Shear modulus master curve of PPG-NH_2 with DP of (a) 6, (b) 67 and PDMS-S-COOH with DP of (c) 13, (d) 83. Their shifting factors are shown in (e) and (f), respectively.

time. The second process appears at lower frequencies. At even lower frequencies, the slopes of 2 and 1 can be seen for G' and G'' in double-logarithmic scale. Thus, the second process is ascribed to the terminal relaxation process. As a result, τ_C for all the associating polymers can be acquired through the fitting method mentioned in Chapter 2 (eq. 2.20 and eq. 2.21). In Fig. 3.6, τ_C acquired from the shear modulus spectra have been labeled as τ_2. $\tau_C(T)$ at different temperatures can be calculated using the shift factor:

$$\tau_C(T) = \frac{\tau_C(T_{ref})}{a(T)} \qquad (3.3)$$

The shear modulus master curves for PDMS-NH_2 and their shift factor are shown in Fig. 3.7. PDMS-NH_2 encounters crystallization at high temperature. Thus, part of the master curve was cut and does not show the final terminal flow very clearly. Despite this fact, we still acquired τ_C from the master curves, as is shown by the left vertical dashed line in Fig. 3.7. $\tau_C(T)$ can be calculated through the shifting factor as well. Thus, $\tau_C(T)$ at different temperatures has been acquired for all telechelic associating polymers involved in the dissertation research.

3.5 Discussion

3.5.1 Activation energy of the transient hydrogen bond with binary association

The activation energy needs to be calculated by taking the segmental relaxation into consideration. In the activation plot (Fig. 3.8), $\tau_\alpha(T)$ have been fit to the Vogel–Fulcher–Tammann (VFT) equation[133-135] which is applied to describe the temperature dependence of the segmental motion:

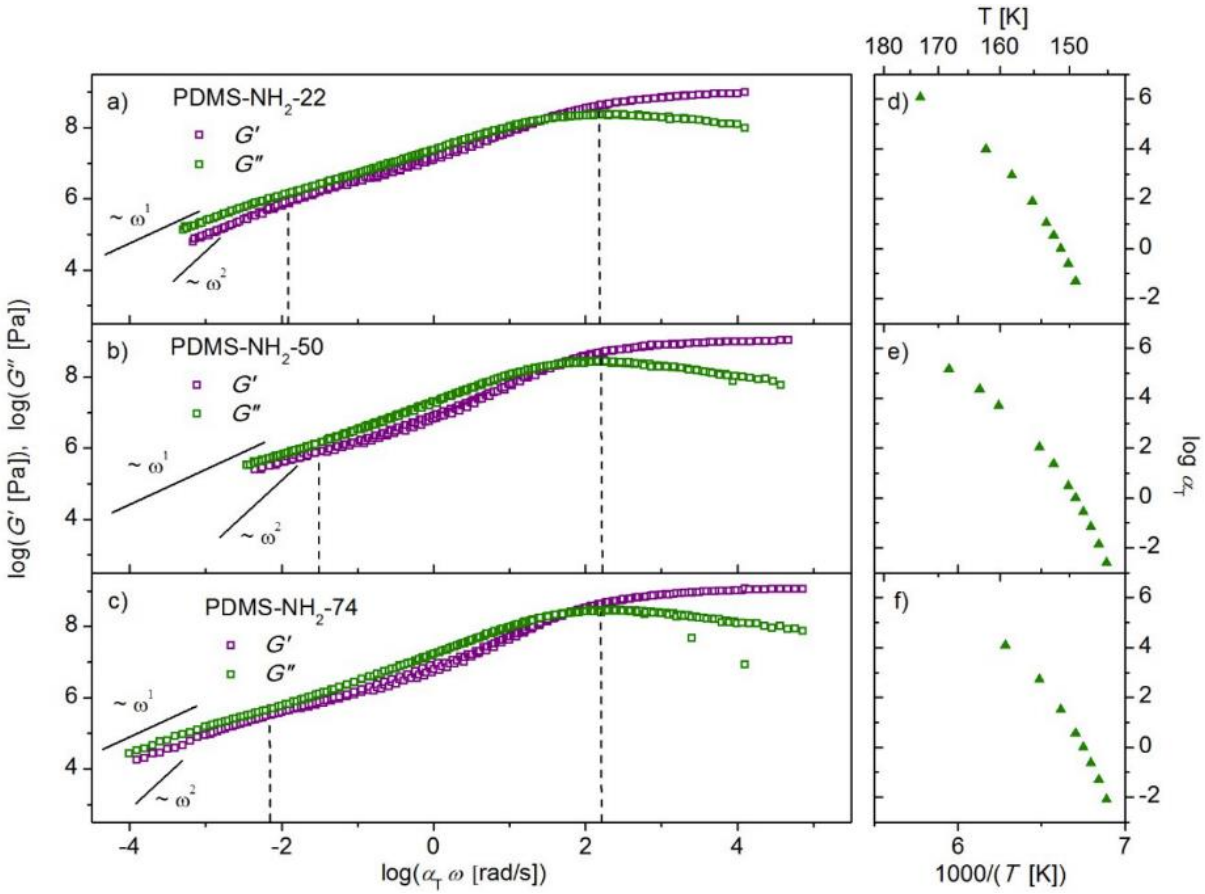

Figure 3.7 Shear modulus master curve for telechelic PDMS-NH_2 with DP of (a) 22, (b) 50 and (c) 74. Their shifting factor is shown in (d), (e) and (f) respectively.

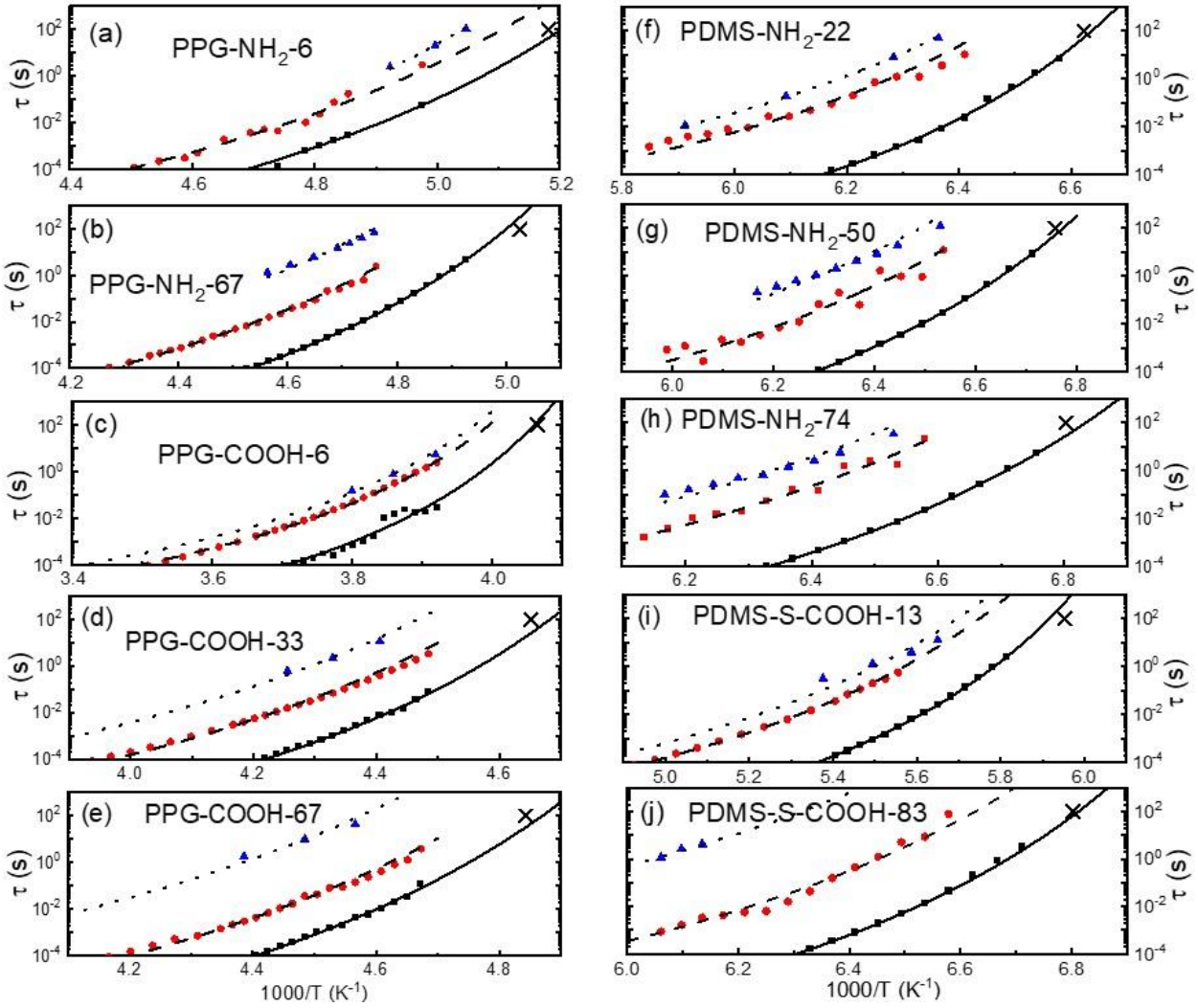

Figure 3.8 Activation plot for PPG-NH_2 with DP of (a) 6, (b) 67; PPG-COOH with DP of (c) 6, (d) 33, (e) 67; PDMS-NH_2 with DP of (f) 22, (g) 50, (h) 74; PDMS-S-COOH with DP of (i) 13, (j) 83. In each activation plot, the solid line indicates the VFT fit for $\tau_\alpha(T)$. The dashed line indicates fit through eq. 3.5. The dotted line indicates the fit through eq. 3.11. The crossover indicates the T_g measured by DSC.

$$\tau_\alpha(T) = \tau_0 \exp\left(\frac{B}{T-T_0}\right) \quad (3.4)$$

Here τ_0 is a limiting relaxation time and B and T_0 are material dependent parameters. During the fitting process, τ_0, B and T_0 were set to be free parameters. The VFT fit shows perfect agreement with measured $\tau_\alpha(T)$ (Fig. 3.8). In addition, if we extrapolate the VFT fit to 100s for each associating polymers, the correspondent temperature matches the T_g in the DSC measurements (Table 4.1 and Figure 3.8). This justifies assignment of the process in the dielectric measurements to the α relaxation (segmental relaxation).

Following these measurements, we utilized the equation which is derived from eq. 1.1 to fit $\tau_\alpha^*(T)$, which is

$$\tau_\alpha^*(T) = \tau_\alpha(\mathrm{T}) \exp\left(\frac{E_a}{RT}\right) = \tau_0 \exp\left(\frac{B}{T-T_0} + \frac{E_a}{RT}\right) \quad (3.5)$$

In this fitting process, τ_0, B and T_0 is fixed to the same parameter as was achieved from the VFT fitting process for $\tau_\alpha(T)$, and E_a is the only free fit parameter. This fitting is in good agreement with the measured $\tau_\alpha^*(T)$ (Fig. 3.8).

The obtained VFT fitting parameters for the segmental motion ($\log\tau_0$, B and T_0), as well as the activation energy for transient bond dissociation are shown in Table 3.3. The activation energy for the studied associating polymer ranges from 6 kJ/mol to 9kJ/mol. That is a reasonable hydrogen bond dissociation energy for NH_2 and COOH. In addition, the estimated E_a for the studied associating polymers is below or comparable to $2\ k_B T ln N$. According to the Bond Lifetime Renormalization model mentioned in Chapter 1, the bond dissociation energy for NH_2 and COOH is in the intermediate bond dissociation energy regime. In such case, bond lifetime

Table 3.3 VFT fitting parameters ($\log\tau_0$, B and T_0) of the α-relaxation, transient bond activation energies E_a and the value of $2k_BTlnN$ for all proposed telechelic associating polymers

Sample	$\log(\tau_0$ [s])	B [K]	T_0 [K]	E_a [kJ/mol]	$2\ k_BTlnN$ [kJ/mol]
PPG-NH_2-6	-13.2	1128	160	5.8±0.1	3.9
PPG-NH_2-67	-12.8	1022	170	8.1±0.1	12.9
PPG-COOH-6	-9.9	633	223	8.4±0.2	4.8
PPG-COOH-33	-12.6	1129	180	8.5±0.1	11.2
PPG-COOH-67	-13.9	1302	169	7.3±0.1	13.4
PDMS-NH_2-22	-12.1	516	135	9.1±0.2	5.6
PDMS-NH_2-50	-13.5	657	129	7.6±0.3	7.8
PDMS-NH_2-74	-13.8	688	127	8.3±0.2	8.8
PDMS-S-COOH-13	-11.5	700	147	8.2±0.4	4.3
PDMS-S-COOH-83	-13.6	679	128	8.1±0.2	9.2

renormalization model can be applied to understand the mechanism of bond rearrangement.

3.5.2 Experimental test of the bond lifetime renormalization model

In the activation plot (Fig. 3.8), the separation of $\tau_\alpha^*(T)$ and $\tau_C(T)$ happens in all associating polymers throughout the presented research, showing that $\tau_C(T)$ can provide an additional contribution beyond the bond dissociation energy. The separation between $\tau_\alpha^*(T)$ and $\tau_C(T)$ becomes increasingly prominent with increase in DP, i.e., with a larger number of Kuhn segments N. If we neglect the temperature dependence and just consider the ratio $\frac{\tau_C}{\tau_\alpha^*}$ averaged over the available temperature range, the data shows a clear trend of an increasing ratio $\frac{\tau_C}{\tau_\alpha^*}$ with the increase in the number of Kuhn segments (N) from less than a half decade to about 4 decades (Fig. 3.9a). In addition, we took the random walk exponent x, as is mentioned by Gold et al.[45], into consideration while analyzing the data using the bond lifetime renormalization model. The derivation of the fitting function for the telechelic associating polymers is presented below.

For telechelic associating polymers with N Kuhn segments, the total concentration of sticky groups is expressed as

$$c_t = \frac{2}{b^3 N} \tag{3.6}$$

Based on eq. 1.24, the concentration of the open sticky group at equilibrium state can be calculated as

$$c_{open} = \frac{1}{b^3\sqrt{N}} \exp\left(-\frac{E_a}{2RT}\right) \tag{3.7}$$

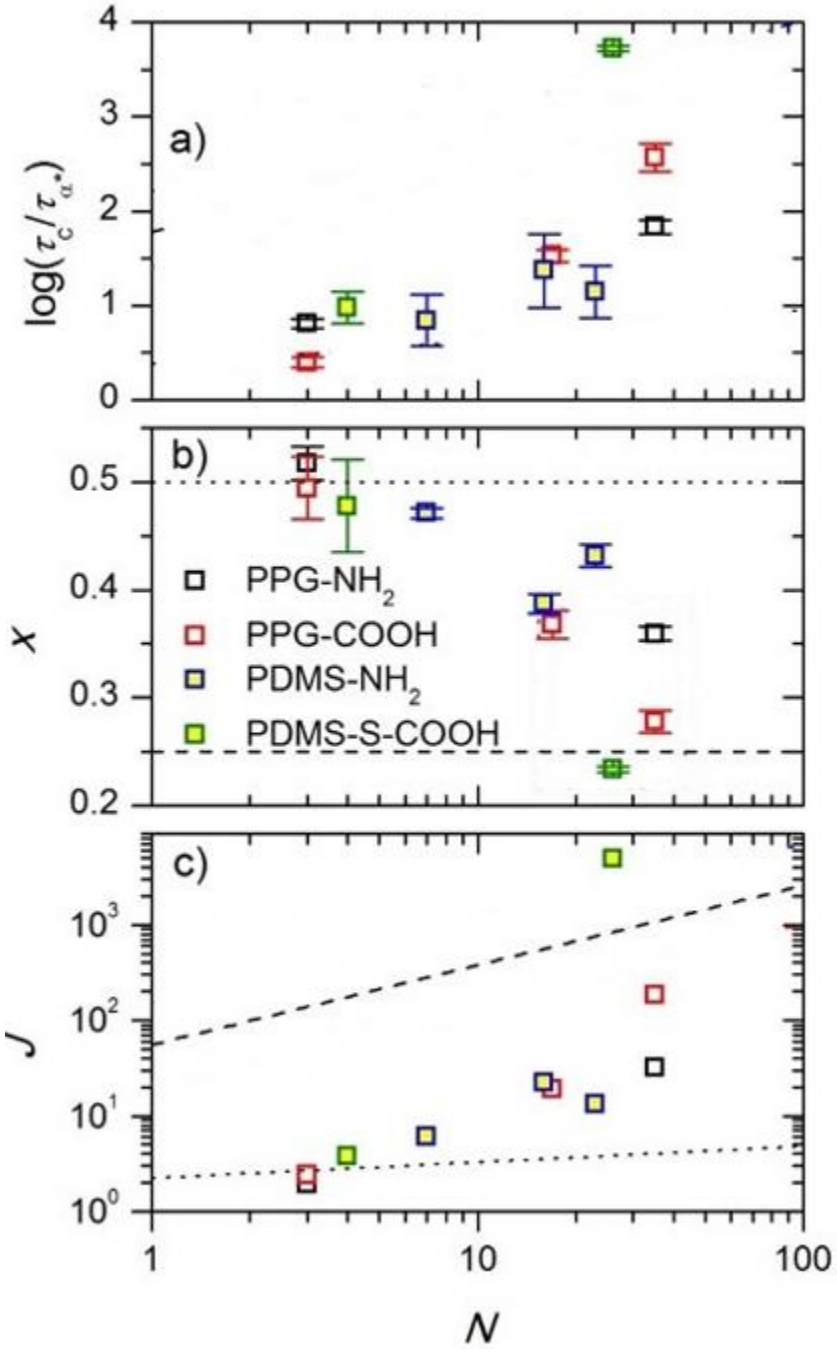

Figure 3.9 (a) Ratio as a function of number of Kuhn segments (N) of the main chain. (b) Random walk exponent x as a function of N. The dotted and dashed lines indicate Rouse (x=0.5) and reptation (x=0.25) dynamics, respectively. (c) Number of returns J as a function of N. The dashed and dotted lines are the predictions of the bond lifetime renormalization model according to eq. 3.10 for reptation (x = 0.25) and Rouse (x = 0.5) dynamics, respectively, using an activation energy of E_a= 8 kJ/mol and a temperature of T = 200 K.

in which E_a is the activation energy acquired from the dielectric measurement.

The distance between open stickers is calculated as

$$r_{open} \approx \left(c_{open}\right)^{-\frac{1}{3}} = b\sqrt[6]{N}\exp\left(\frac{E_a}{6RT}\right) \quad (3.8)$$

Then based on the diffusion function (eq. 1.31), τ_{open} can be calculated as

$$\tau_{open} = \tau_\alpha\left(\frac{r_{open}}{b}\right)^{\frac{2}{x}} \quad (3.9)$$

Based on eq. 1.30, the number of returns can be calculated as

$$J = \frac{\frac{\tau_{open}}{\tau_\alpha}}{\left(\frac{r_{open}}{b}\right)^3} = \left[N\exp\left(\frac{E_a}{RT}\right)\right]^{\left(\frac{1}{3x}-\frac{1}{2}\right)} \quad (3.10)$$

Thus, the normalized bond lifetime, namely $\tau_C(T)$, can be expressed and fit as

$$\tau_C(T) = \tau_b^{renm}(T) = J\tau_\alpha^*(T) + \tau_{open} = \tau_\alpha(T)N^{\frac{1}{3x}}\exp\left(\frac{E_a}{3xRT}\right)\left[N^{-\frac{1}{2}}\exp\left(\frac{E_a}{2RT}\right)+1\right] \quad (3.11)$$

To verify whether the experimentally observed separation between rheological and dielectric relaxation times can be explained by the bond lifetime renormalization model, $\tau_C(T)$ was fit to the eq. 3.11 with fixed $\tau_\alpha(T)$ and fixed E_a. The only free fitting parameter is the random walk exponent x. The random walk exponent x, obtained from the fit, exhibits a pronounced dependence on the chain length (Fig. 3.9b): in PPG-COOH with a DP of 6, one of the shortest investigated chains, it has a value of 0.49 which indicates Rouse dynamics. This decreases with an increasing number of Kuhn segments until it reaches 0.23 in PDMS-S-COOH-83, the longest investigated polymer. The latter value is close to 0.25, characteristic of reptation dynamics[136].

The decrease of the value x reflects a transition from Rouse dynamics to Reptation dynamics with an increase in the chain length.

With the values of E_a and x obtained, the number of returns J can be calculated through eq. 3.10. With a molecular weight increase from 400 to 6000, J increases from ~3 to ~ 10^4 (Fig. 3.9c). These results clearly demonstrate that the number of returns dominates the prominent separation of the bond dissociation and bond rearrangement times. The tremendous increase was explained by what would be expected in the theory scaling, which was calculated through eq. 3.10 by assuming x=0.5 and x=0.25 for Rouse and Reptation dynamics. In addition, the calculation assumes the activation energy to E_a= 8 kJ/mol and a temperature of T = 200 K. The calculation is shown in Fig. 3.9c, which predicts the scaling J to be $J \sim N^{1/6}$ for the Rouse dynamics and on the other hand, $J \sim N^{5/6}$ in the reptation dynamics. However, this can be explained by a transition between the two regimes in which the prefactor also increases from [E_a/(6RT)] to exp[5E_a/(6RT)].

The reptation dynamics is expected to occur in entangled polymer. However, all the associating polymers in this study are lower than the entanglement molecular weight. One of the reasons for the reptation dynamic of the chain end might be that a super-chain has formed in the system. To verify this idea, we measured zero-shear viscosity of the material.

In the Rouse regime, the zero-shear viscosity varies linearly with chain length[137]. Hence, an effective molecular weight of the formed chain can be estimated based on the T_g-scaled zero-shear viscosity of a telechelic associating polymer (η_{as}) and its non-associating counterpart (η_{nonas}) with the molecular weight of M_w, i.e.,

$$M_{w,eff} = \frac{\eta_{as}}{\eta_{nonas}} M_w \quad (3.12)$$

The number of chains effectively connected together can be calculated as

$$N(\eta) = \frac{M_{w,eff}}{M_w} = \frac{\eta_{as}}{\eta_{nonas}} \quad (3.13)$$

Indeed, after being scaled by T_g, the zero-shear viscosity of the associating polymer is always several times larger than its non-associating counterparts (Fig. 3.10), indicating a longer effective super-chain. The number of chains effectively linking together for different associating polymer is shown in Table 3.4. For most of the materials, the effective molecular weight of the super-chain is still below M_C; with the exception of PPG-NH_2 with DP of 67, PPG-COOH with DP of 33 and DP of 67, and PDMS-S-COOH with DP of 83 where it is larger (Table 3.4). These samples also exhibit the smallest values of x (Fig. 3.9b) indicating reptation-like (entangled) dynamics. Thus, the transition from Rouse-like dynamics to reptation-like dynamics observed from the fit of experimental data to the bond lifetime renormalization model seems to be justified by the formation of supramolecular structures.

3.6 Conclusion

Telechelic PDMS and PPG of different molecular weight with two kinds of end groups (amide and carboxylic acid) were investigated by dielectric spectroscopy and linear shear rheology. The former method reveals the segmental motion as well as the dissociation process of the end groups, i.e. the α*-relaxation which is several orders of magnitude slower. In order to estimate the bond dissociation energy, τ_α^* needs to be normalized by τ_α. From the shear modulus spectra,

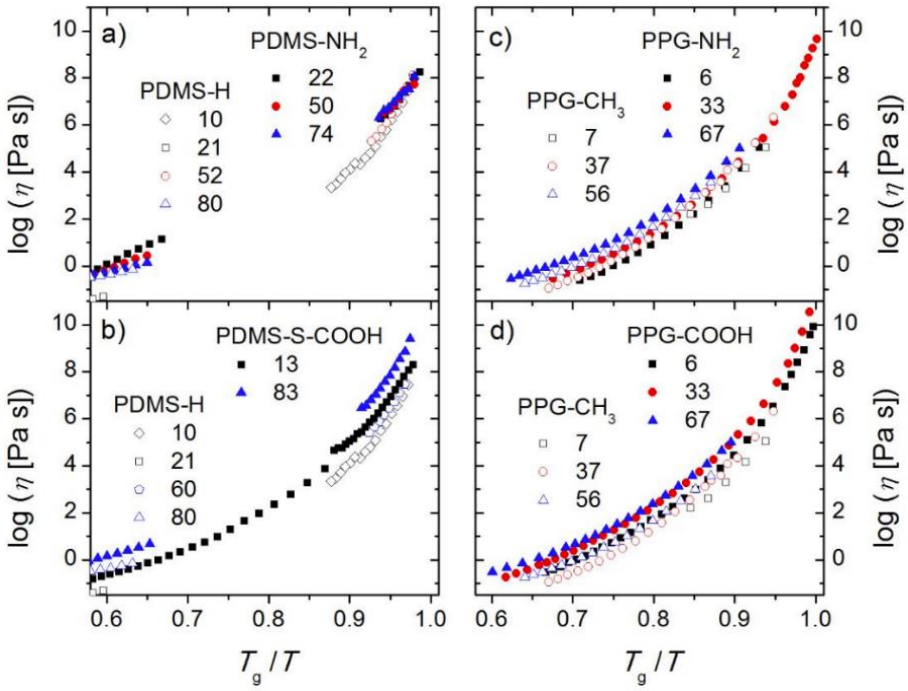

Figure 3.10 Zero-shear viscosity vs. T_g-scaled inverse temperature of (a) PDMS-NH_2 and PDMS-H, (b) PDMS-S-COOH and PDMS-H, (c) PPG-NH_2 and PPG-CH_3, and (d) PPG-COOH and PPG-CH3 of different DP as indicated by numbers.

Table 3.4 Effective super-chain molecular weight ($M_{w,eff}$) and Association number N(η) of each associating polymer

Polymer	$M_{w,eff}$ **[kg/mol]**	$N(\eta)$
PPG-NH_2-6	0.7	1.4
PPG-NH_2-33	2.9	1.4
PPG-NH_2-67	19.4	4.8
PPG-COOH-6	4.4	6.5
PPG-COOH-33	18.7	8.3
PPG-COOH-67	8.8	2.1
PDMS-NH_2-22	8.2	4.7
PDMS-NH_2-50	7.8	2.0
PDMS-NH_2-74	9.5	1.8
PDMS-S-COOH-13	3.6	2.9
PDMS-S-COOH-83	21.4	3.3

we found a terminal relaxation which indicates macroscopic flow in the system. Nevertheless, its characteristic time τ_C is much longer than both the terminal relaxation expected for chains of that length as well as the bond dissociation time τ_α^* deduced from the dielectric spectroscopy. Such a disagreement of bond dissociation time and stress relaxation is predicted by the bond lifetime renormalization model[44], which can be expanded by setting the random walk exponent *x* to be a free parameter[45].

Our detailed analysis demonstrated good agreement of the experimental data with the predictions of the bond lifetime renormalization model. The terminal relaxation time appears to be close to the dissociation time in case of strong interactions (short chains), and the difference of these two times increases strongly with MW. These results agree well with the model predictions assuming a transition to reptation-like dynamics even for the case that polymer backbone MW lower than the entanglement molecular weight (M_e). This indicates the formation of super-chains. An analysis of the viscosity measurement indeed revealed the formation of such super-chains for the samples in which the random walk exponent $x \sim 0.25$ (indicative for the reptation dynamics) was found. We would like to emphasize that a more thorough quantitative test of the bond lifetime renormalization model requires independent measurements of the exponent *x* and the number of returns *J*.

CHAPTER 4 EXPERIMENTAL TEST OF BOND LIFETIME RENORMALIZATION MODEL IN CASE OF HIGH BOND DISSOCIATION ENERGY

4.1 Introduction

Lifetime of dynamic bonds is one of the key factors controlling the viscoelastic properties and self-healing kinetics of associating polymers. If the timescale is shorter than the lifetime of the transient bonds, the network persists, whereas at longer timescales, dynamic bonds dissociate, and polymer chains become free to move leading to network rearrangement. In Chapter 3, we described that well-defined telechelic polymeric systems with hydrogen bonded functional groups indicate that the timescale of the network rearrangement and bond-dissociation timescale measured by dielectric spectroscopy are not the same. This discrepancy has been explained by bond lifetime renormalization model[44]. Based on this model, the above-mentioned timescale difference arises because dissociated sticker can reassociate with its original partner several time before attaching to a new partner. However, these systems fall into the intermediate dissociation energy category of the stickers, $k_BTlnN < E_a < 2k_BTlnN$, where N denotes the number of Kuhn segments and E_a denotes the dissociation energy of the sticker. In this regime of dissociation energy, the bond lifetime is relatively short and as a result, there are plenty of open stickers in the volume pervaded by the dangling chain. Open stickers follow a compact space exploration via sub-diffusive Rouse motion resulting in the bond formation with the same partner repeatedly. In other words, the diffusion time to find another sticker is the major limiting time of network

rearrangement. On the other hand, this situation changes when the interaction energy $E_a > 2k_BTlnN$. With higher bond strength, most of the stickers are in a bonded state for a much longer time and equilibrium concentration of open stickers are very low. In such case, sticker diffusion time is much faster than the bond dissociation time so that the bond dissociation time becomes the determinant factor. Thus, bond lifetime renormalization model predicts the same bond dissociation time and network rearrangement time. However, this model prediction has not been experimentally tested yet.

In this study, we tested the bond lifetime renormalization model with much higher bond dissociation energy ($E_a > 2k_BTlnN$) through the urea functionalized telechelic PDMS (PDMS-U). Indeed, the comparison of the dielectric and rheology data revealed that characteristic relaxation time for bond dissociation and terminal relaxation are the same for urea functionalized telechelic PDMS, verifying the model prediction. In addition, rheological measurement indicates the formation of a supramolecular chain in these polymers, which is much longer than that mentioned in Chapter 3 for systems with intermediate dissociation energy. Moreover, an interesting Debye-like process is found for the bond dissociation process in the dielectric spectra of PDMS-U samples.

4.2 Materials

PDMS-U was synthesized from PDMS-NH_2 with DP 22 and DP 50, which was mentioned in Chapter 4, and react with ethyl isocyanate. The synthesis route is shown in Fig. 4.1a. ^{1}H NMR results are shown in Fig. 4.1b. The peaks in the NMR spectra (labeled from a to f) indicate the different organic groups (labeled from a to f) on the chemical structure. The degree of

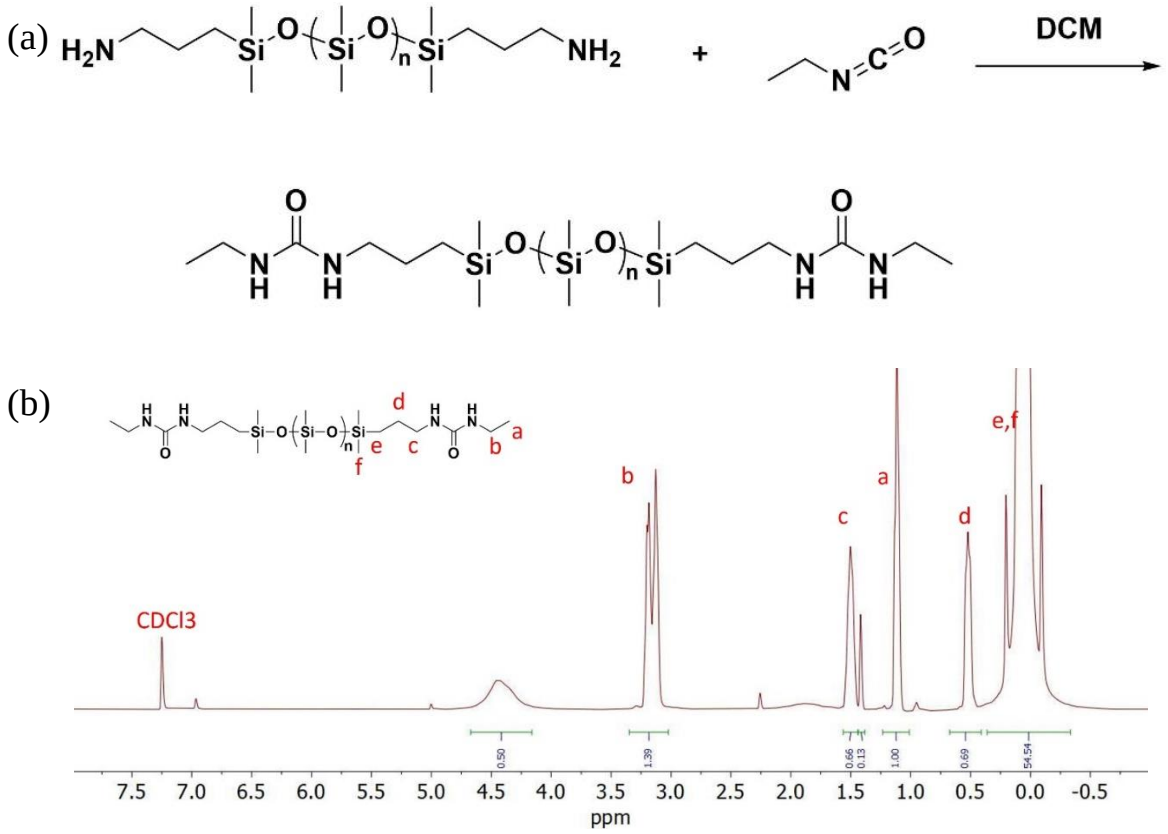

Figure 4.1(a) Synthesis of single urea terminated polydimethylsiloxane (PDMS-U) from amine-terminated polydimethylsiloxane (PPG-NH_2). (b) ^{1}H NMR spectra of PDMS-U.

polymerization, number of Kuhn segments and the actual molecular weight for each PDMS-U associating polymer is shown in the Table 4.1.

4.3 Methods

4.3.1 Differential scanning calorimetry (DSC)

Differential scanning calorimetry (DSC) measurements was employed to probe the glass transition temperature (T_g) of PDMS-U using a Q2500 DSC equipment from TA Instruments. The samples were dried in a vacuum oven at 333 K overnight before being placed into DSC pans. The samples were first equilibrated isothermally at 373 K for 5 minutes to remove the thermal history before being quenched to 113 K (to avoid crystallization). After equilibration for 5 minutes, the samples were heated up to 323 K with a rate of 10 K/min. This procedure was repeated twice for each sample to ensure repeatability.

4.3.2 Broadband Dielectric Spectroscopy (BDS)

Broadband Dielectric Spectroscopy (BDS) in the frequency range from 10^{-2} to 10^{6} Hz were measured utilizing a Novocontrol system that includes an Alpha-A impedance analyzer and a Quatro Cryosystem temperature control unit. DP 19 and DP 50 PDMS-U were placed into a parallel-plate dielectric cell made of sapphire and invar steel with an electrode diameter of 10 mm, and capacitance 3.3 pF with an electrode separation of 210 μm. To prevent crystallization, all samples were quenched from room temperature to about 113 K and reheated to 10 K below

Table 4.1 The degree of polymerization (DP), number of Kuhn segments (N) and the actual molecular weight (M_n) for each PDMS-U associating polymer

Material	DP	N	M_n [g/mol]
PDMS-U-22	22	7	1744
PDMS-U-50	50	16	3816

the T_g before the measurements. All the spectra were measured on heating. After each temperature increase, the samples were equilibrated for 10 min to reach thermal stabilization within 0.1 K.

4.3.3 Shear rheology

Small amplitude oscillatory shear (SAOS) measurements were conducted with the strain-controlled mode of an AR2000ex rheometer (TA Instruments) in the angular frequency range of 10^2–10^{-1} rad s^{-1} utilizing a parallel plate geometry. Plate diameters of 4 and 8 mm were employed depending on the magnitude of the shear modulus. The gap distance between the top and bottom plate was approximately 500 μm and kept constant throughout the temperature range. Prior to the measurement, each sample was dried as described for the DSC measurements. A strain sweep was conducted before each frequency sweep to determine the appropriate strain keeping the SAOS in the linear regime. Before each frequency sweep, the samples were thermally equilibrated for 10 minutes, the maximum permitted temperature deviation was 0.2 K.

4.4 Results

4.4.1 Differential Scanning Calorimeters (DSC)

DSC investigation of PDMS-U showed a single step in the heat flow curve (Fig. 4.2), indicating the glass transition of PDMS segments. The T_g of the PDMS-U (DP 22) is labeled in Fig. 4.2.

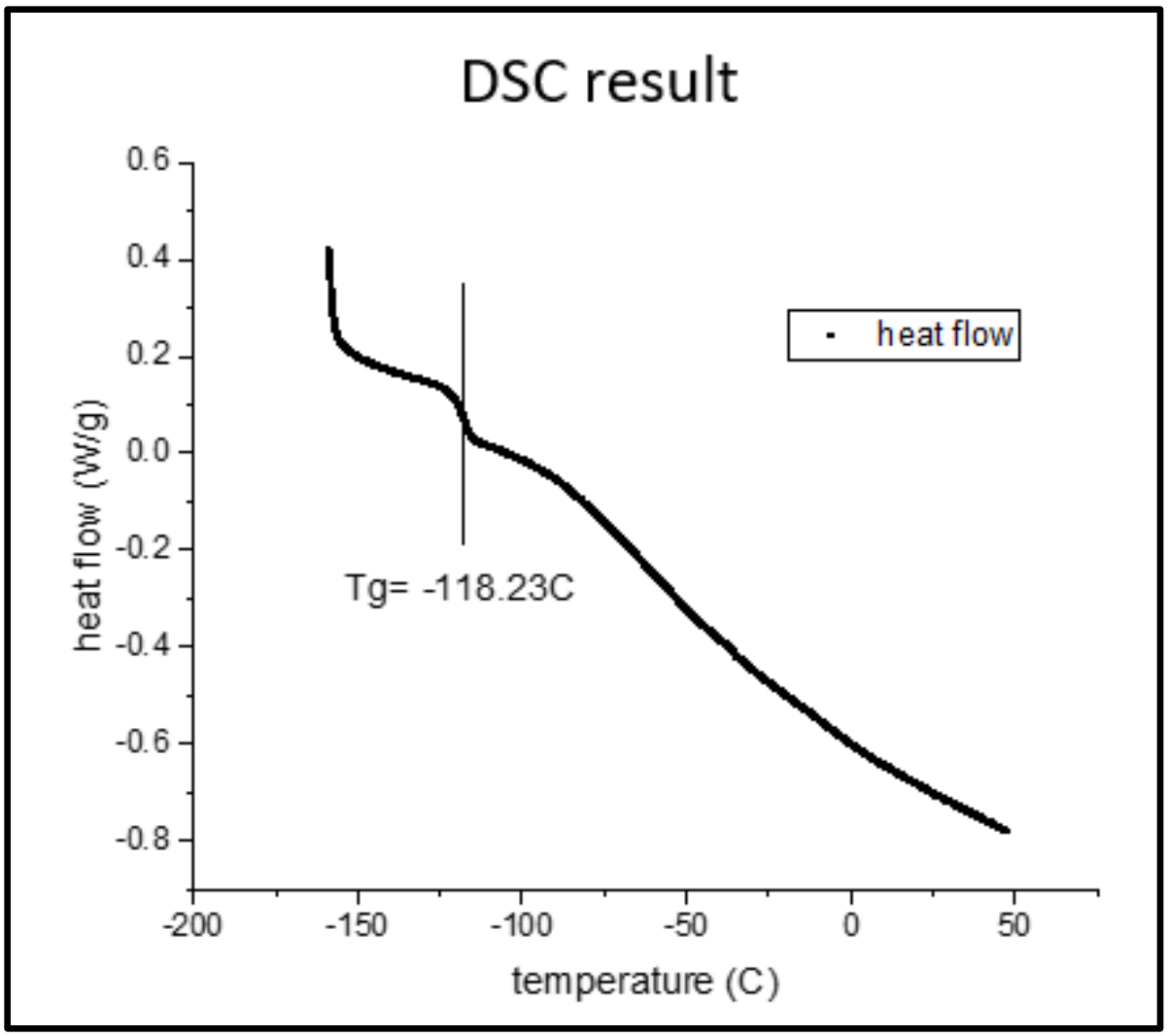

Figure 4.2 Heat flow curves of the telechelic PDMS-U DP22 sample in DSC measurements. Solid lines indicate the T_g of the PDMS matrix.

4.4.2 Broadband Dielectric Spectroscopy

Two dielectric processes were observed for PDMS-U samples. The process which appears at low temperatures is related to the segmental dynamics (also termed as α-relaxation) (Fig. 4.3a for DP 22 sample and Fig. 4.3c for DP 50 sample), and the process observed at higher temperatures might originate from the binary interaction of the sticky groups, indicated as α*-process (Fig.4.3b). For DP 22 sample and Fig. 4.3d for DP 50 sample). To fit the loss spectra and analyzing the relaxation timescales of these processes, Havrilliak-Negami (HN) function was used:

$$\varepsilon''(\upsilon) = -Im \sum_{k=1}^{n} \left\{ \frac{\Delta\varepsilon_k}{\left[1+\left(2\pi i \upsilon \tau_{HN,k}\right)^{\beta_k}\right]^{\gamma_k}} \right\} + \frac{\sigma}{2\pi\upsilon\varepsilon_0} \qquad (4.1)$$

Here ε_0 is the vacuum permittivity, $\Delta\varepsilon_k$ denotes the dielectric relaxation strength, β_k and γ_k represent the shape parameters, and τ_{HN} is HN relaxation time, k indicates number of processes. The second term in eq. 4.1 considers the conductivity (σ) contribution to the loss spectra at higher temperatures. One interesting observation is that the shape of high temperature process has Debye type ($\beta \approx \gamma \approx 1$) (Fig. 4.3e), which is prevalent in monohydroxy alcohols and some secondary amides.

This high temperature process only exists with urea groups. In addition, the comparison of the dielectric strength (Fig. 4.4) of the high temperature process in PDMS-U indicates that the dielectric strength from DP 22 sample is ~ 2 times higher than that from DP 50 sample. This verifies that the high temperature process is α*-relaxation process which indicates the urea group dissociation since the density of the associating stickers is almost 2 times higher in the DP 22 sample.

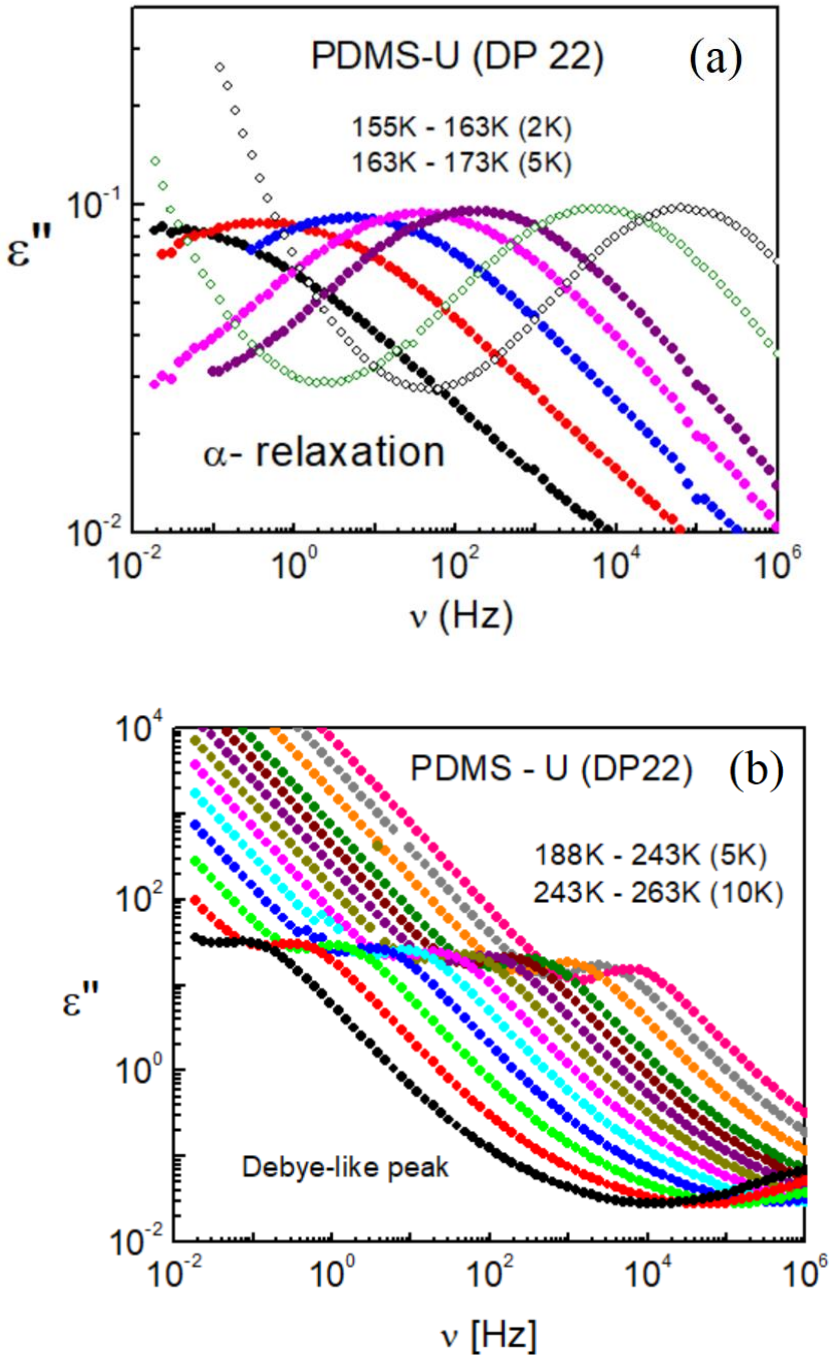

Figure 4.3 Dielectric loss spectra of PDMS-U sample with DP 22 for (a) segmental or α-relaxation regime at low temperatures (b) binary association regime at higher temperatures. Dielectric loss spectra for PDMS-U DP 50 sample (c) in the segmental relaxation regime and (d) binary interaction regime. (e) Representative spectra of the binary association process at 223K for PDMS-U with HN fit (red) line. The peak in dashed line is of Debye-like.

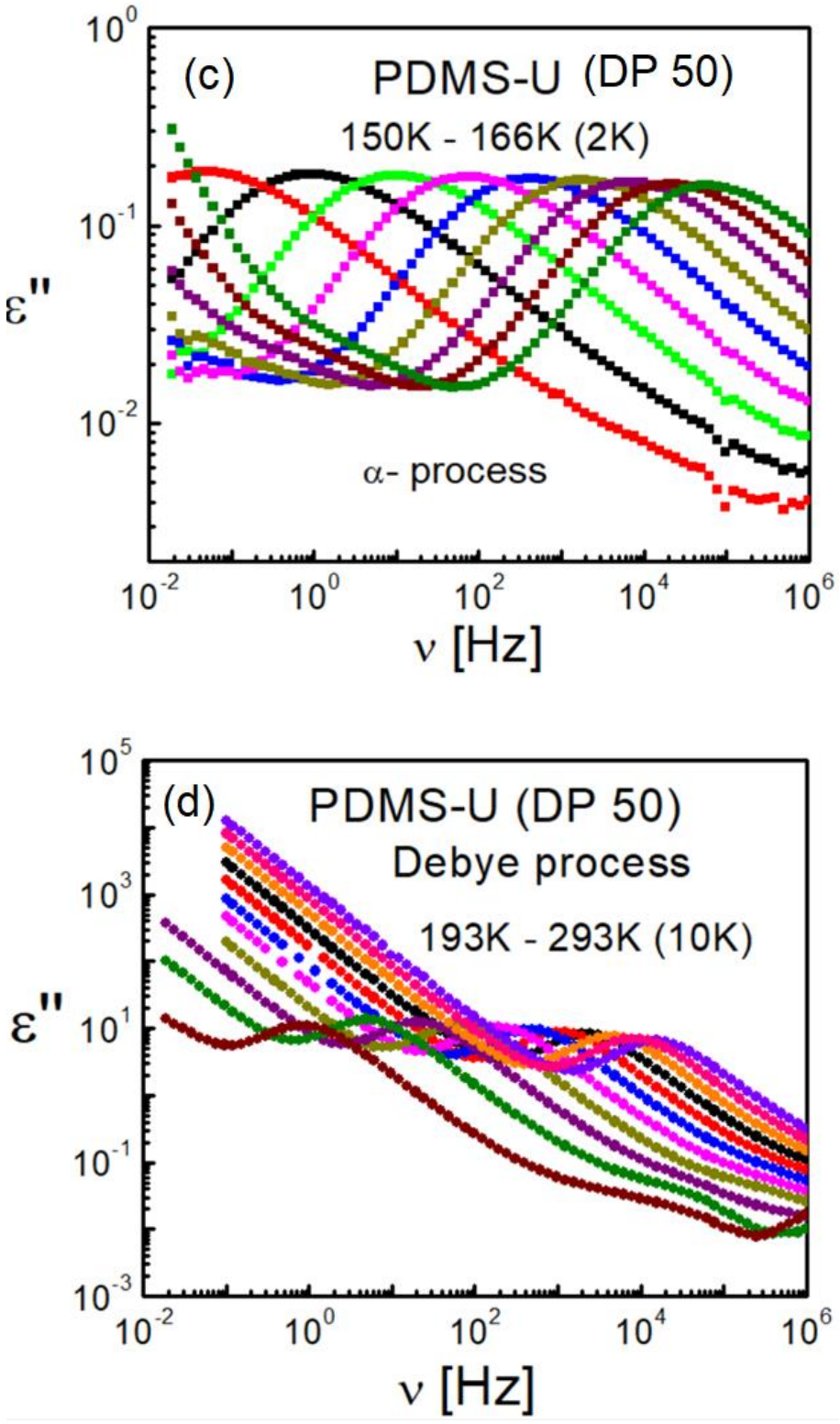

Figure 4.3 Continued

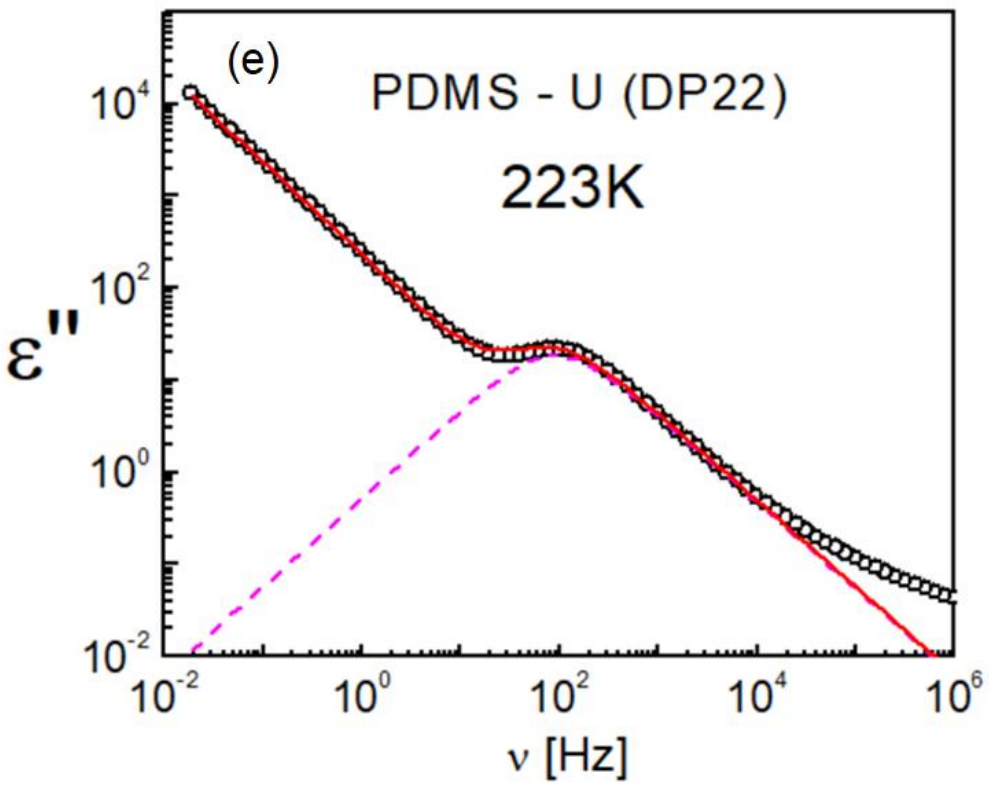

Figure 4.3 Continued

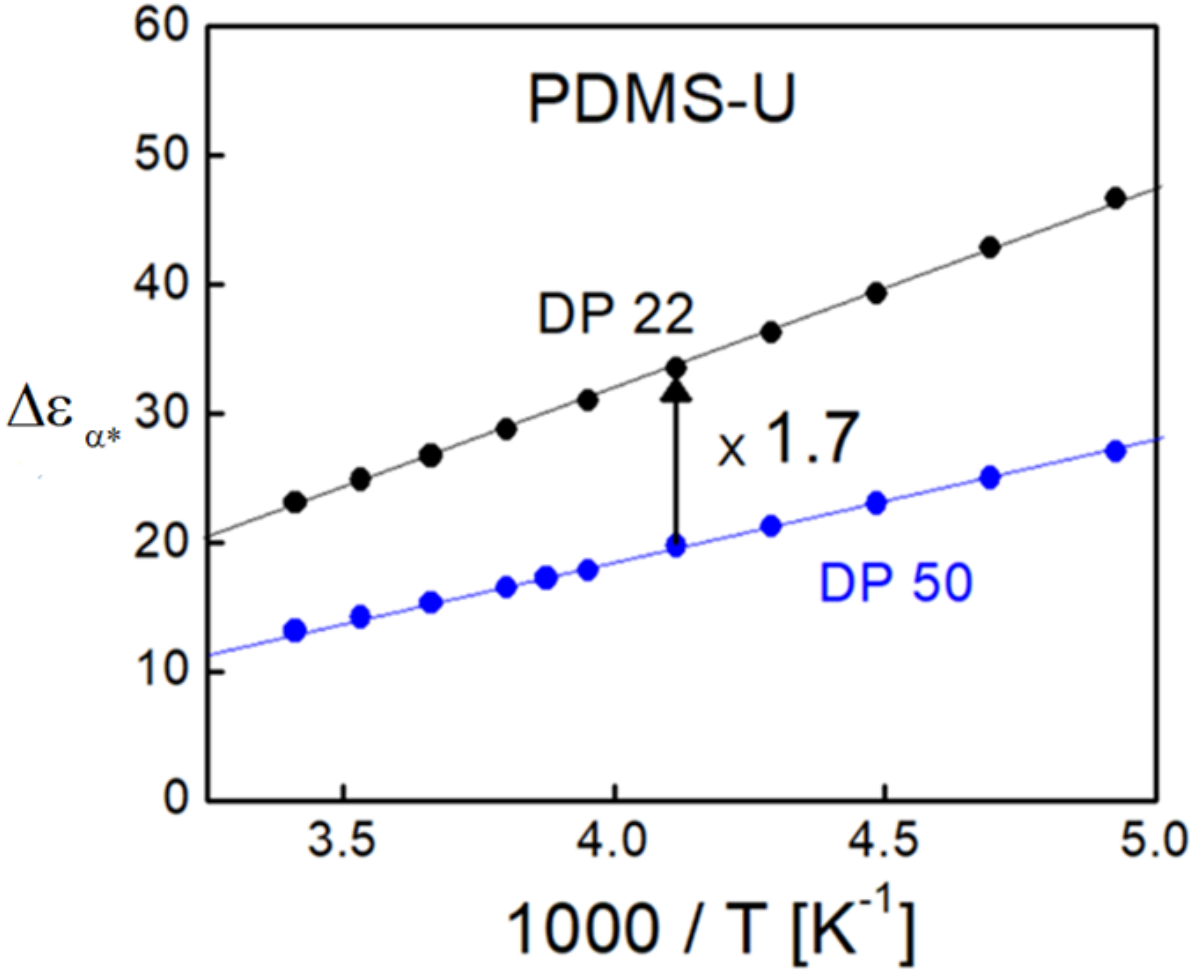

Figure 4.4 The comparison of the dielectric strength of the α*-relaxation process for PDMS-U with DP 22 (black) and DP 50 (blue). The arrow indicates higher dielectric strength for DP 22 sample comparing with DP 50 sample. The solid lines are guide for the eye only.

The relationship between the relaxation time corresponding to the peak position (τ_{max}) with τ_{HN} is as follows:

$$\tau_{max} = \tau_{HN}\left[\sin\left(\frac{\beta\pi}{2+2\gamma}\right)\right]^{-\frac{1}{\beta}}\left[\sin\left(\frac{\beta\gamma\pi}{2+2\gamma}\right)\right]^{\frac{1}{\beta}} \qquad (4.2)$$

τ_{max} is usually used as the characteristic relaxation time for both α and α*-relaxation process acquired from dielectric spectroscopy, namely τ_α and τ_α^*. From the temperature dependence of τ_α and τ_α^* (Fig. 4.5), it is possible to estimate the activation energy E_a required to dissociate the urea bond. The same method used in the last chapter was used here to estimate the bond dissociation energy, i.e., $\tau_\alpha(T)$ have been fit through the Vogel– Fulcher–Tammann (VFT) equation (eq. 4.3) and $\tau_\alpha^*(T)$ has been analyzed by taking the segmental relaxation process into account (eq. 4.4):

$$\tau_\alpha(T) = \tau_0 \exp\left(\frac{B}{T-T_0}\right) \qquad (4.3)$$

$$\tau_\alpha^*(T) = \tau_\alpha(\mathrm{T}) \exp\left(\frac{E_a}{RT}\right) = \tau_0 \exp\left(\frac{B}{T-T_0} + \frac{E_a}{RT}\right) \qquad (4.4)$$

The values of the VFT fitting parameters (including τ_0, B and T_0) and activation energies of α*-processes in the investigated PDMS-U samples are shown in Table 4.2. In addition, if we extrapolate the VFT fit to 100s for DP 22 PDMS-U, the correspondent temperature matches the T_g in the DSC measurements (Figure 4.5a). This justifies assignment of the low temperature process in the dielectric measurements to the α relaxation (segmental relaxation).

For both PDMS-U samples, E_a is approximately ~30 kJ/mol (Table 4.2), which is similar to the reported dissociation energy for urazole functionalized entangled polyisoprene samples (28

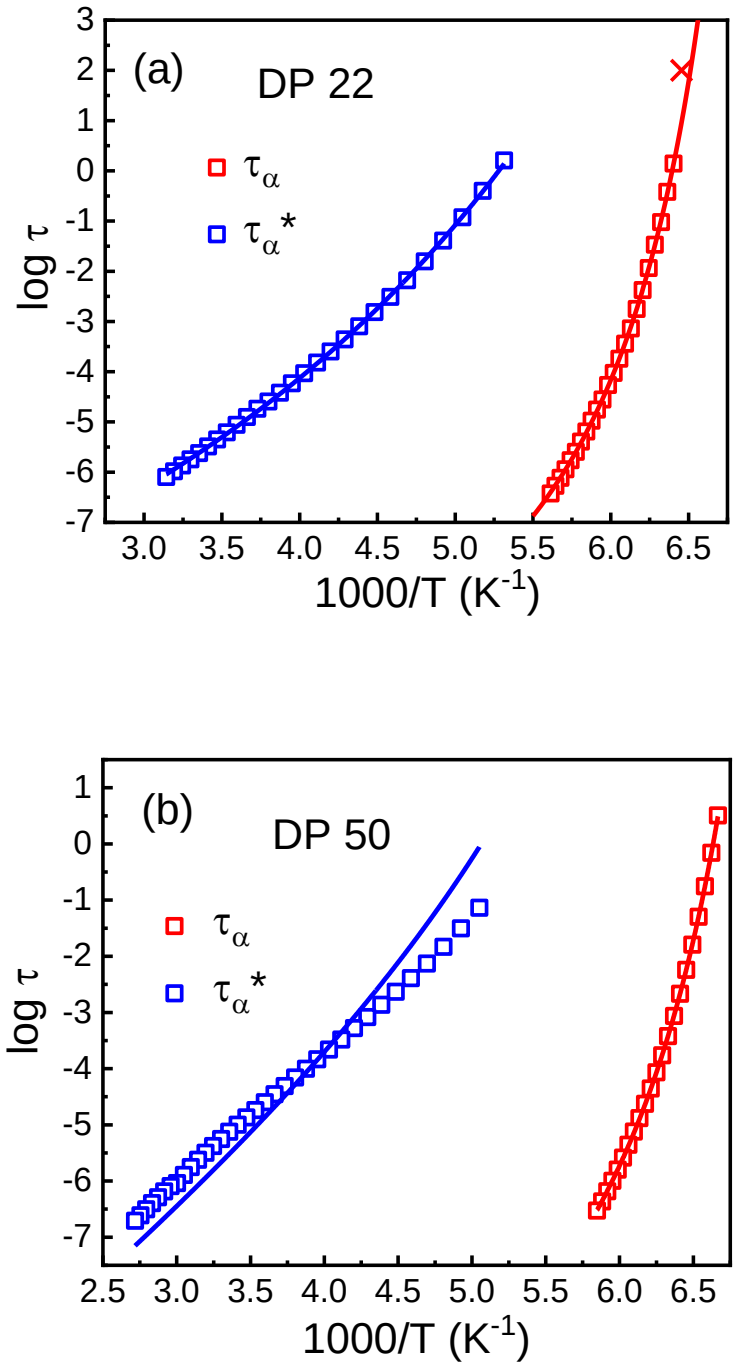

Figure 4.5 Temperature dependence of the segmental relaxation process (red), α*-relaxation process (blue) for PDMS-U sample with (a) DP 22 and (b) DP 50. The crossover indicates the T_g measured by DSC.

Table 4.2 VFT fitting parameters ($\log\tau_0$, B and T_0) of the α-relaxation, Transient bond activation energies E_a and the value of $2k_BTlnN$ for PDMS-U samples.

Sample	$\log(\tau_0$ [s])	B [K]	T_0 [K]	E_a (kJ/mol)	$2k_BTlnN$ (kJ/mol)
PDMS-U-22	-12.3	571	136	28.5±0.1	5.6
PDMS-U-50	-13.2	634	130	34.6±0.4	7.7

kJ/mol)[45] (Fig. 4.6a). The dynamic bonds formed by both Urazole and Urea consists of 2 hydrogen bonds (Fig. 4.6), implying that they should have the similar bond dissociation energy.

4.4.3 Shear rheology

Assuming time-temperature superposition, master curves are created by horizontal shifting of shear modulus spectra measured at several temperatures (Fig. 4.7a). The shifting factor is shown in Fig. 4.7b. The process at high frequency corresponds to the segmental relaxation (storage modulus ~ 1 GPa). At the lowest frequencies, an additional process appears with the distinctive slopes of 2 and 1 in G' and G" (in double-logarithmic representation) respectively. This is a typical terminal relaxation process, which indicates macroscopic network rearrangement in the system. The characteristic time for the terminal relaxation (τ_C) is estimated based on the crossover of G' and G". In addition, we observed a rubbery plateau between these two processes with the modulus value ~1 MPa, which is unusual for polymer with molecular weight lower than the entangled molecular weight. This indicates the formation of a long chain supramolecular polymer which is associated via transient hydrogen bonds between functional urea moieties. To estimate the length of these supramolecular chains, zero shear viscosities for both DP 22 and DP 50 were compared with the non-associating polymer chains (Fig. 4.7c). The viscosity measurement result was normalized by T_g of these 2 associating polymers. Results indicate that after the temperature was normalized by T_g, two associating polymer samples have the identical viscosity vs T_g/T, which is much higher than the viscosity of the non-associating counterpart. This demonstrates that the overall viscosity of these associating polymers is only governed by T_g, implying that they have the same effective chain length which is much higher than that of a

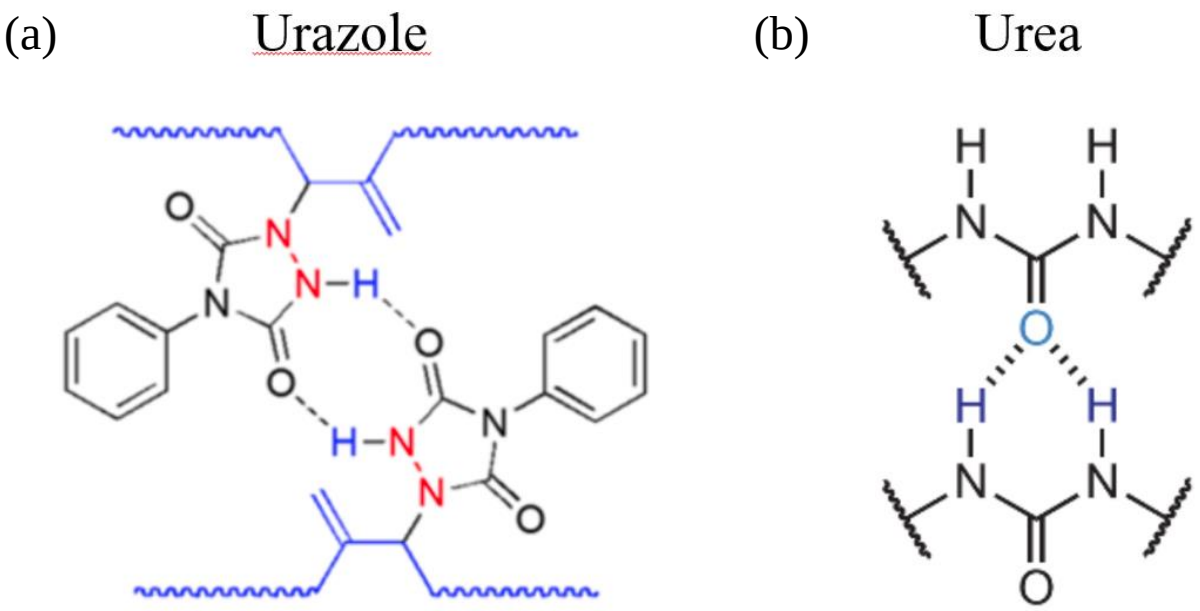

Figure 4.6 Comparison of hydrogen bond formed by (a) Urazole groups and (b) urea groups.

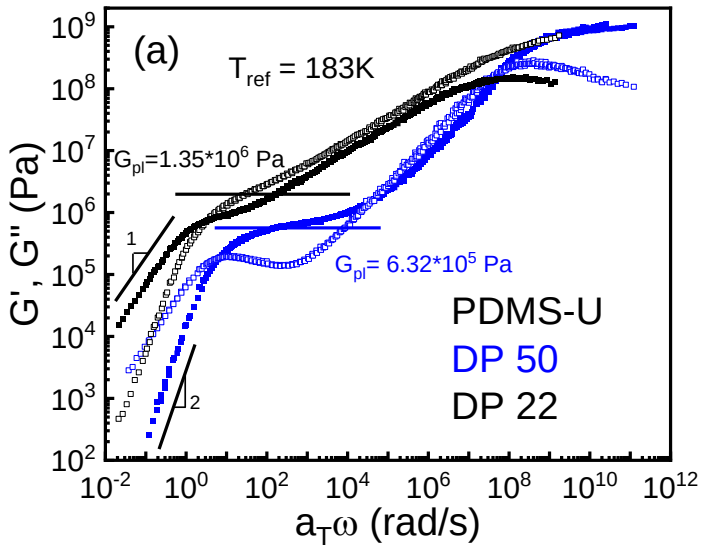

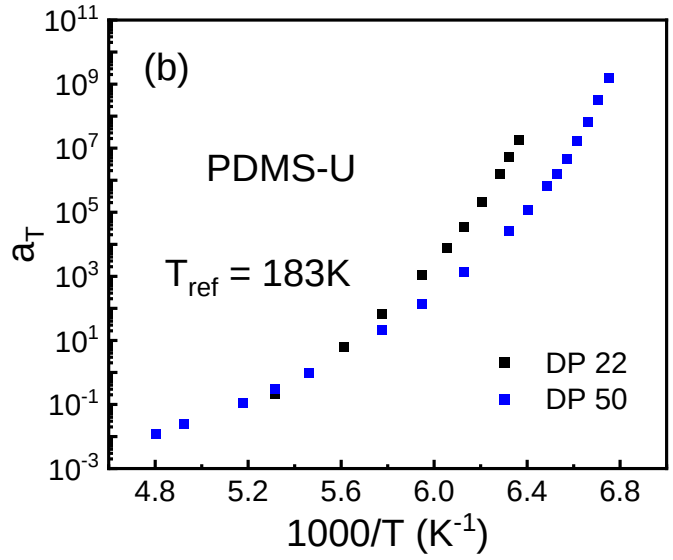

Figure 4.7(a) Shear modulus master curves for PDMS-U sample with DP 50 (blue) and DP 22 (black) against the radial frequency at a reference temperature of 183K. The solid symbols correspond to G', while the open symbols indicate the G" spectra. The plateau modulus level, G_{PL}, are shown with the solid lines. (b) Temperature dependence of horizontal shifting factor for both DP 50 (blue) and DP 22 (black) samples. (c) Zero-shear viscosity vs. T_g-scaled inverse temperature of PDMS-U (DP 22) (red), PDMS-U (DP 50) (blue) with its non-associated counterpart PDMS-H (black).

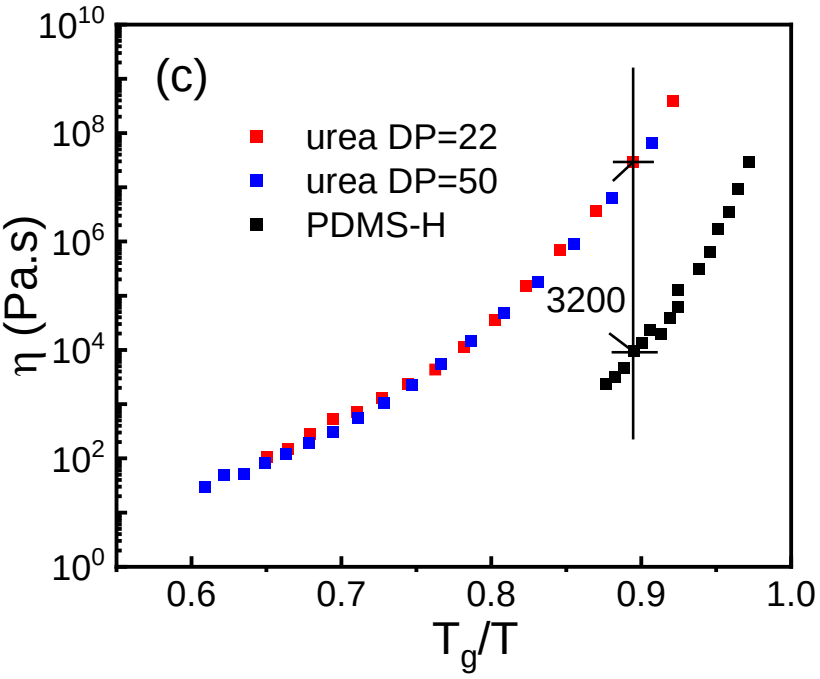

Figure 4.7 Continued

single associating polymer chain.

4.5 Discussion

To compare rheological and dielectric spectra, the latter should be converted form dielectric permittivity $\varepsilon^*(\omega)$ to the dielectric modulus $M^*(\omega)$[138, 139]:

$$M^*(\omega) = \frac{1}{\varepsilon^*(\omega)} = M'(\omega) + iM''(\omega) \qquad (4.5)$$

As an example in PDMS-U (DP 22) at 238K, M" spectra exhibit an additional dielectric process at lower frequencies (Fig. 4.8) which originates from conductivity relaxation (τ_σ)[140, 141]. We also noticed that the timescale of α* relaxation process from M" (τ_{α^*-M}) is faster than that from ε" spectra (τ_{α^*}). This is expected, as the relationship between characteristic relaxation time from M" spectra (τ_M) and ε" spectra (τ_ε) can be expressed by[142]:

$$\tau_M = \frac{\varepsilon_{inf}}{\varepsilon_s}\tau_\varepsilon \qquad (4.6)$$

in which ε_s and ε_{inf} indicates the dielectric constant in the limit of high and low frequencies. Thus, τ_{α^*-M} is shorter than τ_{α^*}, as was already emphasized in[127, 143].

In dielectric modulus spectra, the α* process has also Debye-like shape. To acquire the characteristic relaxation time, the M" spectra were fit based on two Debye-like process, one for α* relaxation process, the other for conductivity relaxation process:

$$M''(\upsilon) = Im\left\{\frac{\Delta M_{\alpha^*}}{1+2\pi i\upsilon\tau_{\alpha^*-M}} + \frac{\Delta M_\sigma}{1+2\pi i\upsilon\tau_\sigma}\right\} \qquad (4.7)$$

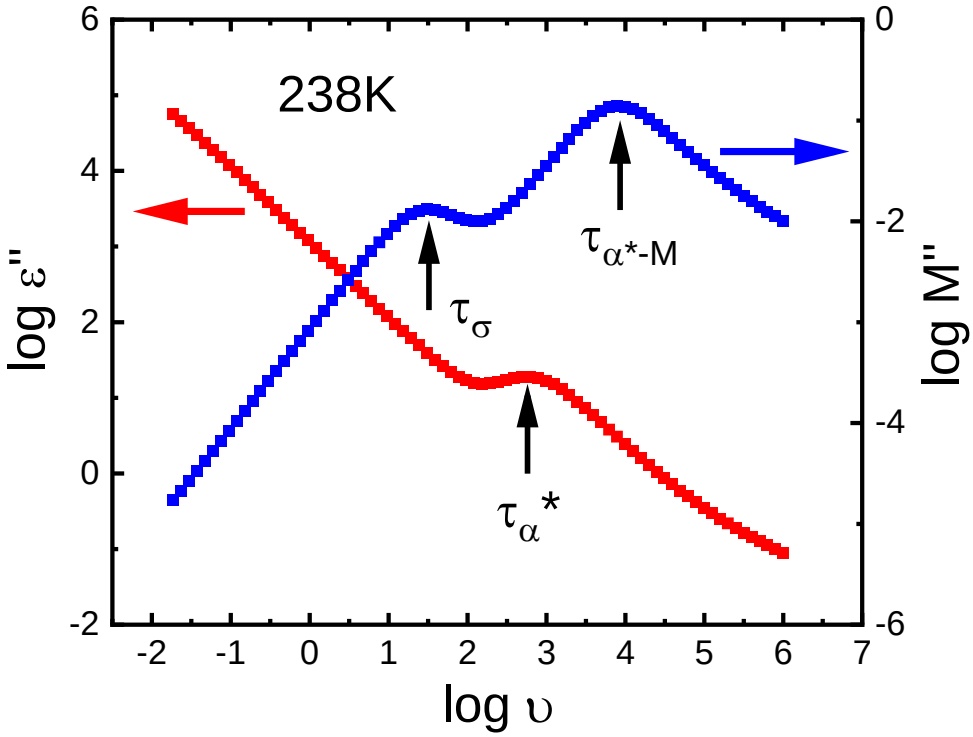

Figure 4.8 Comparison of ε" spectra and M" spectra for PDMS-U with DP 22 in which τ_{α^*}, τ_{α^*-M} and τ_σ are labeled.

in which ΔM_{α^*}, ΔM_{σ} are the "modulus strength" of α*-relaxation process and conductivity process. τ_{α^*-M}, τ_{σ} are the characteristic relaxation time for α^*-relaxation process and the conductivity relaxation process from dielectric modulus. As is shown in the activation plot, τ_{α^*-M} matches very well with τ_C from rheological measurement (Fig. 4.9). As shown in Table 4.2, for PDMS-U sample, the activation energy of the bond dissociation is substantially higher (~30 kJ/mol) than the associating polymer sample (~8 kJ/mol) mentioned in Chapter 3. Based on the obtained values of E_a, we can relate the bond strength regime for each sample considering the criterion introduced by the bond-lifetime renormalization model. The strong binary interaction regime (E_a>2k_BTlnN) is observed for both PDMS-U samples. According to this criterion, the bond lifetime renormalization model predicts the equivalence of the timescale of bond dissociation and network rearrangement, i.e., $\tau_c \approx \tau_{\alpha^*}$, which is indeed confirmed in our experiment based on the comparison of the timescales from dielectric modulus and rheological terminal relaxation timescales. Rheological measurements of the investigated associating polymers also show a rubbery plateau level in their shear modulus master curves. Usually, rubbery regime is observed for the entangled polymer system. For linear PDMS, the entangled molecular weight is ~ 10 kg/mol. However, all our investigated samples are below that threshold value. This indicates that these polymers form effective superlong polymer chains, as was mentioned in Chapter 3. From the viscosity measurements (Fig. 4.7c), it was observed that the viscosity of both PDMS-U DP 22 and PDMS-U DP 50 is almost 3200 times higher than its non-associating counterpart. The separation is much bigger that that mentioned in Chapter 3. This is reasonable because the interaction strength as well as the timescale of the interaction is much higher in urea functionalized sample than the samples studied in the Chapter 3. Based on these

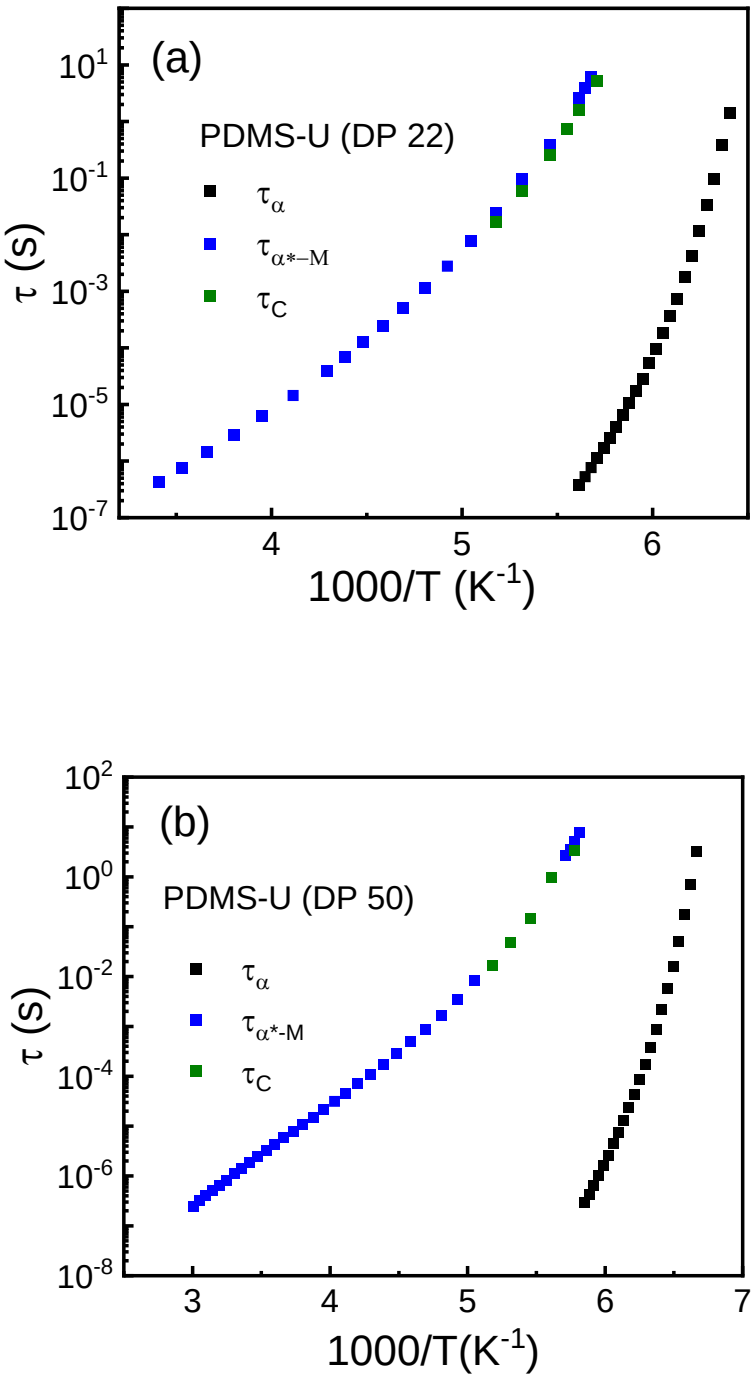

Figure 4.9 Temperature dependence of the segmental relaxation (black), α* relaxation from dielectric modulus (green) and terminal relaxation process (red) for PDMS-U sample with (a) DP 22 and (b) DP 50.

measurements, we found that due to the long-lifetime of the urea groups, PDMS-U DP 22 sample and PDMS-U DP 50 sample form supramolecular chain. The effective molecular weight is calculated based on the zero-shear viscosity. For polymers, the relationship between zero-shear viscosity and molecular weight is expressed as[39]:

$$\begin{cases} \eta_0 \sim M \ (M < 2M_e) \\ \eta_0 \sim M^{3.4} \ (M > 2M_e) \end{cases} \tag{4.8}$$

in which M_e is the entanglement molecular weight. Based on the ratio of zero-shear viscosity between these urea-terminated associating polymers and the non-associating counterpart, the effective molecular weight of both associating polymers is ~ 101 kg/mol, meaning that the number of chains effectively linking together is ~ 53 for DP 22 sample and ~26 for DP 50 sample.

The most intriguing feature of all the investigated associating polymers in this study is the presence of the dielectric Debye-like relaxation process. The Debye relaxation demonstrates the existence of only a single relaxation time, which prevails in hydrogen-bonding dissociation. Previously, Xing et al. suggested that the Debye process originates from the brush-like association of the short polymer chains, where the backbone of the brush is made of OH dipoles[25]. In addition, in a recent report based on the estimation of E_a using FT-IR and dielectric spectroscopy measurement, the authors concluded that the Debye process in 2-ethyl-1-heaxanol is related to the association/dissociation process which is like the binary interaction in our investigated samples[144]. This is in accord with our finding for PDMS-U samples. Thus, we believe that in our PDMS-U sample, this Debye process originates from the binary interaction of the urea functional moiety. Because of the strong interaction energy of the functional groups, this

timescale is closely related to the terminal relaxation of the transient supramolecular chain which is also in agreement with the bond lifetime renormalization model.

4.6 Conclusions

In this study, we investigated dielectric and rheological properties of telechelic PDMS polymers having hydrogen bonded functional groups with higher activation energy. We estimated the activation energy of the bond dissociation in these systems using dielectric spectroscopy. Then, we experimentally tested the bond lifetime renormalization model in the strong association regime. The good matching of the timescale from bond dissociation and rheological terminal relaxation agrees with the model prediction.

Rheological measurements indicate that the viscoelastic properties of the functionalized polymers deviate considerably from their non-associating counterpart due to the formation of supramolecular chains with much longer chain length. In addition, the investigated systems show a unique relaxation peak when bond dissociation happens, which is of Debye shape. The mechanism of how bond dissociation results in Debye-like peak will be investigated in the future.

CHAPTER 5 ORIGIN OF MECHANICAL REINFORCEMENTS IN ASSOCIATING POLYMERS WITH MICROPHASE SEPARATION

A version of this chapter was published in *Macromolecules*, by Sirui Ge, Subarna Samanta, Martin Tress, Bingrui Li, Kunyue Xing, Philippe Dieudonné-George, Anne-Caroline Genix, Peng-Fei Cao, Mark Dadmun, and Alexei P. Sokolov "Critical Role of the Interfacial Layer in Associating Polymers with Microphase Separation" (Macromolecules 2021, 54, 4246−4256)

Alexei P. Sokolov formulated the concept and managed the entire project. Sirui Ge did most of the rheology and dielectric measurement, as well as model analysis and wrote most of the manuscript under the guidance of Alexei P. Sokolov and Subarna Samanta. Subarna Samanta analyzed the dielectric spectra through the dielectric interfacial layer model. Bingrui Li synthesized the PDMS-UU associating polymer. Kunyue Xing synthesized the PDMS-NHCO-COOH associating polymer and did some preliminary measurements. Philippe Dieudonné-George and Anne-Caroline Genix did X-ray scattering measurement. Martin Tress, Peng-Fei Cao and Mark Dadmun provides the general guidance and supervision of the project.

5.1 Introduction

The simplest mode of functional group interaction in associating polymer is binary interaction, in which two complementary functional groups associate together and the dynamics of the polymer

is controlled by the lifetime of the associating bond. In case that functional groups and backbone chains are immiscible[46], the functional groups aggregate in clusters, resulting in a microphase separation. Such microphase separation has been found in different kinds of associating polymers e.g., in ionomers[17, 49] or polymers with hydrogen bonding[48], and even in some vitrimers[50, 145]. The clusters of functional groups can form a solid phase in the polymer melt[146, 147], if their glass transition temperature T_g, or melting temperature T_m are higher than T_g of the polymer backbone. Characteristic structure and morphology of these clusters can also be tuned with the architecture of the polymers[51, 148]. These microphase separated associating polymers demonstrate unique viscoelastic behavior[149-153], which cannot be captured by the model mentioned above. There is no detailed model description existing for these systems.

In heterogeneous polymeric systems, such as polymer nanocomposite, an interfacial polymer layer with significantly different structural and dynamic properties from bulk polymer exists around the solid nanoparticles[154, 155]. In the past few years, Broadband Dielectric Spectroscopy (BDS) has been applied to study the interfacial layer in polymer nanocomposites[66-69, 72, 156, 157]. Through model fitting analysis, the quantitative information, including the characteristic relaxation time and thickness of the interfacial layer, can be estimated[66, 157]. A similar interfacial layer also forms in associating polymers with microphase separation[17, 52]. In ionomers, the existence of the interfacial layer was confirmed by NMR[158] and quasi-elastic neutron scattering[159], and was also characterized by BDS[160, 161]. This interfacial layer changes rheological properties, dramatically broadens the glass-to-rubber transition regime and changes the rubbery plateau level[61]. Based on the rheological and dielectric measurements, an existence of the interfacial layer formed around the cluster was also proposed[28]. However, the interfacial layer in

associating polymers has not been studied in detail, as was done in polymer nanocomposite samples.

In this study, we employed small-angle X-ray scattering (SAXS), BDS and rheology to study structure, segmental relaxation and viscoelastic properties of telechelic associating polymers with poly(dimethyl siloxane) (PDMS) backbone and two different types of associating end groups. Our previous studies revealed strong microphase separation in some of these polymers, which is connected to an unusually high rubbery plateau modulus and demonstrated that their viscosity is controlled by structural relaxation in the clusters of the end groups[26, 162-164]. There we speculated that the high rubbery modulus might be explained by a higher modulus in the polymer interfacial layer[143, 163]. Here, we present a detailed analysis of the microstructure, the interfacial layer volume fraction and thickness in these systems using approach developed for analysis of the dielectric spectra in polymer nanocomposites. We demonstrate that the characteristic inter-cluster distance is defined by the polymer chain length. The analysis of the BDS spectra confirms the formation of an interfacial polymer layer with strongly restricted mobility surrounding these clusters in all the samples. Moreover, this analysis provides estimates of the interfacial layer thickness to be ~0.7-0.9 nm. Finally, we demonstrate that microphase separation of the functional groups and formation of this interfacial layer drastically modify viscoelastic properties of these materials with extremely broad and elevated rubbery plateau. Using the interfacial layer thickness, we estimate that the modulus in the interfacial layer almost reaches glassy modulus value.

5.2 Materials

The polymer involved in this research is the 4-(propylamino)-4-oxobutanoic acid terminated polydimethylsiloxane (PDMS-NHCO-COOH) and double-urea terminated polydimethylsiloxane (PDMS-UU). Both of polymers were synthesized from the PDMS-NH_2, which is a commercially available telechelic associating polymer mentioned in Chapter 4.

5.2.1 Synthesis of PDMS-NHCO-COOH

PDMS-NHCO-COOH was synthesized from PDMS-NH_2 with DP of 13, 22, 50, 74 and react with succinic acid. The synthesis route is shown in Fig. 5.1a.

The chemical structure is confirmed by ^{1}H NMR spectrum (Fig. 5.1b). The peaks in the NMR spectra (labeled from a to g) indicate the different organic groups (labeled from a to g) on the chemical structure.

5.2.2 Synthesis of PDMS-UU

To synthesize PDMS-UU, excessive hexamethylene diisocyanate (HDI) was reacted with methylamine, resulting in one of the two cyanate (NCO) group on HDI being substituted by urea group (forming ICMU). The excessive urea was removed. Then, PDMS-UU was synthesized through the reaction of PDMS-NH_2 with DP of 50 and ICMU. The overall synthesis route is shown in Fig. 5.2a. The chemical structure is confirmed by ^{1}H NMR measurement (Fig. 5.2b). The peaks in the NMR spectra (labeled from a to f) indicate the different organic groups (labeled from a to f) on the chemical structure.

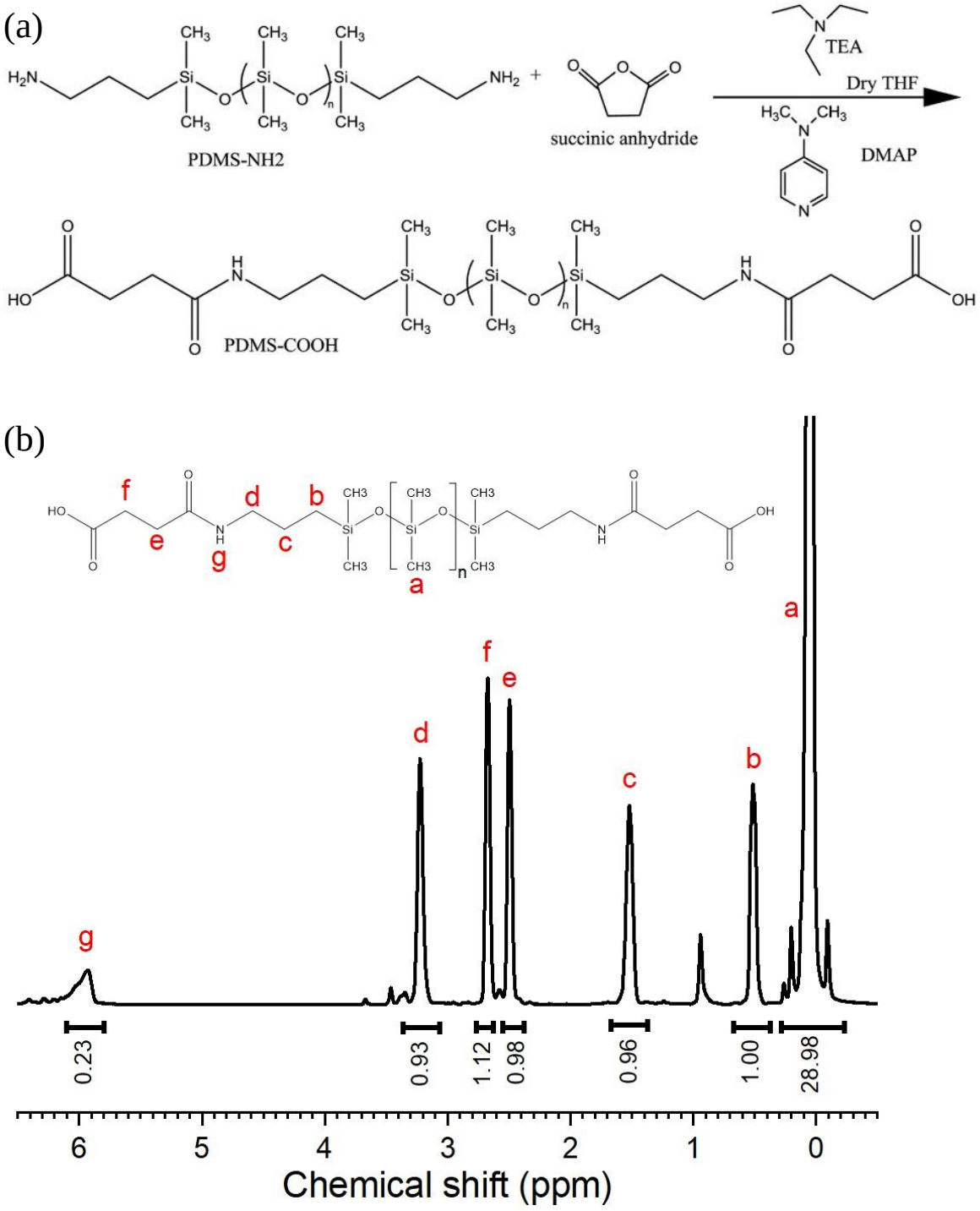

Figure 5.1 (a) Synthesis of 4-(propylamino)-4-oxobutanoic acid terminated polydimethylsiloxane (PDMS-NHCO-COOH) from amine-terminated polydimethylsiloxane (PDMS-NH_2). (b) ^{1}H NMR spectra of PDMS-NHCO-COOH.

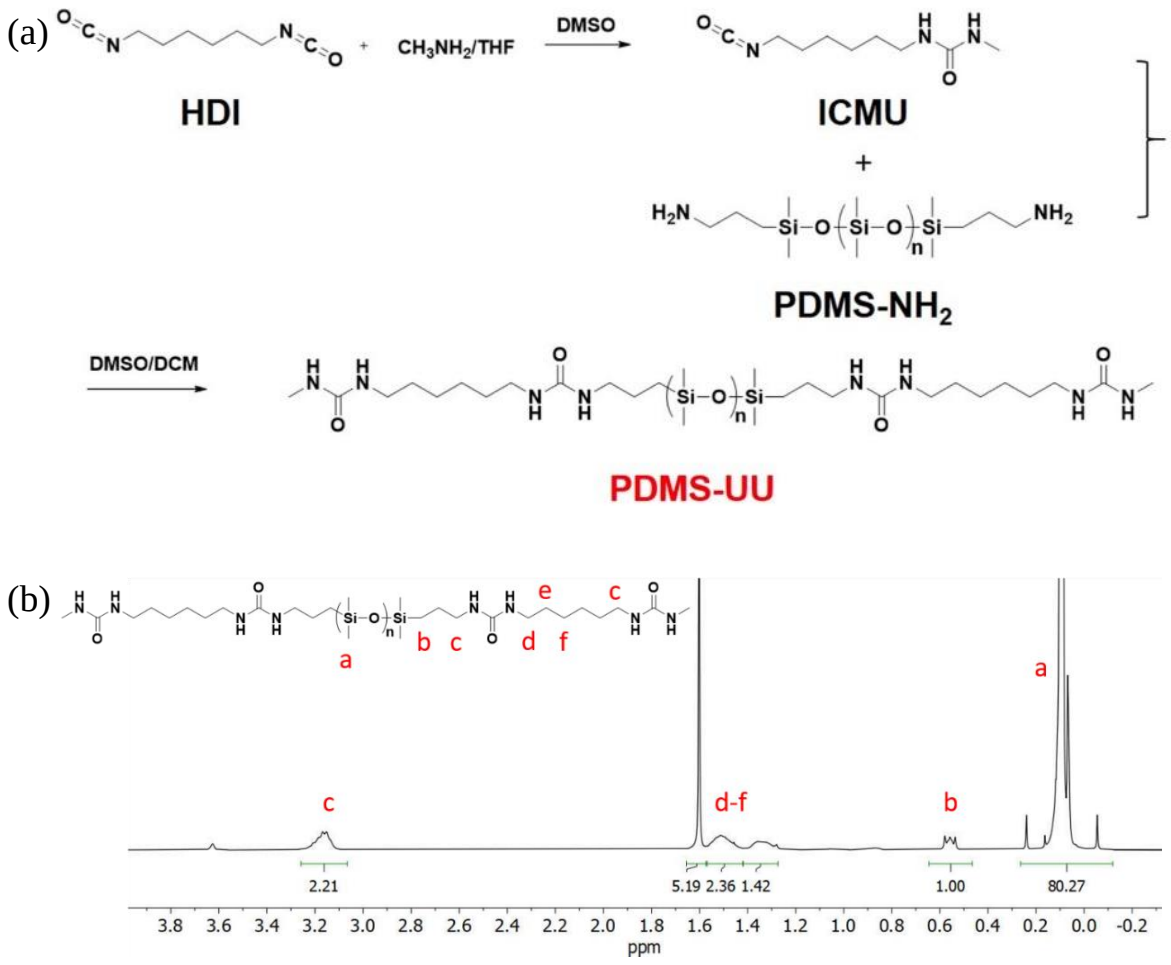

Figure 5.2(a) Synthesis of double-urea terminated polydimethylsiloxane (PDMS-UU) from amine-terminated polydimethylsiloxane (PDMS-NH_2). (b) ^{1}H NMR spectra of PDMS-UU.

5.3 Methods

5.3.1 Differential scanning calorimetry (DSC)

Differential scanning calorimetry (DSC) measurements were performed using a Q2500 DSC from TA Instruments. The samples were dried in vacuum oven at 333 K overnight before placed into the DSC pans. The samples were first equilibrated isothermally at 363 K for 10 minutes to remove the thermal history, and then quenched to 113 K (to avoid crystallization). After equilibration for 10 minutes, the samples were heated up to 363K with a rate of 10K/min. This procedure was repeated twice for each sample to ensure the repeatability.

5.3.2 X-ray Scattering

X-ray Scattering spectra of all the samples were measured using an in-house setup of the Laboratoire Charles Coulomb, "Réseau X et gamma", Université Montpellier, France. A high brightness low power X-ray tube, coupled with aspheric multilayer optic (GeniX3D from Xenocs) delivered an ultralow divergent beam (0.5 mrad, flux 35 Mphotons s^{-1}, λ=1.5418 Å). The scattered intensity was measured by a 2D pixel Pilatus detector with a sample-to-detector distance of 0.2 m. Samples were prepared in glass capillaries. All intensities were corrected for transmission and the empty cell contribution was subtracted. The measurements were performed at room temperature.

5.3.3 Broadband dielectric spectra (BDS)

Broadband dielectric spectra (BDS) in the frequency range 10^{-2}-10^{6} Hz were measured using a Novocontrol system that includes an Alpha-A impedance analyzer and a Quatro Cryosystem temperature control unit. The PDMS-UU sample was placed between two gold-plated electrodes

with diameter of 20 mm, separation between electrodes was 174 μm. PDMS-NHCO-COOH samples were placed into a parallel-plate dielectric cell made of sapphire and invar steel with an electrode diameter of 12 mm. A capacitance of 20 pF was obtained for the cell with an electrode separation of 50 μm. PDMS-CH_3 sample was placed into a parallel-plate dielectric cell made of sapphire and invar steel with an electrode diameter of 10 mm. A capacitance of 3.3 pF was obtained for the cell with an electrode separation of 210 μm. To prevent crystallization, all the samples were quenched from room temperature to about 113 K and reheated to 10 K below the glass transition temperature T_g before the measurements. The spectra were measured on heating. After each temperature increase, the samples were equilibrated for 10 minutes to reach thermal stabilization within 0.1 K. Only PDMS-CH_3 and PDMS-NHCO-COOH (DP 74) samples showed signs of crystallization, and they were measured on heating until crystallization. Measurement of their dielectric spectra during heating and cooling in the temperature range below crystallization confirmed repeatability of the data and ruled out influence of crystallization on the measured spectra. All other samples did not have crystallization, and were measured on heating up to ~300K and then on cooling back to ~T_g to confirm reproducibility of the data.

5.3.4 Rheology

The viscoelastic properties were probed by small-amplitude oscillatory shear (SAOS) measurements through a strain-controlled mode of the AR2000ex (TA Instruments) in an angular frequency range of 10^{-1}–10^{2} rad/s using parallel plate geometry, with a disk diameter of 4mm. The gap between plates was ~ 0.6 - 0.7 mm for all the samples. The samples were quenched to a temperature near T_g before a frequency sweep was conducted at several different temperatures

on heating. Prior to each frequency sweep measurement, the samples underwent thermal stabilization for 5 minutes to make sure that thermal equilibrium has been reached.

5.4 Results

5.4.1 X-ray scattering

The X-ray scattering spectra of all the samples exhibit a strong and sharp peak at q ~0.85 $Å^{-1}$ which reflects spatial correlations between PDMS segments, along with a weaker peak around q ~1.5 $Å^{-1}$ which reflects intra-segmental correlations[165] (Fig. 5.3a). The low-q peak around 0.1 $Å^{-1}$ can be found in spectra of both PDMS-NHCO-COOH and PDMS-UU samples, while no such peak is visible in the spectra of the non-associating PDMS-CH_3 reference sample. Hence this low-q peak is a clear indication of a microphase separation in the former systems. The peak position q_c provides a rough estimate of the average center-to-center distance between the clusters[52], $d \approx \frac{2\pi}{q_c}$, and its intensity should indicate the extent of aggregation. To analyze the intensity of the low-q peak, all the spectra were normalized to the high-q peak of the PDMS backbone after subtracting a baseline (Fig. 5.3b). Then the low-q peak was fitted using a Gaussian peak function (Fig. 5.4):

$$I(q) = \left(\frac{A}{w\sqrt{\pi/2}}\right)\exp\left[-\left(\frac{q-q_c}{w}\right)^2\right] \qquad (5.1)$$

where A is the intensity of the peak defined by the amount of clusters present and their contrast, i.e. the difference of scattering length density between end groups and backbones, w is the width and q_c is the position of the peak. For polymers with shorter chains, the volume fraction of end groups f_e is not negligible, and the obtained A value from fitting needs a correction by the the

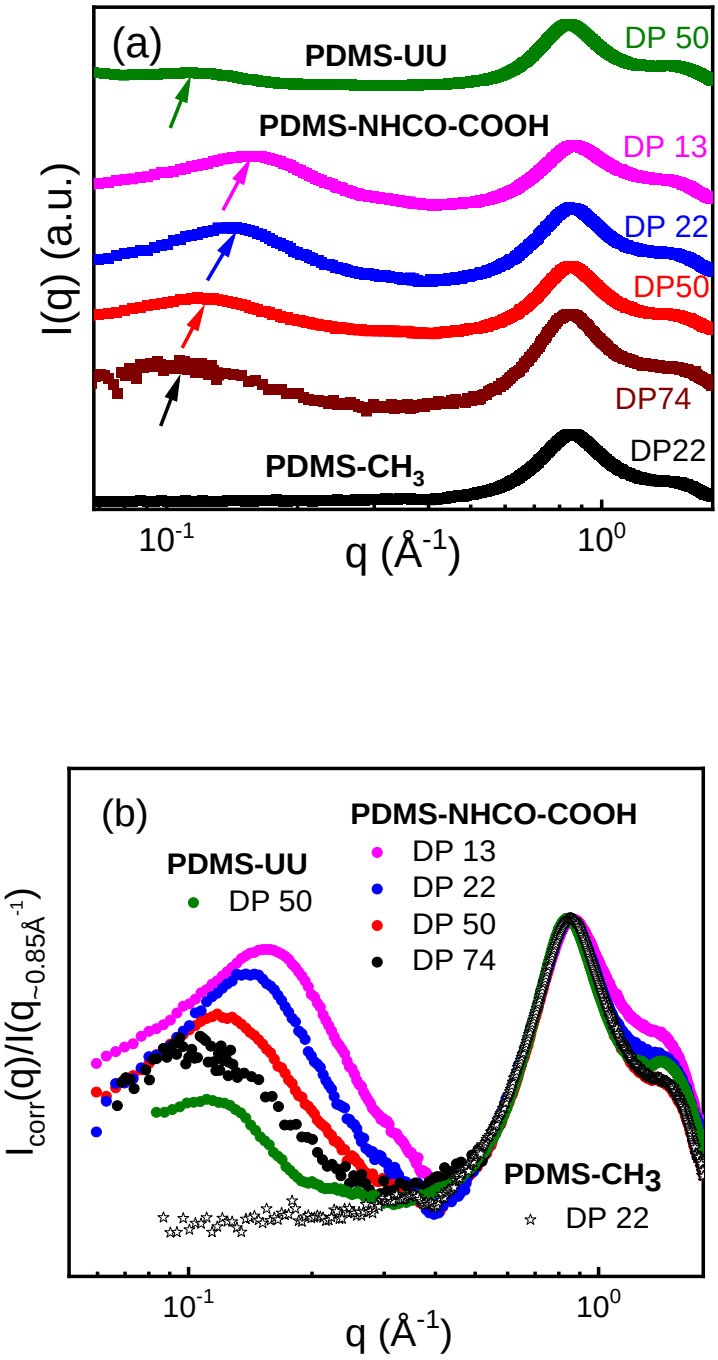

Figure 5.3 (a) X-ray scattering results for all telechelic associating polymers of different degree of polymerization (DP) and PDMS-CH_3 as indicated. The data are offset vertically for clarity. The arrows indicate the low-q peak position. (b) The same X-ray scattering results normalized with respect to the PDMS backbone peak after subtracting a baseline.

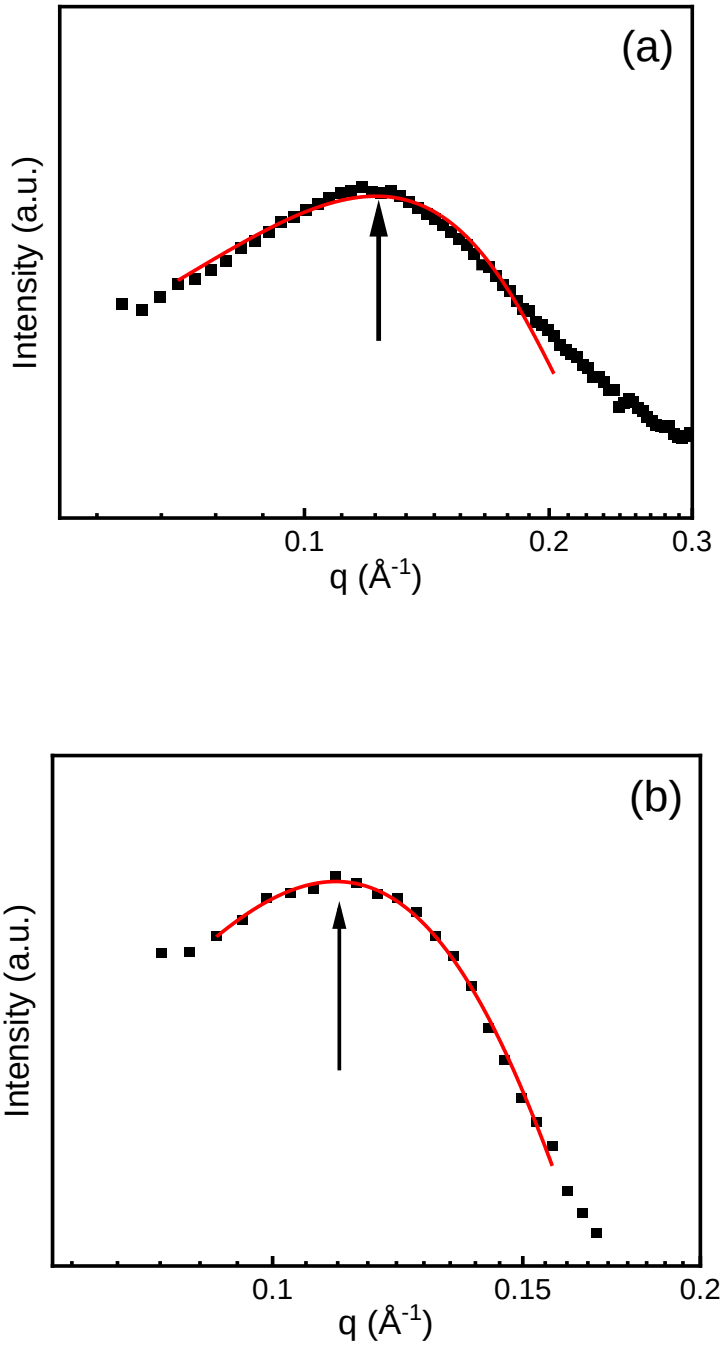

Figure 5.4 Gaussian fits for the low-q peak from the Small Angle X-ray Scattering results after subtracting the baseline for (a) PDMS-NHCO-COOH (DP=50); and (b) PDMS-UU (DP=50).

factor $(1 - f_e)$. Here we assume that the volume fraction of the end groups is the same as their weight fraction, i.e. the density of the end group clusters is about the same as the PDMS density. Thus, $A(1 - f_e)$ is considered as the correct normalized intensity of the low-q peak, that represents the total amount of end groups in the clusters. Indeed, the amplitude of the peak increases with the increase in end group weight fraction (Table 5.1). Assuming that all functional groups form clusters, we can roughly estimate an average cluster radius using the relationship for a cubic arrangement of spherical particles [166]: $R_{cluster} = \frac{d}{2}(\frac{6}{\pi} f_e)^{\frac{1}{3}}$. Table 5.1 presents the cluster center-to-center distance, cluster radius and the normalized intersity of the low-q peak estimated from the SAXS data. The cluster radius appears to increase slightly with the decrease in the backbone DP.

5.4.2 Broadband Dielectric Spectroscopy

The BDS spectra of the studied telechelic associating polymers exhibit several relaxation processes[25-27, 162]. We focus here on a detailed analysis of the PDMS segmental relaxation spectra (Fig. 5.5). Direct comparison of the dielectric loss spectra of a telechelic associating polymer with its non-associating counterpart at the same temperature shows not only a significant shift of the peak position but also a decrease in its amplitude (Fig. 5.5a). In addition, the amplitude of the segmental relaxation peak decreases strongly with decreasing degree of polymerization (DP) of the telechelic associating polymers (Fig. 5.5b). The other remarkable observation is that the peak broadens significantly for the polymers with associating end groups, and the broadening increases drastically with decrease in DP (Fig. 5.5b) and upon cooling (Fig. 5.6a). The observed changes in the BDS spectra are very similar to the ones observed in polymer nanocomposite

Table 5.1 Degree of polymerization (DP), Number of Kuhn segments (N_k), Molecular weight of the PDMS associating polymers including end groups (M_n), weight fraction of the end groups (f_e), center-to-center distance between clusters (d), radius of clusters ($R_{cluster}$) and corrected intensity of the low-q peak A(1-f_e)

Material	DP	N_k	M_n (kg/mol)	f_e (wt%)	d (nm)	$R_{cluster}$ (nm)	A(1-f_e) (a.u.)
PDMS-NHCO-COOH	13	4	1.28	24.7	4.08	1.59	46.8
	22	7	1.94	16.3	4.43	1.50	32.3
	50	16	4.02	7.9	5.12	1.36	23.2
	74	23	5.57	5.7	5.97	1.43	16.2
PDMS-UU	50	16	4.21	12.2	5.70	1.75	7.45

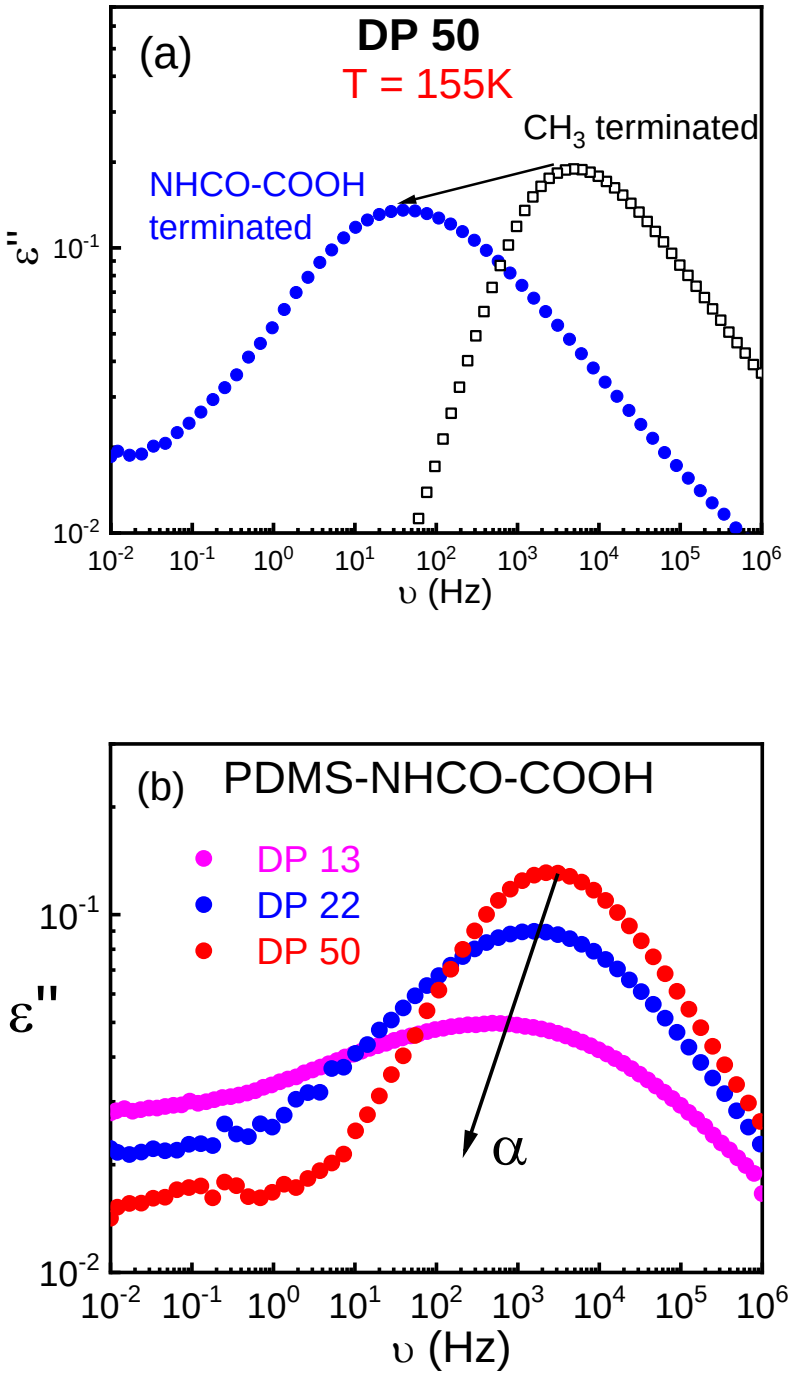

Figure 5.5 Dielectric loss spectra ε'' for (a) PDMS-NHCO-COOH and PDMS-CH_3 with DP=50 at 155K. (b) PDMS-NHCO-COOH with DP = 13 at 168K, DP = 22 at 164K and DP = 50 at 161K. The arrow indicates the decrease in the amplitude of segmental relaxation (α-process). Temperatures were chosen to have the segmental peak in the same frequency range.

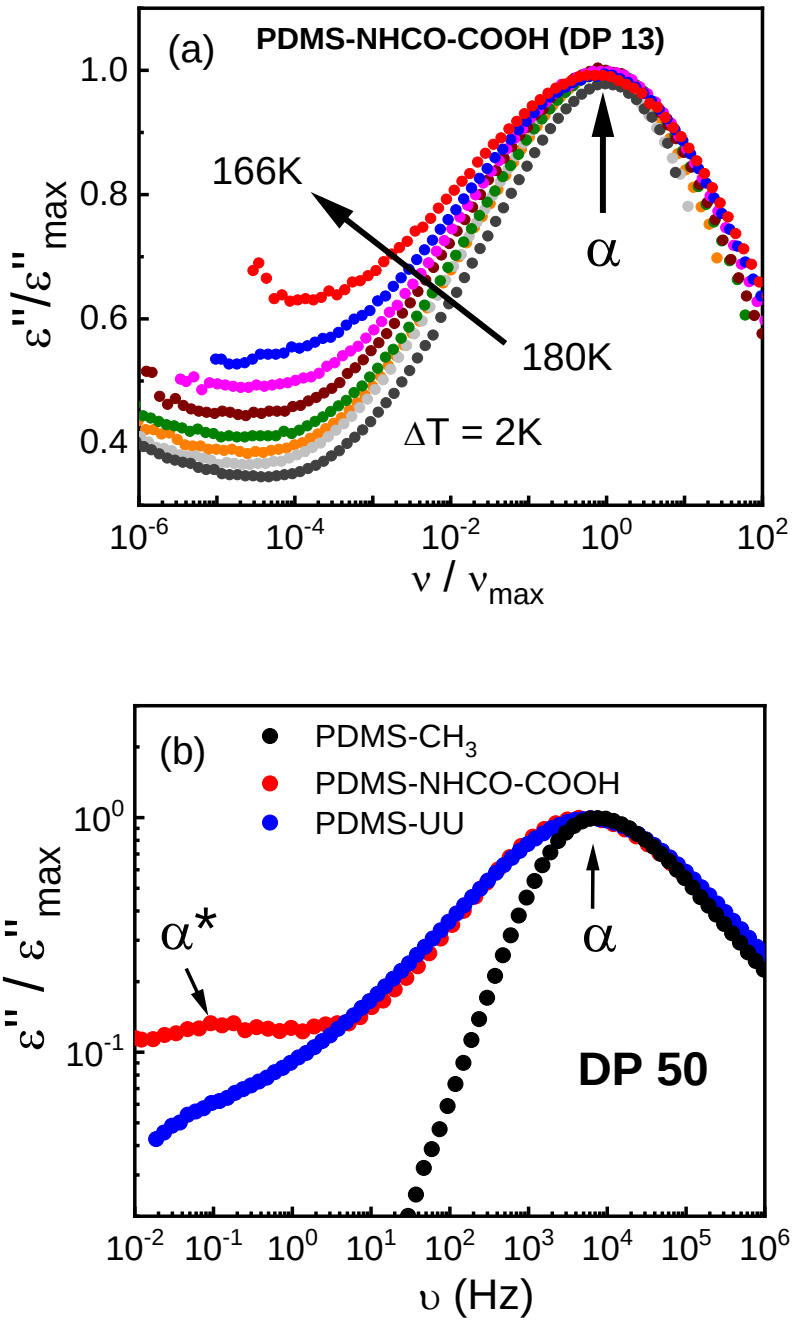

Figure 5.6 (a) Normalized dielectric loss spectra vs. normalized frequency of the α-relaxation of PDMS-NHCO-COOH (DP=13) from 166K to 180K with 2K increment. (b) Normalized dielectric loss spectra vs. frequency PDMS-NHCO-COOH, PDMS-UU and PDMS-CH_3 with DP = 50. The small peak at lower frequencies in PDMS-NHCO-COOH spectra is assigned to binary association (a*-process)[26] .

materials[156, 167]. Moreover, the low frequency side of the segmental peak appears different for UU and COOH terminated chains (Fig. 5.6b). An additional dielectric process is obvious in the spectra of PDMS-NHCO-COOH with DP=50 (Fig. 5.6b). It was called α*-relaxation and was assigned to binary association of the functional groups[26].

To estimate the relaxation time, the loss spectra were initially fit to a single Havriliak-Negami (HN) function[106]:

$$\varepsilon''(\upsilon) = Im\left\{\frac{\Delta\varepsilon}{[1+(2\pi i\upsilon\tau)^{\alpha}]^{\gamma}}\right\} \qquad (5.2)$$

in which $\Delta\varepsilon$ denotes the dielectric relaxation strength, α and γ are the shape parameters. τ is HN relaxation time that is related to the relaxation time at the loss maximum τ_{max}[106]:

$$\tau_{max} = \tau\left[\sin\left(\frac{a\pi}{2+2\gamma}\right)\right]^{-\frac{1}{a}}\left[\sin\left(\frac{a\gamma\pi}{2+2\gamma}\right)\right]^{\frac{1}{a}} \qquad (5.3)$$

The latter is often used as the characteristic segmental relaxation time in polymeric materials. The obtained τ_{max} follows the Vogel–Fulcher–Tammann (VFT) equation (Fig. 5.7a).

$$\tau_{max} = \tau_0 \exp\left(\frac{B}{T-T_0}\right) \qquad (5.4)$$

Here τ_0 is a limiting relaxation time, B and T_0 are material dependent parameters. By extrapolating τ_{max} to $\tau \approx 100$ s, the glass transition temperatures (T_g) from the dielectric measurements are estimated. It is comparable to the calorimetric T_g (Fig. 5.7b), confirming the assignment of the fastest relaxation process in BDS to the segmental motion of the PDMS backbone. The addition of the functional groups at the chain ends shifts the segmental relaxation time and T_g of the backbone, with stronger shift for shorter chains. Changing the functional end

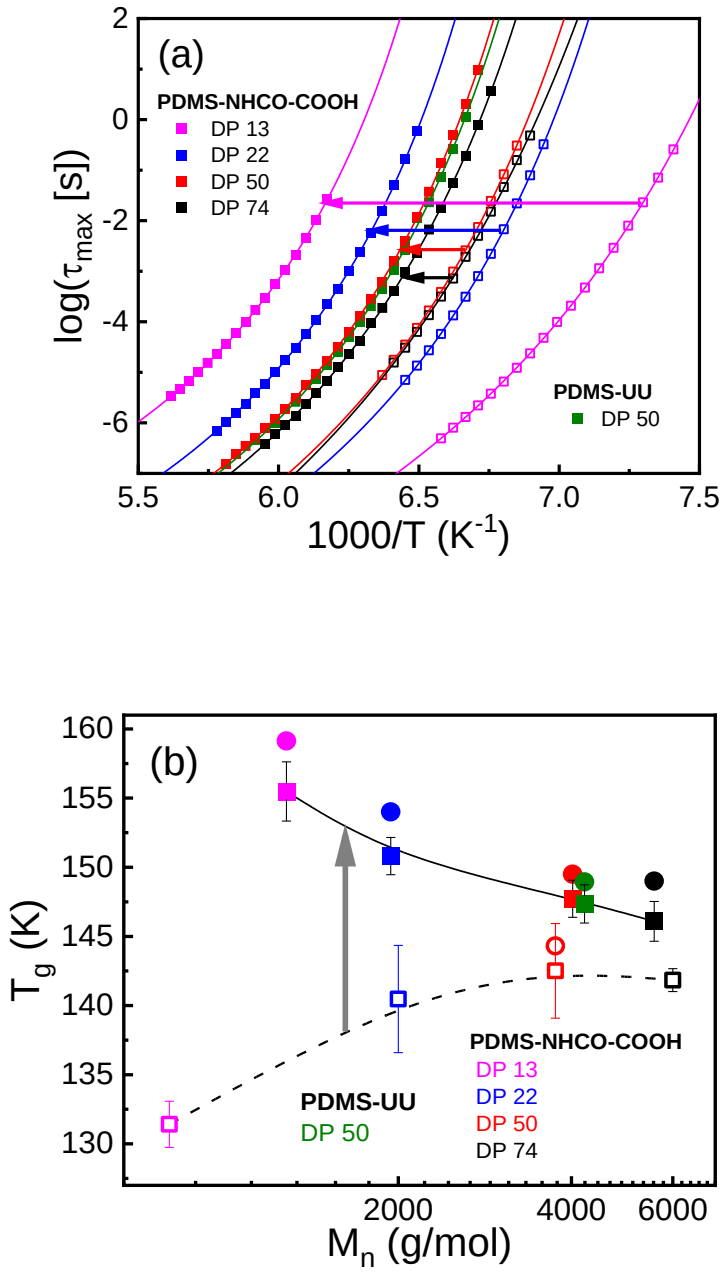

Figure 5.7 (a) Activation plot of the dielectric α-relaxation time of PDMS-NHCO-COOH and PDMS-UU (closed squares) along with their non-associating counterparts PDMS-CH_3 (open squares) with different DP. The solid and dotted lines are VFT fits to the respective data sets. (b) Glass transition temperature (T_g) vs. total molecular weight including end groups (M_n) for PDMS-NHCO-COOH and PDMS-UU (closed symbols) as well as their non-associating counterparts PDMS-CH_3 (open symbols). Squares with error-bars - results from BDS; circles - results from DSC. The lines are guides for the eye.

group of the DP = 50 samples does not affect segmental dynamics and T_g significantly. The broadening of the segmental relaxation peak clearly depends on the chain length, i.e. DP of the samples (Fig. 5.5b, Fig. 5.8). While the sample with DP = 74 shows only a weak broadening on the low frequency side in comparison to the spectrum of PDMS-CH_3, the extent of broadening is significant for DP = 13 sample (Fig. 5.8). In the case of DP = 13, the broadening can even be found on the high frequency side, indicating extremely broad distribution of relaxation times in systems with short chains. In analogy to polymer nanocomposites, we ascribed the broadening of the spectra to the formation of an interfacial layer.

5.4.3 Shear rheology

To analyze the effect of microphase separation on the viscoelastic properties of these samples, we constructed master curves from the shear modulus spectra using time-temperature superposition (TTS). The results for storage (G′) and loss (G″) moduli for PDMS-UU sample are shown in Figure 5.9 together with earlier results for PDMS-NHCO-COOH samples[26, 163]. All the samples demonstrate the prominent rubbery plateau regime. The plateau modulus value is determined as $G_{pl} = G'(\omega_{min})$, where ω_{min} is the frequency of the loss modulus minimum, $G"(\omega_{min})$, in the rubbery region[39]. For the PDMS-NHCO-COOH samples, the plateau modulus is elevated, and its range extends dramatically with decreasing DP. For the DP = 74 and DP = 50 samples, the plateau modulus is ~ 1 MPa, a usual range for rubbery materials, but it increases strongly for samples with smaller DP, reaching around 100 MPa for DP = 13 (Fig. 5.9). The latter is only an order of magnitude lower than the glassy modulus. The PDMS-UU sample shows a higher modulus than PDMS-NHCO-COOH with the same DP = 50, and it shows the

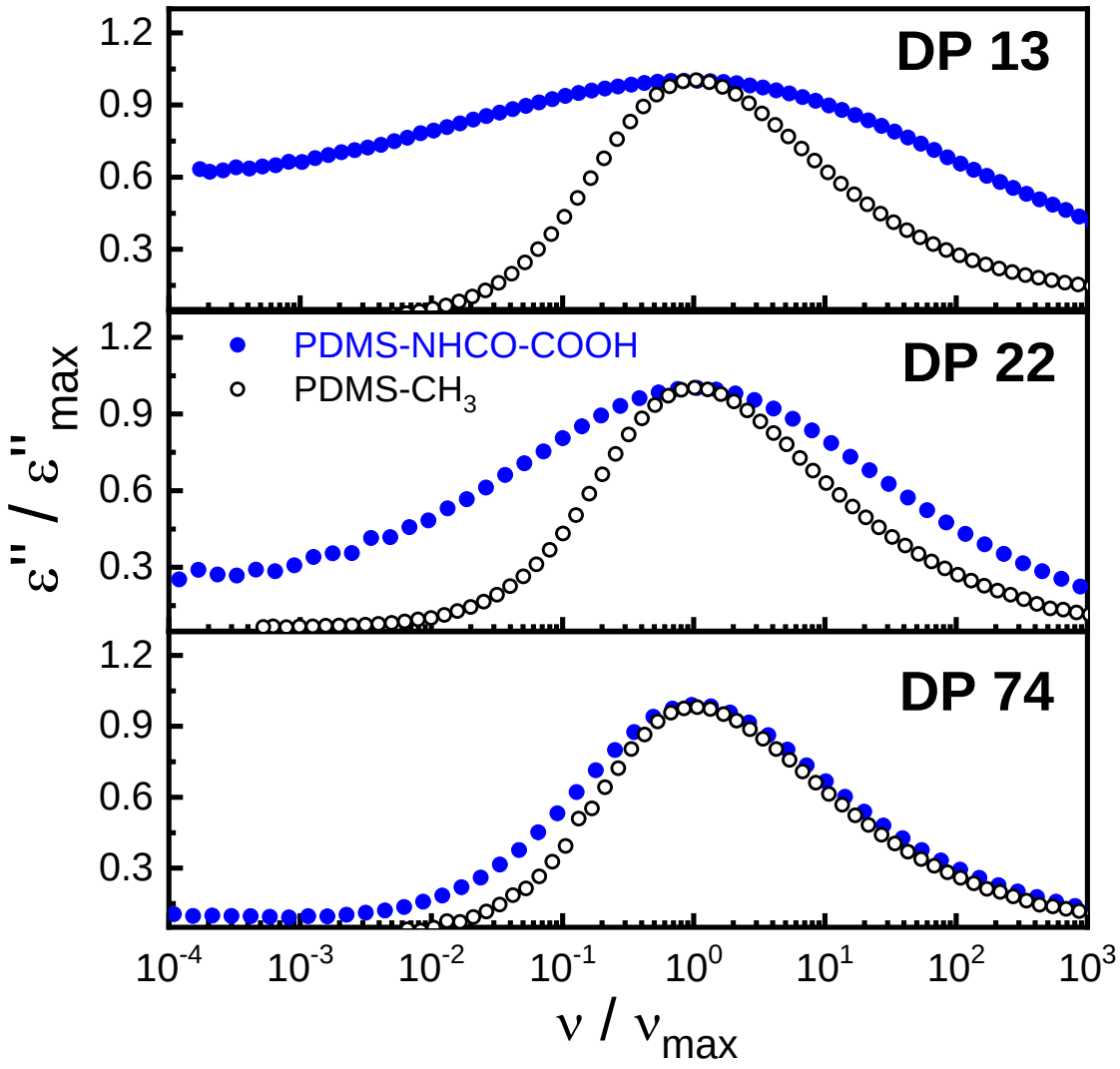

Figure 5.8 Normalized dielectric loss spectra vs. normalized frequency of the α-relaxation for PDMS-NHCO-COOH (blue symbols) and PDMS-CH_3 (black symbols) with DP=74, 22 and 13.

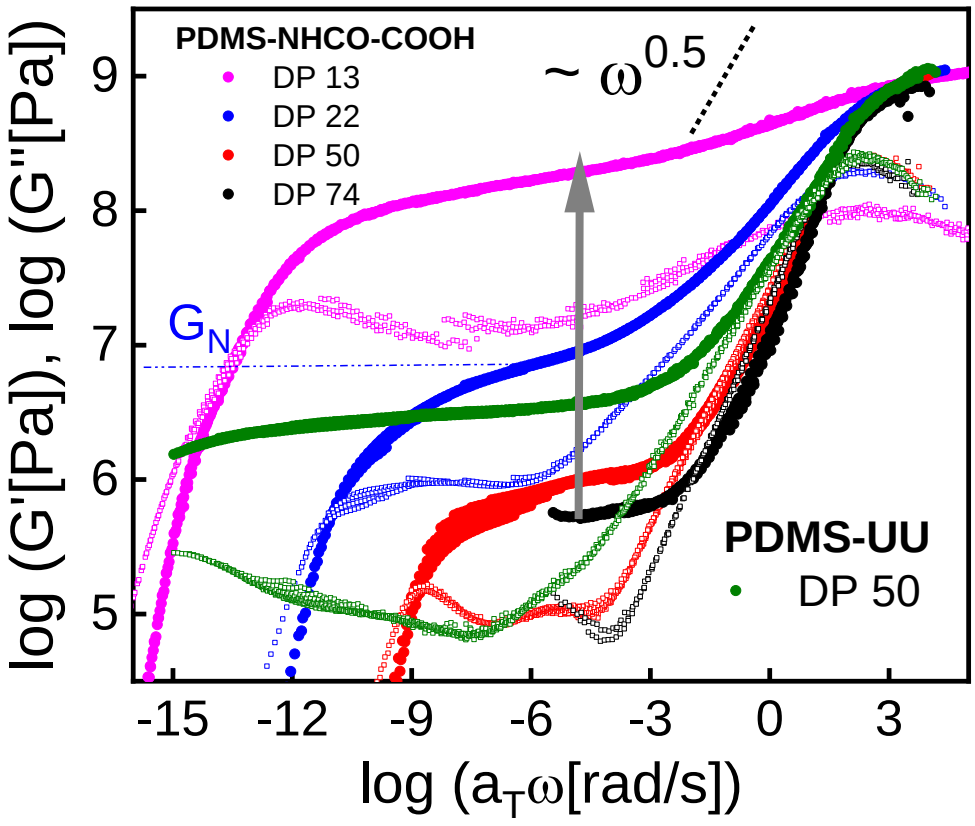

Figure 5.9 Storage (closed symbols) and loss (open symbols) shear moduli master curves for all associating polymers studied here. The reference temperature is taken as 158K for the PDMS-NHCO-COOH (DP=13) sample. The curves of the other samples are horizontally shifted to match the position of the segmental relaxation peak. The vertical arrow indicates the increase in plateau modulus with decrease in DP value from 74 to 13. The horizontal blue dashed line indicates the rubbery plateau modulus level for the PDMS-NHCO-COOH (DP 22) sample.

longest rubbery plateau of any studied sample. The latter can be explained by the higher thermal stability of the clusters formed by the urea groups that is evident from the higher second T_g of the PDMS-UU sample (Fig. 5.10a) compared to PDMS-NHCO-COOH samples (Fig. 5.10b). This second T_g is assigned to the structural relaxation in the clusters of associating groups, which is T_{g2} ~ 280K in UU clusters, while it is T_{g2} ~ 190K in COOH clusters[26].

5.5 Discussion

Analysis of the SAXS data clearly demonstrates that the decreasing DP, i.e. increasing weight fraction of associating chain ends, leads to an increase in amplitude of the low-q peak, a decrease in the distance between clusters d, and a slight increase in the radius of the clusters $R_{cluster}$ (Table 5.1). For the PDMS-UU sample $R_{cluster}$ is larger than in the PDMS-NHCO-COOH sample with the same DP = 50 due to the larger size of the double-urea end groups (Fig. 5.11).

It is expected that the distance between clusters should be controlled by the end-to-end distance of the PDMS backbone R_{ee} because the chain should extend from the surface of one cluster to the surface of another adjacent cluster. The value of unperturbed R_{ee} can be estimated using the classical approximation[130]:

$$\langle R_{ee} \rangle = l_k \sqrt{N_k} \qquad (5.5)$$

Here, $l_k \approx lC_\infty$ and $N_k = \frac{n}{C_\infty}$ are the length and the number of the Kuhn segments, respectively. l = 0.164 nm is the length of the Si-O bond, C_∞ = 6.3 is the characteristic ratio for PDMS[168], and n = 2*DP is the number of backbone bonds. Real R_{ee} of a chain will depend on positions of its end groups in two clusters. The shortest average distance between two surfaces of adjacent clusters is

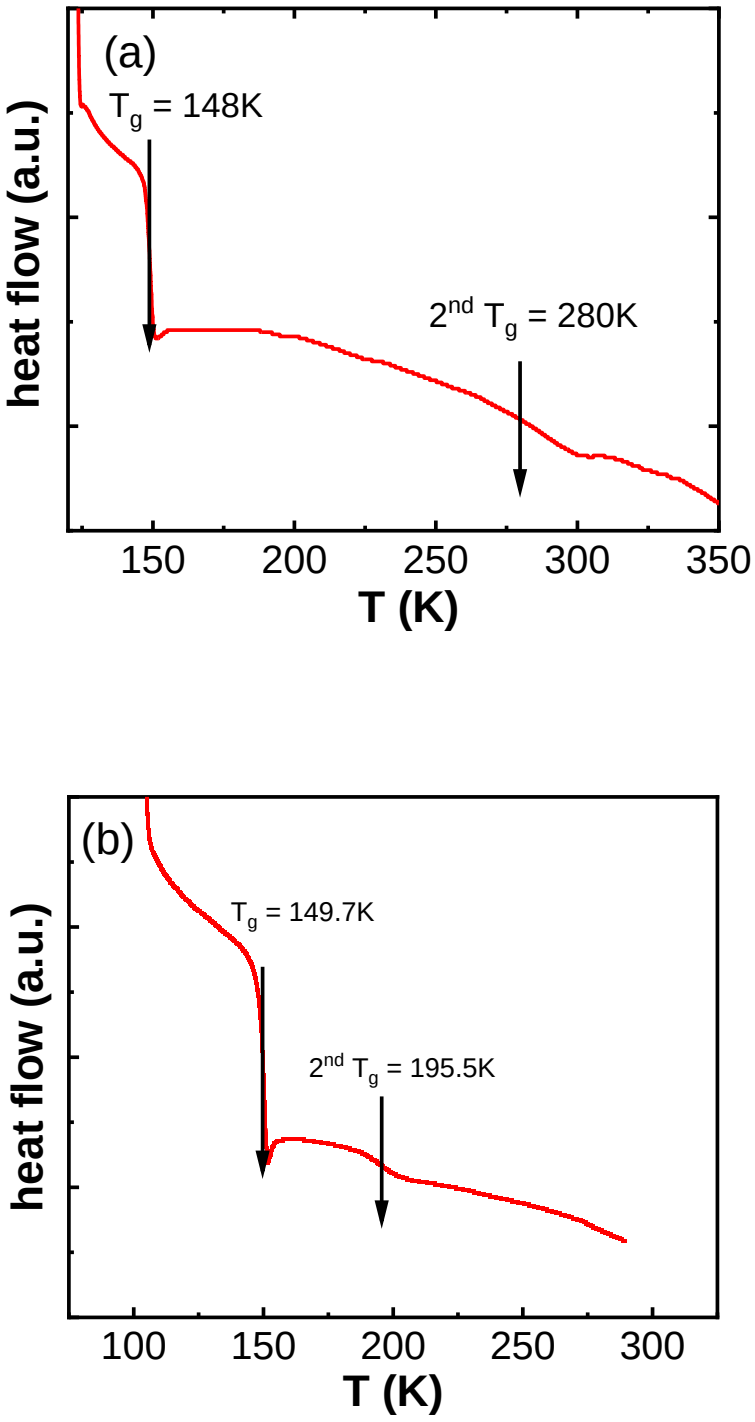

Figure 5.10 Temperature dependence of heat flow measured by differential scanning calorimetry (DSC) for (a) PDMS-UU (DP = 50); (b) PDMS-NHCO-COOH (DP = 50).

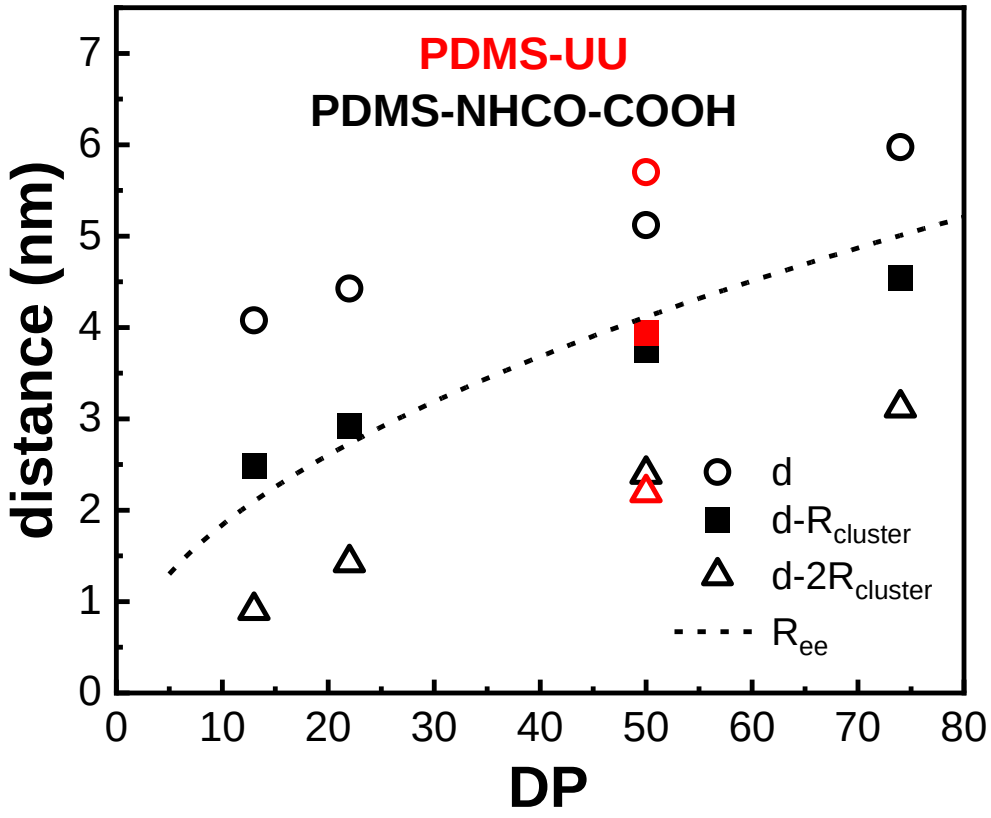

Figure 5.11 Center-to-center distance between clusters d (open circles), d - $R_{cluster}$ (closed squares) and d - $2R_{cluster}$ (open traingles) distances as a function of DP for PDMS-NHCO-COOH (black symbols) and PDMS-UU (red symbols) systems. The dashed line presents the calculated unperturbed PDMS end-to-end distance.

$\sim d - 2R_{cluster}$. But it is unlikely that many connecting chains will have the minimum length. The reason is that there are many chain ends per cluster[26, 163] and most of them are distributed across the entire surface of the cluster. Naively, we would expect that the average R_{ee} for all the chains connecting two neighbor clusters should be between $\sim d - R_{cluster}$ and $\sim d$. Analysis shows that the unperturbed average end-to-end distance of the polymer chains is shorter than d - $R_{cluster}$ for chains with small DP, and is in the range between d - $R_{cluster}$ and d for larger DP (Fig. 5.11). It is interesting that, although d and $R_{cluster}$ are larger in the PDMS-UU system than in the PDMS-NHCO-COOH system with the same DP = 50, d - $R_{cluster}$ is essentially the same, emphasizing that this distance indeed depends on R_{ee}.We note that similar studies of telechelic polyisobutylene revealed that the equlibrium R_{ee} can be comparable and even larger than the distance between clusters d[52]. However, the molecular weight of the studied polyisobutylenes was much higher (up to 30kg/mol)[52]. Thus, analysis of the SAXS data (Fig. 5.11) suggests that the chains in the systems studied here might be stretched especially at smaller DP. In addition, the increased amplitude of the highest-q peak observed in the normalized X-ray scattering with a decrease in DP (Fig. 5.5b) is also a sign of chain stretching. According to the earlier studies[165], intensity of the higher q peaks in PDMS depends on population of the gauche conformational states.

In analogy with the well-known case of polymer nanocomposite, we can ascribe the observed behavior of the dielectric and rheological spectra to the existence of an interfacial polymer layer surrounding the “glassy” clusters of the associating chain ends. In our earlier studies[163] we used this idea to estimate a possible thickness of the interfacial layer using the plateau modulus by assuming the modulus in the interfacial layer to be ~ 1 GPa. However, the dielectric spectra

provide an independent approach to estimate the thickness of the interfacial layer[66, 67, 69]. Knowing the thickness of the interfacial layer, we are able to determine its modulus from the rheological data (Fig. 5.9).

Several approaches to fit the dielectric spectra had been applied to decipher the contribution from an interfacial layer in heterogeneous systems such as polymer nanocomposites[66-71]. Previously, a simple two HN functions fit (an additional HN function to represent the interfacial layer process) and a more convoluted interfacial layer model (ILM) have been used to study the interfacial layer properties in polymer nanocomposites[66]. The ILM is the more accurate method to study the interfacial layer using BDS since it considers the non-additive feature of the dielectric response in heterogeneous systems[70]. Although the two HN functions approach is less accurate[66], it is much simpler and has been utilized in quite a few studies[67, 68, 71] providing reasonable results. Thus, we chose the simpler 2-HN functions approach to analyze the dielectric segmental relaxation spectra in studied here associating polymers. To account for the additional α*-relaxation process, we added a third HN function to fit the dielectric spectra:

$$\varepsilon''(\upsilon) = Im\left\{\frac{\Delta\varepsilon_{bulk}}{[1+(2\pi i\upsilon\tau_{bulk})^{\alpha_1}]^{\gamma_1}} + \frac{\Delta\varepsilon_{int}}{[1+(2\pi i\upsilon\tau_{int})^{\alpha_2}]^{\gamma_2}} + \frac{\Delta\varepsilon_{\alpha*}}{[1+(2\pi i\upsilon\tau_{\alpha*})^{\alpha_3}]^{\gamma_3}}\right\} \qquad (5.6)$$

Here $\Delta\varepsilon_{bulk}$, $\Delta\varepsilon_{int}$ and $\Delta\varepsilon_{\alpha^*}$ are the dielectric relaxation strengths of bulk-like PDMS segments, segments in the interfacial layer, and of the binary association process (α* process), respectively. τ_{bulk}, τ_{int} and $\tau_{\alpha*}$ are the corresponding HN relaxation times; α and γ represent the shape parameters for their respective processes. To reduce the number of free fit parameters, we fixed the shape parameters for bulk-like PDMS segments (α_1, γ_1) to the values from the fit of non-

associated PDMS-CH_3 spectra. The other parameters remained free. Representative fits of the dielectric loss spectra to the eq. 5.6 for all the samples are shown in Fig. 5.12.

Analysis of the results reveals (Fig. 5.13a) that segmental relaxation in the interfacial layer is approximately one order of magnitude slower than in the bulk-like polymer. Interestingly, the ratio τ_{int} to τ_{α} is about the same for all the samples, which is rather independent of temperature as well (Fig. 5.13b). We note that the segmental relaxation time in the interfacial layer was found to be about one order of magnitude slower than that in the bulk polymer also in polymer nanocomposites[66, 72] and polymer grafted nanoparticle samples[73]. However, it was shown that in the case of nanocomposites, the slowdown of segmental dynamics in the interfacial layer depends on the particular polymer-nanoparticles interactions[74, 75].

The fitting results of the dielectric spectra also demonstrate that the amplitude (relaxation strength) of the bulk-like process decreases and that of the interfacial layer increases gradually with decreasing DP, implying an increasing volume fraction of the interfacial region with decrease of the chain length (Fig. 5.14). In the case of the sample with DP=13, almost the entire relaxation spectrum is assigned to the interfacial layer process. Quantitative analysis of the dielectric relaxation strength of the segmental peaks revealed that the bulk-like segmental peak in associating polymers, $\Delta\varepsilon_{bulk}$, is always lower than that in the non-associating polymers, $\Delta\varepsilon_{nonas}$ (Fig. 5.14). For all the non-associating PDMS, the values of $\Delta\varepsilon_{nonas}$ increase upon cooling, following Curie's law (Fig. 5.14). However, $\Delta\varepsilon_{bulk}$ in telechelic polymers shows a much weaker temperature dependence. Moreover, the sample with DP = 22 exhibits essentially no temperature dependence of $\Delta\varepsilon_{bulk}$, while $\Delta\varepsilon_{bulk}$ even decreases upon cooling in sample with DP = 13. These observations are similar to the results known from polymer nanocomposites, and

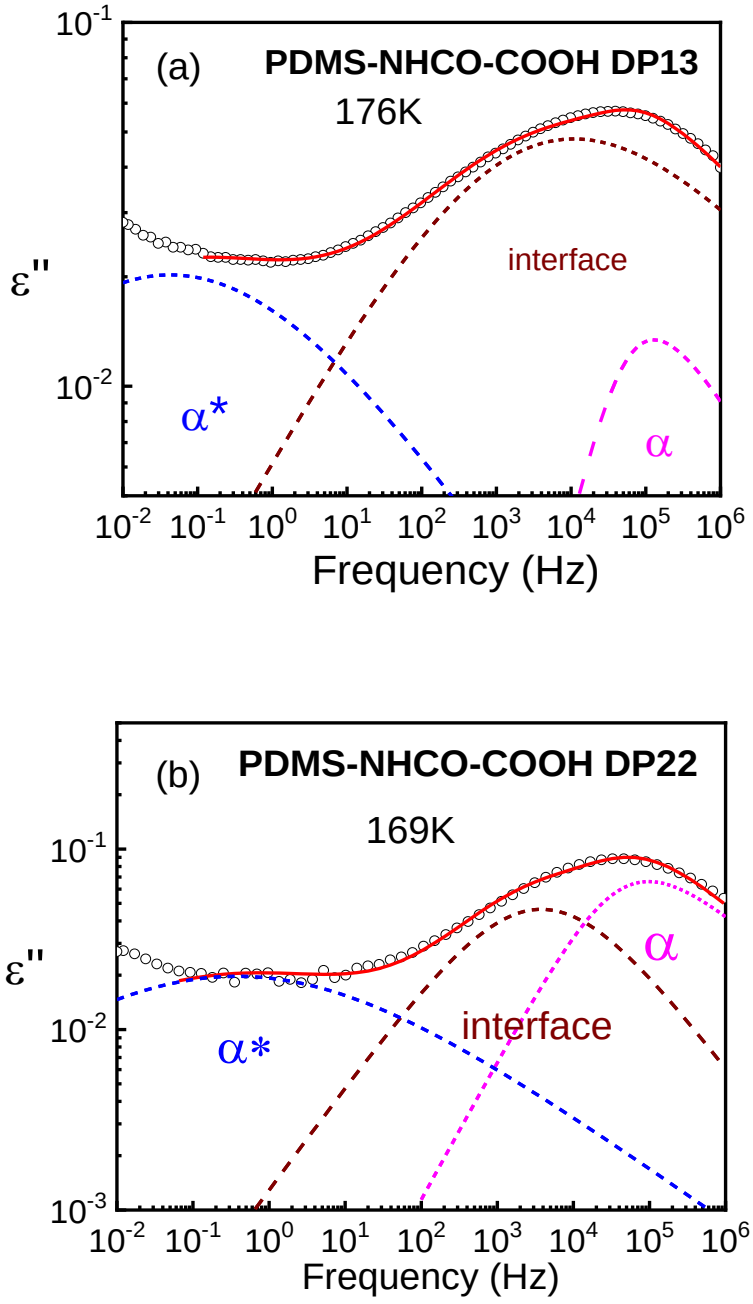

Figure 5.12 Dielectric loss spectra ε”(υ) for (a) PDMS-NHCO-COOH DP 13 at 176K, (b) PDMS-NHCO-COOH DP 22 at 169K, (c) PDMS-NHCO-COOH DP 74 at 163K, (d) PDMS-NHCO-COOH DP 50 at 163K, (e) PDMS-UU DP=50 at 164K. The red solid lines are the fits with three HN functions. The pink, brown and blue dashed lines are the individual contributions of the α, interfacial and α* relaxation processes, respectively.

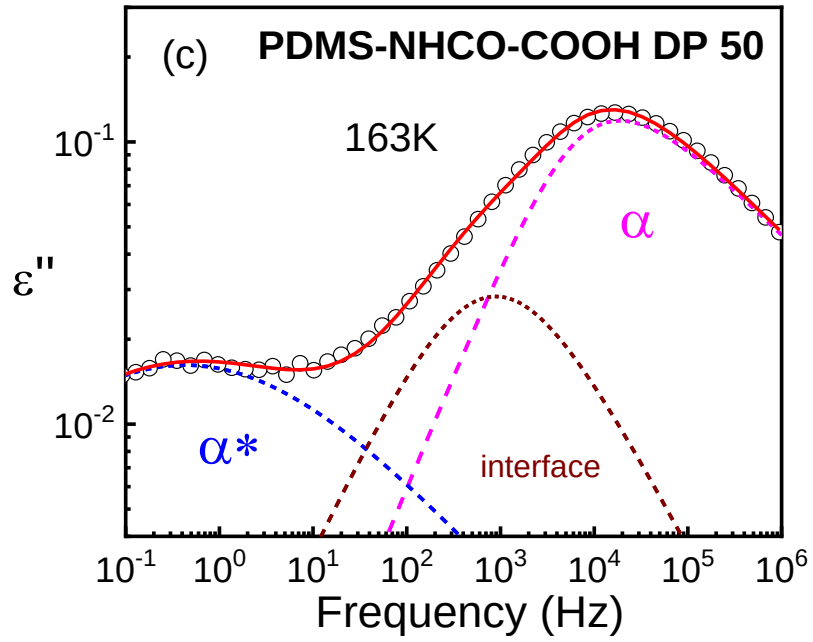

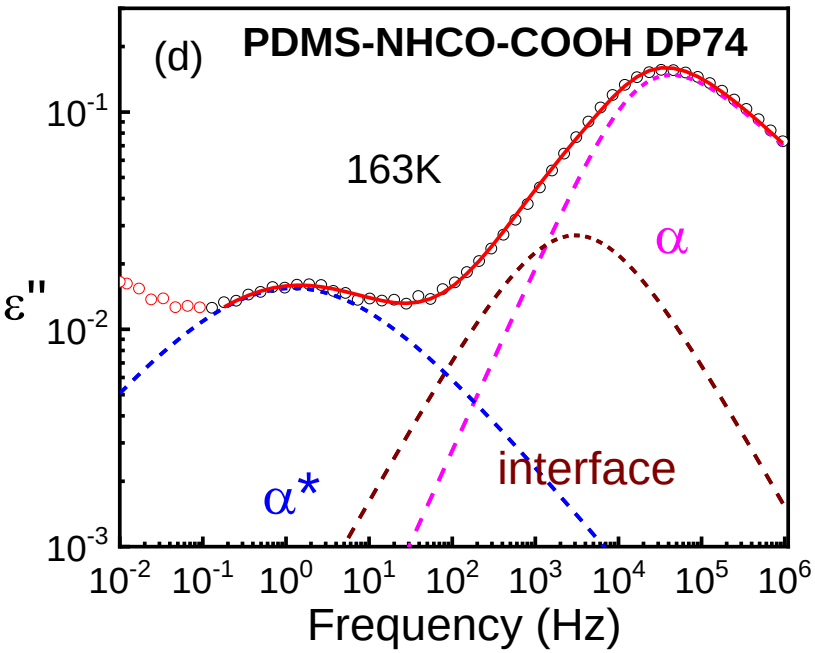

Figure 5.12 Continued

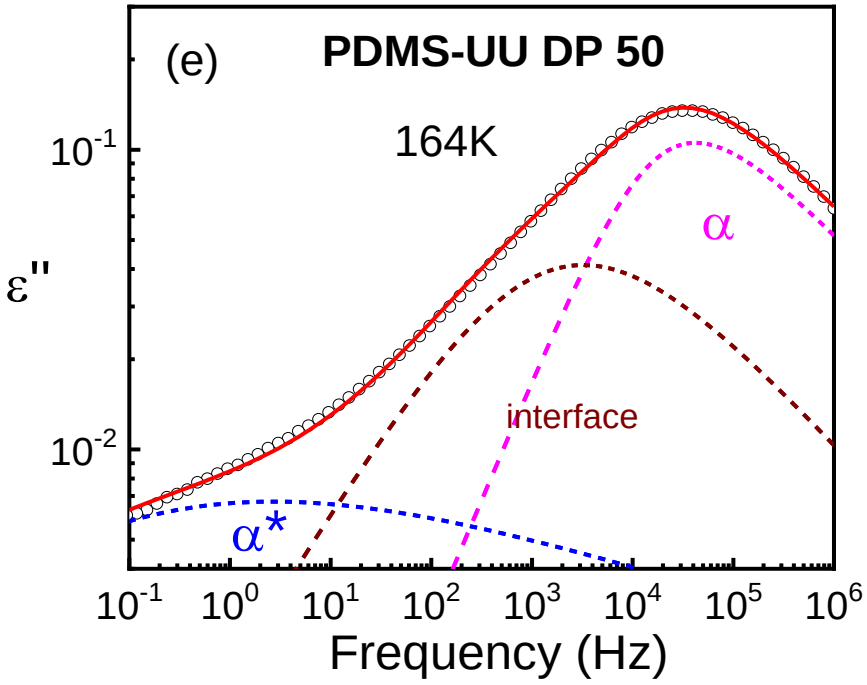

Figure 5.12 Continued

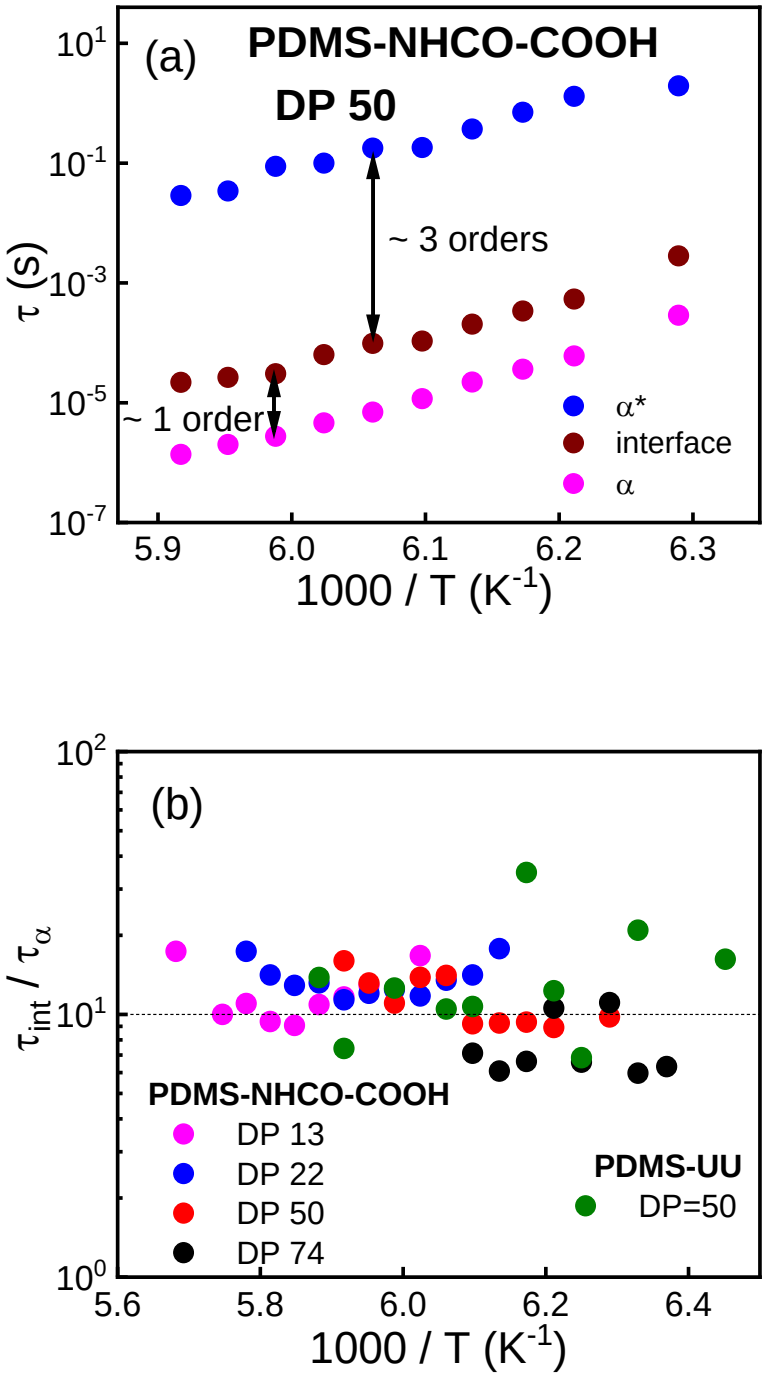

Figure 5.13 (a) Activation plot of the segmental relaxation time in the bulk-like PDMS (pink), in the interfacial layer (brown) and the α* (blue) relaxation time in PDMS-NHCO-COOH DP 50 sample. (b) The ratio between the relaxation times of the interfacial layer and bulk-like PDMS segments for the studied systems.

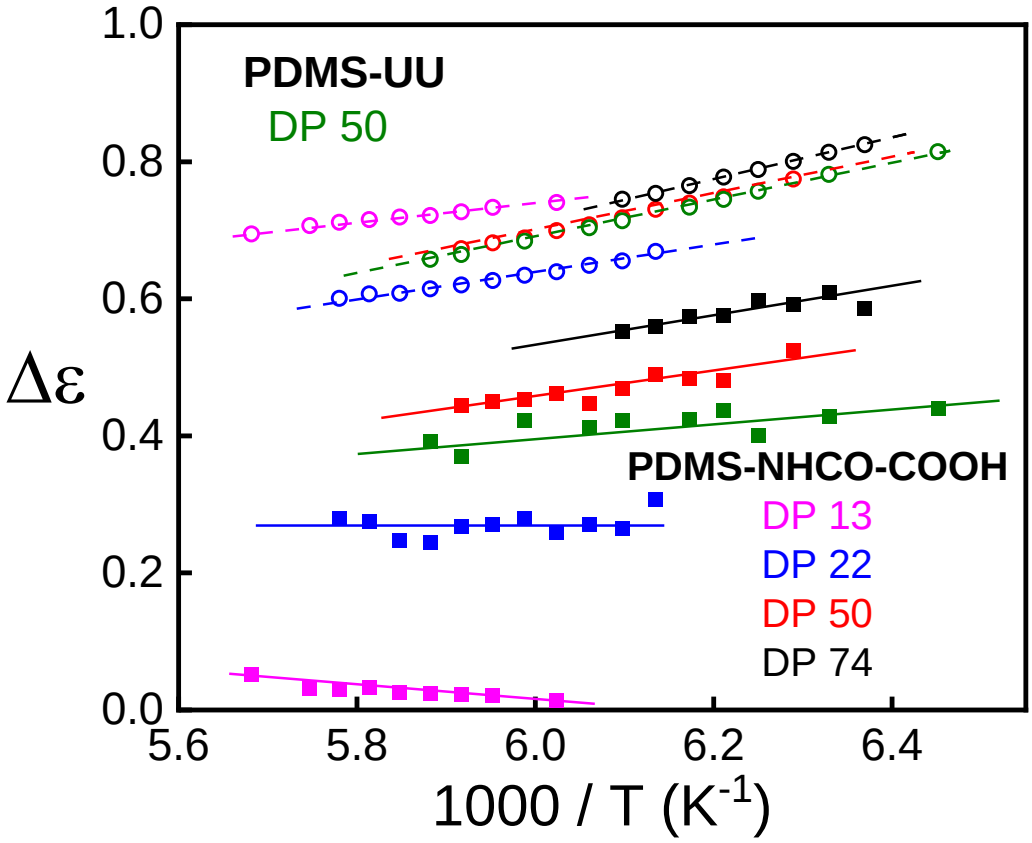

Figure 5.14 Temperature dependence of the dielectric relaxation strength Δε of the α-relaxation of the bulk-like PDMS part in telechelic associating polymers (closed circles) and α-relaxation of the PDMS-CH_3 (open circles).

interpreted as an increase of the interfacial layer thickness upon cooling[73, 169]. This also explains the observed increase in the broadening of the segmental relaxation peak upon cooling (Fig. 5.6a). It is now well documented that the dielectric strength of the segmental relaxation in the interfacial layer, $\Delta\varepsilon_{int}$, of thin polymer films and polymer nanocomposites is strongly suppressed[66, 73, 76]. It was ascribed to a strong restrictions on segmental reorientation in the crowded interfacial layer[73]. Thus, $\Delta\varepsilon_{int}$ does not reflect the true volume fraction of the polymer interfacial layer[73], and one should use $\Delta\varepsilon_{bulk}$ to estimate the volume fraction of the bulk-like polymer, φ_{bulk} [66, 73]. Then the interfacial volume fraction can be estimated using $\varphi_{int} = 1 - \varphi_{NP} - \varphi_{bulk}$, where φ_{NP} is the volume fraction of nanoparticles in the polymer nanocomposite sample.

Following this approach, we use $\Delta\varepsilon_{bulk}$ to calculate the volume fraction of the bulk-like polymer, and then the volume fraction of the interfacial layer:

$$\varphi_{int} = 1 - f_e - \frac{\Delta\varepsilon_{bulk}}{\Delta\varepsilon_{nonas}} \qquad (5.7)$$

The estimated volume fraction of the interfacial layer ranges from 20% to 40%, as DP decreases from 74 to 22, and reaches 70% for the sample with DP=13 (Fig. 5.15a), indicating the strong dominance of the interfacial layer in this sample. Using the estimated φ_{int} and assuming a spherical shape of the chain end group aggregates, we can calculate the interfacial layer thickness using the equation[66]:

$$l_{int} = R_{cluster} \times \left[\left(\frac{\varphi_{int}+f_e}{f_e}\right)^{\frac{1}{3}} - 1\right] \qquad (5.8)$$

The analysis (Fig. 5.15b) reveals that the interfacial layer thickness ranges from 0.7 to 0.9 nm for all telechelic polymer samples studied here, essentially independent of the backbone DP or

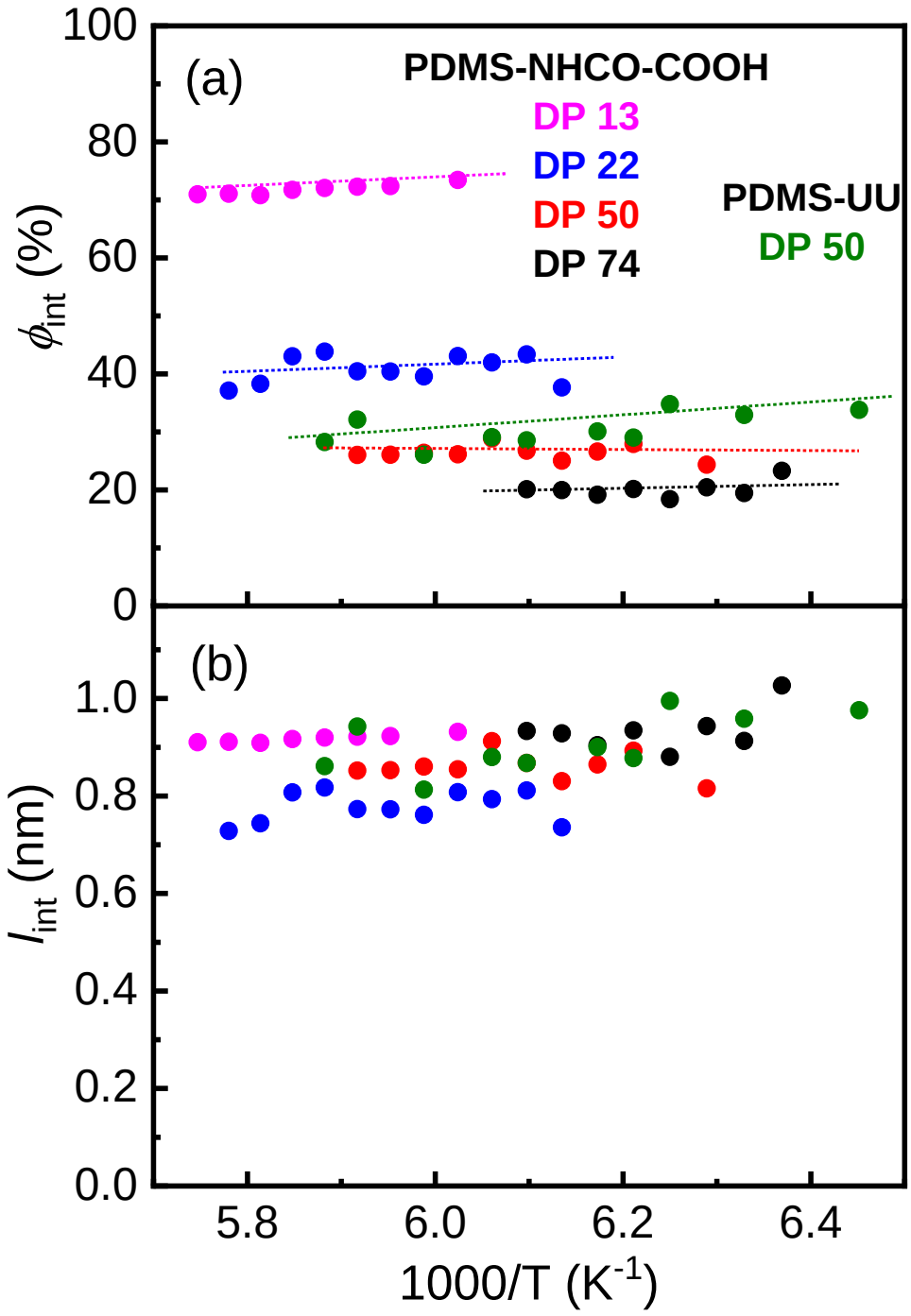

Figure 5.15 Variation of the volume fraction (a) and the thickness (b) of the interfacial layer vs. inverse temperature for the studied telechelic associating polymers.

chemistry of the end group. This value is much smaller than the interfacial layer thickness found in the polymernanocomposites[156]. We explain this result by much smaller cluster size with $R_{cluster}$ ~ 1.4-1.8 nm, while in polymer nanocomposites usually nanoparticles have R ~ 10-20 nm. However, this thickness is consistent with the earlier assumption[17] that it should be comparable to the polymer segment size.

As next step, we analyze the mechanical relaxation spectra (Fig. 5.9). Classical rubber elasticity theory predicts that the rubbery plateau modulus should be inversely proportional to the molecular weight of the PDMS backbone, M: $G_N = \frac{\rho RT}{M}$. Analysis of the experimental data for the longest PDMS chain with DP = 74 revealed that the obtained plateau level is only slightly (~2 times) higher than expected from the classical theory (Fig. 5.16). However, the difference increases strongly with decreasing DP, reaching ~100 times for the sample with DP = 13. As it was shown in our earlier analysis[163], this difference cannot be explained by a hard-filler effect due to the presence of the glassy clusters. This difference clearly indicates that the interfacial layer has a much higher modulus than the bulk-like PDMS matrix. Here, we use again the analogy to Polymer Nanocomposites, especially to polymer grafted nanoparticles. The clusters of chain end groups indeed can be considered as nanoparticles with grafted chains. To analyze the data, we employed the mechanical interfacial layer model used to describe the properties in polymer Nanocomposites, which provides a relationship between the interfacial layer thickness and modulus as well as the macroscopic mechanical strength of the composite material[81]. It assumes a non-slippery condition at the bulk polymer - interfacial layer and interfacial layer - filler boundaries. In the model, the shear modulus of the sample G_c is calculated as:

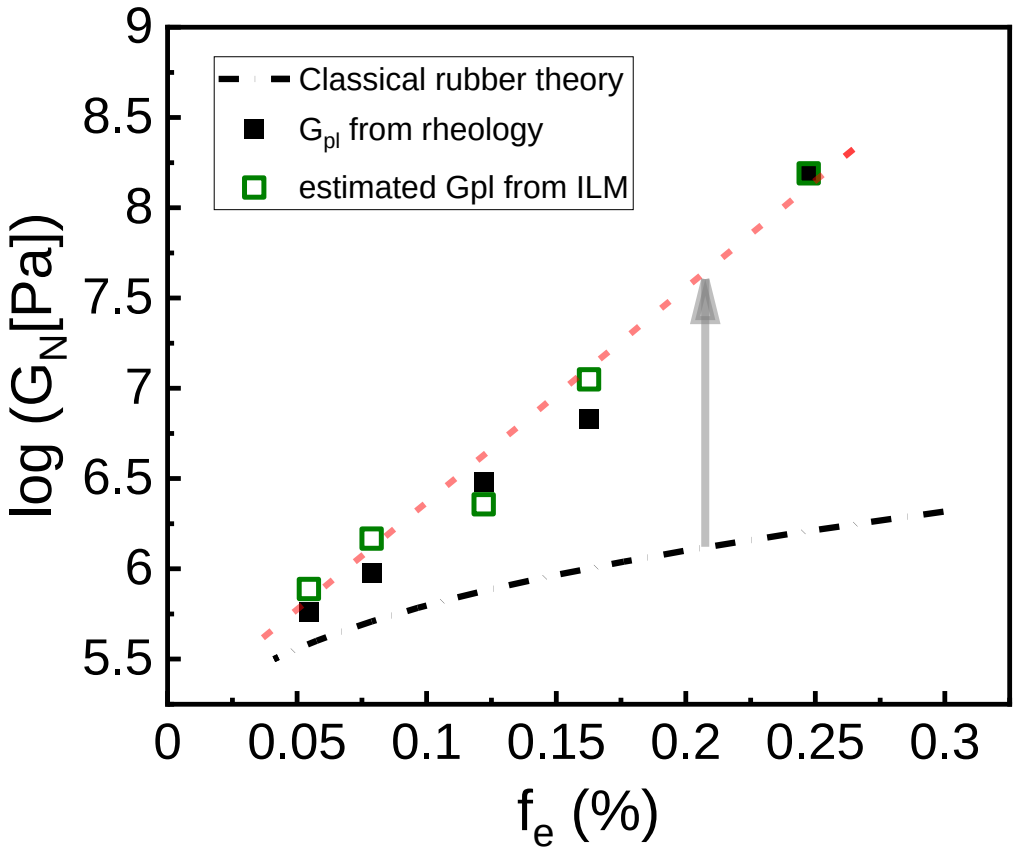

Figure 5.16 Plateau modulus of the studied telechelic associating polymers from rheology measurements (black squares) and calculated from the ILM based on the layer thickness estimated from BDS measurements (green squares) as a function of the weight fraction of the end groups. The black dotted line indicates the relationship between plateau modulus and the weight fraction of end groups according to classical rubber theory. The red dashed line is a trend line guided by the datasets.

$$40(G_c/G_m)^2|X| + \left(\frac{G_c}{G_m}\right)\{2|Y| + 8|Z|\} - 5|T| = 0 \qquad (5.9)$$

where $|X|$, $|Y|$, $|Z|$ and $|T|$ are the determinants of 10×10 matrices which depend on the shear moduli, Poisson's ratios and volume fractions of filler (i.e., end group clusters), interfacial layer and bulk-like matrix, respectively. The full expression of each matrix can be found in Maurer et al.[81].

To analyze the mechanical reinforcement, we used the mechanical ILM with the interfacial layer thickness taken from the BDS measurements (Fig. 5.15b). We assumed that the Poisson's ratio and the modulus of the functional group cluster are the same as in the hydrogen bonding system glycerol[170], i.e. ~ 0.33 and 3GPa, respectively. The Poisson's ratio of the PDMS matrix and of the interfacial layer were assumed to be 0.495, the same as that of neat PDMS[171]. The shear modulus of the bulk-like PDMS matrix is assumed to follow the classical rubbery theory.

The interfacial layer in DP=13 sample occupies essentially the entire polymer fraction (Fig. 5.15a). Thus, the modulus of the interfacial layer even above the PDMS matrix T_g should be comparable to the measured rubbery plateau level in this sample, i.e. ~100 MPa. Indeed, the best agreement between the plateau modulus level and the mechanical ILM estimates for DP = 13 sample is reached (Fig. 5.16). Using this value, a reasonable agreement of the mechanical ILM predictions and the measured plateau modulus is achieved for all other DPs (Fig. 5.16). The decrease in the PDMS backbone length leads to an increase in the volume fraction of associating group clusters and to a significant increase in the interfacial volume fraction (Fig. 5.15a). As a result, the microphase separation of the associating groups leads to a significant mechanical reinforcement with the rubbery modulus of the shortest chains almost reaching a glass-like

modulus value. The reason for so high modulus even at temperatures above the PDMS T_g most probably is related to strong stretching of the chains in the interfacial layer. The estimates show that each cluster contains ~ 35-50 chain ends[163], which would correspond to a grafting density ~ 1.5 chains/nm^2. This is significantly higher than in polymer grafted nanoparticles, where the grafting density is usually ~ 0.5 chains/nm^2 [172]. Such a high grafting density leads to a strong crowding and stretching of the chains in the interfacial layer, leading to their restricted flexibility and high modulus. Thus, BDS and rheological data provide a clear indication of the interfacial polymer layer formed around the clusters of associating end groups. Although this interfacial layer is extremely thin (~0.7 – 0.9 nm), it plays a significant role in relaxation and mechanical properties of associating polymers with microphase separation. The impact of this interfacial layer on the macroscopic properties increases with decreasing chain length due to the increasing volume fraction of the interfacial region. The presented analysis provides a consistent description of both BDS and rheological data for samples with several chain lengths and two different end groups.

5.6 Conclusion

The analysis of the X-ray scattering data of the telechelic polymers studied here reveals that all of them form aggregates of the end groups. This result is consistent with the presence of two T_gs observed in DSC. Moreover, the X-ray scattering data provide a direct estimate of the average distance between the aggregates and allow an estimate of their size. Our analysis suggests that the chain end-to-end distance controls the average distance between aggregates, and aggregates containing ~ 30-55 associating groups increase in size with the decrease in the backbone length.

At the same time, dielectric and rheological data clearly indicate the existence of an interfacial polymer layer surrounding these clusters with relaxation behavior and mechanical properties different from that of the bulk-like polymer.

To analyze the properties and the thickness of the interfacial layer, we employed models developed for polymer nanocomposites. Indeed, structurally the studied samples are analogous to polymer grafted nanoparticles. Using this approach, we found that the segmental dynamics in the interfacial layer is about an order of magnitude slower than that in the bulk-like polymer. The estimated thickness of the interfacial layer is surprisingly small ~ 0.7-0.9 nm, comparable to a length of a single segment. However, this might be reasonable considering the very small size of the aggregates with $R_{cluster}$ ~ 1.4 - 1.8 nm. Using the estimated interfacial layer thickness and the value of the rubbery plateau, we were able to estimate the shear modulus in the interfacial layer. It appears rather high ~ 100 MPa (even at temperatures well above the polymer's T_g), which we explain by a significant chain stretching in this interfacial layer. Thus, the models employed here provide a consistent description of both BDS and rheological data. We emphasize that the employed here analogy with polymer nanocomposite, especially with polymer grafted nanoparticles, yields a suitable approach for describing and predicting properties of polymers with microphase separation. This advances our understanding of polymers with dynamic bonds which is critical for a rational design of novel functional materials with strongly enhanced viscoelastic properties.

CHAPTER 6 MECHANISM OF VISCOELASTICITY IN ASSOCIATING POLYMERS WITH MICROPHASE SEPARATION

A version of this chapter was published in *ACS Nano*, by Sirui Ge, Subarna Samanta, Bingrui Li, Peyton Carden, Peng-Fei Cao, and Alexei P. Sokolov "Unravelling the Mechanism of Viscoelasticity in Polymers with Phase-Separated Dynamic Bonds" (ACS Nano 2022, 16, 3, 4746–4755)

Alexei P. Sokolov formulated most of the concept and managed the entire project. Sirui Ge formulated part of the concept, did most of the rheology and dielectric measurement, as well as model analysis and wrote most of the manuscript under the guidance of Alexei P. Sokolov and Subarna Samanta. Bingrui Li synthesized the associating polymers. Peyton Carden did X-ray scattering measurement and dielectric measurement under the guidance of Sirui Ge. Peng-Fei Cao provides the general guidance for polymer synthesis.

6.1 Introduction

Recent studies[162] suggest that structural relaxation in clusters formed by stickers controls viscosity and terminal relaxation of the polymers with associating groups forming microphase separation. However, a detailed microscopic understanding of how the network rearrangement occurs in the presence of microphase separation is still lacking. Simulations studies[103] suggested that structural rearrangements in this type of systems should go through fusion and dissociation

of the clusters. This idea, however, was questioned in the recent experimental studies[102, 104]. Moreover, a clear separation between the timescale of cluster's structural relaxation time and rheological terminal mode was observed and remains unexplained[26, 104].

Experiments[65,159,143] also indicated the presence of a thin interfacial polymer layer with restricted mobility around these clusters, which also results in the elevated rubbery plateau modulus explained by the mechanical interfacial layer model (ILM). However, the interfacial layers might overlap forming a percolated network [82, 83]. Since the mechanical ILM assumes independent fillers with interfacial layer[81], the previous interpretation from mechanical ILM is questionable. For the polymer nanocomposites systems, the mechanical percolation model has already been utilized to describe the mechanical reinforcement in the presence of percolated network of the overlapping interfacial layers[84, 85, 173]. It has, however, never been used to study the analogous system like the associating polymers with microphase separation. Thus, the mechanism of network rearrangements and its effect on viscoelastic behavior in systems with clusters of the dynamic bonds remains a puzzle. Developing a microscopic understanding of viscoelasticity in polymers with clusters of dynamic bonds will help rational design of materials with multifunctional properties and relatively easy recyclability.

To address this challenge, we provide detailed analysis of the studied earlier model telechelic polymers with microphase-separated functional end groups[26, 163]. We demonstrate that mechanical percolation model indeed explains well the unusually high rubbery plateau modulus in these materials. Most important, based on the analogy to block copolymers, we propose a mechanism of the network rearrangements *via* single chain hopping between clusters controlled by a thermodynamic energy barrier related to the immiscibility of the dynamic end groups and

the polymer matrix. Based on these results, we propose a general scenario of viscoelasticity of polymers with clusters of dynamic bonds[174]. The presented in-depth understanding provides design rules for developing functional materials with tunable viscoelastic properties.

6.2 Materials and Methods

The materials used in this chapter is the PDMS-NHCO-COOH, the same as was mentioned in Chapter 5. Besides that, a new sample with DP of 19 is involved this research. The measurement was the same as mentioned in Chapter 5, including X-ray scattering, broadband dielectric spectroscopy and rheology measurements.

6.3 Results

6.3.1 X-ray scattering

Microphase separation in PDMS-NHCO-COOH has been verified through X-ray scattering in Chapter 6. The low-q weak at around 0.1 $Å^{-1}$ indicates the microphase separation. The similar X-ray scattering result was also observed in DP 19 PDMS-NHCO-COOH (Fig. 6.1). The Gaussian fitting of X-ray scattering spectra (Fig. 6.1) provides information on average center-to-center cluster distance (d) and radius of the cluster ($R_{cluster}$) (Table 6.1). The nearest cluster surface-to-surface distance can be calculated through $d_{IPS} = d - 2R_{cluster}$ (Table 6.1). With $R_{cluster}$, the grafting density (n_e) of PDMS chains on surface of the clusters can be calculated as:

$$n_e = \frac{V_{cluster}}{S_{cluster} V_{end}} = \frac{R\rho N_A}{3M_{end}} \quad (6.1)$$

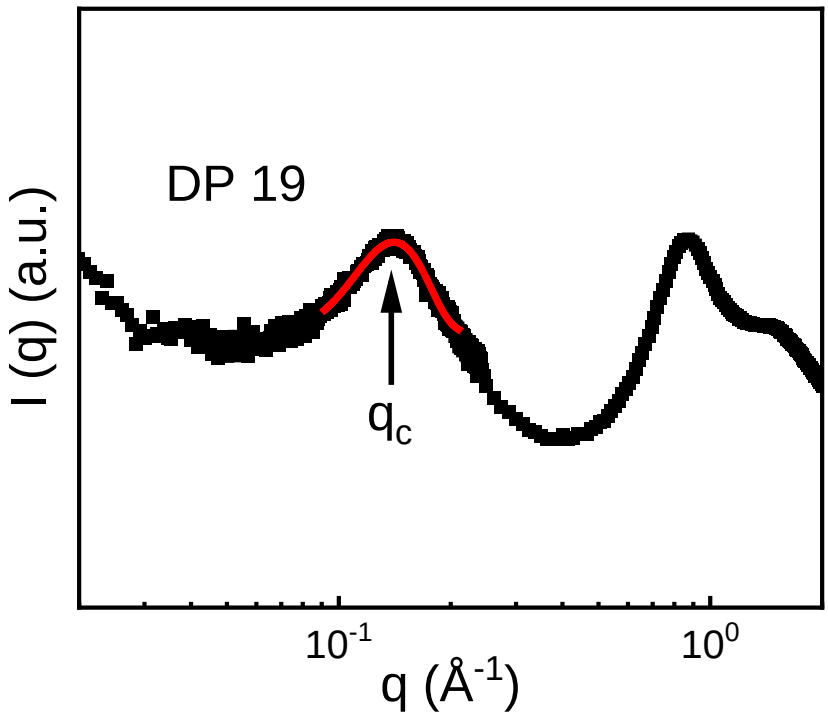

Figure 6.1 X-ray Scattering spectrum for PDMS-NHCO-COOH with DP 19. Red line presents the Gaussian fit of the low-q peak. The peak position is labeled by arrow.

Table 6.1 DP, Molecular Weight of the PDMS-NHCO-COOH samples including end groups (M_n), weight fraction of the end groups (f_e), center-to-center distance between clusters (d), radius of clusters ($R_{cluster}$), cluster nearest surface-to-surface distance (d_{IPS}), number of chain ends in each microphase separated cluster (Z) and grafted density n_e. Details of the X-ray data analysis were presented in Chapter 5.

DP	M_n (kg/mol)	f_e (wt%)	d (nm)	$R_{cluster}$ (nm)	d_{IPS}(nm)	n_e (nm^{-2})
13	1.28	24.7	4.08	1.59	0.9	1.9
19	1.72	18.4	4.47	1.58	1.31	1.9
22	1.94	16.3	4.43	1.50	1.43	1.8
50	4.02	7.9	5.12	1.36	2.4	1.7
74	5.57	5.7	5.97	1.43	3.11	1.8

where M_{end} and ρ are the molecular weight and density of the associating chain end, respectively. N_A is the Avogadro's number. The grafting density was found to be ~1.7-1.9 nm^{-1} for all associating polymers (Table 6.1).

6.3.2 Shear Rheology

Small amplitude oscillatory shear was employed to measure linear viscoelastic behavior of the associating polymers. Shear modulus master curves were constructed (Fig. 6.2a) by using time-temperature superposition (TTS) of the measured rheological spectra at different temperatures in the vicinity of terminal relaxation regime. The shift factor at various temperature used for TTS is shown in Fig. 6.2b. The rubbery plateau modulus (G_{Pl}) increases with decreasing the chain length of the polymer backbone, reaching unusually high level of G_{Pl} ~100 MPa in the shortest chains with DP of 13 (Fig. 6.2c). Terminal relaxation is observed at low frequencies where G' and G" increase with frequency as ω^2 and ω^1, respectively. In addition, the samples with DP of 13, 19 and 22 exhibit an intermediate regime between the rubbery plateau and the terminal relaxation where both G' and G" follow power law behavior $\sim\omega^{\alpha}$ with the exponent $\alpha \sim 0.5$ (Fig. 6.2a). In contrast, this regime is absent in spectra of samples with DP 50 and DP 74, where the terminal relaxation is reached right after the end of the rubbery plateau (Fig. 6.2a). In our previous publication, the terminal relaxation time was determined from the crossover of G' and G"[26, 163]. However, this method is only valid for the Maxwellian relaxation behavior. Due to the presence of the Rouse-like spectra in lower DP samples, the crossover is no longer able to provide the accurate estimation of the terminal relaxation time (Fig. 6.2c). In such case, the longest Rouse timescale is more accurate. Thus, to acquire the accurate terminal relaxation time

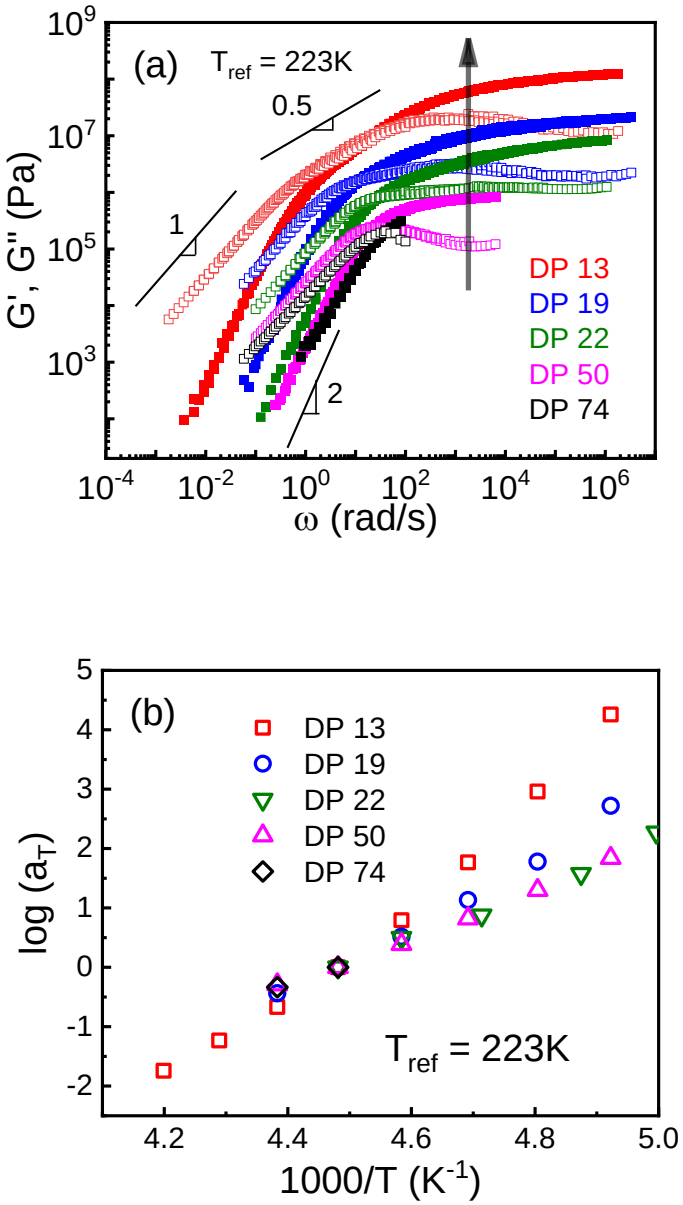

Figure 6.2 (a) Shear modulus master curves for the telechelic PDMS-NHCO-COOH measured at temperatures higher than second T_g. The arrow indicates the telechelic PDMS-NHCO-COOH samples used to create the master curves increased rubbery plateau value for shorter chains. (b) Shift factors of time-temperature superposition (TTS) for the. (c) Master curve of the shear modulus for DP 13 sample based on the reference temperature of 230K. Solid and open symbols refer to G' and G" spectra, respectively. Fits based on the Rouse model are shown as red lines. τ_C refers to terminal relaxation of the material. The values of the rubbery plateau modulus (G_{PL}) and shear modulus at terminal relaxation (G_0) are indicated with arrows.

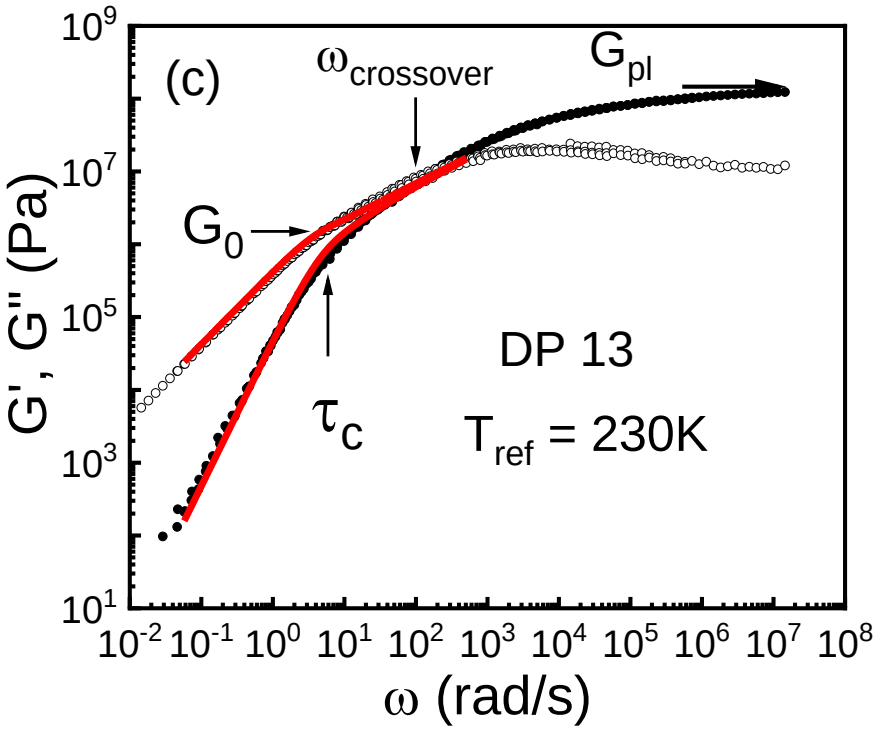

Figure 6.2 Continued

(τ_c) as well as its corresponding shear modulus level (G_0), Rouse model[175] is utilized to fit the shear modulus spectra:

$$G' = G_0 \sum_{j=1}^{N} \frac{\omega^2 \tau_j^2}{1+\omega^2 \tau_j^2} \quad \text{and} \quad G'' = G_0 \sum_{j=1}^{N} \frac{\omega \tau_j}{1+\omega^2 \tau_j^2} \tag{6.2}$$

in which $\tau_j = \frac{\tau_c}{j^2}$. For PDMS-NHCO-COOH with DP of 50 and 74, N is chosen to be 1, which corresponds to the Maxwell relaxation. However, for PDMS-NHCO-COOH with DP of 13, 19 and 22, N is chosen to be an arbitrary number to fit the region of parallel decrease of the G' and G" with slope of 0.5. The proposed fit describes well the shear modulus spectra (see, *e.g.*, Fig. 6.2c for PDMS-NHCO-COOH with DP of 13) and provides estimates of both the G_{Pl} and G_0, as well as τ_c.

6.3.3 Broadband dielectric spectroscopy (BDS)

To analyze microscopic cluster dynamics in the studied systems, we employed dielectric spectroscopy[26, 163]. The dielectric loss spectra (ε") higher than the 2nd T_g of the for all the sample are shown in Fig. 6.3(a-e). The labeled dielectric process is ascribed to motion of associating groups in the clusters, termed as α_2-relaxation[26]. Using the same fitting method mentioned in Chapter 4, i.e., eq. 4.1, we successfully acquired the characteristic relaxation time for α_2-relaxation (τ_{α_2}). The activation plot (Fig. 6.3f) indicates that α_2-relaxation relaxation also follows VFT behavior. If we extrapolate the VFT fitting to 100s, the temperature corresponds to the 2nd Tg, validating the assignment of the dielectric process to the motion of associating groups in the clusters.

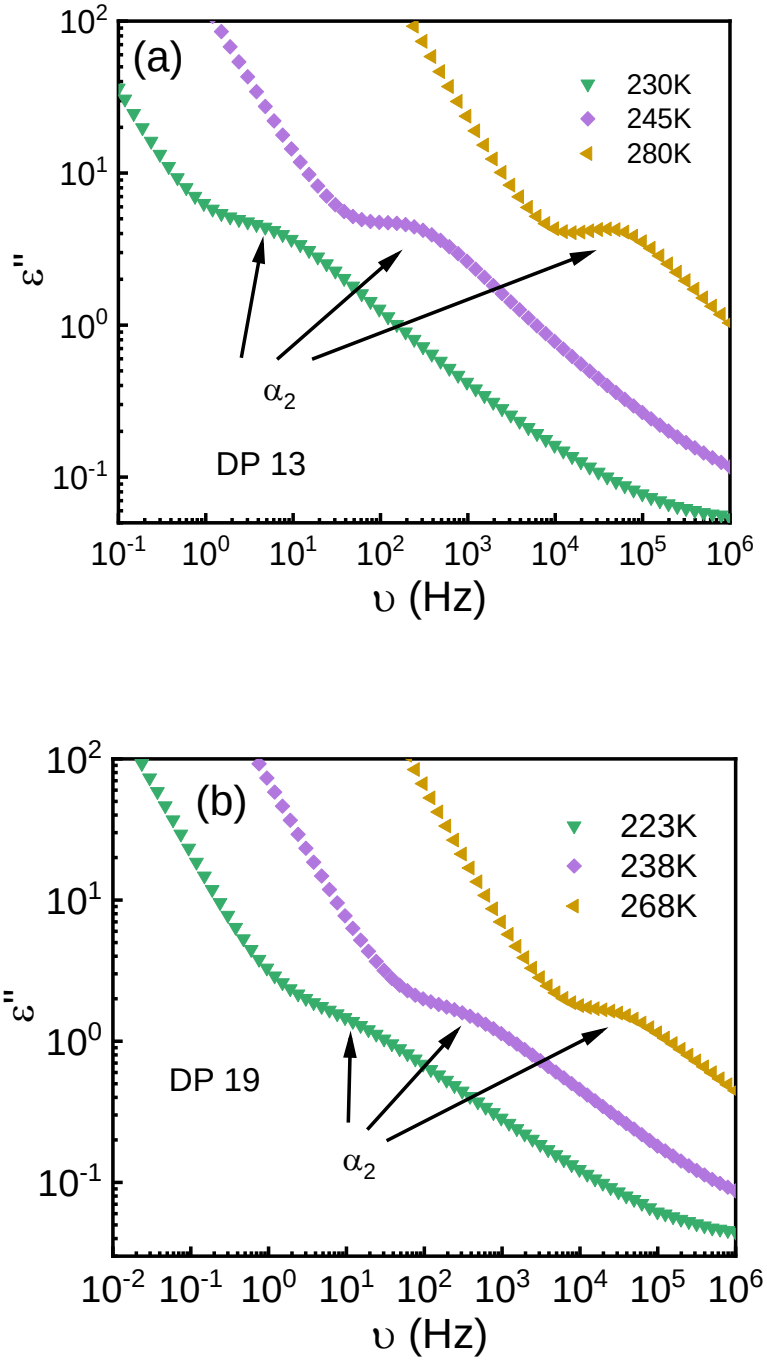

Figure 6.3 (a) Dielectric loss spectra for telechelic PDMS-NHCO-COOH with (a) DP 13, (b) DP 19, (c) DP 22, (d) DP 50, (e) DP 74, (f) $\tau_{\alpha 2}$ as a function of inverse temperature for PDMS-NHCO-COOH, (g) Comparison of ε" spectra and M" spectra for telehelic PDMS-NHCO-COOH with DP of 19 in which $\tau_{\alpha 2}$, $\tau_{\alpha 2\text{-}M}$ and τ_{σ} are labeled.

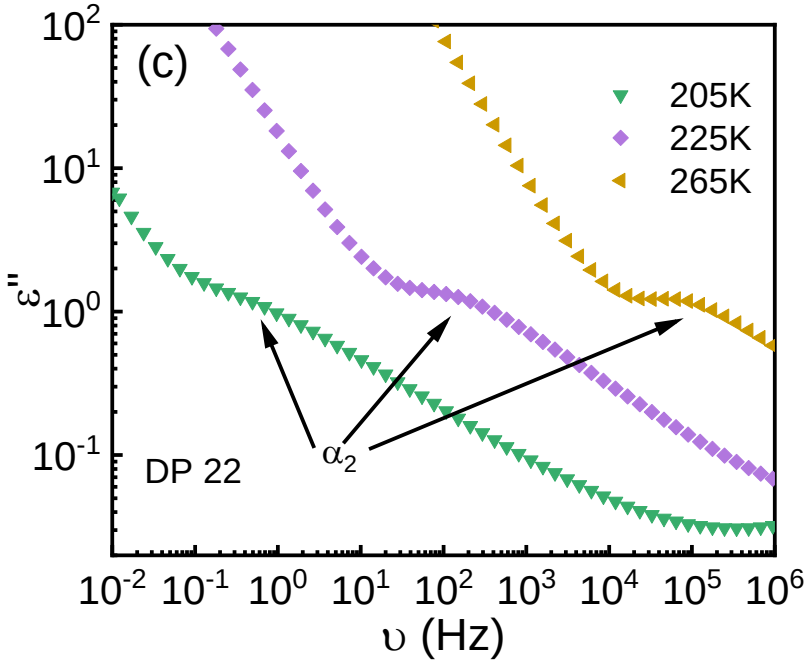

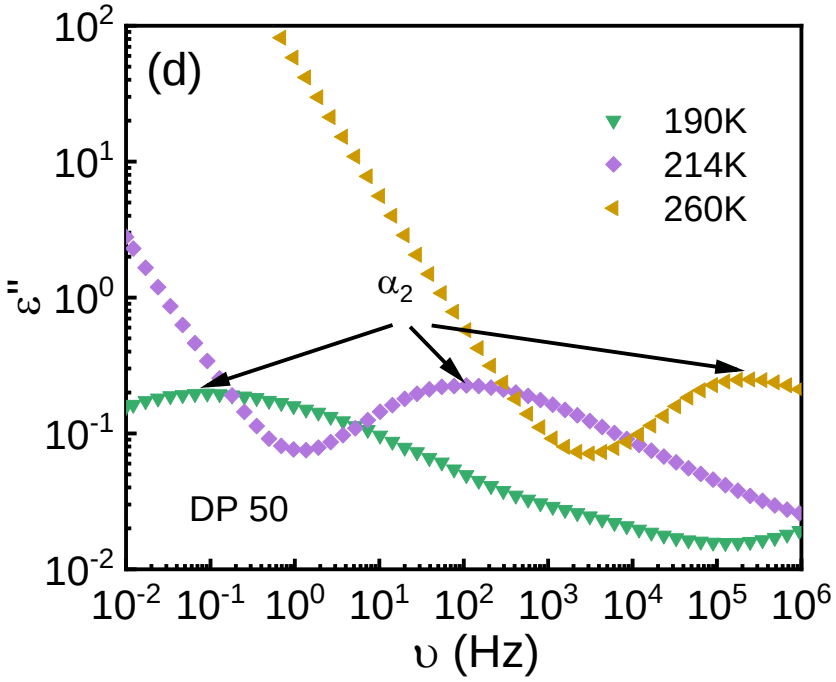

Figure 6.3 Continued

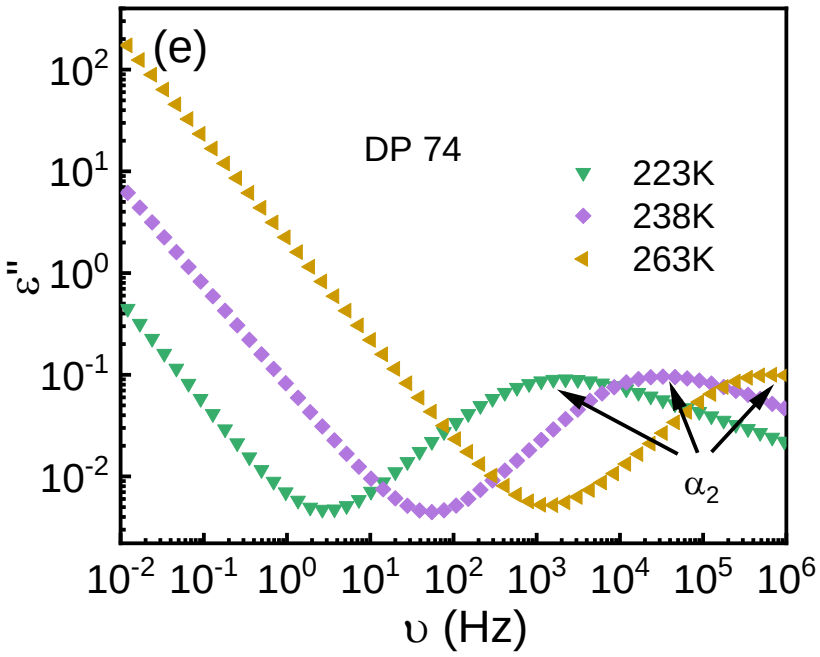

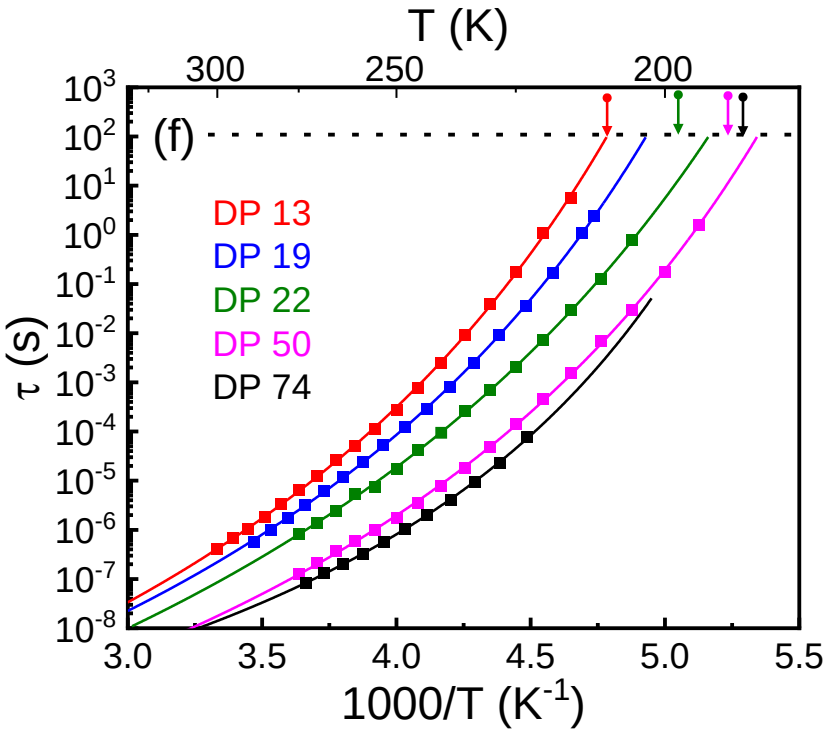

Figure 6.3 Continued

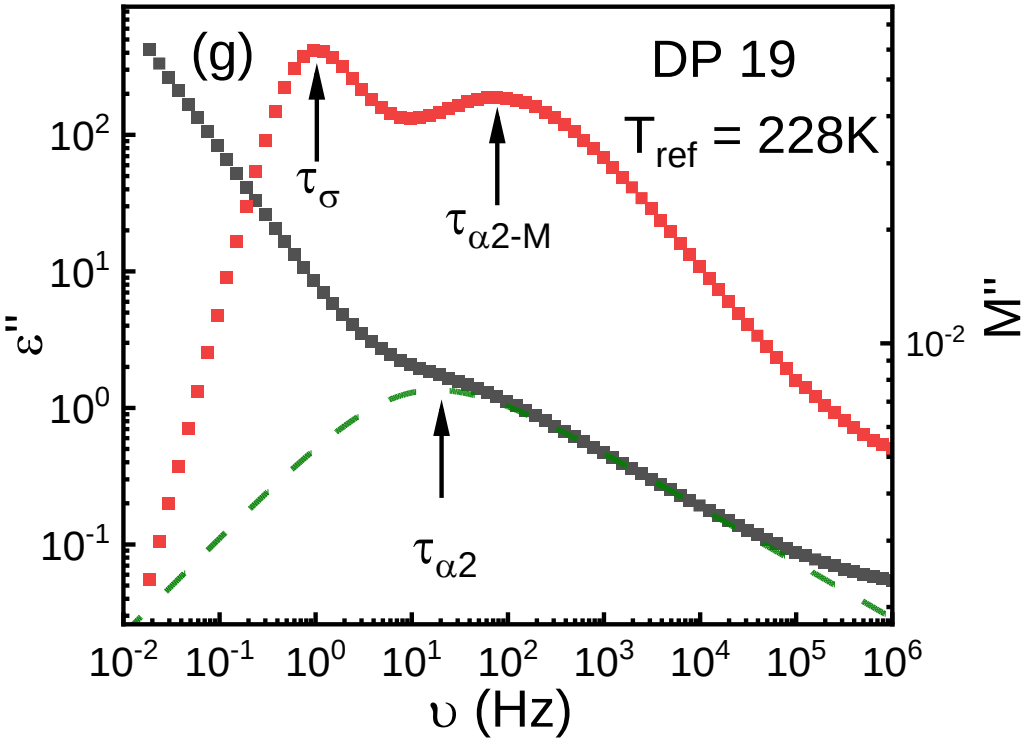

Figure 6.3 Continued

To compare rheological and dielectric data, the latter is converted to the dielectric modulus $M^*(\omega)$[138, 139], as was mentioned in Chapter 4 through eq. 4.5. The M" spectra is shown in Figure 6.3g with an additional dielectric process at lower frequencies originating from conductivity relaxation (τ_σ), as mentioned in Chapter 4. We also noticed that the timescale of α_2 relaxation process from M" (τ_{α_2-M}) is faster than that from ε" spectra (τ_{α_2}), especially for associating polymers with shorter chains such as DP 19 PDMS-NHCO-COOH (Fig. 6.3g). This is expected since the PDMS-NHCO-COOH with shorter PDMS backbone demonstrates higher amplitude of α_2-relaxation process (Fig. 6.3(a-e)), which can theoretically result in larger deviation of characteristic relaxation time from ε" spectra and M" spectra according to eq. 4.6. To acquire the characteristic relaxation time from modulus spectra, the M″ spectra were fit based on one Havrilliak-Negami (HN) function plus one Debye-like process for conductivity relaxation:

$$M''(\upsilon) = Im\left\{\frac{\Delta M_{\alpha_2}}{(1+(2\pi\upsilon\tau_{HN-M})^{\beta_M})^{\gamma_M}} + \frac{\Delta M_\sigma}{1+2\pi i\upsilon\tau_\sigma}\right\} \qquad (6.3)$$

in which ΔM_{α_2}, ΔM_σ are the "modulus strength" of α_2 process and conductivity process. τ_{HN-M}, τ_σ are the HN relaxation time for α_2 process and the conductivity relaxation time from dielectric modulus. β_M and γ_M are the stretching parameters for the α_2 process. The relaxation time corresponding to the peak position of α_2 process in M″ spectra is calculated using[106]:

$$\tau_{\alpha_2-M} = \tau_{HN-M}\left[\sin\left(\frac{\beta_M\pi}{2+2\gamma_M}\right)\right]^{-\frac{1}{\beta_M}}\left[\sin\left(\frac{\beta_M\gamma_M\pi}{2+2\gamma_M}\right)\right]^{\frac{1}{\beta_M}} \qquad (6.4)$$

6.4 Discussion

6.4.1 Mechanical percolation model explaining the mechanical reinforcement:

Our previous studies revealed the existence of an interfacial polymer layer around the microphase-separated clusters with a thickness l_{int} ~ 0.8-0.9 nm regardless of PDMS backbone length[143]. This small thickness was explained by the small radius of the microphase-separated clusters, $R_{cluster}$ ~ 1.4-1.6 nm[143]. When the distance between clusters surfaces $d_{IPS} < 2l_{int}$, the interfacial layers overlap with each other, forming a percolating network. According to the Table 6.1, the percolation of the interfacial regions can happen in PDMS-NHCO-COOH with DP of 13, 19 and 22, while the interfacial layers are expected to be fairly separated in PDMS-NHCO-COOH with DP of 50 and 74 (Fig. 6.4). The critical volume fraction of the cluster, $(f_e)_c$, for percolation is estimated as $d_{IPS} = 2l_{int}$, and appears in the range ~ 13.5 ± 1.2 wt%.

This analysis reveals that indeed interfacial layers form a percolating structure in systems with low DP, and the mechanical percolation model needs to be used to describe the elevated mechanical modulus observed in these samples. According to this model[95], a composite modulus is expressed as:

$$G_c = \frac{(1-2\psi+\psi X_r)G_s G_r+(1-X_r)\psi G_r^2}{(1-X_r)G_r+(X_r-\psi)G_s} \qquad (6.5)$$

in which G_r is the shear modulus of the rigid phase. G_s is the shear modulus of the matrix (in this case PDMS matrix, which can be estimated from the classical rubber elasticity theory). X_r is the volume fraction of the overall rigid phase. ψ is the volume fraction of the spanning rigid phase formed in the percolated network through the overlapping of the interfacial layer, and defined as:

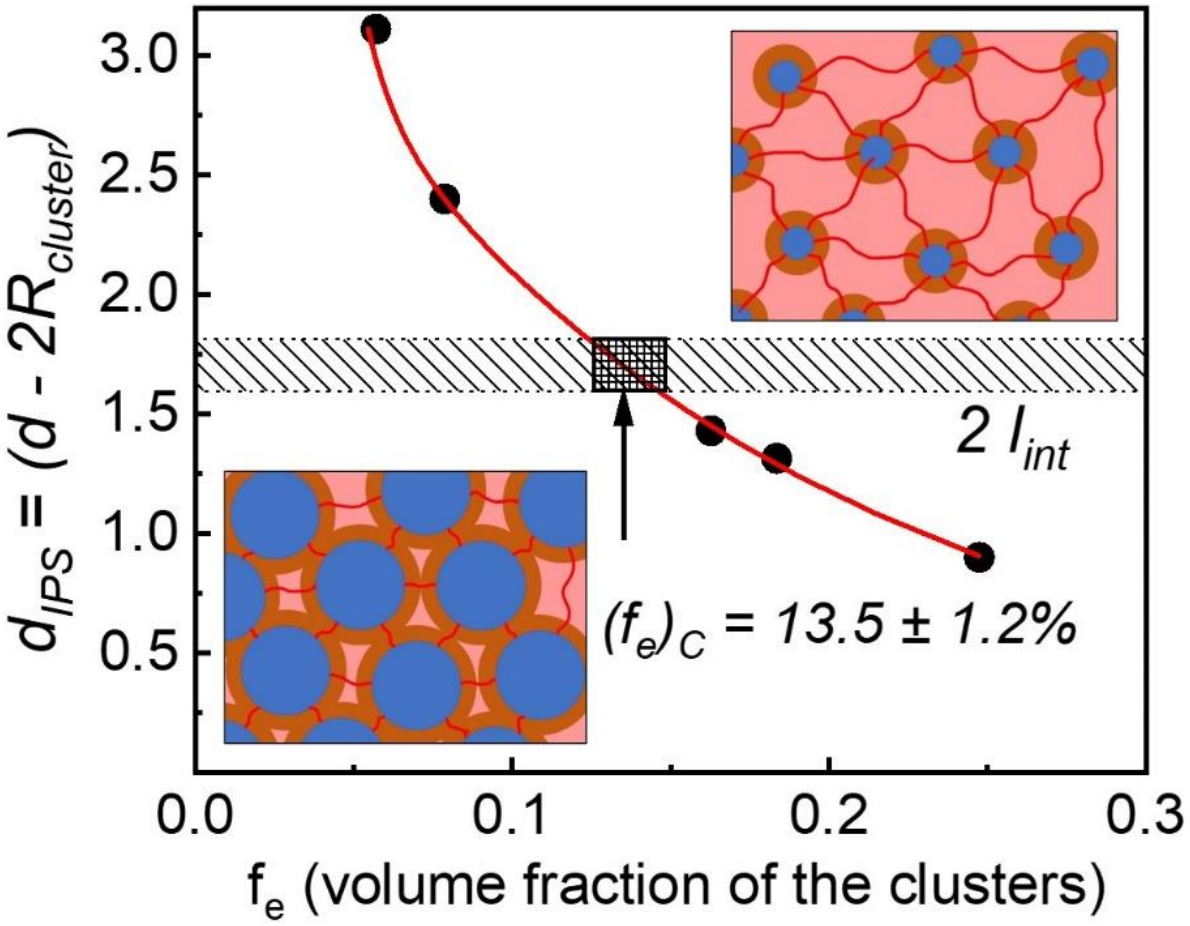

Figure 6.4 d_{IPS} as a function of f_e. Range of $2l_{int}$ value shown as a grey area. The box area indicates the estimated range of percolation threshold, $(f_e)_C$, when $d_{IPS} \sim 2l_{int}$. Above the percolation threshold, interfacial layers overlap to form a percolated network whereas below the threshold, they are well separated. Blue circles represent the clusters of functional groups which are surrounded by interfacial layers (orange) and linked by PDMS chains (red).

$$\psi = \begin{cases} 0, & X_r < X_c \\ X_r\left(\frac{X_r - X_c}{1 - X_c}\right)^b, & X_r \geq X_c \end{cases} \quad (6.6)$$

Here X_c is the volume fraction of the rigid phase at the percolation threshold, b is the percolation exponent characterizing the rate of the percolation structure formation with X_c.

We assume for simplicity that the clusters and their interfacial layers form a single rigid phase with volume fraction $X_r = \varphi_{cluster} + \varphi_{int}$. The mechanical percolation model (eq. 6.5 and eq. 6.6) successfully describes the mechanical reinforcements in studied polymers (Fig. 6.5). The value of X_r at the percolation threshold is found to be 56.5%, which corresponds to the critical volume fraction of the cluster, $(f_e)_c \sim 14.8\%$. The obtained value is in good agreement with the value estimated assuming an ordered cubic arrangement of the clusters (Fig. 6.5). The critical exponent b obtained from the fit is ~1.7, which also agrees with the prediction from scalar elastic model in 3 dimensions developed by de Gennes[176]. Experimental investigations of percolation in various systems including organic polymer blends, polymer gels and nanocomposite indicate the exponent b ranges from 1.6-2.2[177-182]. The model also provides the estimates of the shear modulus of the rigid phase, G_r ~177 MPa.

The obtained G_r value agrees well with the estimates of the shear modulus of the rigid phase using the Two-Phase Model (TPM) (Table 6.2). The two phases are clusters and the interfacial layer. The necessary parameters to estimate the shear modulus using TPM are shear modulus, volume fraction and Poisson ratio of both clusters and the interfacial layer. The modulus of the interfacial layer was estimated to be ~ 100MPa [143]. The Poisson's ratio of the interfacial layer (which consists of PDMS segments) is taken from literature[171] based on the PDMS values. For clusters, the modulus and the Poisson's ratio are assumed to be 3 GPa and 0.33, respectively,

Table 6.2 DP, volume fraction of clusters $\varphi_{cluster}$, volume fraction of the interfacial layer φ_{int}, volume fraction of clusters in the rigid phase $\varphi_{cluster,TPM}$, volume fraction of the interfacial regions in the rigid phase $\varphi_{int,TPM}$, and the overall shear modulus of the rigid phase estimated using TPM for the PDMS-NHCO-COOH associating polymers.

Material	DP	$\varphi_{cluster}$ (%)	φ_{int} (%)	$\varphi_{cluster,TPM}$ (%)	$\varphi_{int,TPM}$ (%)	G_r(TPM) (MPa)
PDMS-NHCO-COOH	13	24.7	71.8	25.6	74.4	171
	19	18.4	59.1	23.7	76.3	164
	22	16.3	40.8	28.5	71.5	183
	50	7.9	26.6	22.9	77.1	161
	74	5.7	19.7	22.4	77.6	159

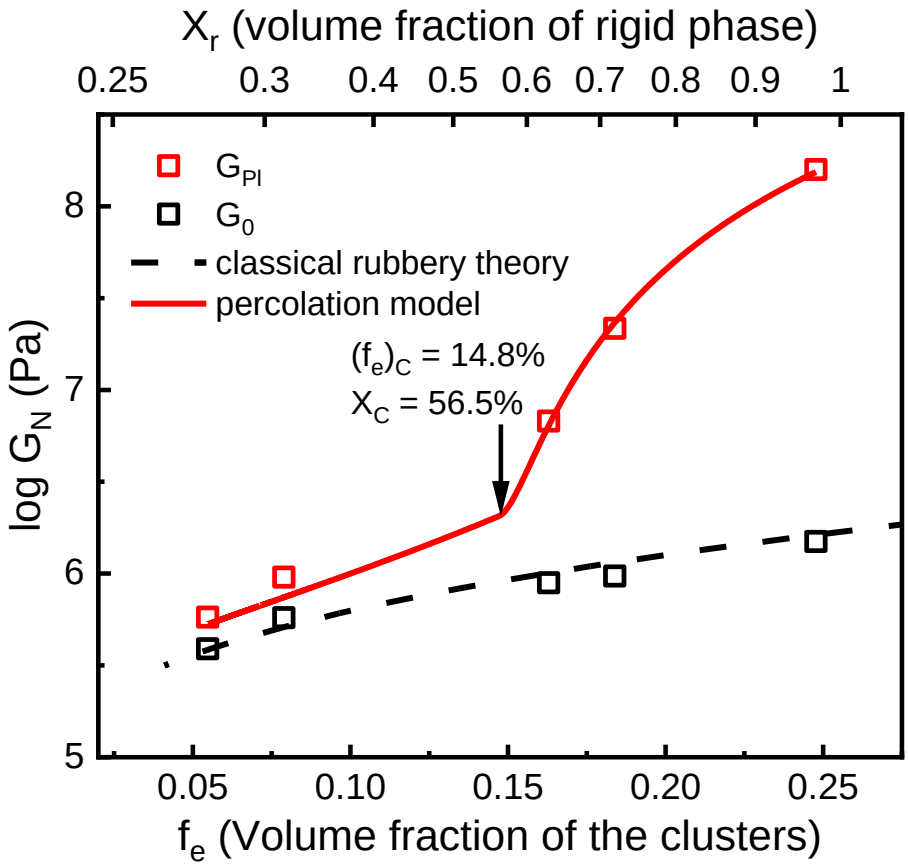

Figure 6.5 Variation of G_{PL} (red squares) and G_0 (black squares) as a function of f_e and X_r. Red line shows the fitting based on the mechanical percolation model (eq. 6.5 and eq. 6.6). Black dashed line indicates the prediction from classical rubber elasticity theory. The arrow indicates percolation threshold estimated from the fit.

which are typical values for glassy hydrogen-bonded systems such as glycerol[183]. The volume fraction of cluster and interfacial layer in the rigid phase were estimated as $\varphi_{cluster,TPM} = \frac{\varphi_{cluster}}{\varphi_{cluster}+\varphi_{int}}$ and $\varphi_{int,TPM} = \frac{\varphi_{int}}{\varphi_{cluster}+\varphi_{int}}$, respectively, where value of $\varphi_{cluster}$ and φ_{int} for PDMS-NHCO-COOH with DP of 13, 22, 50, 74 were demonstrated in Chapter 5 and φ_{int} of PDMS-NHCO-COOH with DP of 19 was estimated through

$$\varphi_{int} = \varphi_{cluster}\left[\left(\frac{l_{int}}{R_{cluster}} + 1\right)^3 - 1\right] \quad (6.7)$$

by using $l_{int} = 0.85nm$, which was estimated in Chapter 6, the results are in good agreement with the value from mechanical percolation model (~177MPa) (Table 6.2), validating that the percolation model explains well the mechanical reinforcement in the studied samples.

6.4.2 Viscoelastic behavior near terminal relaxation

It is interesting that in systems with no percolation (*i.e.*, with DP of 50 and 74) the terminal relaxation demonstrates Maxwellian behavior, *i.e.*, rubbery plateau stops at the terminal relaxation. In contrast, the rubbery plateau in systems with percolating rigid regions (*i.e.*, with DP of 13, 19 and 22) first decreases with a power law before reaching the terminal relaxation (Fig. 6.2a). Consequently, the moduli G_{Pl} and G_0 (eq. 6.2) appear to be comparable for non-percolated systems, while G_{Pl} is much higher than G_0 in percolating systems, and the difference increases with decrease in samples DP (Fig. 6.5). Analysis of these data revealed that G_0 obtained from the fit for all the sample follows the classical rubber elasticity[184] predictions for given length of the PDMS chains (Fig. 6.5), demonstrating that the mechanical reinforcement actually vanishes at terminal relaxation.

To study the viscoelastic properties in associating polymers with microphase separation, we compared shear modulus spectra and dielectric M" spectra (Fig. 6.6a). It is evident that τ_c is significantly slower than τ_{α_2-M}, indicating that motion of stickers inside the clusters is not sufficient for terminal relaxation. Interestingly, the shear modulus in percolating systems starts to decrease from the rubbery plateau level at the time scale comparable to τ_{α_2-M} (Fig. 6.6a), suggesting that the stickers motions within the clusters lead to the softening of the modulus down to the level predicted from classical rubber elasticity. Indeed, when chain ends in clusters are unable to move, the whole system is similar to nanoparticles with extremely high grafting density ~1.7-1.9 chains/nm^2 (Table 6.1). This grafting density is ~3 times higher than in usual polymer grafted nanoparticles, leading to strong crowding and stretching of the chains in the interfacial layer. Stretching of the chain is supported by larger population of the gauche states found from wide-angle X-ray scattering results[143]. All these factors strongly hinder bending of the PDMS segments in the interfacial layer and lead to high modulus. However, when chain ends start to move inside the clusters, the PDMS segments in the interfacial layer can be easily rearranged and change their conformations under external force, and the macroscopic deformation is easier to reach. This results in a gradual softening of the polymer interfacial layer, which is demonstrated through the parallel decrease of the G' and G" with decrease in frequency. This softening reaches the modulus level expected from the rubber elasticity at the time of the terminal relaxation. Moreover, similar temperature dependence of both τ_{α_2-M} and τ_C (Fig. 6.6(b-f)) suggest that dynamics in the clusters might act as a precursor for the macroscopic rearrangement of the network.

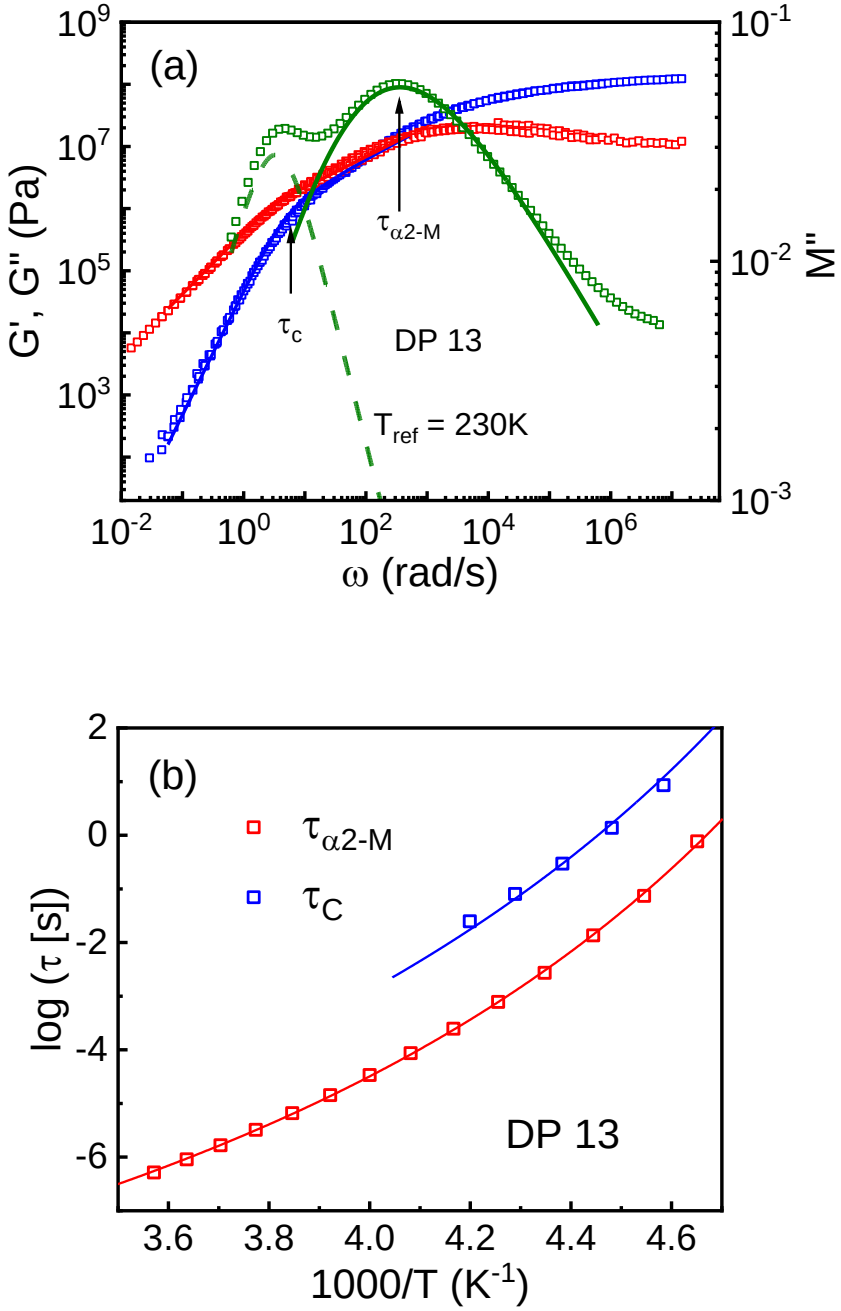

Figure 6.6 (a) Comparison between the shear modulus (red and blue symbols) and the dielectric loss modulus spectra (green symbols) for PDMS-NHCO-COOH with DP of 13 sample at 230K. Terminal relaxation timescale (τ_C) and α_2-relaxation timescale ($\tau_{\alpha 2\text{-}M}$) are labeled with arrows. (b-f) Temperature dependence of the two timescales (symbols), and their fit based on eq. 6.10 and eq. 6.9 (lines) for PDMS-NHCO-COOH with DP of 13, 19, 22, 50 and 74.

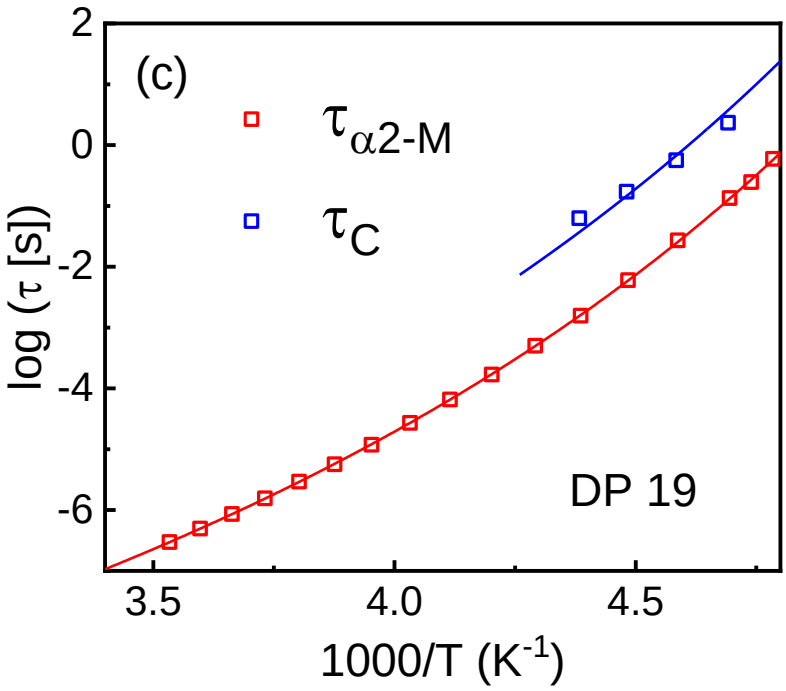

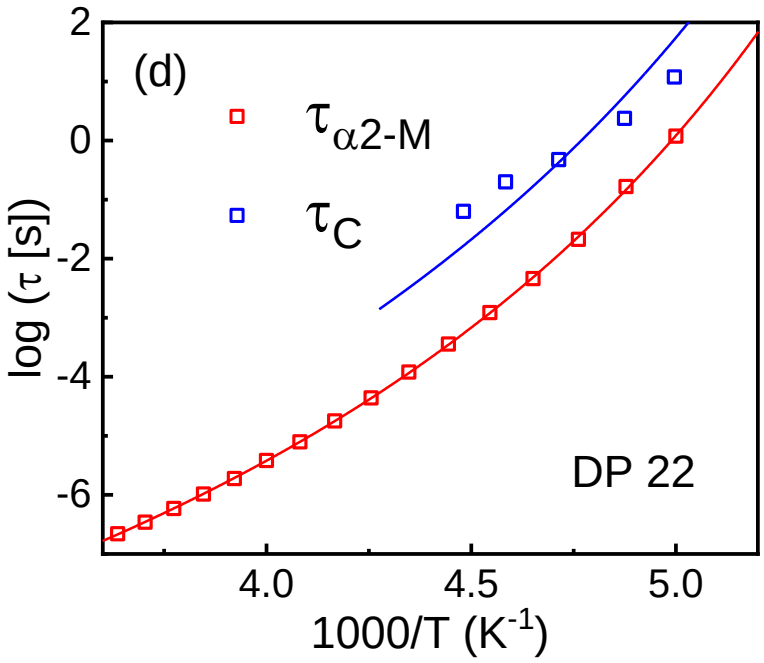

Figure 6.6 Continued

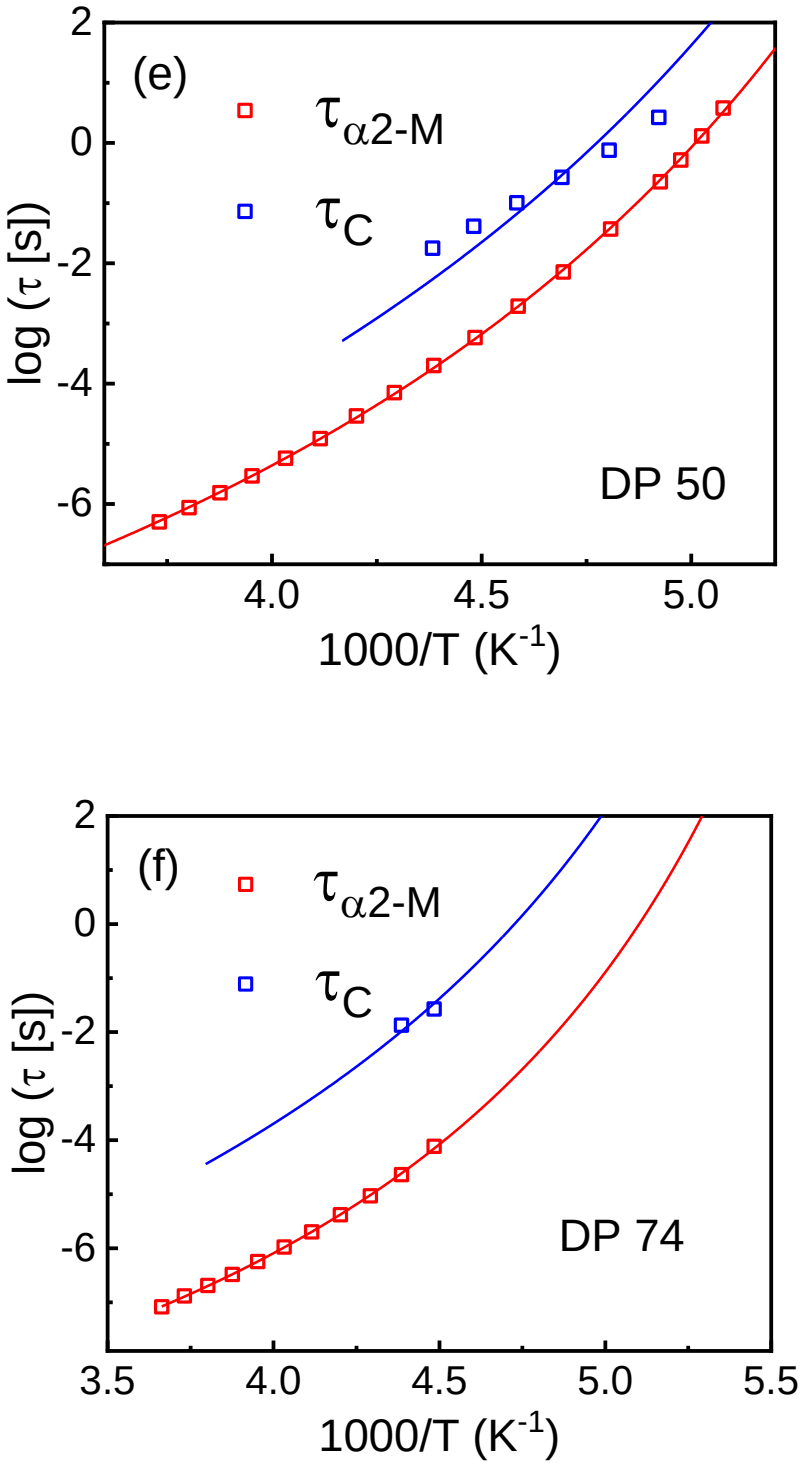

Figure 6.6 Continued

6.4.3 Mechanism of network rearrangement

The mechanism of network rearrangement in associating polymers with microphase separation remains a puzzle. It is obvious that the network rearrangement should involve exchange of the stickers between different clusters[103, 185]. Based on computer simulations, Amin *et al.* suggested that exchange should go through a merge of different clusters[103]. This mechanism was questioned by Mordvinkin *et al.*[102, 104], where telechelic poly(isobutylene) (PIB) with functional end groups were studied. These systems, like the studied here polymers, have well separated clusters and merging of these clusters is not feasible due to the presence of multiple chains between the clusters. These systems, however, are similar to triblock copolymers with microphase separation. In triblock copolymers with microphase separation, network rearrangement process is dominated by chain pullout process, which needs to overcome the free energy penalty from the immiscibility of different blocks[185-187]. In other words, the block in the microphase-separated cores need to be pulled out and diffuse to another microphase-separated core to complete the rearrangement process. According to[188-190] the pullout timescale is expressed as:

$$\tau_{pullout} = \tau_{Rouse} \exp(\alpha \chi N_{core}) \quad (6.8)$$

in which τ_{Rouse} is Rouse relaxation time of the block inside the microphase-separated cores. χ is the Flory−Huggins parameter. N_{core} is the number of Kuhn segments of the block forming microphase-separated cores. α is a constant in the order of unity. We hypothesize that the similar mechanism controls bond rearrangements in the studied here telechelic systems, and the free energy barrier to "chain end pullout" process determines the network rearrangement process (Fig. 6.10a).

Borrowing the idea of chain exchange kinetics in block copolymer micelles[185-187, 191], relationship between τ_c and τ_{α_2-M} can be expressed as:

$$\tau_c(T) = \tau_{\alpha_2-M}(T)\exp\left(\frac{E_a}{RT}\right) = \tau_{\alpha_2-M}(\mathrm{T})\exp\left(\alpha\chi N_{core}\right) \quad (6.9)$$

in which the activation energy barrier, E_a, is related to the thermodynamic penalty for the sticker to be placed in the polymer matrix $\sim\alpha\chi N_{core}$. To estimate the activation barrier from the experimental result, $\tau_{\alpha_2-M}(T)$ was fit to the Vogel–Fulcher–Tammann (VFT) equation (Fig. 6.6(b-f), red line):

$$\tau_{\alpha_2-M}(T) = \tau_0\exp\left(\frac{B}{T-T_0}\right) \quad (6.10)$$

Here τ_0, B and T_0 are the VFT fit parameters. Then, $\tau_C(T)$ was fitted using eq. 6.9, in which τ_{α_2-M} is substituted by the VFT equation, with the energy barrier E_a as the only free fit parameter (Fig. 6.6(b-f)). The fitting results revealed the average activation energy to be ~ 6.6 kJ/mol (Fig. 6.7). Strong deviation in the case of the sample with DP 74 might be caused by crystallization that strongly limited the studied temperature range.

The obtained activation energy can be compared to the expected $\sim\alpha\chi N_{core}$. N_{core} of the end group is 1, and the Flory-Huggins parameter, χ, can be estimated from the solubility parameters (δ) and molar volume of the chain end instead of the molar volume of a copolymer block[192]

$$\chi = \frac{(\delta_{end}-\delta_{PDMS})^2 V_{end}}{RT} \quad (6.11)$$

The solubility parameter of the PDMS backbone δ_{PDMS} is 7.3 $cal^{1/2}cm^{-3/2}$ [193]. The solubility parameter of the chain end (COOH), δ_{end}, is estimated *via* Hansen Solubility Parameter (HSP)[194]

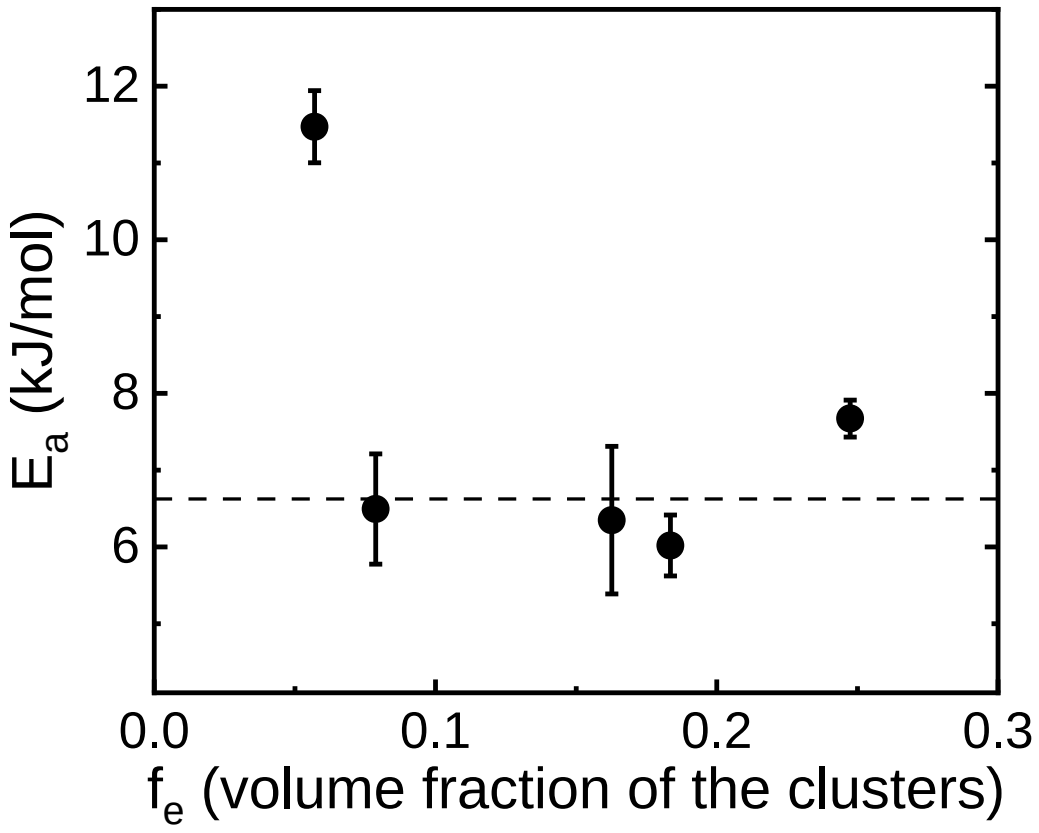

Figure 6.7 Estimated energy barrier for single sticker “pullout” into PDMS matrix. The solid dashed line indicates the average activation energy for this process.

approach, which divides the solubility parameter into 3 partial components: dispersion, polarity and hydrogen-bonding. The total solubility parameter is calculated as

$$\delta_t = \sqrt{\delta_d^2 + \delta_p^2 + \delta_{hb}^2} \quad (6.12)$$

Each partial parameter can be estimated through the group contribution method[195]:

$$\delta_d = \left(\sum_i N_i C_i + \sum_j M_j D_j + 959.11\right)^{0.4126} (MPa)^{\frac{1}{2}} \quad (6.13)$$

$$\delta_p = \left(\sum_i N_i C_i + \sum_j M_j D_j + 7.6134\right) (MPa)^{\frac{1}{2}} \quad (6.14)$$

$$\delta_{hb} = \left(\sum_i N_i C_i + \sum_j M_j D_j + 7.7003\right) (MPa)^{\frac{1}{2}} \quad (6.15)$$

where C_i is the contribution of the first-order groups of type i that appears N_i times in the compound and D_j is the contribution of the second-order groups of type j that appears M_j times in the compound.

According to the PDMS-NHCO-COOH chain end structure, it possesses 4 different First-order groups in the Table A.1. in[195]. (Fig. 6.8). By using the equations (eq. 6.16 – eq. 6.18), 3 partial parameters are calculated as shown below.

$$\delta_d = \left(3\delta_{d,CH2} + \delta_{d,CH2CO} + \delta_{d,COOH} + \delta_{d,CH2NH} + 959.11\right)^{0.4126} = 18.233\ (MPa)^{\frac{1}{2}} \quad (6.16)$$

$$\delta_p = \left(3\delta_{p,CH2} + \delta_{p,CH2CO} + \delta_{p,COOH} + \delta_{p,CH2NH} + 7.6134\right) = 11.258\ (MPa)^{\frac{1}{2}} \quad (6.17)$$

$$\delta_{hb} = \left(3\delta_{hb,CH2} + \delta_{hb,CH2CO} + \delta_{hb,COOH} + \delta_{hb,CH2NH} + 7.7003\right) = 11.392\ (MPa)^{\frac{1}{2}} \quad (6.18)$$

Thus, $\delta_{end} = 24.27\ (MPa)^{\frac{1}{2}} = 11.86\ cal^{\frac{1}{2}} cm^{-\frac{3}{2}}$.

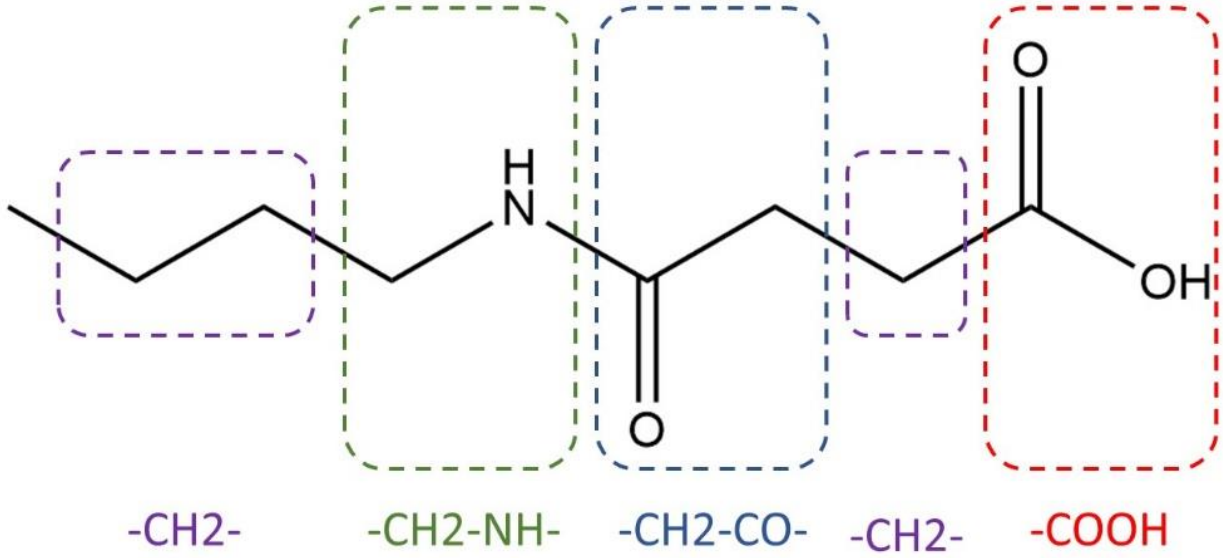

Figure 6.8 Chemical structure of chain ends dividing into 4 parts, all of which are included in the Table A.1 in[195].

The molar volume of chain ends V_{end} is calculated using $V_{end} = \frac{M_{end}}{\rho_{end}}$, where the molecular weight of chain ends M_{end} is 158 g/mol, and the density of chain ends is assumed to be the same as that of glycerol, ρ_{end} = 1.26 g/cm^3. Thus, $(\delta_{end} - \delta_{PDMS})^2 V_{end}$ is estimated to be ~ 11 kJ/mol, in reasonable agreement with the experimentally estimated E_a assuming α value ~0.6. The value of α close to 0.6 has been reported in several studies of chain exchange kinetics in different block copolymer micelles[187, 196, 197]. Thus, the single chain hopping mechanism provides reasonable estimates of the energy barrier controlling terminal relaxation in associating polymers with microphase separation.

Based on these results and analysis, we propose the following mechanism of the terminal relaxation in polymers with phase separated reversible bonds (stickers). Network rearrangements require mobility of stickers in the clusters and a sticker escape from the cluster requires to overcome an energy barrier controlled by miscibility of stickers in a polymer matrix. Once the sticker escaped from the cluster, it will diffuse through the polymer matrix to another cluster with a timescale of $\tau_{\text{diffusion}}$, which is mainly governed by Rouse sub-diffusive motion, *i.e.*, $\tau_{diffusion} \sim \tau_\alpha (\frac{d}{l_k})^4$, here d is the distance between clusters (~ 5 nm, Tables 6.1) and l_k is the Kuhn segment length of PDMS (~ 1 nm). This provides estimates of $\tau_{diffusion} \sim 10^3\ \tau_\alpha$. At the onset of 2nd T$_g$, where stickers can move inside the clusters, τ_α is ~ 10^{-9} s and $\tau_{diffusion}$ is ~ 10^{-6} s. This time is many orders faster than terminal relaxation time at the same temperatures. Thus, we can safely assume that sticker escape from the cluster is the rate-determining step in the single chain hopping process. This mechanism is similar to that describing the network rearrangement of Butyl ionomer[198]. However, we introduce the microscopic mechanism of these

rearrangements and identify the energy barrier controlling the sticker hopping process. This mechanism also explains the difference between the timescale of network rearrangement and the dynamic bonds motion inside the clusters. The proposed mechanism is consistent with the recent NMR studies[102, 104] revealing that single chain relaxation is responsible for the terminal relaxation in the associating polymer with phase separation. These studies of telechelic PIBs with barbituric acid end groups and with thymine end groups also revealed that cluster relaxation process observed in dielectric spectra is faster than the terminal relaxation, and the ratio of these time scales depends on chemistry of the stickers[104] (Fig. 6.9). Following the proposed mechanism, we estimated the energy barrier (through eq. 6.9) to be E_a ~ 16-17 kJ/mol for more polar barbituric acid end groups and ~ 9 kJ/mol for less polar thymine end group (Table 6.3). The obtained energy barrier (E_a) with error is presented in the Table 6.3.

We assume that this energy barrier also originates from the immiscibility between polymer backbone and chain ends can be estimated using $\alpha(\delta_{end} - \delta_{PIB})^2 V_{end}$. The solubility parameter of chain end δ_{end} is 28 $MPa^{\frac{1}{2}}$ and 27 $MPa^{\frac{1}{2}}$ for BA[199] and TH[194], respectively. The solubility parameter for the PIB backbone is 15.8 $MPa^{\frac{1}{2}}$ [200]. According to the chemical structure, the molecular weight of the chain end is $M_{BA} = 128\ g/mol$ and $M_{TH} = 126\ g/mol$. In terms of the density, it is $\rho_{BA} = 0.72 g/cm^3$ and $\rho_{TH} = 1.23\ g/cm^3$, respectively. Thus, by using the similar methods mentioned above, $(\delta_{end} - \delta_{PIB})^2 V_{end}$ is estimated to be 26 kJ/mol for PIB associating polymers with BA, and 13 kJ/mol for PIB associating polymers with TH, respectively. Comparison of these values with the estimated (Table 6.3) suggests that α value is ~0.6-0.7. Thus, the proposed mechanism provides also good understanding for the network rearrangement in other associating polymer systems with microphase separation.

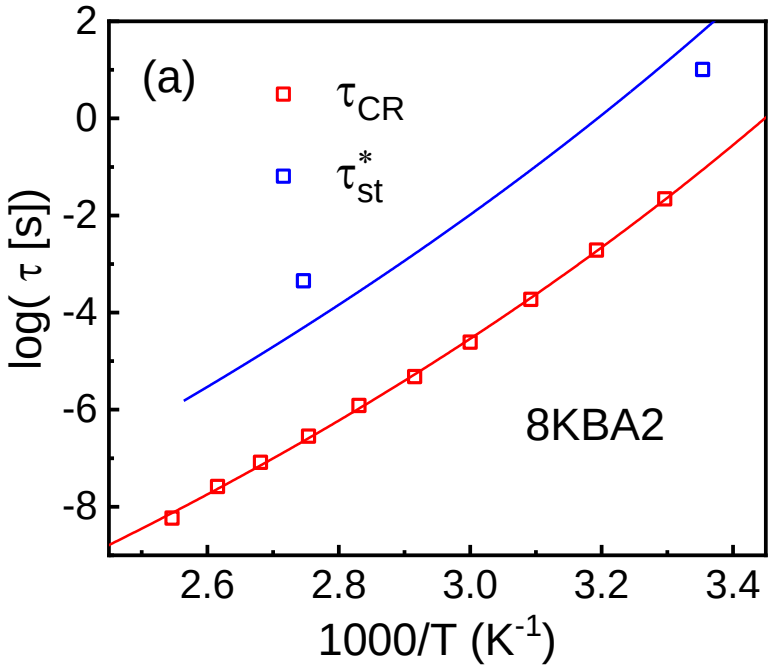

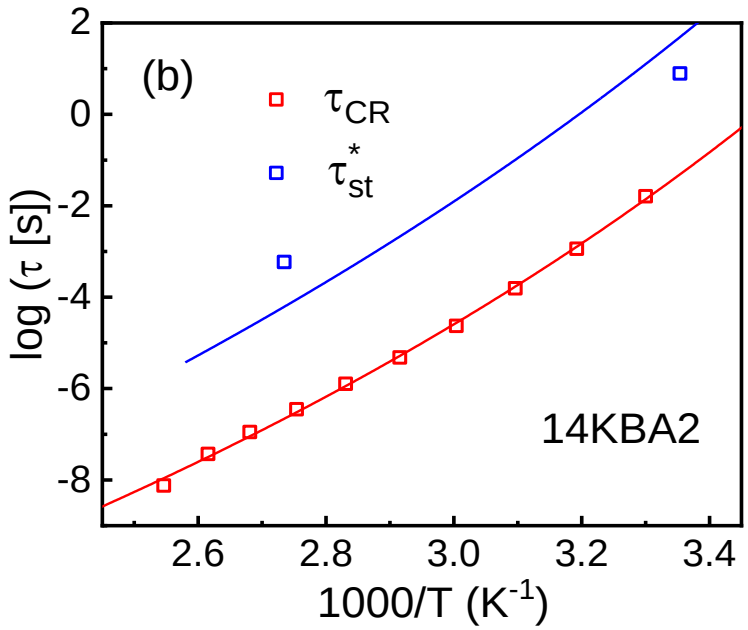

Figure 6.9 Activation plot of the telechelic PIB associating polymer (a) 8KBA2, (b) 14KBA2, (c) 4KTH2 reflecting the separation between τ_{CR} and τ_{st}*. Data from[104] .

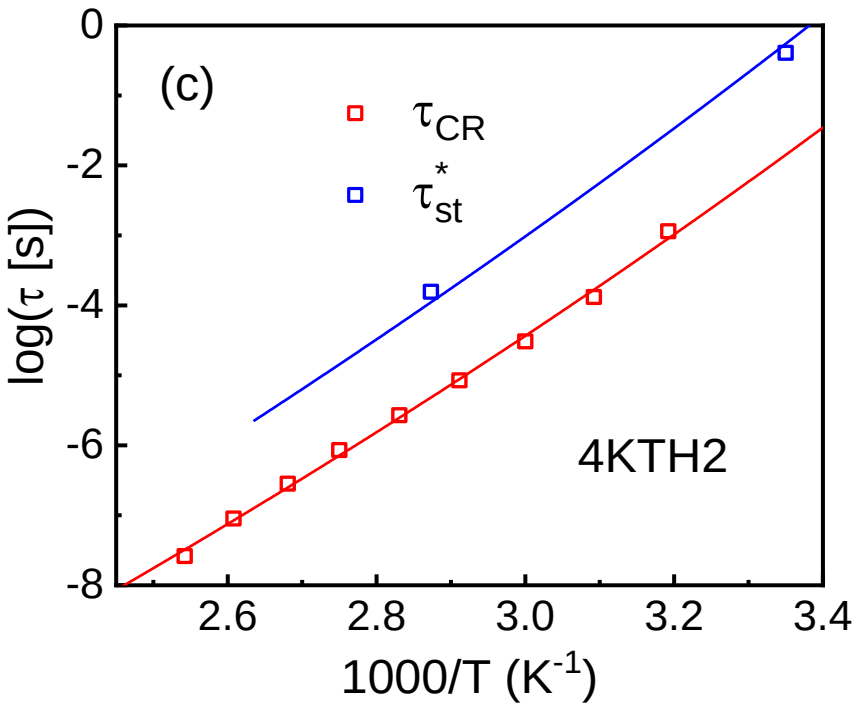

Figure 6.9 Continued

Table 6.3 The estimated energy barrier E_a for 3 telechelic PIB associating polymers

Sample	E_a(kJ/mol)
8KBA2	16.3 ± 5.5
14KBA2	17.1 ± 5.6
4KTH2	9.1 ± 0.9

6.4.4 A general molecular picture

Based on analysis of the presented above results, we propose a general picture of viscoelasticity in associating polymers with microphase separation (Fig. 6.10b). Microphase separated clusters possess a higher T_g value than the polymer matrix and their dynamics is governed by a timescale of structural relaxation in these clusters, τ_{α_2}. At times $t < \tau_{\alpha_2}$, clusters are glassy and control the rubbery plateau level. In such case, not only chain ends are fixed, but also the grafting density is extremely high, resulting in chains crowding and stretching in an interfacial layer around these clusters. These severely restrict segmental mobility and chain bending (similar to polymer grafted nanoparticles), leading to a much higher elastic modulus[143, 163]. In the absence of percolation of the interfacial polymer regions, the mechanical reinforcement from the interfacial layer is small, and mechanical strength of the associating polymer is mostly defined by the rubber elasticity of network structure crosslinked by the clusters. However, in the case where interfacial regions overlap, significant mechanical reinforcement is observed, which can be ascribed to a percolation phenomenon (Fig. 6.10b). On time scale $\tau_{\alpha_2} < t < \tau_c$, stickers become mobile within the clusters, and even if the grafting density is high, the segments in the vicinity of clusters can easily rearrange and change conformations. This leads to a subsequent decrease of the mechanical modulus in the interfacial layer down to the level expected in the rubber elasticity theory. As a result, the macroscopic modulus level drops down significantly in the case of percolated network as the effect of percolation fades away with the gradual softening of the modulus in the interfacial layer. When there is no percolation, the decrease in the macroscopic shear modulus is negligible until topological reorganization of network occurs at the terminal relaxation time (τ_c). At $t > \tau_c$, sticky ends start to move out of the cluster overcoming the free

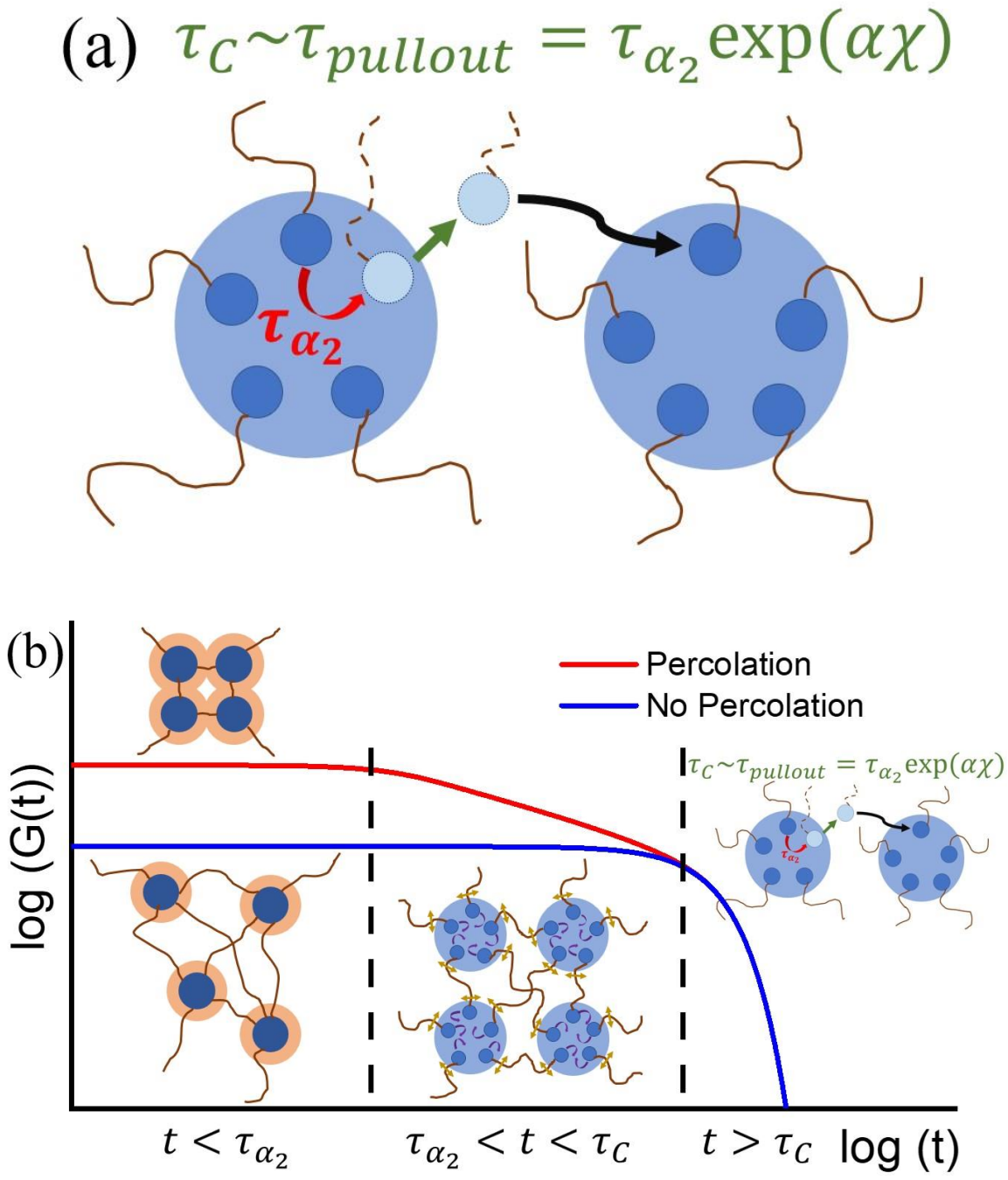

Figure 6.10 (a) Cartoon of a single chain exchange process between two clusters which leads to a macroscopic rearrangement of the network. (b) A qualitative picture of the shear modulus variation with time for a microphase-separated associated polymer network with percolated interfacial layers (red line) and with no percolation (blue line). Dashed lines mark two important time scales of the system, $\tau_{\alpha 2}$ – relaxation in clusters of dynamic bonds, and τ_C – terminal relaxation defined by the network rearrangement time.

energy barrier due to their immiscibility with the polymer matrix, and subsequently diffuse to another cluster. Through this single chain exchange process, macroscopic stress relaxation happens within the network.

6.5 Conclusions

In this study, we investigated telechelic PDMS with functional groups forming microphase separation due to their immiscibility with the polymer backbone. We demonstrated that mechanical percolation model describes well the strong mechanical reinforcement observed in these systems. Although the result is similar to what we achieved in Chapter 6 using mechanical ILM, the percolation model is more appropriate to explain the mechanical reinforcement since interfacial layers overlap in most of the studied samples. Moreover, our results and analysis question the proposed earlier mechanism[103] of network relaxation through a merger of microphase-separated clusters. Instead, we propose a chain-hopping mechanism of network rearrangement borrowed from the field of microphase-separated block copolymer. It provides a reasonably good description of the presented data even on a quantitative level. This mechanism also describes earlier data on telechelic PIB[104]. Finally, we formulate a general molecular picture describing the viscoelastic behavior of associating polymers. When microphase-separated clusters are frozen, the system behaves as a permanent network, which show strong mechanical reinforcement depending on whether there is percolation or not. Then, the softening of the interfacial layer occurs upon the motion of functional groups inside the microphase separated clusters, followed by the network rearrangement controlled by additional energy barrier defined by immiscibility of stickers and polymer matrix.

The presented analysis and the proposed mechanism provide a detailed understanding of the viscoelastic behavior of associating polymers with microphase separation. These mechanisms should not only work for telechelic associating polymers, but also for any associating polymer with microphase separation. The developed understanding is of paramount importance for rational design of advanced materials with enhanced mechanical properties, and better recyclability.

Conclusion Remarks and Future Directions

The research presented in this thesis provides a clear microscopic understanding and quantitative description of how transient reversible bonds influence the dynamics and viscoelastic behavior of associating polymers in the case of binary association and microphase separation. The results are of vital importance for understanding how microscopic parameters controlling macroscopic properties of associating polymers. The developed knowledge is also very important for understanding the dynamic of soft matter in general.

For associating polymers with only binary association, we found a disagreement of bond rearrangement timescale estimated from rheological measurement and bond dissociation time estimated from dielectric measurement due to the bond lifetime renormalization mechanism. The characteristic timescale of bond dissociation from dielectric measurement should be considered as the true bond lifetime. Also, segmental relaxation process is essential to be considered to estimate the bond dissociation energy. The systematical study of associating polymer with only binary association provides a thorough experimental test of bond lifetime renormalization model, with both intermediate bond strength and higher bond strength. Moreover, the Effective long chains forms and reptation-like diffusion behavior found for telechelic polymers with molecular weight far below the entanglement molecular weight.

In terms of the associating polymer with microphase separation, X-ray scattering measurement verifies the existence of microphase separation of the functional groups, which also characterizes the size of the clusters as well as the distance between clusters. Through careful analysis of the dielectric spectra, the interfacial layer with restricted segmental mobility was characterized

quantitatively with a thickness of ~ 0.7-0.9 nm. Then, through the analysis using mechanical interfacial layer model and mechanical percolation model, the crucial role of the interfacial layer on the mechanical reinforcement in microphase separated associating polymers was unambiguously demonstrated. In addition, the research also demonstrates a mechanism of how network rearrangement happens in associating polymer with microphase separation. We found that it is the single chain hopping that results in network rearrangement. The chain pullout process is the rate determining step for network rearrangement to happen, which needs to overcome the enthalpy penalty due to the immiscibility. Finally, a clear molecular picture is proposed about how the stress relaxation happens in associating polymer with microphase separation, depending on whether there is percolation of the interfacial layer or not.

Some future directions of the research of associating polymers are presented as follow:

Recently, theoretical study unraveled that it is the sticker fraction that determines T_g and segmental relaxation timescale of the associating polymers[201]. However, this idea has not been experimentally tested yet. We are going to study associating polymers with several functional groups placed as side groups along the chain, with functional groups either forming binary interactions or microphase separated domains. In such case, we expect to see the same microscopic dynamics as the telechelic associating polymer on condition that the functional group have the same fraction. In terms of the macroscopic dynamics, the terminal relaxation is expected to have Rouse-like behavior even without percolation, which is predicted by the Sticky-Rouse model.

We are also planning to go into the field of vitrimers, which is another kind of associating polymer with dynamic covalent bonds. The topic of vitrimers has been a heated research

direction in the field of associating polymers in the past few years[202-204]. However, the research is still in rudimental stage, especially the estimation of the stress relaxation time and activation energy in many publications are questionable. Based on our experience of the study of associating polymers with hydrogen bonding, we are trying to use similar methods to study vitrimers. One of the important tasks is to observe bond dissociation process of the dynamic covalent bond in vitrimers through dielectric measurement. In terms of the material, we are trying to design and synthesize vitrimers with PDMS chain and imine bond or disulfide bond, and study how such dynamic covalent bonds alter the overall viscoelastic behavior.

References

(1) Sijbesma, R. P.; Beijer, F. H.; Brunsveld, L.; Folmer, B. J.; Hirschberg, J. K.; Lange, R. F.; Lowe, J. K.; Meijer, E. Reversible polymers formed from self-complementary monomers using quadruple hydrogen bonding. *Science* **1997**, *278* (5343), 1601-1604.

(2) Wei, M.-H.; Li, B.; David, R. A.; Jones, S. C.; Sarohia, V.; Schmitigal, J. A.; Kornfield, J. A. Megasupramolecules for safer, cleaner fuel by end association of long telechelic polymers. *Science* **2015**, *350* (6256), 72-75.

(3) Brunsveld, L.; Folmer, B.; Meijer, E. W.; Sijbesma, R. Supramolecular polymers. *Chemical reviews* **2001**, *101* (12), 4071-4098.

(4) De Greef, T. F.; Smulders, M. M.; Wolffs, M.; Schenning, A. P.; Sijbesma, R. P.; Meijer, E. Supramolecular polymerization. *Chemical Reviews* **2009**, *109* (11), 5687-5754.

(5) Cao, P. F.; Li, B.; Hong, T.; Townsend, J.; Qiang, Z.; Xing, K.; Vogiatzis, K. D.; Wang, Y.; Mays, J. W.; Sokolov, A. P. Superstretchable, Self-Healing Polymeric Elastomers with Tunable Properties. *Advanced Functional Materials* **2018**, *28* (22), 1800741.

(6) Zhang, Z.; Ghezawi, N.; Li, B.; Ge, S.; Zhao, S.; Saito, T.; Hun, D.; Cao, P. F. Autonomous Self-Healing Elastomers with Unprecedented Adhesion Force. *Advanced Functional Materials* **2021**, *31* (4), 2006298.

(7) Zhang, Z.; Ghezawi, N.; Li, B.; Ge, S.; Zhao, S.; Saito, T.; Hun, D.; Cao, P. F. Self-Healing Elastomers: Autonomous Self-Healing Elastomers with Unprecedented Adhesion Force (Adv. Funct. Mater. 4/2021). *Advanced Functional Materials* **2021**, *31* (4), 2170025.

(8) Wang, C.; Wu, H.; Chen, Z.; McDowell, M. T.; Cui, Y.; Bao, Z. Self-healing chemistry enables the stable operation of silicon microparticle anodes for high-energy lithium-ion batteries. *Nature chemistry* **2013**, *5* (12), 1042-1048.

(9) Gao, S.; Cannon, A.; Sun, F.; Pan, Y.; Yang, D.; Ge, S.; Liu, N.; Sokolov, A. P.; Ryan, E.; Yang, H. Glass-fiber-reinforced polymeric film as an efficient protecting layer for stable Li metal electrodes. *Cell Reports Physical Science* **2021**, *2* (8), 100534.

(10) Li, B.; Zhao, S.; Zhu, J.; Ge, S.; Xing, K.; Sokolov, A. P.; Saito, T.; Cao, P.-F. Rational polymer design of stretchable poly (ionic liquid) membranes for dual applications. *Macromolecules* **2020**, *54* (2), 896-905.

(11) Pan, Y.; Ge, S.; Rashid, Z.; Gao, S.; Erwin, A.; Tsukruk, V.; Vogiatzis, K. D.; Sokolov, A. P.; Yang, H.; Cao, P.-F. Adhesive polymers as efficient binders for high-capacity silicon electrodes. *ACS Applied Energy Materials* **2020**, *3* (4), 3387-3396.

(12) Liu, G.; Ding, X.; Cao, Y.; Zheng, Z.; Peng, Y. Shape memory of hydrogen-bonded polymer network/poly (ethylene glycol) complexes. *Macromolecules* **2004**, *37* (6), 2228-2232.

(13) Lu, W.; Le, X.; Zhang, J.; Huang, Y.; Chen, T. Supramolecular shape memory hydrogels: a new bridge between stimuli-responsive polymers and supramolecular chemistry. *Chemical Society Reviews* **2017**, *46* (5), 1284-1294.

(14) Wang, C.; Wu, H.; Chen, Z.; McDowell, M. T.; Cui, Y.; Bao, Z. Self-healing chemistry enables the stable operation of silicon microparticle anodes for high-energy lithium-ion batteries. *Nature chemistry* **2013**, *5* (12), 1042.

(15) Madueno, R.; Räisänen, M. T.; Silien, C.; Buck, M. Functionalizing hydrogen-bonded surface networks with self-assembled monolayers. *Nature* **2008**, *454* (7204), 618-621.

(16) Hirschberg, J. K.; Brunsveld, L.; Ramzi, A.; Vekemans, J. A.; Sijbesma, R. P.; Meijer, E. Helical self-assembled polymers from cooperative stacking of hydrogen-bonded pairs. *Nature* **2000**, *407* (6801), 167-170.

(17) Eisenberg, A.; Hird, B.; Moore, R. A new multiplet-cluster model for the morphology of random ionomers. *Macromolecules* **1990**, *23* (18), 4098-4107.

(18) Zhang, L.; Brostowitz, N. R.; Cavicchi, K. A.; Weiss, R. A. Perspective: Ionomer Research and Applications. *Macromolecular Reaction Engineering* **2014**, *8* (2), 81-99. DOI: 10.1002/mren.201300181.

(19) Erwin, A. J.; Lee, H.; Ge, S.; Zhao, S.; Korolovych, V. F.; He, H.; Matyjaszewski, K.; Sokolov, A. P.; Tsukruk, V. V. Viscoelastic properties and ion dynamics in star-shaped polymerized ionic liquids. *European Polymer Journal* **2018**, *109*, 326-335.

(20) Khusnutdinova, J. R.; Milstein, D. Metal–ligand cooperation. *Angewandte Chemie International Edition* **2015**, *54* (42), 12236-12273.

(21) Holten-Andersen, N.; Harrington, M. J.; Birkedal, H.; Lee, B. P.; Messersmith, P. B.; Lee, K. Y. C.; Waite, J. H. pH-induced metal-ligand cross-links inspired by mussel yield self-healing polymer networks with near-covalent elastic moduli. *Proceedings of the National Academy of Sciences* **2011**, *108* (7), 2651-2655.

(22) Tsuzuki, S.; Honda, K.; Uchimaru, T.; Mikami, M.; Tanabe, K. Origin of attraction and directionality of the π/π interaction: model chemistry calculations of benzene dimer interaction. *Journal of the American Chemical Society* **2002**, *124* (1), 104-112.

(23) Filot, I. A.; Palmans, A. R.; Hilbers, P. A.; van Santen, R. A.; Pidko, E. A.; de Greef, T. F. Understanding cooperativity in hydrogen-bond-induced supramolecular polymerization: a

density functional theory study. *The Journal of Physical Chemistry B* **2010**, *114* (43), 13667-13674.

(24) Jeffrey, G. A.; Jeffrey, G. A. *An introduction to hydrogen bonding*; Oxford university press New York, 1997.

(25) Xing, K.; Chatterjee, S.; Saito, T.; Gainaru, C.; Sokolov, A. P. Impact of hydrogen bonding on dynamics of hydroxyl-terminated Polydimethylsiloxane. *Macromolecules* **2016**, *49* (8), 3138-3147.

(26) Xing, K.; Tress, M.; Cao, P.; Cheng, S.; Saito, T.; Novikov, V. N.; Sokolov, A. P. Hydrogen-bond strength changes network dynamics in associating telechelic PDMS. *Soft Matter* **2018**, *14* (7), 1235-1246. DOI: 10.1039/c7sm01805c.

(27) Xing, K.; Tress, M.; Cao, P.-F.; Fan, F.; Cheng, S.; Saito, T.; Sokolov, A. P. J. M. The Role of Chain-End Association Lifetime in Segmental and Chain Dynamics of Telechelic Polymers. **2018**, *51* (21), 8561-8573.

(28) Goldansaz, H.; Fustin, C.-A.; Wübbenhorst, M.; van Ruymbeke, E. How Supramolecular Assemblies Control Dynamics of Associative Polymers: Toward a General Picture. *Macromolecules* **2016**, *49* (5), 1890-1902. DOI: 10.1021/acs.macromol.5b01535.

(29) Chen, Q.; Colby, R. H. Linear viscoelasticity of sulfonated styrene oligomers near the sol-gel transition. *Korea-Australia Rheology Journal* **2014**, *26* (3), 257-261. DOI: 10.1007/s13367-014-0030-4.

(30) Ng, W.; Tam, K.; Jenkins, R. Lifetime and network relaxation time of a HEUR-C20 associative polymer system. *Journal of Rheology* **2000**, *44* (1), 137-147.

(31) Knaebel, A.; Skouri, R.; Munch, J.; Candau, S. Structural and rheological properties of hydrophobically modified alkali-soluble emulsion solutions. *Journal of Polymer Science Part B: Polymer Physics* **2002**, *40* (18), 1985-1994.

(32) Liao, D.; Dai, S.; Tam, K. C. Rheological properties of hydrophobic ethoxylated urethane (HEUR) in the presence of methylated β-cyclodextrin. *Polymer* **2004**, *45* (25), 8339-8348. DOI: 10.1016/j.polymer.2004.10.016.

(33) Tanaka, F.; Edwards, S. Viscoelastic properties of physically crosslinked networks: Part 1. Non-linear stationary viscoelasticity. *Journal of Non-Newtonian Fluid Mechanics* **1992**, *43* (2-3), 247-271.

(34) Matsumiya, Y.; Watanabe, H.; Urakawa, O.; Inoue, T. Experimental test for viscoelastic relaxation of polyisoprene undergoing monofunctional head-to-head association and dissociation. *Macromolecules* **2016**, *49* (18), 7088-7095.

(35) Samanta, S.; Kim, S.; Saito, T.; Sokolov, A. P. Polymers with Dynamic Bonds: Adaptive Functional Materials for a Sustainable Future. *The Journal of Physical Chemistry B* **2021**, *125* (33), 9389-9401.

(36) Chen, Q.; Tudryn, G. J.; Colby, R. H. Ionomer dynamics and the sticky Rouse model. *Journal of Rheology* **2013**, *57* (5), 1441-1462. DOI: 10.1122/1.4818868.

(37) Müller, M.; Fischer, E.; Kremer, F.; Seidel, U.; Stadler, R. The molecular dynamics of thermoreversible networks as studied by broadband dielectric spectroscopy. *Colloid and Polymer Science* **1995**, *273* (1), 38-46.

(38) Chen, Q.; Zhang, Z.; Colby, R. H. Viscoelasticity of entangled random polystyrene ionomers. *Journal of Rheology* **2016**, *60* (6), 1031-1040. DOI: 10.1122/1.4955432.

(39) Wang, S.-Q. *Nonlinear Polymer Rheology: Macroscopic Phenomenology and Molecular Foundation*; John Wiley & Sons; Hoboken, NJ, 2018.

(40) Shabbir, A.; Javakhishvili, I.; Cerveny, S.; Hvilsted, S.; Skov, A. L.; Hassager, O.; Alvarez, N. J. Linear viscoelastic and dielectric relaxation response of unentangled UPy-based supramolecular networks. *Macromolecules* **2016**, *49* (10), 3899-3910.

(41) De Gennes, P.-G. Reptation of a polymer chain in the presence of fixed obstacles. *The journal of chemical physics* **1971**, *55* (2), 572-579.

(42) Doi, M.; Edwards, S. F. *The theory of polymer dynamics*; oxford university press, 1988.

(43) Doi, M.; Edwards, S. Dynamics of concentrated polymer systems. Part 4.—Rheological properties. *Journal of the Chemical Society, Faraday Transactions 2: Molecular and Chemical Physics* **1979**, *75*, 38-54.

(44) Stukalin, E. B.; Cai, L. H.; Kumar, N. A.; Leibler, L.; Rubinstein, M. Self-Healing of Unentangled Polymer Networks with Reversible Bonds. *Macromolecules* **2013**, *46* (18). DOI: 10.1021/ma401111n.

(45) Gold, B. J.; Hövelmann, C. H.; Lühmann, N.; Székely, N. K.; Pyckhout-Hintzen, W.; Wischnewski, A.; Richter, D. Importance of Compact Random Walks for the Rheology of Transient Networks. *ACS Macro Letters* **2017**, *6* (2), 73-77. DOI: 10.1021/acsmacrolett.6b00880.

(46) Kiran, E. Polymer miscibility, phase separation, morphological modifications and polymorphic transformations in dense fluids. *The Journal of Supercritical Fluids* **2009**, *47* (3), 466-483.

(47) Chen, L.-J.; Yang, H.-B. Construction of stimuli-responsive functional materials via hierarchical self-assembly involving coordination interactions. *Accounts of chemical research* **2018**, *51* (11), 2699-2710.

(48) Stuparu, M. C.; Khan, A.; Hawker, C. J. Phase separation of supramolecular and dynamic block copolymers. *Polymer Chemistry* **2012**, *3* (11). DOI: 10.1039/c2py20368e.

(49) Hall, L. M.; Seitz, M. E.; Winey, K. I.; Opper, K. L.; Wagener, K. B.; Stevens, M. J.; Frischknecht, A. L. Ionic aggregate structure in ionomer melts: effect of molecular architecture on aggregates and the ionomer peak. *J Am Chem Soc* **2012**, *134* (1), 574-587. DOI: 10.1021/ja209142b.

(50) Scheutz, G. M.; Lessard, J. J.; Sims, M. B.; Sumerlin, B. S. Adaptable crosslinks in polymeric materials: resolving the intersection of thermoplastics and thermosets. *Journal of the American Chemical Society* **2019**, *141* (41), 16181-16196.

(51) Yan, T.; Schröter, K.; Herbst, F.; Binder, W. H.; Thurn-Albrecht, T. Nanostructure and Rheology of Hydrogen-Bonding Telechelic Polymers in the Melt: From Micellar Liquids and Solids to Supramolecular Gels. *Macromolecules* **2014**, *47* (6), 2122-2130. DOI: 10.1021/ma402007f.

(52) Yan, T.; Schröter, K.; Herbst, F.; Binder, W. H.; Thurn-Albrecht, T. What Controls the Structure and the Linear and Nonlinear Rheological Properties of Dense, Dynamic Supramolecular Polymer Networks? *Macromolecules* **2017**, *50* (7), 2973-2985. DOI: 10.1021/acs.macromol.6b02507.

(53) Gill, P.; Moghadam, T. T.; Ranjbar, B. Differential scanning calorimetry techniques: applications in biology and nanoscience. *Journal of biomolecular techniques: JBT* **2010**, *21* (4), 167.

(54) D'Amelia, R. P.; Stracuzzi, V.; Nirode, W. F. Introduction of Differential Scanning Calorimetry in a General Chemistry Laboratory Course: Determination of Heat Capacity of Metals and Demonstration of the Law of Dulong and Petit. *Journal of chemical education* **2008**, *85* (1), 109.

(55) Hollamby, M. J. Practical applications of small-angle neutron scattering. *Physical chemistry chemical physics* **2013**, *15* (26), 10566-10579.

(56) Seiffert, S. Scattering perspectives on nanostructural inhomogeneity in polymer network gels. *Progress in Polymer Science* **2017**, *66*, 1-21.

(57) Herbst, F.; Schröter, K.; Gunkel, I.; Gröger, S.; Thurn-Albrecht, T.; Balbach, J.; Binder, W. H. Aggregation and chain dynamics in supramolecular polymers by dynamic rheology: cluster formation and self-aggregation. *Macromolecules* **2010**, *43* (23), 10006-10016.

(58) Appel, W. P.; Portale, G.; Wisse, E.; Dankers, P. Y.; Meijer, E. Aggregation of ureido-pyrimidinone supramolecular thermoplastic elastomers into nanofibers: a kinetic analysis. *Macromolecules* **2011**, *44* (17), 6776-6784.

(59) Hawke, L. G. D.; Ahmadi, M.; Goldansaz, H.; van Ruymbeke, E. Viscoelastic properties of linear associating poly(n-butyl acrylate) chains. *Journal of Rheology* **2016**, *60* (2), 297-310. DOI: 10.1122/1.4942231.

(60) Ahmadi, M.; Jangizehi, A.; van Ruymbeke, E.; Seiffert, S. Deconvolution of the Effects of Binary Associations and Collective Assemblies on the Rheological Properties of Entangled Side-

Chain Supramolecular Polymer Networks. *Macromolecules* **2019**, *52* (14), 5255-5267. DOI: 10.1021/acs.macromol.9b00323.

(61) Wu, S.; Liu, S.; Zhang, Z.; Chen, Q. Dynamics of Telechelic Ionomers with Distribution of Number of Ionic Stickers at Chain Ends. *Macromolecules* **2019**, *52* (6), 2265-2276. DOI: 10.1021/acs.macromol.8b01776.

(62) Williams, M. L.; Landel, R. F.; Ferry, J. D. The temperature dependence of relaxation mechanisms in amorphous polymers and other glass-forming liquids. *Journal of the American Chemical society* **1955**, *77* (14), 3701-3707.

(63) Stadler, F. J.; Pyckhout-Hintzen, W.; Schumers, J.-M.; Fustin, C.-A.; Gohy, J.-F. o.; Bailly, C. Linear Viscoelastic Rheology of Moderately Entangled Telechelic Polybutadiene Temporary Networks. *Macromolecules* **2009**, *42* (16), 6181-6192. DOI: 10.1021/ma802488a.

(64) Nyrkova, I. A.; Khokhlov, A. R.; Doi, M. Microdomains in block copolymers and multiplets in ionomers: parallels in behavior. *Macromolecules* **1993**, *26* (14), 3601-3610.

(65) Vanhoorne, P.; Jérôme, R.; Teyssié, P.; Laupretre, F. Direct NMR evidence for a local restriction in the segmental chain mobility of a model ionomer. *Macromolecules* **1994**, *27* (9), 2548-2552.

(66) Carroll, B.; Cheng, S.; Sokolov, A. P. Analyzing the Interfacial Layer Properties in Polymer Nanocomposites by Broadband Dielectric Spectroscopy. *Macromolecules* **2017**, *50* (16), 6149-6163. DOI: 10.1021/acs.macromol.7b00825.

(67) Klonos, P.; Kulyk, K.; Borysenko, M. V.; Gun'ko, V. M.; Kyritsis, A.; Pissis, P. Effects of Molecular Weight below the Entanglement Threshold on Interfacial Nanoparticles/Polymer Dynamics. *Macromolecules* **2016**, *49* (24), 9457-9473. DOI: 10.1021/acs.macromol.6b01931.

(68) Klonos, P.; Kyritsis, A.; Pissis, P. Interfacial and confined dynamics of PDMS adsorbed at the interfaces and in the pores of silica–gel: Effects of surface modification and thermal annealing. *Polymer* **2016**, *84*, 38-51.

(69) Gong, S.; Chen, Q.; Moll, J. F.; Kumar, S. K.; Colby, R. H. Segmental dynamics of polymer melts with spherical nanoparticles. *ACS Macro Letters* **2014**, *3* (8), 773-777.

(70) Steeman, P.; Maurer, F. An interlayer model for the complex dielectric constant of composites. *Colloid and Polymer Science* **1990**, *268* (4), 315-325.

(71) Füllbrandt, M.; Purohit, P. J.; Schönhals, A. Combined FTIR and dielectric investigation of poly (vinyl acetate) adsorbed on silica particles. *Macromolecules* **2013**, *46* (11), 4626-4632.

(72) Holt, A. P.; Bocharova, V.; Cheng, S.; Kisliuk, A. M.; White, B. T.; Saito, T.; Uhrig, D.; Mahalik, J. P.; Kumar, R.; Imel, A. E.; et al. Controlling Interfacial Dynamics: Covalent Bonding versus Physical Adsorption in Polymer Nanocomposites. *ACS Nano* **2016**, *10* (7), 6843-6852. DOI: 10.1021/acsnano.6b02501.

(73) Popov, I.; Carroll, B.; Bocharova, V.; Genix, A.-C.; Cheng, S.; Khamzin, A.; Kisliuk, A.; Sokolov, A. P. Strong Reduction in Amplitude of the Interfacial Segmental Dynamics in Polymer Nanocomposites. *Macromolecules* **2020**, *53* (10), 4126-4135.

(74) Mortezaei, M.; Famili, M. H. N.; Kokabi, M. The role of interfacial interactions on the glass-transition and viscoelastic properties of silica/polystyrene nanocomposite. *Composites science and technology* **2011**, *71* (8), 1039-1045.

(75) Carrillo, J.-M. Y.; Cheng, S.; Kumar, R.; Goswami, M.; Sokolov, A. P.; Sumpter, B. G. Untangling the effects of chain rigidity on the structure and dynamics of strongly adsorbed polymer melts. *Macromolecules* **2015**, *48* (12), 4207-4219.

(76) Napolitano, S.; Capponi, S.; Vanroy, B. Glassy dynamics of soft matter under 1D confinement: How irreversible adsorption affects molecular packing, mobility gradients and orientational polarization in thin films. *The European Physical Journal E* **2013**, *36* (6), 1-37.

(77) van der Poel, C. On the rheology of concentrated dispersions. *Rheologica Acta* **1958**, *1* (2), 198-205. DOI: 10.1007/BF01968867.

(78) Hashin, Z.; Shtrikman, S. A variational approach to the theory of the elastic behaviour of multiphase materials. *Journal of the Mechanics and Physics of Solids* **1963**, *11* (2), 127-140.

(79) Smith, J. C. Correction and extension of van der Poel's method for calculating the shear modulus of a particulate composite. *Journal of research of the National Bureau of Standards. Section A, Physics and chemistry* **1974**, *78* (3), 355.

(80) Hashin, Z. Thermoelastic properties of particulate composites with imperfect interface. *Journal of the Mechanics and Physics of Solids* **1991**, *39* (6), 745-762.

(81) Maurer, F. An interlayer model to describe the physical properties of particulate composites. In *Controlled interphases in composite materials*, Springer, 1990; pp 491-504.

(82) Essam, J. W. Percolation theory. *Reports on progress in physics* **1980**, *43* (7), 833.

(83) Stauffer, D.; Aharony, A. *Introduction to percolation theory*; CRC press, 2018.

(84) Musino, D.; Genix, A.-C.; Chauveau, E.; Bizien, T.; Oberdisse, J. Structural identification of percolation of nanoparticles. *Nanoscale* **2020**, *12* (6), 3907-3915.

(85) Baeza, G. P.; Dessi, C.; Costanzo, S.; Zhao, D.; Gong, S.; Alegria, A.; Colby, R. H.; Rubinstein, M.; Vlassopoulos, D.; Kumar, S. K. Network dynamics in nanofilled polymers. *Nat Commun* **2016**, *7*, 11368. DOI: 10.1038/ncomms11368.

(86) Nadiv, R.; Fernandes, R. M.; Ochbaum, G.; Dai, J.; Buzaglo, M.; Varenik, M.; Biton, R.; Furo, I.; Regev, O. Polymer nanocomposites: Insights on rheology, percolation and molecular mobility. *Polymer* **2018**, *153*, 52-60.

(87) Consiglio, R.; Baker, D.; Paul, G.; Stanley, H. Continuum percolation thresholds for mixtures of spheres of different sizes. *Physica A: Statistical Mechanics and its Applications* **2003**, *319*, 49-55.

(88) Rintoul, M. D. Precise determination of the void percolation threshold for two distributions of overlapping spheres. *Physical Review E* **2000**, *62* (1), 68.

(89) Van der Marck, S. Network approach to void percolation in a pack of unequal spheres. *Physical review letters* **1996**, *77* (9), 1785.

(90) Wu, S.; Qiu, M.; Tang, Z.; Guo, B. Interphase Percolation Mechanism Underlying Elastomer Reinforcement. *The Journal of Physical Chemistry C* **2017**, *121* (51), 28594-28603. DOI: 10.1021/acs.jpcc.7b11239.

(91) Zheng, Z.; Song, Y.; Yang, R.; Zheng, Q. Direct Evidence for Percolation of Immobilized Polymer Layer around Nanoparticles Accounting for Sol-Gel Transition in Fumed Silica Dispersions. *Langmuir* **2015**, *31* (50), 13478-13487. DOI: 10.1021/acs.langmuir.5b03899.

(92) Hassanabadi, H. M.; Wilhelm, M.; Rodrigue, D. A rheological criterion to determine the percolation threshold in polymer nano-composites. *Rheologica Acta* **2014**, *53* (10-11), 869-882. DOI: 10.1007/s00397-014-0804-0.

(93) Zare, Y.; Rhee, K. Y. Development of Conventional Paul Model for Tensile Modulus of Polymer Carbon Nanotube Nanocomposites After Percolation Threshold by Filler Network Density. *Jom* **2020**, *72* (12), 4323-4329. DOI: 10.1007/s11837-020-04398-9.

(94) Sugimoto, S.; Inutsuka, M.; Kawaguchi, D.; Tanaka, K. The effect of interfacial dynamics on the bulk mechanical properties of rubber composites. *Polymer Journal* **2020**, *52* (2), 217-223.

(95) Favier, V.; Cavaille, J.; Canova, G.; Shrivastava, S. Mechanical percolation in cellulose whisker nanocomposites. *Polymer Engineering & Science* **1997**, *37* (10), 1732-1739.

(96) Takayanagi, M.; Uemura, S.; Minami, S. Application of equivalent model method to dynamic rheo-optical properties of crystalline polymer. In *Journal of Polymer Science Part C: Polymer Symposia*, 1964; Wiley Online Library: Vol. 5, pp 113-122.

(97) Ouali, N.; Cavaille, J.; Perez, J. Plastics Rubber Compos. In *Proc. Appl*, 1991; Vol. 16, p 55.

(98) Semenov, A.; Joanny, J.-F.; Khokhlov, A. Associating polymers: equilibrium and linear viscoelasticity. *Macromolecules* **1995**, *28* (4), 1066-1075.

(99) Semenov, A.; Rubinstein, M. Dynamics of entangled associating polymers with large aggregates. *Macromolecules* **2002**, *35* (12), 4821-4837.

(100) Green, M. S.; Tobolsky, A. V. A new approach to the theory of relaxing polymeric media. *The Journal of Chemical Physics* **1946**, *14* (2), 80-92.

(101) Tanaka, F.; Edwards, S. Viscoelastic properties of physically crosslinked networks. 1. Transient network theory. *Macromolecules* **1992**, *25* (5), 1516-1523.

(102) Mordvinkin, A.; Döhler, D.; Binder, W. H.; Colby, R. H.; Saalwächter, K. Terminal Flow of Cluster-Forming Supramolecular Polymer Networks: Single-Chain Relaxation or Micelle Reorganization? *Physical review letters* **2020**, *125* (12), 127801.

(103) Amin, D.; Likhtman, A. E.; Wang, Z. Dynamics in Supramolecular Polymer Networks Formed by Associating Telechelic Chains. *Macromolecules* **2016**, *49* (19), 7510-7524. DOI: 10.1021/acs.macromol.6b00561.

(104) Mordvinkin, A.; Döhler, D.; Binder, W. H.; Colby, R. H.; Saalwächter, K. Rheology, Sticky Chain, and Sticker Dynamics of Supramolecular Elastomers Based on Cluster-Forming Telechelic Linear and Star Polymers. *Macromolecules* **2021**.

(105) Tschoegl, N. W. *The phenomenological theory of linear viscoelastic behavior: an introduction*; Springer Science & Business Media, 2012.

(106) Kremer, F.; Schönhals, A. *Broadband Dielectric Spectroscopy*; Springer-Verlag; Berlin, 2003.

(107) Havriliak, S.; Negami, S. A complex plane representation of dielectric and mechanical relaxation processes in some polymers. *Polymer* **1967**, *8*, 161-210.

(108) Tress, M.; Vielhauer, M.; Lutz, P.; Mülhaupt, R.; Kremer, F.; Xing, K.; Ge, S.; Cao, P.; Saito, T.; Sokolov, A. Polymer Dynamics in Nanostructured Environments: Structure-Property Relations Unraveled by Dielectric Spectroscopy. In *Broadband Dielectric Spectroscopy: A Modern Analytical Technique*, ACS Publications, 2021; pp 223-238.

(109) Wübbenhorst, M.; Van Turnhout, J. J. J. o. N.-C. S. Analysis of complex dielectric spectra. I. One-dimensional derivative techniques and three-dimensional modelling. **2002**, *305* (1-3), 40-49.

(110) Ng, W. K.; Tam, K. C.; Jenkins, R. D. Lifetime and network relaxation time of a HEUR-C20 associative polymer system. *Journal of Rheology* **2000**, *44* (1), 137-147. DOI: 10.1122/1.551078.

(111) Knaebel, A.; Skouri, R.; Munch, J. P.; Candau, S. J. Structural and rheological properties of hydrophobically modified alkali-soluble emulsion solutions. *Journal of Polymer Science Part B: Polymer Physics* **2002**, *40* (18), 1985-1994. DOI: 10.1002/polb.10249.

(112) Manassero, C.; Raos, G.; Allegra, G. Structure of Model Telechelic Polymer Melts by Computer Simulation. *Journal of Macromolecular Science, Part B* **2007**, *44* (6), 855-871. DOI: 10.1080/00222340500364759.

(113) Manassero, C.; Castellano, C. Telechelic Melt Polymer's Structure Variation Depending on Shear Deformation. *Journal of Macromolecular Science, Part B* **2013**, *52* (10), 1465-1477. DOI: 10.1080/00222348.2013.771019.

(114) Zhuge, F.; Hawke, L. G. D.; Fustin, C.-A.; Gohy, J.-F.; van Ruymbeke, E. Decoding the linear viscoelastic properties of model telechelic metallo-supramolecular polymers. *Journal of Rheology* **2017**, *61* (6), 1245-1262. DOI: 10.1122/1.4997593.

(115) Park, G. W.; Ianniruberto, G. A new stochastic simulation for the rheology of telechelic associating polymers. *Journal of Rheology* **2017**, *61* (6), 1293-1305. DOI: 10.1122/1.4997592.

(116) Meng, X.-X.; Russel, W. B. Rheology of telechelic associative polymers in aqueous solutions. *Journal of Rheology* **2006**, *50* (2), 189-205. DOI: 10.1122/1.2167467.

(117) Ozaki, H.; Koga, T. Network Formation and Mechanical Properties of Telechelic Associating Polymers with Fixed Junction Multiplicity. *Macromolecular Theory and Simulations* **2017**, *26* (2). DOI: 10.1002/mats.201600076.

(118) Chen, Q.; Huang, C.; Weiss, R. A.; Colby, R. H. Viscoelasticity of Reversible Gelation for Ionomers. *Macromolecules* **2015**, *48* (4), 1221-1230. DOI: 10.1021/ma502280g.

(119) Zhang, Z.; Huang, C.; Weiss, R. A.; Chen, Q. Association energy in strongly associative polymers. *Journal of Rheology* **2017**, *61* (6), 1199-1207. DOI: 10.1122/1.4997586.

(120) Indei, T. Rheological study of transient networks with junctions of limited multiplicity. *J Chem Phys* **2007**, *127* (14), 144904. DOI: 10.1063/1.2747607.

(121) Indei, T. Rheological study of transient networks with junctions of limited multiplicity. II. Sol/gel transition and rheology. *J Chem Phys* **2007**, *127* (14), 144905. DOI: 10.1063/1.2747610.

(122) Gold, B. J.; Hövelmann, C. H.; Lühmann, N.; Pyckhout-Hintzen, W.; Wischnewski, A.; Richter, D. The microscopic origin of the rheology in supramolecular entangled polymer networks. *Journal of Rheology* **2017**, *61* (6), 1211-1226. DOI: 10.1122/1.4998159.

(123) Tress, M.; Xing, K.; Ge, S.; Cao, P.; Saito, T.; Sokolov, A. What dielectric spectroscopy can tell us about supramolecular networks⋆. *The European Physical Journal E* **2019**, *42* (10), 1-12.

(124) Müller, M.; Fischer, E.; Kremer, F.; Seidel, U.; Stadler, R. J. C.; Science, P. The molecular dynamics of thermoreversible networks as studied by broadband dielectric spectroscopy. **1995**, *273* (1), 38-46.

(125) Xing, K.; Tress, M.; Cao, P.; Cheng, S.; Saito, T.; Novikov, V. N.; Sokolov, A. P. Hydrogen-bond strength changes network dynamics in associating telechelic PDMS. *Soft Matter* **2018**.

(126) Ge, S.; Tress, M.; Samanta, S.; Xing, K.; Cao, P.-F.; Saito, T.; Sokolov, A. Experimental test of the bond lifetime renormalization model in telechelic associating polymers. In *APS March Meeting Abstracts*, 2021; Vol. 2021, p A04. 002.

(127) Ge, S.; Tress, M.; Xing, K.; Cao, P.-F.; Saito, T.; Sokolov, A. P. Viscoelasticity in associating oligomers and polymers: experimental test of the bond lifetime renormalization model. *Soft Matter* **2020**, *16* (2), 390-401.

(128) Ding, Y.; Sokolov, A. P. Comment on the dynamic bead size and Kuhn segment length in polymers: Example of polystyrene. *Journal of Polymer Science Part B: Polymer Physics* **2004**, *42* (18), 3505-3511. DOI: 10.1002/polb.20235.

(129) Kokubo, S.; Vana, P. Easy Access to the Characteristic Ratio of Polymers Using Ion-Mobility Mass Spectrometry. *Macromolecular Chemistry and Physics* **2017**, *218* (1). DOI: 10.1002/macp.201600373.

(130) Rubinstein, M.; Colby, R. H. *Polymer physics*; Oxford university press New York, 2003.

(131) Wagner, H.; Richert, R. J. T. J. o. P. C. B. Equilibrium and non-equilibrium type β-relaxations: d-sorbitol versus o-terphenyl. **1999**, *103* (20), 4071-4077.

(132) Adrjanowicz, K.; Kaminski, K.; Dulski, M.; Wlodarczyk, P.; Bartkowiak, G.; Popenda, L.; Jurga, S.; Kujawski, J.; Kruk, J.; Bernard, M. Communication: Synperiplanar to antiperiplanar conformation changes as underlying the mechanism of Debye process in supercooled ibuprofen. *The Journal of chemical physics* **2013**, *139* (11), 09B401_401.

(133) Vogel, H. Das temperaturabhängigkeitsgesetz der viskosität von flüssigkeiten. *Phys. Z.* **1921**, *22*, 645-646.

(134) Tammann, G.; Hesse, W. Die Abhängigkeit der Viscosität von der Temperatur bie unterkühlten Flüssigkeiten. *Zeitschrift für anorganische und allgemeine Chemie* **1926**, *156* (1), 245-257.

(135) Fulcher, G. S. Analysis of recent measurements of the viscosity of glasses. *Journal of the American Ceramic Society* **1925**, *8* (6), 339-355.

(136) Ge, S.; Zhu, X.; Wang, S.-Q. Watching shear thinning in creep: Entanglement-disentanglement transition. *Polymer* **2017**, *125*, 254-264.

(137) Ge, S. The Entanglement-Disentanglement Transition (EDT) During Creep With Either Constant Or Oscillatory Stress In Highly-Entangled Polybutadiene Solution. University of Akron, 2016.

(138) Kremer, F.; Schönhals, A. *Broadband dielectric spectroscopy*; Springer Science & Business Media, 2002.

(139) Tarnacka, M.; Jurkiewicz, K.; Hachuła, B.; Wojnarowska, Z.; Wrzalik, R.; Bielas, R.; Talik, A.; Maksym, P.; Kaminski, K.; Paluch, M. Correlation between Locally Ordered (Hydrogen-Bonded) Nanodomains and Puzzling Dynamics of Polymethysiloxane Derivative. *Macromolecules* **2020**, *53* (22), 10225-10233.

(140) Richert, R.; Agapov, A.; Sokolov, A. P. Appearance of a Debye process at the conductivity relaxation frequency of a viscous liquid. *The Journal of chemical physics* **2011**, *134* (10), 104508.

(141) Gainaru, C.; Stacy, E. W.; Bocharova, V.; Gobet, M.; Holt, A. P.; Saito, T.; Greenbaum, S.; Sokolov, A. P. Mechanism of conductivity relaxation in liquid and polymeric electrolytes: Direct link between conductivity and diffusivity. *The Journal of Physical Chemistry B* **2016**, *120* (42), 11074-11083.

(142) Richert, R.; Wagner, H. The dielectric modulus: relaxation versus retardation. *Solid State Ionics* **1998**, *105* (1-4), 167-173.

(143) Ge, S.; Samanta, S.; Tress, M.; Li, B.; Xing, K.; Dieudonné-George, P.; Genix, A.-C.; Cao, P.-F.; Dadmun, M.; Sokolov, A. P. Critical Role of the Interfacial Layer in Associating Polymers with Microphase Separation. *Macromolecules* **2021**, *54* (9), 4246-4256.

(144) Soszka, N.; Hachuła, B.; Tarnacka, M.; Kaminska, E.; Pawlus, S.; Kaminski, K.; Paluch, M. Is a Dissociation Process Underlying the Molecular Origin of the Debye Process in Monohydroxy Alcohols? *The Journal of Physical Chemistry B* **2021**, *125* (11), 2960-2967.

(145) Rahman, M. A.; Bowland, C.; Ge, S.; Acharya, S. R.; Kim, S.; Cooper, V. R.; Chen, X. C.; Irle, S.; Sokolov, A. P.; Savara, A. Design of tough adhesive from commodity thermoplastics through dynamic crosslinking. *Science advances* **2021**, *7* (42), eabk2451.

(146) Kan, L.; Zhang, P.; Jiang, H.; Zhang, S.; Liu, Z.; Zhang, X.; Ma, N.; Qiu, D.; Wei, H. Microphase separation of a quadruple hydrogen bonding supramolecular polymer: effect of the steric hindrance of the ureido-pyrimidone on their viscoelasticity. *RSC Advances* **2019**, *9* (16), 8905-8911. DOI: 10.1039/c8ra08861f.

(147) Appel, W. P. J.; Portale, G.; Wisse, E.; Dankers, P. Y. W.; Meijer, E. W. Aggregation of Ureido-Pyrimidinone Supramolecular Thermoplastic Elastomers into Nanofibers: A Kinetic Analysis. *Macromolecules* **2011**, *44* (17), 6776-6784. DOI: 10.1021/ma201303s.

(148) Tress, M.; Ge, S.; Xing, K.; Cao, P.-F.; Saito, T.; Genix, A.-C.; Sokolov, A. P. Turning rubber into a glass: mechanical reinforcement by Microphase separation. *ACS Macro Letters* **2021**, *10* (2), 197-202.

(149) Lehmann, M. L.; Yang, G.; Gilmer, D.; Han, K. S.; Self, E. C.; Ruther, R. E.; Ge, S.; Li, B.; Murugesan, V.; Sokolov, A. P. Tailored crosslinking of Poly (ethylene oxide) enables

mechanical robustness and improved sodium-ion conductivity. *Energy Storage Materials* **2019**, *21*, 85-96.

(150) Yang, G.; Cao, P.; Chen, X. C.; Self, E. C.; Zhao, S.; Ge, S.; Zhu, C.; Lehmann, M.; Saito, T.; Delnick, F. M. The Impact of Selectively Plasticized Poly (ethylene oxide)(PEO) Block in Nanostructured Polystyrene− PEO− Polystyrene Triblock Copolymer Electrolytes. In *ECS Meeting Abstracts*, 2019; IOP Publishing: p 641.

(151) Yang, G.; Cao, P.-F.; Self, E. C.; Lehmann, M.; Chen, X. C.; Zhao, S.; Ge, S.; Zhu, C.; Saito, T.; Delnick, F. M. Selective Plasticization of Poly (ethylene oxide)(PEO) Block in Nanostructured Polystyrene− PEO− Polystyrene Triblock Copolymer Electrolytes. *Journal of The Electrochemical Society* **2022**, *169* (5), 050506.

(152) Zhang, Z.; Luo, J.; Zhao, S.; Ge, S.; Carrillo, J.-M. Y.; Keum, J. K.; Do, C.; Cheng, S.; Wang, Y.; Sokolov, A. P. Surpassing the stiffness-extensibility trade-off of elastomers via mastering the hydrogen-bonding clusters. *Matter* **2022**, *5* (1), 237-252.

(153) Yang, G.; Lehmann, M. L.; Zhao, S.; Li, B.; Ge, S.; Cao, P.-F.; Delnick, F. M.; Sokolov, A. P.; Saito, T.; Nanda, J. Anomalously high elastic modulus of a poly (ethylene oxide)-based composite electrolyte. *Energy Storage Materials* **2021**, *35*, 431-442.

(154) Papon, A.; Montes, H.; Lequeux, F.; Oberdisse, J.; Saalwächter, K.; Guy, L. Solid particles in an elastomer matrix: impact of colloid dispersion and polymer mobility modification on the mechanical properties. *Soft Matter* **2012**, *8* (15), 4090-4096.

(155) Kim, S. Y.; Meyer, H. W.; Saalwächter, K.; Zukoski, C. F. Polymer dynamics in PEG-silica nanocomposites: Effects of polymer molecular weight, temperature and solvent dilution. *Macromolecules* **2012**, *45* (10), 4225-4237.

(156) Cheng, S.; Carroll, B.; Bocharova, V.; Carrillo, J.-M.; Sumpter, B. G.; Sokolov, A. P. Focus: Structure and dynamics of the interfacial layer in polymer nanocomposites with attractive interactions. *The Journal of Chemical Physics* **2017**, *146* (20), 203201.

(157) Cheng, S.; Mirigian, S.; Carrillo, J.-M. Y.; Bocharova, V.; Sumpter, B. G.; Schweizer, K. S.; Sokolov, A. P. Revealing spatially heterogeneous relaxation in a model nanocomposite. *The Journal of chemical physics* **2015**, *143* (19), 194704.

(158) Vanhoorne, P.; Jérôme, R.; Teyssié, P.; Laupretre, F. J. M. Direct NMR evidence for a local restriction in the segmental chain mobility of a model ionomer. **1994**, *27* (9), 2548-2552.

(159) Sinha, K.; Maranas, J. K. Segmental dynamics and ion association in PEO-based single ion conductors. *Macromolecules* **2011**, *44* (13), 5381-5391.

(160) Castagna, A. M.; Wang, W.; Winey, K. I.; Runt, J. Influence of the Degree of Sulfonation on the Structure and Dynamics of Sulfonated Polystyrene Copolymers. *Macromolecules* **2010**, *43* (24), 10498-10504. DOI: 10.1021/ma102206f.

(161) Castagna, A. M.; Wang, W.; Winey, K. I.; Runt, J. Influence of Cation Type on Structure and Dynamics in Sulfonated Polystyrene Ionomers. *Macromolecules* **2011**, *44* (13), 5420-5426. DOI: 10.1021/ma2009657.

(162) Tress, M.; Xing, K.; Ge, S.; Cao, P.; Saito, T.; Sokolov, A. What dielectric spectroscopy can tell us about supramolecular networks⋆. *The European Physical Journal E* **2019**, *42* (10), 133.

(163) Tress, M.; Ge, S.; Xing, K.; Cao, P.-F.; Saito, T.; Genix, A.-C.; Sokolov, A. P. Turning Rubber into a Glass: Mechanical Reinforcement by Microphase Separation. *ACS Macro Letters* **2021**, *10*, 197-202. DOI: 10.1021/acsmacrolett.0c00778.

(164) Samanta, S.; Ge, S.; Tress, M.; Li, B.; Xing, K.; Cao, P.-F.; Sokolov, A. Mechanical Reinforcement by Interfacial Layer in Phase-separating Associating Telechelic Polymers. In *APS March Meeting Abstracts*, 2021; Vol. 2021, p A04. 004.

(165) Mitchell, G. R.; Odajima, A. The local conformation of poly (dimethylsiloxane). *Polymer journal* **1984**, *16* (4), 351-357.

(166) Wu, S. Phase structure and adhesion in polymer blends: a criterion for rubber toughening. *Polymer* **1985**, *26* (12), 1855-1863.

(167) Cheng, S.; Xie, S.-J.; Carrillo, J.-M. Y.; Carroll, B.; Martin, H.; Cao, P.-F.; Dadmun, M. D.; Sumpter, B. G.; Novikov, V. N.; Schweizer, K. S. Big effect of small nanoparticles: A shift in paradigm for polymer nanocomposites. *ACS nano* **2017**, *11* (1), 752-759.

(168) Ding, Y.; Sokolov, A. Comment on the dynamic bead size and Kuhn segment length in polymers: Example of polystyrene. *Journal of Polymer Science Part B: Polymer Physics* **2004**, *42* (18), 3505-3511.

(169) Cheng, S.; Carroll, B.; Lu, W.; Fan, F.; Carrillo, J.-M. Y.; Martin, H.; Holt, A. P.; Kang, N.-G.; Bocharova, V.; Mays, J. W. Interfacial properties of polymer nanocomposites: Role of chain rigidity and dynamic heterogeneity length scale. *Macromolecules* **2017**, *50* (6), 2397-2406.

(170) Lyapin, A.; Gromnitskaya, E.; Danilov, I.; Brazhkin, V. Elastic properties of the hydrogen-bonded liquid and glassy glycerol under high pressure: comparison with propylene carbonate. *RSC advances* **2017**, *7* (53), 33278-33284.

(171) Müller, A.; Wapler, M. C.; Wallrabe, U. A quick and accurate method to determine the Poisson's ratio and the coefficient of thermal expansion of PDMS. *Soft Matter* **2019**, *15* (4), 779-784.

(172) Moll, J. F.; Akcora, P.; Rungta, A.; Gong, S.; Colby, R. H.; Benicewicz, B. C.; Kumar, S. K. Mechanical reinforcement in polymer melts filled with polymer grafted nanoparticles. *Macromolecules* **2011**, *44* (18), 7473-7477.

(173) Nadiv, R.; Fernandes, R. M. F.; Ochbaum, G.; Dai, J.; Buzaglo, M.; Varenik, M.; Biton, R.; Furó, I.; Regev, O. Polymer nanocomposites: Insights on rheology, percolation and molecular mobility. *Polymer* **2018**, *153*, 52-60. DOI: 10.1016/j.polymer.2018.07.079.

(174) Ge, S.; Samanta, S.; Li, B.; Carden, G. P.; Cao, P.-F.; Sokolov, A. P. Unravelling the mechanism of viscoelasticity in polymers with phase-separated dynamic bonds. *ACS nano* **2022**, *16* (3), 4746-4755.

(175) Ferry, J. D. *Viscoelastic properties of polymers*; John Wiley & Sons, 1980.

(176) De Gennes, P.-G. On a relation between percolation theory and the elasticity of gels. *Journal de Physique Lettres* **1976**, *37* (1), 1-2.

(177) Tokita, M.; Niki, R.; Hikichi, K. Percolation theory and elastic modulus of gel. *Journal of the Physical Society of Japan* **1984**, *53* (2), 480-482.

(178) Evingür, G. A.; Pekcan, Ö. Elastic percolation of swollen polyacrylamide (PAAm)–multiwall carbon nanotubes composite. *Phase Transitions* **2012**, *85* (6), 553-564.

(179) Djabourov, M.; Leblond, J.; Papon, P. Gelation of aqueous gelatin solutions. II. Rheology of the sol-gel transition. *Journal de Physique* **1988**, *49* (2), 333-343.

(180) Hsu, W. Y.; Wu, S. Percolation behavior in morphology and modulus of polymer blends. *Polymer Engineering & Science* **1993**, *33* (5), 293-302.

(181) Gauthier-Manuel, B.; Guyon, E. Critical, elasticity of polyacrylamide above its gel point. *Journal de Physique Lettres* **1980**, *41* (21), 503-505.

(182) Le Strat, D.; Dalmas, F.; Randriamahefa, S.; Jestin, J.; Wintgens, V. Mechanical reinforcement in model elastomer nanocomposites with tuned microstructure and interactions. *Polymer* **2013**, *54* (5), 1466-1479.

(183) Lyapin, A. G.; Gromnitskaya, E. L.; Danilov, I. V.; Brazhkin, V. V. Elastic properties of the hydrogen-bonded liquid and glassy glycerol under high pressure: comparison with propylene carbonate. *RSC advances* **2017**, *7* (53), 33278-33284.

(184) Hayashi, M.; Noro, A.; Matsushita, Y. Viscoelastic properties of supramolecular soft materials with transient polymer network. *Journal of Polymer Science Part B: Polymer Physics* **2014**, *52* (11), 755-764. DOI: 10.1002/polb.23479.

(185) Ma, Y.; Lodge, T. P. Chain exchange kinetics in diblock copolymer micelles in ionic liquids: The role of χ. *Macromolecules* **2016**, *49* (24), 9542-9552.

(186) Wang, E.; Lu, J.; Bates, F. S.; Lodge, T. P. Effect of corona block length on the structure and chain exchange kinetics of block copolymer micelles. *Macromolecules* **2018**, *51* (10), 3563-3571.

(187) Wang, E.; Zhu, J.; Zhao, D.; Xie, S.; Bates, F. S.; Lodge, T. P. Effect of solvent selectivity on chain exchange kinetics in block copolymer micelles. *Macromolecules* **2019**, *53* (1), 417-426.

(188) Lu, J.; Bates, F. S.; Lodge, T. P. Remarkable effect of molecular architecture on chain exchange in triblock copolymer micelles. *Macromolecules* **2015**, *48* (8), 2667-2676.

(189) Peters, A. J.; Lodge, T. P. Comparison of gel relaxation times and end-block pullout times in ABA triblock copolymer networks. *Macromolecules* **2016**, *49* (19), 7340-7349.

(190) Zhao, D.; Ma, Y.; Lodge, T. P. Exchange kinetics for a single block copolymer in micelles of two different sizes. *Macromolecules* **2018**, *51* (6), 2312-2320.

(191) Lu, J.; Bates, F.; Lodge, T. Chain exchange in binary copolymer micelles at equilibrium: confirmation of the independent chain hypothesis. *ACS Macro Letters* **2013**, *2* (5), 451-455.

(192) Chremos, A.; Nikoubashman, A.; Panagiotopoulos, A. Z. Flory-Huggins parameter χ, from binary mixtures of Lennard-Jones particles to block copolymer melts. *The Journal of chemical physics* **2014**, *140* (5), 054909.

(193) Lee, J. N.; Park, C.; Whitesides, G. M. Solvent Compatibility of Poly(dimethylsiloxane)-Based Microfluidic Devices. *Analytical Chemistry* **2003**, *75* (23), 6544-6554. DOI: 10.1021/ac0346712.

(194) Hansen, C. M. *Hansen solubility parameters: a user's handbook*; CRC press, 2007.

(195) Stefanis, E.; Panayiotou, C. A new expanded solubility parameter approach. *International journal of pharmaceutics* **2012**, *426* (1-2), 29-43.

(196) Choi, S.-H.; Lodge, T. P.; Bates, F. S. Mechanism of molecular exchange in diblock copolymer micelles: hypersensitivity to core chain length. *Physical review letters* **2010**, *104* (4), 047802.

(197) Kim, S.; Lee, S.; Choi, S.-H.; Char, K. Chain Exchange Kinetics of Bottlebrush Block Copolymer Micelles. *Macromolecules* **2021**, *54* (10), 4739-4746.

(198) Mordvinkin, A.; Suckow, M.; Böhme, F.; Colby, R. H.; Creton, C.; Saalwächter, K. Hierarchical Sticker and Sticky Chain Dynamics in Self-Healing Butyl Rubber Ionomers. *Macromolecules* **2019**, *52* (11), 4169-4184. DOI: 10.1021/acs.macromol.9b00159.

(199) Barton, A. F. *CRC handbook of solubility parameters and other cohesion parameters*; Routledge, 2017.

(200) Kim, C. A.; Choi, H. J.; Sung, J. H.; Lee, H. M.; Jhon, M. S. Effect of Solubility Parameter of Polymer-Solvent Pair on Turbulent Drag Reduction. In *Macromolecular Symposia*, 2005; Wiley Online Library: Vol. 222, pp 169-174.

(201) Ghosh, A.; Samanta, S.; Ge, S.; Sokolov, A. P.; Schweizer, K. S. Influence of Attractive Functional Groups on the Segmental Dynamics and Glass Transition in Associating Polymers. *Macromolecules* **2022**, *55* (6), 2345-2357.

(202) Shen, T.; Vernerey, F. J. Rate-dependent fracture of transient networks. *Journal of the Mechanics and Physics of Solids* **2020**, *143*, 104028.

(203) Shen, T.; Song, Z.; Cai, S.; Vernerey, F. J. Nonsteady fracture of transient networks: The case of vitrimer. *Proceedings of the National Academy of Sciences* **2021**, *118* (29).

(204) Porath, L.; Soman, B.; Jing, B. B.; Evans, C. M. Vitrimers: Using Dynamic Associative Bonds to Control Viscoelasticity, Assembly, and Functionality in Polymer Networks. *ACS Macro Letters* **2022**, *11* (4), 475-483.

VITA

Sirui Ge graduated from East China University of Science and Technology with a B.S. degree in Materials Physics and Finance minor in June 2015. In August 2014, Sirui was enrolled in a 3+2 BS/MS program in Department of Polymer Science in University of Akron. During that time, he conducted Master's research under the supervision of Dr. Shi-Qing Wang on the study of Entanglement-Disentanglement Transition of highly entangled polymer under creep deformation. Sirui was graduated with a M.S. degree in May 2016. After that, Sirui went to Department of Materials Science and Engineering in University of Tennessee as a PhD student. In May 2017, Sirui Ge began his PhD studies under the guidance of Dr. Alexei P. Sokolov. His research focus on the understanding of dynamics and viscoelastic behavior of polymers with dynamic bonds. Sirui has presented at APS and NGRPC conferences and has published 17 peer reviewed publications and 1 book chapter, including 4 first-authored publications.